KATHOLIEKE UNIVERSITEIT LEUVEN
FACULTEIT TOEGEPASTE WETENSCHAPPEN
DEPARTEMENT ELEKTROTECHNIEK
Kardinaal Mercierlaan 94 - 3001 Leuven (Heverlee)

MODEL BASED OPTIMIZATION AND CONTROL OF BIOPROCESSES
From Theory to Practice

Jury :
Voorzitter Prof. E. Aernoudt, pro-dekaan
Prof. J. Van Impe, promotor
Prof. B. De Moor, promotor
Prof. J. Vandewalle
Prof. G. Bastin (UCL)
Prof. M. Hendrickx
Prof. B. Nicolaï
Dr. H. Stigter

Proefschrift voorgedragen tot
het behalen van het doctoraat
in de toegepaste wetenschappen

door

Vincent RYCKAERT

U.D.C. 621.3.049.77

Mei 1998

© Katholieke Universiteit Leuven - Faculteit Toegepaste Wetenschappen
Arenbergkasteel, B-3001, Heverlee

Alle rechten voorbehouden. Niets uit deze uitgave mag worden vermenigvuldigd en/of openbaar gemaakt worden door druk, fotocopie, microfilm, elektronisch of op welke andere wijze ook zonder voorafgaande schriftelijke toestemming van de uitgever.

All rights reserved. No part of the publication may be reproduced in any form by print, photoprint, microfilm or any other means without written permission from the publisher.

D/1998/7515/31
ISBN 90-5682-130-X

Dankwoord

De gedrevenheid van wetenschappers is ongetwijfeld te vinden in hun immense drang naar een totaal beeld over een bepaald studie onderwerp. Helaas zijn enkel briljante wetenschappers in staat de resultaten van analyse van bepaalde deelaspecten te unificeren tot een harmonieus geheel. De afgelopen 10 jaar aan de Universiteit heb ik dan ook ervaren als een voortdurende confrontatie tussen enerzijds ongetwijfeld door jeugdig idealisme gevoede zoektocht naar vormen van unificatie en anderzijds de persoonlijke beperkingen.

Slechts door een uitstekende begeleiding kan in dergelijke omstandigheden resultaten worden geboekt. Professor Jan Van Impe heeft met veel geduld en discrete aanmaningen de uitwerking van een realistisch onderzoeksproject mogelijk gemaakt zonder evenwel het leggen van persoonlijke klemtonen onmogelijk te maken. Ik besef dat dit voor hem niet altijd gemakkelijk is geweest en wens hem daarvoor uitdrukkelijk te bedanken.

Dat het aansnijden van zo'n verscheidenheid aan onderwerpen tijdens mijn onderzoek toch tot resultaten heeft geleid is te danken aan de grote inzet van de verschillende uitmuntende thesis- en projectstudenten waarmee ik graag heb samengewerkt. Jan en Kris, Carl, Marc, Erik, Katleen, Tom, Didier, Ronald, David en Grim bedankt voor alles.

Onderzoek mag dan misschien wel een individuele bezigheid zijn, het meest heb ik genoten van de intense discussies en samenwerking met en de warme vriendschap van mijn collega van het eerste uur, Johan. De andere collega's waarmee ik heb samengewerkt, Carl, Kurt, Chantal en Leen wens ik te bedanken voor het vertrouwen dat zij in mij hebben gesteld. Ook de andere collega's van de onderzoeksgroep BioTeC, het Laboratorium voor Industriële Microbiologie en Biochemie en SISTA wil ik bedanken voor de aangename werksfeer.

Graag had ik ook de Faculteit Landbouwkundige en Toegepaste Biologische Wetenschappen bedankt voor zoveel gastvrijheid. Ik heb me als ingenieur van de dode materie altijd welkom gevoeld en veel opgestoken van mijn collega's (bio-)ingenieurs van de levende materie. In het bijzonder wens ik de vorige Decaan Prof. V. Goedseels, de huidige Decaan Prof. R. Schoonheydt en het bureau van de Faculteit te bedanken voor de vlotte en constructieve samenwerking.

Ook Prof. H. Verachtert, wiens kritische houding tegenover al die nieuwlichterij, mij heeft doen inzien dat een intensieve dialoog met collega's uit andere disciplines broodnodig is, wil ik graag bedanken.

De samenwerking met SEGHERSengineering Water en ALMA, universiteitsrestaurants heeft gezorgd voor een belangrijke industriële component in mijn onderzoek. Ron, Kris, Marc, Luc en Kris, Luc, Mia, Toon bedankt voor jullie inspanningen.

Professor Bart De Moor, wiens gedrevenheid en ruime inzet, inspirerend heeft gewerkt om zelf mijn horizon te verruimen, wil ik bedanken omdat ik op enkele cruciale momenten op hem beroep kon doen.

Professor Joos Vandewalle wil ik bedanken omdat hij naast lid te zijn van mijn wetenschappelijk begeleidingscomité steeds een luisterend oor had op die momenten dat het eens wat minder ging.

The book of Bastin and Dochain was my first introduction to estimation and control of bioprocesses and influenced my work considerably. I would like to thank Professor George Bastin for his continuous interest in my work the last four years and his considerable input while preparing the thesis.

Professor Marc Hendrickx wil ik bedanken omdat hij via zijn opmerkingen als jurylid van twee van mijn thesisstudenten ongetwijfeld mijn werk heeft beïnvloed.

Professor Bart Nicolaï, wiens werk het me mogelijk maakte mijn project met ALMA in een ruimer perspectief te plaatsen, wil ik bedanken voor de kansen die hij creëerde voor mij om ook zijn onderzoeksterrein te leren kennen.

Hans Stigter wil ik bedanken omdat zijn positieve geestesingesteldheid een grote steun was tijdens de laatste maanden.

Bedankt Nico en Marc voor het nalezen van de tekst.

Het I.W.T. wil ik bedanken voor de financiële steun gedurende mijn doctoraatswerk. Met dank gaat ook uit naar de Faculteit Toegepaste Wetenschappen, die mijn werk in een onderzoeksgroep van een andere faculteit, wist te appreciëren.

Ook de verschillende mensen waarmee ik heb samengewerkt als A.A.P.-B.A.P.-vertegenwoordiger wil ik bedanken voor hun inzet.

Gelukkig moet ik Ingrid niet steeds opnieuw uitleggen waarom het vaak zo druk is. Toch is de onvoorwaardelijke steun die ik van haar gekregen heb niet evident, waarvoor dank.

Dank ook voor de familie en vrienden, die ondanks onze geringe aandacht voor hen, er nog altijd zijn voor ons.

Vincent Ryckaert
Leuven, April 1998

Abstract

Model based optimization and control, which is a generally accepted methodology in engineering fields such as electronics, mechanics, thermodynamics and hydraulics, is shown to be feasible also for bioprocesses, when the specific nature of these processes (time-varying, nonlinear, complex and uncertain dynamics) is taken into account explicitly.

In the thesis the different aspects of model based optimization and control (modeling, optimization, monitoring and control) are discussed. The applicability of several techniques (dynamical and sensitivity analysis, optimal control theory, nonlinear estimation and control theory) for bioprocesses is examined. Performance measures, inspired from a process engineering point of view, are used.

The thesis aims at closing the gap between theory and practice by providing results of case studies about cyclically operated activated sludge wastewater treatment systems (carbon- and nitrogen removal) and fermentation processes.

Modelgebaseerde optimalisering en regeling is een algemeen geaccepteerde methodologie in technische domeinen zoals electronica, mechanica, thermodynamica en hydraulica. In het proefschrift wordt aangetoond dat deze technieken ook toepasbaar zijn voor bioprocessen als de specifieke karakteristieken van deze processen (tijdsvariërend, niet-lineair, complexe en onzekere dynamica) expliciet in rekening wordt gebracht.

In het proefschrift worden de verschillende aspecten van modelgebaseerde optimisatie en regeling (modellering, optimisatie, meten en regeling) behandeld. De toepasbaarheid van verschillende technieken (dynamische en sensitiviteitsanalyse, *optimal control* theorie, niet-lineair schatten en regelen) voor bioprocessen wordt onderzocht. De beoordeling gebeurt vanuit de invalshoek van de procesingenieur.

Het proefschrift beoogt het dichten van de kloof tussen theorie en praktijk. Daarom worden de resultaten geïllustreerd met toepassingen voor cyclisch opererende aktief slib afvalwaterzuivering (koolstof- en nitraatverwijdering) en fermentatieprocessen.

Contents

0 Introduction xi
0.1 Motivation . . . xi
0.2 Own contributions . . . xvi
0.3 Prototype model . . . xxi

I Modeling of biotechnological processes 1

1 Modeling of cyclically operated activated sludge wastewater treatment systems 3
1.1 Introduction . . . 3
1.2 Cyclically operated biological wastewater treatment plants . . 4
1.2.1 Single stage system . . . 4
1.2.2 Two stage system . . . 5
1.3 Simulation study of the single stage system . . . 7
1.3.1 Mathematical model . . . 7
1.3.2 Dynamic behavior of the system . . . 8
1.3.3 Equilibrium lines in the state space . . . 9
1.3.4 State space analysis . . . 12
1.4 Simulation study of the two stage system . . . 13
1.4.1 Unstructured model . . . 13
1.4.2 Structured model . . . 15
1.4.3 Dynamic behavior of the system . . . 17
1.4.4 Physical analysis . . . 19
1.5 Model validation . . . 21
1.5.1 Lab-scale experiments . . . 21
1.5.2 Full-scale experiments . . . 26
1.6 Application of the models . . . 30
1.7 Nitrogen removal systems . . . 31
1.7.1 Biological Nitrogen Removal . . . 32
1.7.2 Redox potential . . . 33
1.8 Conclusions . . . 34

II Optimization of biotechnological processes 37

2 Optimal control of fed-batch fermentation processes with multiple limiting substrates 39
2.1 Introduction . . . 39
2.2 General framework . . . 40
2.2.1 General state space model for biotechnological processes 40
2.2.2 Optimal control of biotechnological processes . . . 42
2.3 Multiple limiting substrates . . . 45
2.3.1 Model description . . . 45
2.3.2 Dynamical costate equations . . . 47
2.3.3 Optimal control strategy . . . 48
2.3.4 A general singular control law . . . 51
2.4 Case study . . . 53
2.4.1 Case 1: double Haldane kinetic . . . 55
2.4.2 Case 2: Haldane/Monod kinetic . . . 58
2.4.3 Case 3: double Monod kinetic . . . 60
2.5 Optimization . . . 60
2.6 Simulations . . . 64
2.6.1 Case 1: double Haldane kinetic . . . 65
2.6.2 Case 2: Haldane/Monod kinetic . . . 66
2.6.3 Case 3: double Monod kinetic . . . 67
2.7 Conclusions . . . 68

3 Optimization of cyclically operated activated sludge wastewater treatment plants 69
3.1 Introduction . . . 69
3.2 Optimal control of a single tank system . . . 70
3.2.1 Problem formulation . . . 71
3.2.2 Derivation of the optimal control solution . . . 72
3.2.3 Optimal control solution . . . 75
3.2.4 Simulations . . . 75
3.3 Optimal control of complex systems . . . 76
3.3.1 Optimal control solution for a single tank system with partially fixed state . . . 77
3.3.2 Optimal control solution for a combined aerator and sedimentation tank . . . 82
3.3.3 Optimal control solution for a combination of two aerators . . . 83
3.4 Optimization of cyclically operated multi tank systems . . . 85
3.4.1 Two tank systems . . . 86
3.4.2 Three tank systems . . . 87
3.5 Conclusions . . . 89

III Monitoring of biotechnological processes 91

4 State and parameter estimation of bioprocess models 93
4.1 Introduction . . . 93
4.2 Observability and identifiability analysis of the prototype model 94
4.2.1 Problem statement . . . 94
4.2.2 Transformations . . . 95
4.2.3 State observers . . . 97
4.2.4 Observer based estimators . . . 100
4.2.5 Least squares estimation . . . 100
4.2.6 Reparameterizations . . . 101
4.2.7 Summary . . . 104
4.3 State estimation and the redox sensor . . . 107
4.3.1 Problem statement . . . 107
4.3.2 State estimation of ammonium and nitrate concentration . . . 108
4.3.3 Summary . . . 112
4.4 Conclusions . . . 114

5 Performance analysis of nonlinear observers 115
5.1 Introduction . . . 115
5.2 Prototype model and observers . . . 117
5.3 Method 1: Exact linearization . . . 118
5.4 Local linearization . . . 121
5.4.1 Method 2: Local linearization in original coordinates . 121
5.4.2 Method 3: Local linearization in observer coordinates 122
5.5 Method 4: High gain observers . . . 124
5.6 Simulation results . . . 126
5.7 Performance analysis . . . 126
5.8 Convergence region . . . 127
5.9 Noise sensitivity and speed of convergence . . . 129
5.10 Robustness analysis . . . 132
5.10.1 Equilibrium analysis . . . 133
5.10.2 Dynamical analysis . . . 139
5.10.3 Conclusions . . . 144
5.11 Discretization . . . 147
5.12 Conclusions . . . 150

6 Optimal tuning of observers and observer based estimators 153
6.1 Introduction . . . 153
6.2 General problem statement . . . 154
6.3 Case study 1: Observer based estimators . . . 155
6.3.1 Introduction . . . 155
6.3.2 Oxygen uptake rate estimator, independent of the oxygen transfer rate . . . 156

6.3.3 Oxygen transfer rate estimator . . . 162
6.3.4 Oxygen uptake rate estimator, dependent on the oxygen transfer rate . . . 169
6.3.5 Case study: carbon removal wastewater treatment systems . . . 171
6.3.6 Case study: nitrogen removal wastewater treatment systems . . . 172
6.3.7 Case study: fermentation processes . . . 175
6.3.8 Case study: germination processes . . . 178
6.4 Case study 2: Nonlinear observers . . . 179
6.4.1 Problem statement . . . 179
6.4.2 Performance analysis . . . 181
6.4.3 Trade-off analysis . . . 183
6.4.4 Simulations . . . 184
6.5 Conclusions . . . 185

IV Control of biotechnological processes 187

7 Nonlinear control of bioprocesses 189
7.1 Introduction . . . 189
7.2 Robustness analysis . . . 190
7.2.1 Problem statement . . . 190
7.2.2 Nonlinear controller design techniques . . . 190
7.2.3 Robustness against parametric uncertainty . . . 193
7.2.4 Conclusions . . . 199
7.3 Combined observers-controllers . . . 199
7.3.1 Problem statement . . . 199
7.3.2 Nonlinear controller design . . . 200
7.3.3 Nonlinear observer design I . . . 201
7.3.4 Nonlinear separation principle I . . . 202
7.3.5 Nonlinear observer design II . . . 205
7.3.6 Nonlinear separation principle II . . . 205
7.3.7 Application . . . 206
7.3.8 Conclusions . . . 210
7.4 Optimal tuning of nonlinear controllers . . . 210
7.4.1 Problem statement . . . 210
7.4.2 Performance analysis . . . 211
7.4.3 Trade-off analysis . . . 212
7.4.4 Simulations . . . 213
7.4.5 Conclusions . . . 214
7.5 General conclusions . . . 215

8 Conclusions 217
8.1 Overview of the contributions 217
8.2 Suggestions for further research 219

V Appendices 221

A Estimation theory 223
A.1 Introduction 223
A.2 General dynamical model for biotechnological processes . . . 223
A.3 State observers 224
A.4 Observer based parameter estimators 225
A.5 Least squares estimation 226
A.6 Transformations 227
A.7 Reparametrizations 228
A.8 Adaptive state estimation 230

B Technical lemmas 233
B.1 Introduction 233
B.2 Technical Lemma 1 233
B.3 Technical Lemma 2 234
B.4 Technical Lemma 3 236

C Differential geometry in nonlinear controller and observer design 237
C.1 Introduction 237
C.2 Basic definitions 238
C.3 Basic theorems 239
C.3.1 Leibniz formula 239
C.3.2 Lemma 240
C.3.3 Inverse Function Theorem 240
C.3.4 Frobenius Theorem 240
C.3.5 Simultaneous Rectification Theorem 240
C.3.6 Remarks 240
C.4 Nonlinear controller design 241
C.4.1 Input-output linearizing controller 241
C.4.2 Input-state linearizing controller 242
C.5 Nonlinear observer design 244
C.5.1 Canonical forms 244
C.5.2 Observers without input derivatives 245
C.5.3 Observers with input derivatives 246
C.6 Conclusions 250

D Notations, units and parameter values 251

E Bibliography 259

F Nederlandse samenvatting 269
F.1 Motivatie 270
F.2 Eigen bijdragen 275
F.2.1 Hoofdstuk 1. Modellering van cyclisch opererende actief slib afvalwaterzuiveringsinstallaties 275
F.2.2 Hoofdstuk 2. Optimale regeling van fed-batch fermentatieprocessen met meerdere limiterende substraten . 276
F.2.3 Hoofdstuk 3. Optimale regeling van cyclisch opererende actief slib afvalwaterzuiveringsinstallaties 276
F.2.4 Hoofdstuk 4. Toestand- en parameterschatters voor bioprocesmodellen 277
F.2.5 Hoofdstuk 5. Performantie van niet-lineaire toestandschatters 278
F.2.6 Hoofdstuk 6. Optimale afstelling van toestand- en parameterschatters 279
F.2.7 Hoofdstuk 7. Niet-lineaire regeling van bioprocessen . 279
F.2.8 Appendix C. Differential geometry in niet-lineaire regelaar en toestandschatterontwerp 280
F.3 Conclusies 281

Chapter 0

Introduction

0.1 Motivation

Model based optimization and control is a generally accepted methodology in engineering fields such as electronics, mechanics, thermodynamics and hydraulics. The use of model based approaches for *bioprocesses*, which are systems involving *living* material (e.g. micro-organisms, ...), is often criticized. Besides technical reasons, such as the intrinsically complex, time-varying nonlinear dynamics of biotechnological processes and the lack of cheap, reliable and accurate on-line measurements, basically the modeling of the bioprocess is considered not to be feasible. Two basic reasons for the rejection of modeling of bioprocesses can be distinguished. The first reason is the psychological fact that humans can hardly accept that bioprocesses, involving living material (in the limit humans), can be described mathematically. The second reason is a misunderstanding of what a model is. When referring to other sciences (mechanics, electronics, ...) it is often stated that for these systems basic physical laws are known while for bioprocesses this is hardly the case. One does not sufficiently realize at that moment that these famous physical laws are nothing else than (although rather accurate) models of the reality.

A first theme of the thesis is to indicate the fundamental role the process model plays in model based optimization and control techniques. It is emphasized that excellent performance is obtained even if the model is a rough, approximate description of reality. This fact makes application of model based techniques to bioprocesses feasible.

This theme is elaborated as follows in the different chapters (Table 0.1).

Chapter 1. The modeling of a particular bioprocess is studied. It is illustrated that *simple process models* are sufficient for analyzing the main dynamics of the system, studied in this chapter. Moreover the parameters of such a model can be determined in practice.

Chapters 2 and 3. Optimal control strategies for bioprocesses are derived. The main features of the obtained control strategy are only depending on a *qualitative* notion of the process kinetics, which is often the uncertain part in bioprocess models.

Chapter 4. *Observability* and *identifiability* of bioprocess models is discussed with two case studies. The model serves here as framework for data interpretation. The concept of *minimal modeling*, discussed here, emphasizes that the model must not be completely specified.

Chapters 5 and 7. *Robustness* of nonlinear observers and controllers against parametric and structural uncertainty on their design model is analyzed. The performance of these algorithms remains acceptable for reasonable magnitudes of uncertainty on the model.

Chapters 6 and 7. *Model based tuning* of nonlinear estimators and controllers is illustrated. It is demonstrated how even with models with low complexity important insights in the tuning problem can be obtained.

In electronics and mechanics model based techniques are often developed within the framework of linear time-invariant systems, which becomes commonly known and has widely accepted standard concepts and notations. By adaptation, enabled by the availability of fast and accurate on-line sensors, of the linear models used in these applications, one can deal with nonlinearities and time-varying dynamics.

Due to the intrinsic nonlinear time-varying dynamics of bioprocesses and the lack of cheap, reliable and accurate on-line sensors model based techniques for bioprocesses should originate from *nonlinear systems* and *control theory*. This research field is currently developing. This results in a large variety of concepts and notations, which are mainly introduced from a mathematical point of view. Moreover, the resulting methods are at first sight not always directly implementable.

A second theme of the thesis is, instead of developing new nonlinear techniques, to illustrate the potential of existing approaches (with case studies) and to introduce general concepts for evaluation of the methods from a process engineering point of view.

This theme is considered in detail in the following chapters (Table 0.1).

Chapter 1. *Dynamical simulations, state space* and *sensitivity analysis* are introduced as tools for understanding the main dynamics of the plant under consideration. Moreover the model is used as basis for the design of an advanced sampling and measurement system.

Chapters 2 and 3. *Optimal control theory* (minimum principle of Pontryagin) is presented as a powerful tool for obtaining optimal control inputs, in spite of the intrinsic sensitivity of the method on model uncertainties, typically encountered in bioprocess modeling. The resulting optimal control strategies serve as starting point for practically implementable heuristic control strategies.

Chapter 4. Analysis of *observability* and *identifiability* is more than evaluation of some mathematical properties of a model. The analysis establishes a direct link between the design of the system under consideration and the measurability. Moreover, it provides a tool for determining an optimal sensor investment policy.

Chapters 5 and 7. *Nonlinear observer and controller design techniques* are reviewed and illustrated for a prototype model for bioprocesses. *Performance analysis tools*, enabling selection of an appropriate observer and controller structure and inspired from a process engineering point of view, are introduced.

Chapters 6 and 7. The proper selection of tuning parameters in the different algorithms is of major importance for the process engineer. Optimal tuning of nonlinear estimators and controllers is discussed. *Performance analysis* is used here as one of the tools for determination of an appropriate parameter set. *Trade-off analysis*, based on objective function optimization, is a complementary tool.

A third theme of the thesis is to demonstrate the potential of model based optimization and control techniques on bioprocesses by considering several quite diverse applications.

The following case studies are discussed (Table 0.1).

Activated sludge wastewater treatment plants. Modeling of carbon removal treatment systems is discussed in **Chapter 1**. Nitrogen removal systems are shortly introduced in this chapter. The optimal control strategy for a carbon removal plant is derived in **Chapter 3**. The results of the observability and identifiability analysis of a prototype model for bioprocesses are interpreted in the context of carbon removal processes in **Chapter 4**. In the same chapter the use of the redox potential as extra on-line measurement in nitrogen removal systems is illustrated. Tuning of observer based estimators, useful for on-line monitoring of the carbon removal plant is discussed and illustrated with real data in **Chapter 6**. Results obtained with methods of this chapter are used in **Chapter 1** on modeling.

Fermentation processes. Derivation of optimal control strategies by application of the *minimum principle of Pontryagin* for fermentation processes with one biomass and multiple limiting substrates is presented in **Chapter 2**. The tuning of observer based estimators and nonlinear observers is discussed for fermentation processes (both liquid and solid state fermentations) in **Chapter 6**. The performance of an observer based estimator is illustrated with real data. Tuning of nonlinear controllers is also discussed in the context of fermentations in **Chapter 7**.

It must be emphasized that the prototype model used for analysis of identifiability and observability (**Chapter 4**), performance analysis and tuning of nonlinear observers (**Chapter 5, 6**) and controllers (**Chapter 7**) can be used both in the context of biological wastewater treatment and fermentation.

Conceptually *modeling, optimization, monitoring* and *control* of bioprocesses are strongly related problems. The resulting optimal control strategy depends on the model while the implementability of this control strategy depends on the monitoring and control properties of the model under consideration. From this observation one could conclude that these topics should be considered simultaneously, which is practically not feasible.

A fourth theme of the thesis is to illustrate that model based optimization and control of bioprocesses can roughly be decomposed into four subproblems: (i) modeling of the process, (ii) derivation of an optimal control strategy, (iii) design of software sensors and (iv) controller design. Problems due to the interaction between the different subproblems can most often be overcome by applying rules, originating from common sense and engineering experience. This decomposition is also expressed in the structure of the thesis.

The structure of the thesis is depicted in Table 0.1.

Modeling. In **Chapter 1** modeling of cyclically operated activated sludge wastewater treatment plants is presented. Development of *models with low complexity* prevents appearing of problems (lack of identifiability and observability of parameters and states, mathematical unsolvable optimization, observer and controller design problems, ...) while considering the other subproblems.

Optimization. In **Chapter 2** the optimization of fermentation processes with one biomass and multiple limiting substrates is discussed while

carbon removal treatment systems are considered in **Chapter 3**. Insight in the nature of the optimization problem enables determination of the important parts of the model of the process under consideration and even decomposition of the optimization problem in (analytically solvable) subproblems. *Reformulation* of the obtained optimal solution in new nearly optimal control objectives enables practical implementation.

Monitoring. A first step to consider while dealing with a monitoring problem is to perform an *observability* and *identifiability analysis* as presented in **Chapter 4.** In **Chapter 5** the design and performance analysis of nonlinear observers is treated. Such an analysis enables the *selection* of an appropriate design methodology. This selection can be considered as a second step in solving monitoring problems. The *tuning* of observer based estimators and observers, which is the third step to consider, is presented in **Chapter 6**. Both performance analysis and trade-off analysis are discussed. Observability, identifiability and performance analysis indicate which model parts are important with respect to the monitoring problem.

Control. In **Chapter 7** performance analysis of nonlinear controllers, the tuning of these algorithms and the combination with estimators is treated. Analysis of the combined estimator-controller algorithm indicates the interactions between the *monitoring* and *control* problem. Performance analysis indicate which model parts are important with respect to the control problem.

Chapters 2, 5, 7 are considered to be of theoretical nature while **Chapters 1, 3, 4, 6** are more practically oriented because a specific system is considered and/or real data are used as illustration. Notice that the organization of the thesis in 4 parts (1 *modeling*, 2 *optimization*, 3 *monitoring* and 4 *control*) reflects the problem decomposition.

From the thesis it must be clear that modeling is **not** *the bottleneck for application of model based optimization and control to bioprocesses. The typical characteristics of bioprocesses (complex, time-varying nonlinear dynamics with large uncertainty) only require a specific approach when using model based techniques. The presentation of various techniques and their evaluation from process engineering point of view should facilitate their use in process industry. The potential of model based approaches is demonstrated by the different applications considered throughout the thesis. The 'divide et impera' strategy, visualized in the structure of the thesis, indicates that model based optimization and control problems, can be decomposed in relatively easily solvable subproblems.*

	Theory	Practice
Modeling		**Chapter 1.** Modeling of cyclically operated activated sludge wastewater treatment systems
Optimization	**Chapter 2.** Optimal control of fed-batch fermentation processes with multiple limiting substrates	**Chapter 3.** Optimal control of cyclically operated activated sludge wastewater treatment plants
Monitoring	**Chapter 5.** Performance analysis of nonlinear state observers	**Chapter 4.** State and parameter estimation of bioprocess models
		Chapter 6. Optimal tuning of observers and observer-based estimators
Control	**Chapter 7.** Nonlinear control of bioprocesses	

Table 0.1: Outline of the thesis

0.2 Own contributions

Chapter 1. Modeling of cyclically operated activated sludge wastewater treatment systems.

1. The *dynamic analysis methodology*, enabling easy interpretation of the dynamics of cyclically operated systems, is developed. Principally the method relies on the construction of the regime trajectory with dynamic simulations and the interpretation of the dynamics in the state space with equilibrium lines.

2. A *sensitivity analysis* of cyclically operated activated sludge wastewater treatment systems is performed. With this analysis feasible regions for the main process parameters can be deduced.

3. It is illustrated that dynamical analysis and sensitivity analysis are basic elements in *model selection*. Process models incorporating the basic design philosophy of the systems under study are derived and incorporated in a simulator.

4. Process parameters are determined both from lab- and full-scale experiments. The *identifiability* of the model parameters is studied. An

automatic sampling and measuring system, which is one of the key elements of an advanced control strategy for the treatment plants, is developed. The measurements are interpreted in terms of the process model.

Dynamical analysis of a single stage cyclically operated activated sludge wastewater treatment system is reported in [Ryckaert *et al.* 1994]. Dynamical and sensitivity analysis of single and two stage systems is presented in [Ryckaert *et al.* 1997a]. Practical identifiability of the parameters of the process models is discussed in [Claes *et al.* 1996a; 1996b]. Models, involving multiple species, are discussed in the context of combined biotransformation-sedimentation in [Cenens *et al.* 1997]. Redox based control of nitrogen removal systems is presented in [Ryckaert *et al.* 1998a].

Chapter 2. Optimal control of fed-batch fermentation processes with multiple limiting substrates.

1. The optimal control equations are derived for a general model for biotechnological processes and reveal a particular structure.
2. The optimal control problem of fed-batch fermentation processes with multiple limiting substrates and one biomass is solved. It is shown that from the optimal control solution a *suboptimal heuristic control strategy* can be derived.
3. The optimization of other degrees of freedom in combination with the optimal control strategy is discussed. A *two-step procedure* for optimization of the process is established.

The topics, discussed in this chapter, are presented in [Ryckaert and Van Impe 1998e].

Chapter 3. Optimal control of cyclically operated activated sludge wastewater treatment plants.

1. It is illustrated how optimal control theory can be used as basis for the derivation of a heuristic control strategy, even for complex systems such as cyclically operated activated sludge wastewater treatment plants. The approach relies on solving a low complexity optimal control problem for a hypothetical treatment system and evaluating the effect of increasing the complexity until a reasonable plant description is obtained.
2. A *heuristic control strategy* for the cyclically operated activated sludge wastewater treatment plants is derived. Also a design formula for the volume of the systems is obtained which enables the evaluation of a trade-off between operating and investment costs.

3. The features of an automatic sampling and measuring system, based on the developed process model, are discussed from the point of view of implementing the heuristic control strategy.

Optimal control of cyclically operated wastewater treatment systems is reported in [Ryckaert *et al.* 1996d; 1998d]. The modeling, monitoring of these systems from the point of view of implementing a heuristic control strategy is discussed in [Claes *et al.* 1997]. A preliminary result on optimization of nitrogen removal systems is presented in [Herremans *et al.* 1997].

Chapter 4. State and parameter estimation of bioprocess models.

1. The *observability* and *identifiability* of a prototype model for bioprocesses is examined for different measurement sets. The analysis can be considered as a tool for determining an optimal sensor investment policy.
2. The results of the analysis are interpreted in the case of the cyclically operated activated sludge wastewater treatment system. A link between the design of the plant and the measurability is pointed out.
3. In the analysis estimators found in literature are used. Some extensions, mainly dealing with the transport terms in the model, are introduced.
4. It is shown what can be gained by using redox potential measurements as additional on-line sensor in activated sludge wastewater treatment systems for nitrogen removal.

The observability and identifiability analysis is reported in [Ryckaert *et al.* 1996a] and [Ryckaert and Van Impe 1997b].

Chapter 5. Performance analysis of nonlinear observers.

1. Several mathematical *performance analysis tools* for nonlinear observers are constructed. Methods for evaluation and interpretation of the performance measures are discussed.
2. The performance of four different nonlinear observer design methodologies are evaluated for a prototype model for bioprocesses. Conclusions for the case study in particular and *observer design selection* in general are presented.

Performance analysis of nonlinear observers is presented in [Ryckaert and Van Impe 1996c; 1997c] and [Ryckaert *et al.* 1998f]. Robustness improvements are discussed in [Ryckaert *et al.* 1997d].

Chapter 6. Optimal tuning of observers and observer based estimators.

1. *Performance analysis* of observers and observer based estimators is introduced as a tool for tuning of these algorithms. This method relies on the determination of an analytical relation between the performance measures and the tuning parameters.

2. Tuning of observers and observer based estimators with *trade-off analysis* is discussed. This method relies on representative simulations.

3. The advantages and disadvantages of performance and trade-off analysis as tools for optimal tuning of nonlinear observers and observer based estimators are discussed and compared.

4. The observer based estimators are illustrated on real data obtained from wastewater treatment plants, both carbon and nitrogen removal and fermentation processes.

The application of observer based estimators in cyclically operated activated sludge wastewater treatment systems is reported in [Ryckaert *et al.* 1995]. Optimal tuning is presented in [Ryckaert and Van Impe 1998b].

Chapter 7. Nonlinear control of bioprocesses.

1. *Performance analysis* of nonlinear controllers is introduced and illustrated for two different nonlinear controller design methodologies.

2. *Performance analysis* and *trade-off analysis* as tools for tuning of nonlinear controllers is discussed.

3. The combination of nonlinear observers based on exact linearization and nonlinear controllers based on state feedback linearization is studied.

4. The tuning of the combined nonlinear observers and controllers is discussed.

Combined estimation and control of bioprocesses is reported in [Ryckaert and Van Impe 1998g]. Model based temperature control of oven cavities in the context of food processes is presented in [Ryckaert *et al.* 1996b; 1998h].

Appendix A. Estimation theory.
A general dynamical model for biotechnological processes, software sensors based on this model, model transformations and reparametrization are introduced. These methods are basically adopted from the work of Bastin and Dochain (1990). However, a more general transport model is considered in the appendix.

Appendix B. Technical lemmas.
Extensions of the technical lemmas found in Bastin and Dochain (1990) are presented.

Appendix C. Differential geometry in nonlinear controller and observer design.
A brief introduction of concepts, terminologies and theorems (including proofs) of differential geometry are presented. A considerable effort has been made to present all the proofs in a similar way. Finally an observer, originating from differential algebraic techniques, is reformulated in the differential geometric framework.

Appendix D. Notations, units and parameter values.
The notations and units of the variables and the parameter values, used throughout the thesis, are given. Also some information on the hard- and software used is provided.

Finally it must be emphasized that (i) the results of **Chapters 2 and 3** on *optimal control* can be considered as extensions of the work by [Van Impe 1993a], (ii) **Chapters 4, 5, 6** and partly **Chapter 7** on *estimation and control of bioprocesses* are inspired by [Bastin and Dochain 1990] and (iii) the application of *nonlinear design techniques* in **Chapters 5, 6 and 7** is essentially based on the work of [Isidori 1989] and [Marino and Tomei 1995]. The references [Vanrolleghem 1994], [Axelsson 1989], [Keulers 1993] provided excellent background material on modeling and monitoring of activated sludge wastewater treatment plants and model based control of fermentation processes while [Sepulchre *et al.* 1996] served as motivation for application of nonlinear techniques. Standard references on nonlinear systems are [Khalil 1992] and [Vidyasagar 1993].

0.3 Prototype model

The prototype biotechnological system used throughout this thesis is introduced here. Below the basic scheme (autocatalytic reaction) of an aerobic biological process is shown. Substrate S is consumed for growth of biomass X with μ the specific biomass growth rate. Oxygen O is consumed during the biotransformation.

$$S + O \xrightarrow[X]{\mu} X \tag{0.1}$$

In **Chapters 1, 3** and **4** this basic process is used in the context of aerobic carbon removal wastewater treatment systems. In this application the emphasis is on the substrate (which is in fact the wastewater) consumption. In **Chapter 2** and partly **Chapter 7** aerobic fermentation processes are discussed while more theoretical issues are presented in **Chapters 5, 6** and partly **Chapter 7**.

The substrate, biomass and oxygen concentration C_S [mg/L], C_X [g/L], C_O [mg O_2/L] and the volume V [L], [m^3] of the liquid phase in the bioreactor considered are describing the state of the system. In carbon removal wastewater treatment systems the substrate or carbon concentration C_S is often expressed in mgCOD/L or mgBOD/L, referring to the Chemical Oxygen Demand and Biological Oxygen Demand respectively. The biomass or activated sludge concentration C_X is often described in gMLSS/L (Mixed Liquor Suspended Solids) in wastewater treatment systems while in fermentation processes gDW/L (Dry Weight) is often used. An alternative approach, used in the context of wastewater treatment, is to express the biomass concentration also in gCOD/L or gBOD/L.

Below the dynamic equation of the system is given.

$$\begin{aligned}
\frac{dC_S}{dt} &= -\sigma(C_S)C_X + D\cdot(C_{S,in} - C_S) \\
\frac{dC_X}{dt} &= \mu(C_S)C_X + D\cdot(C_{X,in} - C_X) \\
\frac{dC_O}{dt} &= -OUR(C_S, C_X) + OTR(C_O) - D\cdot C_O
\end{aligned} \tag{0.2}$$

The different terms of the model are now introduced. First the dynamics of the substrate and biomass concentration due to the biotransformation process are discussed. Second the operation modes of bioreactors are presented because this determines the dynamics of these state variables due to transport. Finally the dynamics of the oxygen concentration is discussed.

Biotransformation process. The specific substrate consumption rate $\sigma(C_S, C_O)$ [1/h] and the specific biomass growth rate $\mu(C_S, C_O)$ [1/h] are often related via the linear law (0.3). $Y_{X/S}$ [-] and m [1/h] are the yield of

biomass on substrate and the maintenance coefficient respectively.

$$\sigma = \frac{\mu}{Y_{X/S}} + m \tag{0.3}$$

The specific rates can be modeled in several ways. Some examples are given below [Bastin and Dochain 1990, Marsili-Libelli 1989].

- **First order model.**

$$\mu(C_S) = a\cdot C_S \tag{0.4}$$

- **Monod model.**

$$\mu(C_S) = \mu_{max}\frac{C_S}{K_S + C_S} \tag{0.5}$$

- **Haldane model.**

$$\mu(C_S) = \mu_m\frac{C_S}{K_S + C_S + \frac{C_S^2}{K_I}} \tag{0.6}$$

- **Maynard-Smith or Volterra-Leslie model.**

$$\mu(C_S, C_X) = (a\cdot C_S - b\frac{C_X}{C_S}) \quad ; \quad \sigma(C_S) = c\cdot C_S \tag{0.7}$$

The specific rates are not linearly related here. Notice that the specific growth rate μ is assumed to be function of the biomass concentration C_X.

The prototype biotechnological process is assumed to be aerobic. As such the dependence of the specific rates on the oxygen concentration is not made explicitly as it is assumed that by an appropriate aeration process sufficient dissolved oxygen is available.

Operation modes. The biotechnological process takes place in a perfectly mixed aerated and stirred reactor.

Besides in *batch* mode (no transport), such a reactor can operate in *continuous* or in *fed-batch* mode.

- Continuous reactor (Figure 0.1 left).
  The volume of the liquid phase in the reactor is constant. The volumetric input flow is equal to the output flow.

- Fed-batch reactor (Figure 0.1 right).
  There is no output flow. The volume is changing due to the input flow.

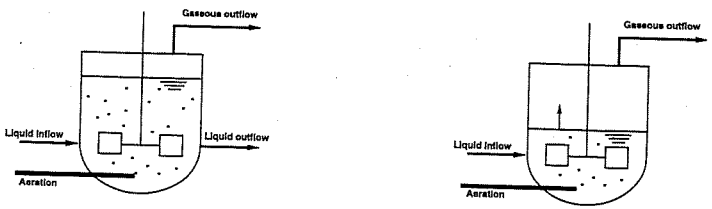


Figure 0.1: Stirred tank biological reactors. Left: continuous operation. Right: fed-batch operation

There is an influent stream with substrate concentration $C_{S,in}$ [g/L] and biomass concentration $C_{X,in}$. F [L/h] is the volumetric flow rate through the system in the case of continuous operation, and the input flow rate in fed-batch operation. $D = F/V$ [1/h] is the so-called dilution rate and is considered as the *input variable* of the system.

Aeration process. The oxygen consumption rate OUR [mg O_2/L h] is function of the biomass concentration C_X and the substrate concentration C_S. The oxygen consumption rate OUR consists of two parts.

1. The endogenous respiration OUR_{end} modeled by the parameter m [mgO_2/gDW h] multiplied with the biomass concentration C_X.
2. The exogenous respiration OUR_{ex} related to the specific growth rate $\mu(C_S)$ [1/h] and the biomass concentration C_X by the yield coefficient $Y_{X/O}$ [mgO_2/gMLSS].

$$OUR \;=\; \frac{1}{Y_{X/O}} \cdot \mu(C_S) \cdot C_X \;+\; m \cdot C_X \tag{0.8}$$

The oxygen transfer rate OTR is proportional with the difference between the actual oxygen concentration C_O and the oxygen saturation concentration C_{SAT} [mg O_2/L]. The proportionality constant k_La [1/h] is called the oxygen transfer coefficient. The dilution of oxygen by transport is neglected in the wastewater treatment applications studied in the thesis. This can be motivated for the plant considered.

$$OTR \;=\; k_La \cdot (C_{SAT} - C_O) \tag{0.9}$$

It must be emphasized that in **Chapter 5, 6, 7** mainly the first order model for the specific biomass growth rate is used. As such a rather simple *second order multilinear* model is obtained. The motivation for this choice is that models are preferred for which *observer and controller design methods*, not relying on local linearizations, exist. In **Chapter 1** also some experimental evidence for this choice for the growth kinetic is given. On the other hand in **Chapter 1, 2, 3** the Monod and Haldane kinetics are used for the *modeling and optimization* of the bioprocesses. Notice that in **Chapter 4** on *observability and identifiability* the kinetics are not specified at all.

Part I

Modeling of biotechnological processes

Chapter 1

Modeling of cyclically operated activated sludge wastewater treatment systems

1.1 Introduction

Several mathematical models for (classical) wastewater treatment processes have already been published (e.g. Busby and Andrews 1975, Henze *et al.* 1995). The complexity of these models is highly related with their aim.

Models used for *simulation* of wastewater treatment plants, typically have many states and parameters and are based on biological knowledge. However, models used for *on-line process control* should have as few variables as possible (*minimal modeling concept* [Bastin and Dochain 1990]), due to the measurement problems encountered when dealing with biological systems.

The main goal of the chapter is to illustrate the modeling of cyclically operated activated sludge wastewater treatment plants. Simple models, which can be experimentally validated and useful for optimization, monitoring and control, can describe the main dynamics of the system fairly well. Moreover some techniques enabling model selection and plant analysis are introduced.

It is illustrated that (i) *dynamical (state space) analysis* and (ii) *sensitivity studies* of different model structures are useful tools in determining an appropriate model structure for cyclically operated carbon removal systems. Dynamical and sensitivity analysis of cyclically operated carbon removal

wastewater treatment systems is reported in [Ryckaert and Van Impe 1994, 1997a]. *The chapter is organized as follows. Two types of cyclically operated biological wastewater treatment systems (single stage and two stage) for carbon removal are described in Section 1.2. In Section 1.3 an unstructured model is presented for a single stage system. The behavior of the system is analyzed in detail in the state space with the use of equilibrium lines. In Section 1.4 an unstructured model is compared with a structured model for a two stage system, by using dynamical analysis and sensitivity studies. In Section 1.5 model validation with both lab- and full-scale experiments (including respirometric experiments) is presented. In Section 1.7 cyclically operated nitrogen removal systems and oxydo reduction potential measurements are shortly introduced. The unstructured model of Section 1.3 is used for determination of an optimal design and control strategy for cyclically operated systems in Chapter 3. Respirometry is the basic concept in the advanced sampling and monitoring system, also shortly presented in Chapter 3. Section 1.7 serves as background material for Chapters 4 and 6. In these chapters (i) state estimation from oxydo reduction potential measurements and (ii) redox knee detection are discussed respectively.*

1.2 Cyclically operated biological wastewater treatment plants

A classical wastewater treatment plant for carbon removal typically consists of two tanks. In the aeration tank the wastewater is consumed by micro-organisms and converted into water, gases and new micro-organisms. In the sedimentation tank the effluent and biomass are separated. Recycling of biomass from the sedimentation tank to the aeration tank is necessary to keep the biomass amount at a sufficient high value. Notice that tanks in this classical setup have a specific function, namely, aeration or sedimentation tank. In the systems analyzed in this chapter the function of the tanks is switched following a cyclic pattern. Two configurations are considered: the single stage UNITANK® system (SSU) (Section 1.2.1) and the two stage UNITANK® system (TSU) (Section 1.2.2). A detailed description of such systems can be found in [Ghekiere *et al.* 1990].

1.2.1 Single stage system

A single stage system (Figure 1.1) consists of three tanks. The function of the outer tanks is switched between *aeration mode* and *sedimentation mode*. During aeration mode the biodegradation takes place, because the tank is aerated and stirred. During the sedimentation mode there is no aeration and stirring. This results in separation of the biomass and effluent.

The system has four operational phases (Figure 1.1): two main phases and two intermediate phases. In the first main phase, the first and second

tank are in aeration mode while the third tank is in sedimentation mode. The influent enters the system in tank 1. The wastewater flows from tank 1 to tank 3. The effluent leaves the system at the top of the third tank, while at the bottom of the third tank an amount of biomass can be wasted. Because there is no recycling, biomass shifts towards the third tank. Therefore, after some time the system is switched to the second main phase. During this phase the flow direction through the system is reversed. Biomass shifts back to the first tank. The first and second main phase are similar in the sense that the function of tank 1 and tank 3 is interchanged.

Between the two main phases there is an intermediate phase. During this phase the outer aeration tank is prepared for sedimentation: this tank is not aerated nor stirred. The second tank is still in aeration mode and is fed with influent. The outer sedimentation tank is still in sedimentation mode.

Although the description of the operation may seem rather involved, the construction of this cyclic system is very easy and cheap. It consists of one big tank with three (hydraulically interconnected) compartments. There is no need for pumps for transport between the different compartments.

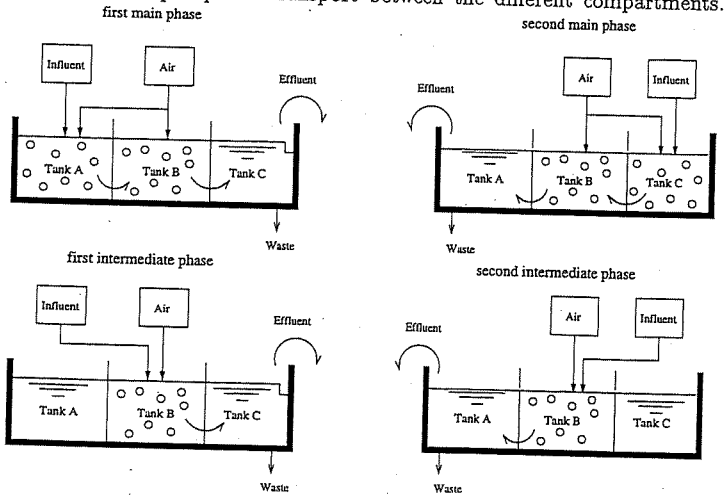


Figure 1.1: Cyclic operation of the single stage system

1.2.2 Two stage system

The two stage system consists of two single stage systems in series, which may result in better effluent quality (Figure 1.2). The activated sludge of

the first stage consumes rapidly biodegradable substrates, while the biomass of the second stage is specialized in removal of slowly biodegradable substrates.

The operation of the system consists again of four phases as shown in Figure 1.2. During the first main phase the influent enters the system in the first tank of the first stage. The first and second tank of this stage are in aeration mode. The third tank is in sedimentation mode. The effluent of the first stage enters the second stage in tank 4. The fourth and fifth tank operate as aeration tanks, while the sixth tank is in sedimentation mode. The final effluent comes out of tank 6.

During the intermediate phase, the first stage is not fed. The influent enters the second stage in tank 5. This direct feeding of the second stage is necessary to provide from time to time the biomass of this stage with enough substrate for growth. The fifth tank is used as aeration tank, while the sixth tank is in sedimentation mode. The fourth tank is prepared for sedimentation in the next phase. The second main phase and second intermediate phases are similar in the sense that the functions of tanks 1 and 3 of the first stage and of tanks 4 and 6 of the second stage are switched.

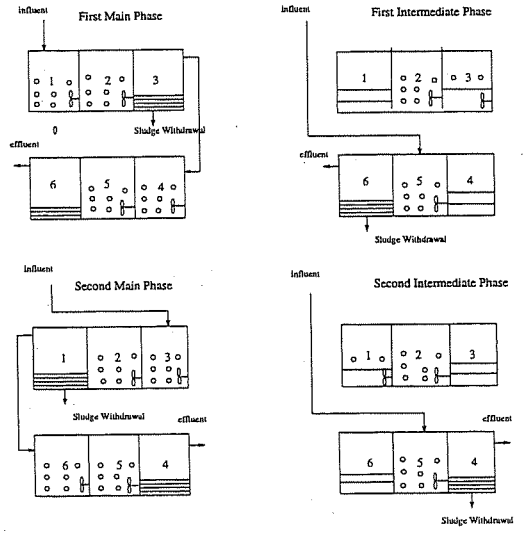


Figure 1.2: Cyclic operation of the two stage system

1.3 Simulation study of the single stage system

1.3.1 Mathematical model

In biological systems such as wastewater treatment plants, on-line measurements are hard to obtain due to the lack of accurate and cheap sensors. Models useful for on-line control of wastewater treatment systems should therefore contain as few variables (states and parameters) as possible. Nevertheless, the model should be accurate enough, as it forms the basic ingredient for the design of model based control laws. For simulation of the single stage system an unstructured model is introduced.

The model is a lumped model with three fractions (substrate S, active biomass X and inactive biomass X_d) for each tank, resulting in nine state variables necessary to describe the complete three tank system. The state variables are the (volumetric) concentrations of the substrate C_S [mgCOD/L], the active biomass C_X [gMLSS/L] and the inactive biomass C_{Xd} [gMLSS/L]. The state equations are basically mass balances. The right hand side consists of two terms representing *biotransformation* and *transport*. For the biotransformation part (Equation (1.1)) the well known Monod/decay model has been used, with μ_{max} [1/h] the maximum specific growth rate, K_S [mgCOD/L] the Monod constant, $Y_{X/S}$ [gMLSS/mgCOD] the yield coefficient of biomass on substrate, and K_d [1/h] the specific decay rate for the active biomass. The transport terms can be described in a rather straightforward manner (by checking the process scheme) except for the sedimentation part. The sedimentation model (Equation (1.2)) expresses that the concentration of the wasted biomass is proportional to the biomass concentration in the sedimentation tank. The proportionality constant β [-] represents sludge thickening. The complete model consists of four sets of nine differential equations, due to the four operational phases. The influent flow rate [L/h] and sludge waste rate [L/h] are considered to be constant during the simulation. During the intermediate phase the aeration tank is assumed to be in steady state because there is no transport nor biodegradation (the aerator is switched off which results in oxygen limitation).

- Model for aeration mode

$$\begin{aligned}
\frac{dC_X}{dt} &= \mu_{max}\frac{C_S}{K_S+C_S}C_X - K_d\,C_X + (\textit{transport terms})\\
\frac{dC_S}{dt} &= -\frac{1}{Y_{X/S}}\mu_{max}\frac{C_S}{K_S+C_S}C_X + (\textit{transport terms})\\
\frac{dC_{Xd}}{dt} &= +K_d\,C_X + (\textit{transport terms})
\end{aligned} \tag{1.1}$$

- Model for sedimentation mode

$$C_{X,effluent} = 0 \;;\; C_{X,waste} = \beta C_X \tag{1.2}$$

The sludge waste flow [L/h] can be described as a fraction of the total flow by using a proportionality constant w [-].

1.3.2 Dynamic behavior of the system

When a constant loading (flow rate multiplied with the influent substrate concentration) is considered, then in regime the dynamical behavior of the system is periodical. This can easily be visualized in the state space spanned by the (active) biomass and substrate concentration. The evolution of the state in each tank is represented by a closed regime trajectory in this state space. The parameters used for these simulations are given in Appendix D.

In Figure 1.3 the regime trajectories for the three tanks are plotted. The regime trajectories of tank 1 and tank 3 (which are identical) are at the right of Figure 1.3. The left one is the trajectory for tank 2. The trajectory for tank 2 is passed counter clockwise.

Tank 1.

First main phase (1)-(2)-(3). At the beginning of this phase, the substrate and biomass concentration is given by point (1). During this phase the biomass concentration decreases. The substrate concentration decreases first but at point (2) there is a sudden change in behavior. The substrate concentration increases now up to point (3).

First intermediate phase (3). The tank is in steady state, represented by point (3).

Second main phase (3)-(4). The first tank operates in sedimentation mode. The biomass concentration increases during this phase while the substrate concentration is decreasing.

Second intermediate phase (4)-(5)-(1). The behavior of the previous phase continues until a sudden change in behavior of the substrate concentration in the point (5). This concentration decreases first and then increases until point (1) is reached again. The biomass concentration still increases.

Tank 3. The regime trajectory of this tank is equal to the regime trajectory of tank 1 since the process cycle of tank 3 is equal to the process cycle of tank 1 shifted over half a cycle in time.

Tank 2. The trajectory of the second tank is passed twice during a complete process cycle since for this tank there is no difference between the first main (respectively intermediate) and second main (respectively intermediate) phase. Due to the low substrate concentration in the second tank the detailed evolution can not be clearly visualized on the scale of this figure.

Main phase (6)-(7)-(8)-(9). This phase starts in point (6). The biomass concentration increases until point (8) and then decreases until point

(9) is reached. The substrate degradation is very fast until point (7) is reached and then increases until point (9) is reached.

Intermediate phase (9)-(6). This phase starts in point (9) and is characterized by a fast increase of the substrate concentration in the beginning of the phase and then by a slow increase until point (6) is reached again. For the biomass the opposite behavior is observed. First a small decrease and then a fast decrease until the end of the phase.

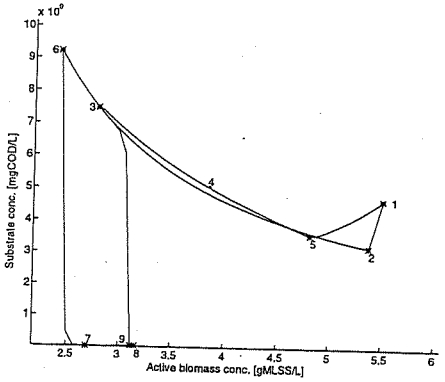


Figure 1.3: State space representation for the single stage system simulated with an unstructured model

1.3.3 Equilibrium lines in the state space

The behavior of this system is rather difficult to analyze due to the interaction between the several tanks and the switching of the function of the tanks.

An efficient tool to interpret the system behavior are the *equilibrium lines* for the several state variables. These lines provide (i) an instantaneous indication about the future evolution of the state and (ii) illustrate clearly the interactions between the several compartments.

These equilibrium lines are found by setting the time derivative of the state variables equal to zero. This results in an expression between state variables. These lines divide the state space into several zones. Each zone is characterized by the increase or decrease of a state variable. In Figure 1.3 the 9 dimensional state space, spanned by the concentrations in each tank, is visualized by two 2 dimensional state spaces (active biomass and substrate for the first and second tank respectively) superimposed on each

other. Notice that the inactive biomass X_d can be omitted because this fraction does not alter the dynamics of the active biomass X and the substrate S. Further, the state of the third tank is equal to the state of the first tank, shifted over a half process cycle and can therefore be omitted. As a result, the 9 dimensional state space can be reduced to the four states (active biomass and substrate for the first and second tank) as mentioned above.

The equilibrium lines are in general functions of all the state variables. Due to the fact that the 9 dimensional state space is represented by a 2 dimensional plot, a complete representation can only be obtained by plotting the equilibrium lines for particular values of the non-visualized states. This results in a set of equilibrium lines, parameterized by the non-visualized state variables. In Figure 1.4 at the end of this section the equilibrium lines for the substrate concentration of tank 1 are visualized. They are obtained as follows.

Tank 1.

First main phase. When the time derivative of the substrate concentration balance of tank 1 is set equal to zero during the first main phase, an expression (Equation (1.3)) between the substrate concentration $C_{S,1}$ and the biomass concentration $C_{X,1}$ of that tank is found with D [1/h] the dilution rate defined as the flow rate divided by the tank volume V [L], C_{SIN} [mgCOD/L] the influent substrate concentration, and σ [1/h] the actual specific substrate degradation rate defined as the actual specific growth rate μ [1/h] divided by the yield of biomass on substrate $Y_{X/S}$ [gMLSS/mgCOD]. In this equation no other state variables are involved because this tank is the first tank of the cascade. There is no influence of the other tanks. This equilibrium line is visualized in Figure 1.4 by a dashed dot line. It is called the *feed* line throughout this chapter, because its position is determined by the substrate concentration of the influent. When the system is in the region above this line the substrate concentration decreases. In the region below this line the substrate concentration will increase.

$$C_{X,1} = D\frac{C_{SIN} - C_{S,1}}{\sigma(C_{S,1})} \tag{1.3}$$

When the time derivative of the biomass concentration is set to zero (Equation (1.4)), there are two possibilities.

1. Transport and decay of biomass can not be compensated by the biomass growth. In that case equilibrium for biomass concentration is reached when the biomass concentration is equal to zero.
2. Biomass growth is larger than the decay and transport terms. In that case the biomass would accumulate. In UNITANK® systems

in normal operation only the first case is realistic. Notice that the equilibrium line (Equation (1.4)) coincides with the substrate concentration axis.

$$(\mu(C_{S,1}) - K_d - D) \cdot C_{X,1} = 0 \quad (1.4)$$

First intermediate phase. During this phase the tank is in equilibrium.

Second main phase. The same calculations as for the first main phase can be done for the second main phase. Now the equilibrium lines are function of the variables of the second tank because the first tank is the last tank of the cascade and is fed by the second tank. The line for the substrate concentration is a horizontal line (Equation (1.5)), marked by a dashed line in Figure 1.4, with a height depending on the substrate concentration in the second tank. If this concentration increases, the height of the equilibrium line will also increase. Above this line the substrate concentration in the first tank will decrease and under this line it will increase.

$$C_{S,1} = \frac{C_{S,2}}{1-w} \quad (1.5)$$

The line for the biomass concentration is a vertical line (Equation (1.6)) situated at the right side of the regime trajectories (not visualized in Figure 1.4). It is situated more to the right if the biomass in the second tank is increased. At the right of this line the biomass in the first tank will decrease and at the left it will increase.

$$C_{X,1} = \frac{C_{X,2}}{\beta \cdot w} \quad (1.6)$$

Second intermediate phase. The equations for the equilibrium lines for the second intermediate phase are equal to the equations of the equilibrium lines (Equations (1.5)(1.6)) of the second main phase.

Tank 3. Recall that the same description as for tank 1 can be applied because the regime trajectory of tank 3 is equal to the regime trajectory of tank 1 shifted over half a cycle in time.

Tank 2.

Main phase. For the second tank similar expressions are found. It is clear that the position of these lines is now also dependent on the state variables of the first (respectively third) tank during the first main phase (respectively second main phase). The lines for the substrate concentrations have the same structure as the feed line (Equation (1.3)). The concentration C_{SIN} in Equation (1.3) has been replaced

by the concentration $C_{S,1}$. These lines (Equation (1.7)) are situated higher if the substrate concentration of the preceding tank increases.

$$C_{X,2} = D\frac{C_{S,1} - C_{S,2}}{\sigma(C_{S,2})} \quad (1.7)$$

The equilibrium lines for the biomass are given by Equation (1.8) and move to the right if the biomass in the preceding tank increases.

$$C_{X,2} = DC_{X,1}\frac{1}{\mu(C_{S,2}) - K_d - D} \quad (1.8)$$

Intermediate phase. During this phase the equilibrium lines are not dependent on other state variables in the intermediate phases, because the second tank is fed directly during this intermediate phases. The equilibrium line for the substrate is equal to the feed line (Equation (1.3)) but now expressed in the substrate and biomass concentration of the second tank. The biomass concentration is again in equilibrium when the biomass concentration is zero.

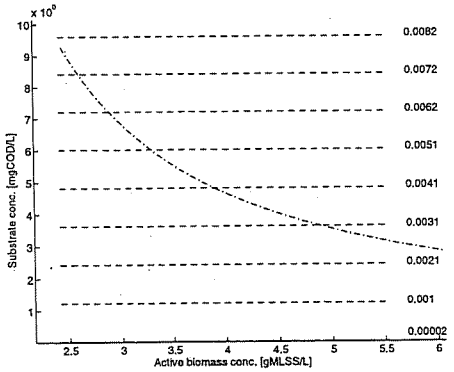


Figure 1.4: Equilibrium lines for tank 1

1.3.4 State space analysis

The behavior of the complete system can be better understood if the system dynamics are analyzed in the state space subdivided by equilibrium lines. In Figure 1.5 at the end of this section both the closed regime trajectories and the equilibrium lines relevant for tank 1 are shown.

By referring to the appropriate equilibrium line the driving force for substrate and biomass concentration increase or decrease becomes immediately

clear. Sudden behavioral changes can easily be related to the corresponding interaction between the compartments.

The use of these equilibrium lines is illustrated in the description of the regime trajectory of the first (and thus also of the third) tank.

First main phase (1)-(2)-(3). Starting in point (1) the substrate concentration decreases because the system is in the zone above the feed line (Equation (1.3)). The biomass concentration decreases because the equilibrium concentration for biomass is zero. When the state reaches the feed line in point (2), the remaining driving force is the dynamics of the biomass concentration. Due to the fact that the substrate dynamics is faster than the biomass dynamics the substrate concentration comes in a steady state described by the feed line and the biomass concentration at that particular moment.

First intermediate phase (3). The system is in the steady state, reached at the end of the first main phase.

Second main phase (3)-(4). The equilibrium lines for tank 1 are determined by the concentrations in tank 2. At the beginning of the second main phase the equilibrium line (Equation (1.5) for the substrate is situated very low because the substrate concentration in tank 2 is low. That is why the substrate concentration in the first tank decreases.

The first tank is fed with biomass of the second tank. The corresponding equilibrium line (Equation (1.6)) is situated at the right of the regime trajectory which explains why the biomass concentration is increasing.

Second intermediate phase (4)-(5)-(1). Because the substrate concentration of the second tank is increasing due to the direct feeding, the corresponding equilibrium line is also varying, resulting in a sudden change of behavior of the substrate concentration of tank 1 at the point (5). The corresponding substrate and biomass concentration in the second tank is indicated by the point (A).

For the second tank a similar way of reasoning can be set up [Ryckaert *et al.* 1994].

1.4 Simulation study of the two stage system

In this Section the dynamical behavior of the two stage system is examined. First the unstructured model is considered. The simulation results and the conclusions of a sensitivity analysis are summarized. Second a structured model is introduced.

1.4.1 Unstructured model

The model equations are similar to the equations (1.1)(1.2) used for the single stage system. Only the transport terms are adapted, according to the process scheme of Figure 1.2. The complete model consists of four sets

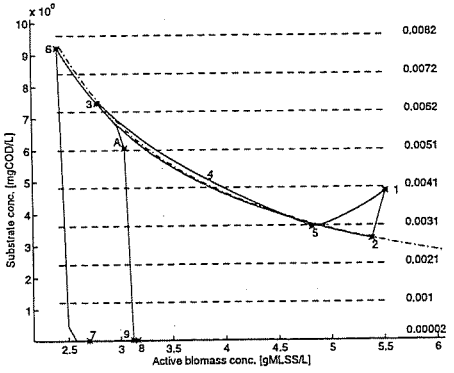


Figure 1.5: State space analysis for tank 1

(4 phases) of eighteen differential equations (6 tanks × 3 states per tank).

Extensive simulations for the two stage system reveal unrealistic values for the substrate concentration in the second stage and the final effluent for a large set of parameter values, including parameter values found in literature [Henze *et al.* 1995].

For this model, a sensitivity study has been performed. In such a sensitivity analysis the effect of a small change in a parameter on the dynamical behavior is examined. The maximum growth rate μ_{max}, the thickening parameter β, and the biomass withdrawal rate w are studied in [Ryckaert *et al.* 1994]. As an example the sensitivity analysis results for the maximum specific growth rate μ_{max} are illustrated for each tank of the two stage system for both the substrate and the biomass concentration. The effect on the maximum, minimum (dashed lines) and average (full line) substrate and biomass concentrations in the tanks is indicated in Figure 1.6. When the true value of the maximum specific growth rate is small, a small perturbation of its value results in a large change of substrate and biomass concentrations. When the true value of the parameter is large, the resulting maximum, minimum and average biomass and substrate concentrations remain almost constant under a perturbation of the parameter. Notice that this parameter μ_{max} is difficult to estimate from experimental data.

In fact, for certain parameter sets the unstructured model can simulate more realistic substrate concentrations in the tanks and in the effluent, also for the two stage system. However, these parameter sets differ a lot from parameter values found in literature. For instance, μ_{max} must be chosen in the order of magnitude 0.01 1/h, while a typical value is 0.1 1/h. In addition, the sensitivity analysis reveals that variations on these parameters are found to have a tremendous effect on the system behavior (see Figure

1.6 for $\mu_{max} = \mathcal{O}(0.01)$ 1/h). For this region of parameters the system is very sensitive, so the unstructured model is found not to be appropriate for modeling the two stage system.

As a conclusion it can be stated that the unstructured model is not appropriate for simulation of the two stage system. The main problem with this model is that it does not reflect the underlying philosophy of the two stage system because the substrate is not structured. This problem can be solved with the introduction of a more structured model.

1.4.2 Structured model

In this Section a structured model for simulation of the two stage system is described. The following assumptions are made:

- The substrate is subdivided into (i) a rapidly biodegradable fraction C_{Sr}, and (ii) a slowly biodegradable fraction C_{Ss}.
- In the first stage only the rapidly biodegradable fraction $C_{Sr,1}$ is consumed.
- In the second stage the remaining rapidly biodegradable fraction $C_{Sr,2}$ and the slowly biodegradable fraction $C_{Ss,2}$ are removed but at different biodegradation rate. For the degradation of the rapidly biodegradable fraction the same kinetics is used as in the first stage.
- The active and inactive biomass concentration in the first (denoted $C_{X,1}$, $C_{Xd,1}$) and second stage (denoted $C_{X,2}$, $C_{Xd,2}$) have different characteristics. The parameters for the degradation of the rapidly biodegradable substrate are $\mu_{max,r}$, $K_{S,r}$, $Y_{X/S,r}$ for both the first and the second stage. The parameters for the degradation of the slowly biodegradable substrate in the second stage are $\mu_{max,s}$, $K_{S,s}$, $Y_{X/S,s}$. The parameters describing the decay of biomass are $K_{d,r}$ and $K_{d,s}$ for the first stage and the second stage respectively.

This results in the following set of equations (only the biotransformation terms are shown). Notice that the subscript 1 or 2 refers to stage 1 or 2 of the system (and not to the tank number as in Section 1.3).

Stage 1

$$\begin{aligned}
\frac{dC_{X,1}}{dt} &= \mu_{max,r}\frac{C_{Sr,1}}{K_{S,r}+C_{Sr,1}}C_{X,1} - K_{d,r}\ C_{X,1} \\
\frac{dC_{Sr,1}}{dt} &= -\frac{1}{Y_{X/S,r}}\mu_{max,r}\frac{C_{Sr,1}}{K_{S,r}+C_{Sr,1}}C_{X,1} \\
\frac{dC_{Ss,1}}{dt} &= 0 \\
\frac{dC_{Xd,1}}{dt} &= +K_{d,r}\ C_{X,1}
\end{aligned} \tag{1.9}$$

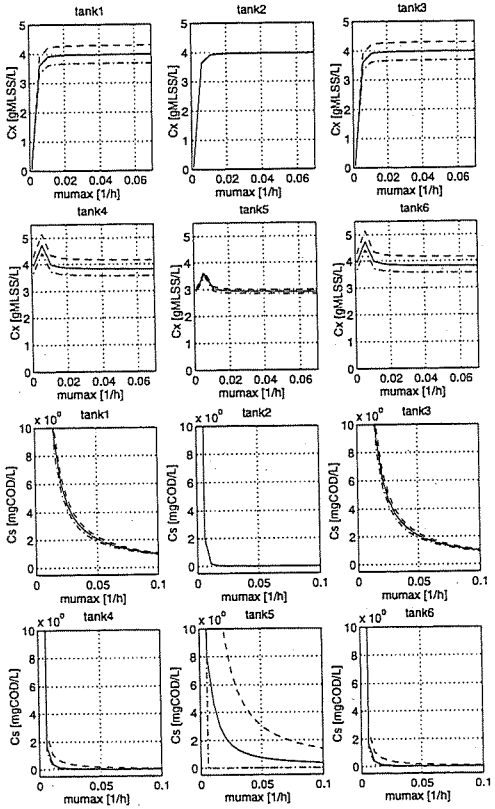


Figure 1.6: Sensitivity analysis for the maximum specific growth rate μ_{max}

Stage 2

$$
\begin{aligned}
\frac{dC_{X,2}}{dt} &= \mu_{max,r}\frac{C_{Sr,2}}{K_{S,r}+C_{Sr,2}}C_{X,2} \\
&+ \mu_{max,s}\frac{C_{Ss,2}}{K_{S,s}+C_{Ss,2}}C_{X,2} \qquad -K_{d,s}\ C_{X,2} \\
\frac{dC_{Sr,2}}{dt} &= -\frac{1}{Y_{X/S,r}}\mu_{max,r}\frac{C_{Sr,2}}{K_{S,r}+C_{Sr,2}}C_{X,2} \\
\frac{dC_{Ss,2}}{dt} &= -\frac{1}{Y_{X/S,s}}\mu_{max,s}\frac{C_{Ss,2}}{K_{S,s}+C_{Ss,2}}C_{X,2} \\
\frac{dC_{Xd,2}}{dt} &= +K_{d,s}\ C_{X,2}
\end{aligned}
\tag{1.10}
$$

The Equations (1.9) for the aeration tanks in the first stage are similar to the Equations (1.1) used in the unstructured model for the single stage system. An additional equation for the slowly biodegradable substrate is introduced containing only transport terms. Equations (1.10) for the aeration tanks in the second stage contain balances for the active and inactive biomass and both the slowly and rapidly biodegradable substrate. The mass balance of the biomass $C_{X,2}$ of the second stage consists of two terms, one depending on the rapidly biodegradable substrate C_{Sr} and one depending on the slowly biodegradable substrate C_{Ss}.

1.4.3 Dynamic behavior of the system

When a constant load is assumed, the system is again converging to a set of regime trajectories. The parameter values used for simulation are given in Appendix D. In Figure 1.7 the regime trajectories are shown for the biomass versus the rapidly biodegradable substrate, denoted with $C_{S,r}$, and the biomass versus the slowly biodegradable substrate, denoted with $C_{S,s}$. For the first stage the slowly biodegradable substrate is not indicated, because it is not biodegraded in this stage. In the following the behavior of the system in each tank is described. In Section 1.4.4 a physical interpretation of this behavior is provided.

Tank 1.

First main phase. At the beginning of the first main phase the biomass concentration and substrate concentration are given by the lower right point (denoted with $*$) in the state space. During the aeration both the biomass concentration and substrate concentration are initially decreasing. The state evolves along the lower line of the regime trajectory.

First intermediate phase. The system is in steady state, represented by the upper left point (also denoted with $*$) of the trajectory.

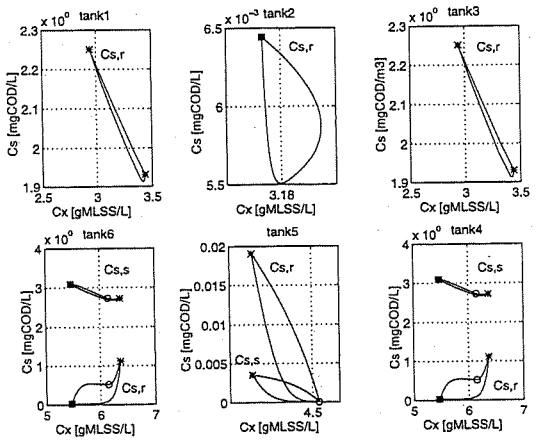


Figure 1.7: State space representation for the two stage system, simulation with a structured model

Second main phase. The biomass is increasing, while the substrate concentration is decreasing. The state is described by the upper part of the regime trajectory.

Second intermediate phase. The system is assumed to be in steady state during this phase.

Tank 2. The system evolves twice counter-clockwise along this regime trajectory during one operational cycle.

Main phase. At the beginning of the main phase the state of the system is represented by the upper point (denoted with $*$) of the regime trajectory. During the main phase there is first a small increase of biomass concentration and a decrease in substrate concentration. After a while both the substrate and biomass concentration increase. The biomass concentration reaches then its maximum value and decreases again till the steady state point is reached.

Intermediate phase. During the intermediate phase the system is in steady state, represented by the upper point of the regime trajectory.

Tank 3. The regime trajectory of tank 3 is identical to the regime trajectory of tank 1 shifted over half a cycle in time.

Tank 4.

First main phase. At the beginning of the first main phase the concentration of the rapidly biodegradable substrate and the biomass concentration are represented by the upper point (denoted with $*$) of the lower regime trajectory. During the main phase the rapidly biodegradable substrate concentration and the biomass concentration are decreasing. The system evolves along the lower curve of the lower regime trajectory. The slowly biodegradable substrate concentration (starting also in $*$) is initially slightly decreasing but increases afterwards. This is described by the lower part of the upper closed trajectory.

First intermediate phase. The system is in steady state, represented by the lower left point (denoted with $\circledast$) of the lower trajectory and the upper left point (denoted with $\circledast$) of the upper trajectory.

Second main phase. During the second main phase, there is an increase in rapidly biodegradable substrate concentration and an increase in biomass. The slowly biodegradable substrate concentration is decreasing.

Second intermediate phase. The second intermediate phase starts in the point denoted with a $\circ$, both in the upper and lower regime trajectory. During the second intermediate phase there is an increase in rapidly biodegradable substrate concentration. The biomass increases also. This evolution is described by the upper curve of the lower trajectory. There is a slight increase of slowly biodegradable substrate.

Tank 5. The regime trajectory is passed twice clockwise during one operational cycle.

Main phase. During the main phase (starting in the point denoted with $*$) the substrate concentration of both rapidly and slowly biodegradable substrate is decreasing, while the biomass concentration is increasing.

Intermediate phase. During the intermediate phase (starting in the point denoted with $\circ$) the substrate concentration of both fractions of the substrate is increasing, while the biomass concentration is decreasing.

Tank 6. The regime trajectory of tank 3 is identical to the regime trajectory of tank 1 shifted over half a cycle in time.

1.4.4 Physical analysis

Again, the dynamical behavior can be analyzed with the method of the equilibrium lines in the state space. The analysis provides insight in the dynamics of the system but is rather tedious. In this section only a physical interpretation of the behavior is given.

Tank 1. The decrease in the biomass concentration, during the first main phase, is due to the outflow of biomass to tank 2. This results in a higher substrate equilibrium concentration [given by the feed line (Equation (1.3))], which explains the substrate concentration increase. During the first intermediate phase the system is in steady state because the tank is prepared for sedimentation. During the second main phase, the biomass concentration is increasing due to the inflow of biomass out of tank 2. The substrate concentration is decreasing, because the substrate input flow comes from tank 2. This input flow contains less substrate than the influent stream. During the second intermediate phase the system is considered to be in steady state.

Tank 2. The substrate concentration is decreasing at the beginning of the main phases, because the substrate input is initially lower than the substrate input at the end of the previous main phase. After a while the substrate concentration is increasing due to the substrate concentration increase in the first tank. The biomass concentration initially increases due to the inflow of biomass of tank 1. This inflow is decreasing, due to the behavior of tank 1. After a while, the outflow out of tank 2 towards tank 3 becomes dominant. During the intermediate phase the system is considered to be in steady state.

Tank 3. The regime trajectory is identical to the regime trajectory of the first tank shifted over half a cycle.

Tank 4. During the first main phase, the biomass concentration is decreasing due to biomass outflow. The rapidly biodegradable substrate is consumed immediately. The equilibrium of the concentration of the slowly biodegradable substrate is increasing because the biomass concentration is decreasing. During the intermediate phase the tank is prepared for sedimentation and is in steady state. During the second intermediate and main phase, the biomass is increasing due to the outflow out of tank 5. During the second intermediate phase the concentration of rapidly and slowly biodegradable substrate increases because now the system is fed in tank 5.

Tank 5. During the main phase the biomass concentration is increasing, due to the outflow out of tank 4 or 6. The concentration of both rapidly and slowly biodegradable substrate is decreasing. During the intermediate phase these concentrations are increasing due to the direct feeding. The biomass concentration is decreasing due to the outflow.

Tank 6. The regime trajectory of tank 6 is identical to the regime trajectory of tank 4 shifted over half a cycle.

1.5 Model validation

Lab-scale (Section 1.5.1) and *full-scale* (Section 1.5.2) experiments are used for model validation. *The main goals are (i) to verify whether the models, proposed above, describe the main dynamics, found in the experiments, rather well and (ii) to analyze the practical issues involved.*

Many experiments are based on the oxygen dynamics. The basic model for the oxygen dynamics is introduced in Chapter 0.

Details on the lab-scale experiments are reported in detail in [Bieswal 1995, Vandenbroeck 1996]. Identification from full-scale data can be found in [Claes *et al.* 1996a, 1996b]. Observer based estimation algorithms, presented in [Ryckaert *et al.* 1995] and discussed in Chapter 6, are used for data processing.

1.5.1 Lab-scale experiments

Lab-scale experiments have been performed with influent and activated sludge of a full-scale wastewater treatment system.

These experiments are used for (1) identification of the kinetic parameters (the maximal specific biomass growth rate μ_{max}, the Monod constant K_S and the yield of biomass on substrate $Y_{X/S}$), (2) identification of the respirometric parameters (the yield of biomass on oxygen $Y_{X/O}$ and the specific endogenous respiration m) and (3) for influent characterization (by determining different fractions).

Identification of kinetic parameters Identification of the kinetic parameters μ_{max} [1/h], K_S [mgCOD/L] and $Y_{X/S}$ [gMLSS/mgCOD] from (i) batch and (ii) fed-batch experiments has been considered.

The yield $Y_{X/S}$ is determined in batch experiments by calculating the change of the biomass concentration C_X [gMLSS/L] divided by the change of substrate concentration C_S [mgCOD/L]. This approach can also be used in fed-batch experiments, but the addition of substrate and the dilution of the biomass during the experiment must be taken into account. The identification of $Y_{X/S}$ can be performed independently of the other parameters [Bastin and Dochain 1990], when maintenance is neglected (which is a rough approximation).

It is known from literature [Holmberg 1982] that an identifiability problem pops up when one wants to determine μ_{max} and K_S from data obtained from batch experiments. This is illustrated in Figure 1.8. The model fit for two considerably different parameter sets is shown. It is clear that hardly any difference can be observed. Figure 1.8 shows the contour plot of the least squares estimation error. A sum of quadratic errors on both substrate and biomass concentration measurements are used. A weighting between the substrate and biomass contributions is made such that these contributions have the same order of magnitude. It is clear from the figure that infinitely many sets of parameters minimizes the least squares error.

To cure the identifiability problem fed-batch experiments are considered. Figure 1.9 shows the substrate and biomass concentration of a fed-batch experiment and the model fit. The experiment can be considered as three batch experiments. Notice that the volume of the liquid is constant. This is realized by replacing the supernatants with influent. The contour plot of the least squares estimation error for this experiment is shown in Figure 1.9. This figure shows that the identifiability of the model parameters is improved (Table 1.1). Nevertheless further research on the identifiability problem must be conducted. The question arises when to add new influent

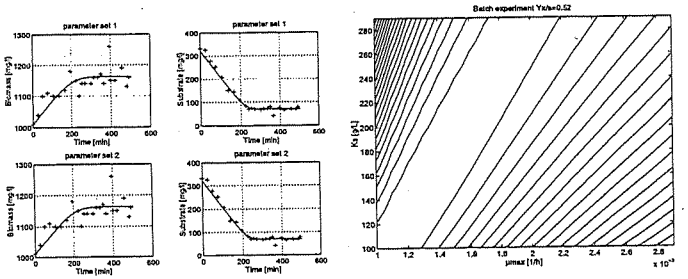


Figure 1.8: Identification of kinetic parameters from batch experiments. Left: dynamics of the biomass and substrate concentration and model fit for two different parameter sets. Right: contour plot of the least squares estimation error.

to the reactor when performing fed-batch experiments. Recall that the substrate and biomass concentration are not on-line available during the experiment. A practical approach is to monitor the oxygen uptake rate. When the oxygen uptake rate becomes low (approximately equal to the expected endogenous respiration) new influent is added. This approach is illustrated in Figure 1.10. The dynamics of the substrate and biomass concentration and the specific oxygen uptake rate is shown.

Continuous experiments, although from theoretical viewpoint interesting for parameter identification, are not considered because (1) identification with such experiments would last very long and (2) practically it is not easy (e.g., pump failures, temperature variations, ...) to keep all environmental conditions constant over such a long period, which is a key requirement for continuous experiments.

It must be emphasized that from theoretical point of view the Monod model is only valid under balanced growth conditions (constant substrate concentration). This fact results in practical constraints on the substrate concentration variations allowed in parameter identification experiments.

The parameters μ_{max} and K_S can be determined alternatively with the RODTOX measurement system [Vanrolleghem 1994]. The measurement

system estimates the exogenous uptake rate in a reactor when an amount of influent is added. This uptake rate is related to the specific biomass growth rate. When the yield of biomass on oxygen and the biomass concentration in the reactor is known, μ can be determined. The maximum specific uptake rate is now determined for increasing amounts of influent. The related specific biomass growth rate is illustrated in Figure 1.11 (left). Each measurement point ($*$) indicates a different RODTOX experiment. The parameters, determined with Lineweaver-Burk linearization (plot of μ^{-1} versus C_S^{-1})), are given in Table 1.1. The parameters found with the

Experiment	μ_{max} [1/h]	K_S [mgCOD/L]	$Y_{X/S}$ [gMLSS/mgCOD]
Batch exp. 1	-	-	0.00058
Fed-batch exp. 1	0.083	92.4	-
RODTOX exp.	0.121	13.31	-

Table 1.1: Kinetic parameters

RODTOX experiment are probably related to fast biodegradable substrate, which explains the difference between the parameter sets in Table 1.1.

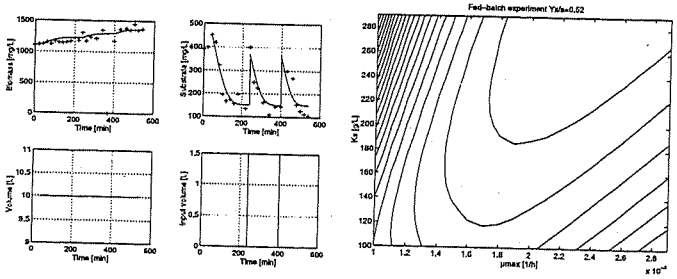


Figure 1.9: Identification of kinetic parameters from fed-batch experiments. Left: dynamics of the biomass and substrate concentration and model fit. Right: contour plot of the least squares estimation error

Identification of respirometric parameters The specific endogenous respiration coefficient m [mgO_2/gMLSS h] equals the specific oxygen uptake rate if the substrate concentrations of the biodegradable fractions are zero.

In Table 1.2 the results obtained from different experiments are summarized. The first result originates from the first batch experiment, used for identification of the kinetic parameters. The second set of results are found with a second batch experiment, used for influent characterization. The high value of m is obtained after 270 minutes while the lower value is found after two days of aeration. The difference between the two values can be due to (i) consumption of adsorbed substrate or (ii) by degradation

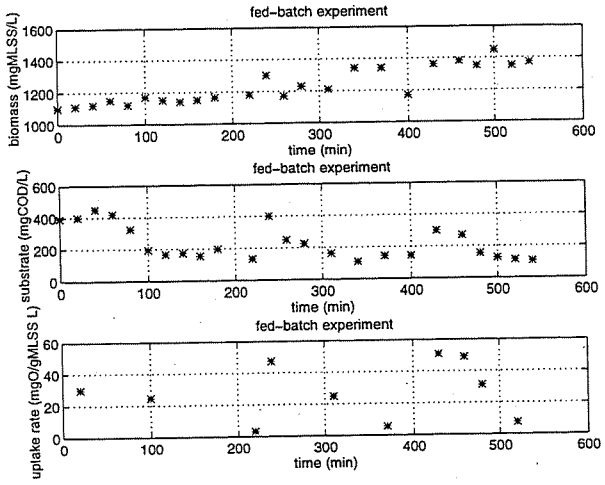


Figure 1.10: Identification of kinetic parameters from fed-batch experiments. Substrate addition based on respiration monitoring. Top: dynamics of the substrate. Middle: dynamics of the biomass. Bottom: dynamics of the respiration

of the biomass (due to the lack of substrate). The third result is obtained from the fed-batch experiment (Figure 1.10) used for identification of the kinetic parameters. The specific oxygen uptake rate is measured at the time instance 210 min. The biodegradable substrate concentration is assumed to be zero at that time instance. The other lab-scale results are obtained from a batch experiment and a fed-batch experiment (considered as a repeated batch experiments here) described in [Vandenbroeck 1996]. The last value is determined from full-scale experiments, described in Section 1.5.2.

The yield $Y_{X/O}$ [gMLSS/mgO_2] of biomass on oxygen is found with a linear regression between the specific exogenous respiration rate (found from the total uptake rate minus the endogenous respiration) and the specific biomass growth rate. The results are also indicated in Table 1.2. The oxygen transfer coefficient k_La and oxygen saturation concentration C_{SAT} are parameters that must be determined on the full-scale installation (Section 1.5.2).

Influent characterization Although batch experiments are found not to be useful for the identification of the kinetic parameters, these experiments can be used for influent characterization.

Figure 1.12 shows the dynamics of the substrate and biomass concentration and the specific oxygen uptake rate for two batch experiments. One

Experiment	m [$mgO_2/gMLSS\ h$]	$Y_{X/O}$ [$gMLSS/mgO_2$]
Batch exp.1 (490 min.)	3.54	-
Batch exp. 2 (270 min.)	4.69	0.0020
Batch exp. 2 (48 h.)	2.08	0.0020
Fed-batch exp. 1 (210 min.)	3.18	-
Batch exp. 3	5.5	-
Fed-batch exp. 2a	6.8	0.0037
Fed-batch exp. 2b	5.7	0.0034
Fed-batch exp. 2c	4.5	0.0039
Full-scale exp.	3.4	-

Table 1.2: Respirometric parameters

Experiment	non degr.	fast degr.	slow degr.
Batch exp. 1	25 %	75 %	-
Batch exp. 2	30 %	10 %	60 %
Batch exp. 3	25 %	75 %	

Table 1.3: Influent characterization

can observe that not all the substrate is consumed. The non biodegradable fraction can be determined.

From analysis of the dynamics of the specific oxygen uptake rate (and the dynamics of the substrate concentration) one can conclude whether the influent must be modeled as one substrate or more substrates with different biodegradation rates [Vanrolleghem 1994]. Figure 1.12 illustrates the one substrate and two substrates case respectively. Figure 1.11 (right) shows the specific biomass growth rate (calculated from the substrate concentration dynamics and the yield of biomass on substrate) in function of the substrate concentration. This figure suggests that the specific biomass growth rate is represented as a sum of Monod type relations. Each measurement ($*$) is related to a different time instance. Recall that the substrate concentration is decreasing with time.

In Table 1.3 the fractions (non biodegradable fraction, the fast biodegradable fraction, the slow biodegradable fraction (if relevant)), determined from the batch experiments, are indicated.

The percentages of the fast and slow degradable fraction can be approximated by calculation of the area under the specific oxygen uptake rate profile. The integral from 0 till 25 minutes represents the fast biodegradable fraction, the integral from 0 till 125 minutes represents the sum of the slow and fast degradable fraction. The obtained values must be transformed in the appropriate dimensions by using the yields $Y_{X/S}$ and $Y_{X/O}$.

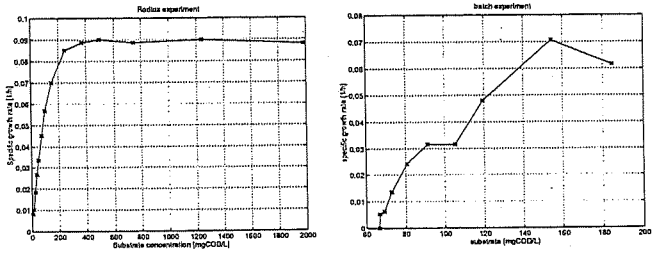


Figure 1.11: Specific biomass growth rates in function of the substrate concentration. Left: Rodtox experiment. Right: batch influent characterization experiment

1.5.2 Full-scale experiments

Respirometric experiments The oxygen transfer rate k_La [1/h] and the oxygen saturation concentration C_{SAT} [mgO_2/L] must be determined on the full-scale installation under consideration.

Figure 1.13 shows the dynamics of the oxygen concentration in an outer tank of the first stage. The normal process operation is disturbed by on-off control of the aerator and the influent flow rate.

In [Vanrolleghem 1994] it is demonstrated that the oxygen transfer rate can be found by disturbing the oxygen equilibrium by (i) on-off control of the aerator (time interval 0-35 minutes) or (ii) by adding a pulse of substrate (time intervals 43-65, 71-89 and 109-127 minutes). The average value of the k_La found by these four experiments is 18.25 [1/h].

The oxygen uptake rate equals minus the slope of the decreasing oxygen concentration when the aerator is off (time instance 34 minutes). As the influent flow rate is zero over the time interval 0-43 minutes it is assumed that this oxygen uptake rate approximates the endogenous respiration. The biomass concentration in the reactor is 3.19 gMLSS/L. The specific endogenous respiration coefficient can then be determined and is found in Table 1.2. The oxygen saturation concentration can be determined from the equilibrium concentration (at time instance 34 minutes), the oxygen transfer coefficient and the oxygen uptake estimate. An approximate value of 6.8 [mgO_2/L] is found.

In the time intervals ([43-71], [71-108], [108-136]) influent has been added for a certain time period. The area between the oxygen equilibrium concentration (approximately 6 mgO_2/L) and the oxygen concentration profile is a measure for the amount of substrate added. Because the influent flow rate and the influent substrate concentration are known here, one can evaluate whether the respirometric determination of the amount of substrate is reliable. The results are shown in Table 1.4. The second column is the

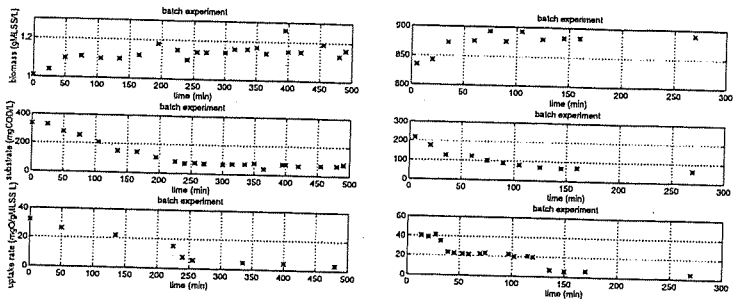


Figure 1.12: Influent characterization with batch experiments. Left: batch experiment 1: one sudden oxygen uptake rate decay implies single substrate and non biodegradable fraction. Right: batch experiment 2: two sudden oxygen uptake rate decays imply two substrates and non biodegradation fraction. Top: biomass concentration. Middle: substrate concentration. Bottom: specific oxygen uptake rate

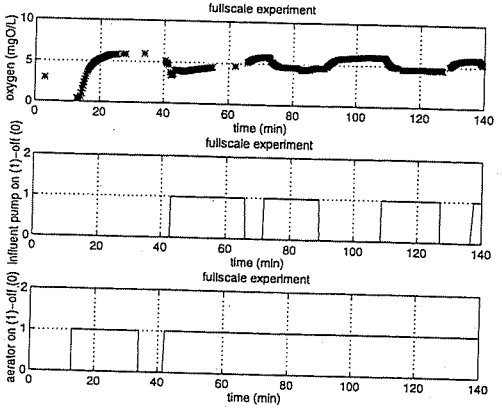


Figure 1.13: Full-scale respirometric experiments. Top: oxygen concentration dynamics. Middle: influent control. Bottom: aerator control

amount added while the third column represents the amount estimated with respirometry. Notice that a large error on the first result appears because the oxygen concentration is not in equilibrium at the beginning of the addition.

Interval [min.]	Added influent [kgCOD]	Estimated influent [kgCOD]
43-71	7	12,6
71-108	6	8.7
108-136	6	8.7

Table 1.4: Determination of amount of added substrate

Identification of kinetic parameters In [Claes *et al.* 1996a] the identifiability of the kinetic parameters K_S and μ_{max} from mean daily measurements of biomass and substrate concentration in the first stage of a two stage cyclically operated activated sludge wastewater treatment system is discussed.

It is found that unique identifiability of the kinetic parameters from such a data set is not possible. The main reason for the bad identifiability is that fact that the Monod constant K_S of the Monod model (Chapter 0) (found from lab-scale experiments) is considerably higher than the average substrate concentration in the system.

A modified model, in which the specific biomass growth rate is described with a first order model (Chapter 0), is presented. The single kinetic parameter a of this modified model can be determined in a unique way from the available data set. Naturally the effect of such a model approximation on the performance of algorithms based on such an approximation must be analyzed. In Chapter 5 such an analysis is provided for state observers.

Identification of respirometric parameters From on-line oxygen concentration measurements of a two stage cyclically operated wastewater treatment system the oxygen uptake rates are estimated with observer based estimators [Ryckaert *et al.* 1995].

Observer based estimation of the oxygen uptake rate. The aerator configuration of the installation under consideration is as follows. In the outer tanks of the first stage two aerators are used both controlled with an on-off control strategy, but with different bounds. In the other tanks of the system one aerator with an on-off control strategy is used.

Due to this aerator configuration the observer based estimation algorithms of Chapter 6 could only be applied to the second tank of the first stage and the tanks of the second stage, although extensions to other aeration configurations are theoretically possible.

In the subplots of Figure 1.14 the dynamical behavior of the oxygen uptake rate OUR [mg O_2/L h] is given versus time, for the several tanks. Also information about the actual phase is provided. Some additional information about the feeding is also displayed.

The duration of the main phase is 360 minutes, while the intermediate phase lasts 90 minutes. The direct feeding during the main phase in the second tank of the first stage starts after 220 minutes and lasts 40 minutes.

In top left subplot of Figure 1.14 the oxygen uptake rate of the second tank of the first stage is shown. The full lines in the lower plot indicate whether there is direct feeding in this tank or not. One can notice that due to the direct feeding there is a slight increase in the *OUR*. This is due to the increase of the substrate in the tank, which results in a higher exogenous respiration.

The top right subplot of Figure 1.14 shows the oxygen uptake rate of the fifth tank. This tank is fed during the intermediate phases, indicated by the full lines. This results in a doubling of the *OUR*.

In bottom subplots of Figure 1.14 the oxygen uptake rate of the fourth and sixth tank of the system is shown respectively. Information of the oxygen uptake rate is only given when the tank is in aeration mode. The full lines do not indicate the direct feeding of this tanks, as in the previous figures, but the feeding in the fifth tank. The dynamics of the oxygen uptake rate is here mainly determined by the transport of the biomass. During the aeration phase the oxygen uptake rate is decreasing because the biomass is shifting towards the other tanks. Recall that the substrate concentration is the second stage is low. The biomass growth is negligible. It is found that the rate of change of the oxygen uptake rate is determined by the dilution rate. Notice that the oxygen uptake rate at the beginning of an aeration phase is approximately the same over the different phases and for the two tanks, which illustrates the cyclical dynamics of the system.

The calculation of the oxygen uptake rate with the observer based estimation algorithm has been done off-line but the method can easily be implemented on-line. This results in an on-line monitoring of the biological activity.

Parameter identification from oxygen uptake rate measurements. In [Claes *et al.* 1996b] the identifiability of the respirometric parameters $Y_{X/O}$ and m_O from the obtained oxygen uptake rates for the second tank is analyzed.

The process model predicts a peak in the oxygen uptake rate profile when the influent is directly fed into the tank. Notice that this is indeed confirmed by the oxygen uptake rate data.

It is found with simulation based analysis that unique identifiability of the respirometric parameters from full-scale data is however not feasible because (i) peak absence and (ii) system response delay. Because the oxygen uptake rate is not continuously monitored, the maximal oxygen uptake rate in the tank is not necessarily available in the data set. The model shows a direct change in the oxygen uptake rate when the feeding is changed. In practice some delay is found.

Nevertheless the comparison of the oxygen uptake rate data with the model simulations show that (i) the dynamics of the oxygen uptake rate is not due to the convergence of the observer, but represents the dynamics of

the system and (ii) the model describes the main dynamics of the system well.

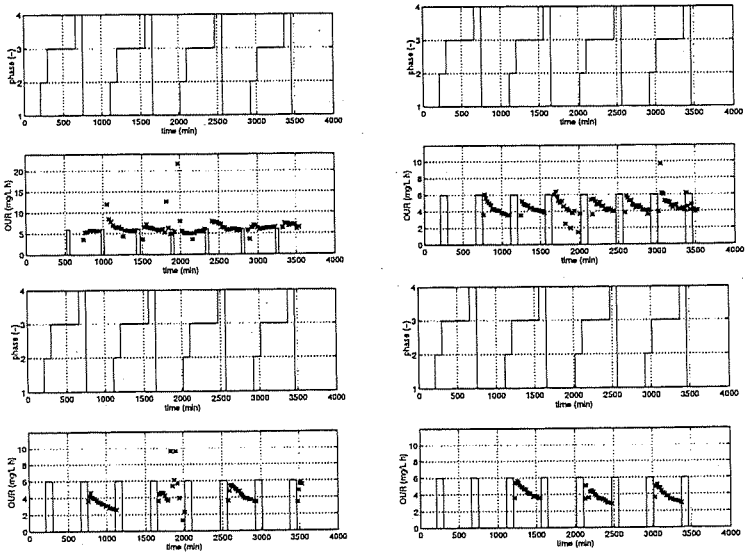


Figure 1.14: Top left: tank 2. Top right: tank 5. Bottom left: tank 4. Bottom right: tank 6. Upper plot: first main phase (1), first intermediate phase (2), second main phase (3), second intermediate phase (4). Lower plot: estimates of *OUR* (*) and indication of feeding instances

1.6 Application of the models

The obtained models (unstructured for the single stage system and structured for the two stage system) can describe the main dynamics of the UNITANK® systems under study although the complexity is kept considerably low.

Due to their low complexity these models can be used for both dynamical optimization of the system design and advanced model based controller design. The application of models for estimation and control of wastewater treatment systems is discussed in detail in [Marsili-Libelli 1989].

In Figure 1.15 the effluent pattern of the second stage of the two stage system (which is the final effluent) is shown. This effluent pattern is periodic. The periodically occurring peaks are due to the direct feeding in tank 5. This indicates that the relative duration of the different phases within

a complete process cycle has an important impact on the effluent quality. A simulation model, as developed above, is very useful to determine the optimal phase switching pattern (and thus the optimal performance) of the installation [Ryckaert *et al.* 1994]. In the same contribution the unstructured model has been used in the design of a nonlinear linearizing controller [Dochain and Perrier 1992] for the waste flow rate w, resulting in control of the active biomass concentration at a setpoint. This setpoint can be again be optimizated with respect to several performance criteria. In [Ryckaert *et*

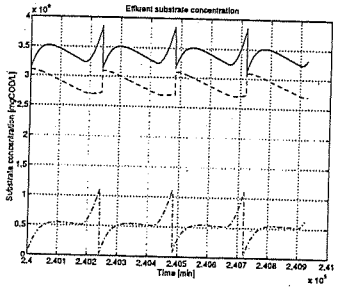


Figure 1.15: Effluent pattern for a two stage system

al. 1995] the use of low complexity models for state and parameter estimation in wastewater treatment systems has been illustrated. The application of such estimators on data from a full-scale plant revealed that the simulation results obtained with the low complexity models are realistic.

Recall that in Chapter 3 (model based) optimal design and control of cyclically operated carbon removal systems is considered while in Chapter 4 and 6 parameter and state estimation are discussed in the context of wastewater treatment systems.

1.7 Nitrogen removal systems

In Section 1.7.1 the two phase nitrogen removal process is shortly described. The implementation of this two phase nitrogen removal process in cyclically operated but continuous systems (e.g., UNITANK® systems) is considered.

In Section 1.7.2 the oxydo reduction potential (redox potential) is introduced. The automatic control of cyclically operated nitrogen removal systems with *on-line* measurements of the redox potential is shortly discussed.

1.7.1 Biological Nitrogen Removal

The two phase nitrogen removal process is introduced. A detailed description of this process in a more mathematical setting is reported in [Henze *et al.* 1995]. The two phase nitrogen removal process consists of two phases.

1. Nitrification phase. Ammonium (NH_4^+) is oxidized into nitrite (NO_2^-) and nitrate (NO_3^-) by autotrophic biomass (X_A) under aerobic conditions (free oxygen available). During this process a part of the BOD is oxidized.

2. Denitrification phase. Nitrate (NO_3^-) and nitrite (NO_2^-) are transformed into inert nitrogen gas (N_2) by heterotrophic biomass (X_H) under anoxic conditions (no free but fixed oxygen available). BOD serves in this reaction as electron donor.

A straightforward implementation of this two phase biological process would consist of two bioreactors in series. In the first aerated tank the nitrification process takes place. In the second stirred but not aerated tank the denitrification goes on. Such a process scheme requires however an unnecessary oxidative consumption of BOD. A modified scheme called the predenitrification scheme switches the flow. First the denitrification process takes place in the stirred but not aerated tank in which the influent is fed, followed by the nitrification process, in an aerated tank. Clearly, this approach requires a recirculation of the wastewater and biomass mixture because the nitrate and the nitrite are only formed in the second reactor. The basic and modified process scheme described above are based on *control in place*. The two processes proceed in different bioreactors. The duration of the aerobic and anoxic phase is determined by the flow rates and the volume of the reactors. Another implementation, based on *control in time*, only requires one reactor and no equipment for recirculation. By switching the aerator on or off the duration of the aerobic and anoxic phases is chosen respectively. The latter control principle has been applied in the UNITANK® systems for N removal. Another configuration is discussed in [Isaacs 1996].

The UNITANK® system for nitrogen removal (Figure 1.16) is discussed now. This system consists of four tanks. During the first main phase the basins A and B are periodically aerated (aerobic conditions) or stirred (anoxic conditions). This approach results in the *control in time* implementation of the nitrification/denitrification process. Basin C is aerated and is used for the removal of the remaining BOD, the oxidation of nitrite to nitrate and blowing out the nitrogen gas while tank D is used as sedimentation tank. As in the basic carbon removal system a second main phase exist in which tank C and D are used for the nitrification/ denitrification process. Tank B is now used as extra aeration tank while tank A is in sedimentation mode. Details on the process operation of cyclically operated nitrogen removal systems are found in [Ghekiere *et al.* 1990].

1.7.2 Redox potential

The redox potential or the oxido reduction potential (ORP) is a measure of the oxidative or reductive capacity of a system. Biochemical reactions requiring transfer of electrons are called redox reactions. The electrons are given free by the reductans (B_{RED}) and collected by the oxidans (A_{OX}). The reaction scheme is given below with stoechiometric coefficients a, b, c and d .

$$aA_{OX} + bB_{RED} + ne^- \rightarrow cA_{RED} + dB_{OX} \qquad (1.11)$$

The oxidative and reductive capacity of a component is described by the redox potential. When an appropriate measuring electrode is used, a half-reaction can take place at the contact area between the electrode and the liquid phase. Due to the electron transfer between the electrode and the liquid phase a potential difference will appear. The electron transfer can only take place when a certain electric force is available. The required electric force increases during the course of the process because the potential difference becomes larger. An equilibrium situation is reached when the electric force becomes equal to the affinity of the component in the liquid phase for electrons. The final electronic potential difference between electrode and liquid phase is the so-called redox potential of the liquid [Héduit and Thévenot 1989, 1992; Koch and Oldham 1985].

Theoretically the redox potential E [mV] of a reaction (1.11) can be calculated by using the law of Nernst (1.12) with E_o the so-called normal potential (defined for standard conditions), n [-] the amount of electrons involved in the reaction, T [°K] the absolute temperature, F the constant of Faraday and the concentration of the components [mol/L] involved in the reaction.

$$E = E_o + \frac{RT}{nF} \log \frac{(A_{RED})^c (B_{OX})^d}{(A_{OX})^a (B_{RED})^b} \qquad (1.12)$$

In a biochemically complex system such as a biological wastewater treatment plant there exists no equilibrium situation. Under this condition the oxido reduction potential can not be calculated from a thermodynamic point of view. The potential measured in a wastewater treatment process must be considered as a measure of the netto electron activity of all the reactions involved. From this point of view the measured values will be specific for a certain installation and the wastewater treated in this system. This fact is shown to be correct also in practice. *Although the values of the redox potential are case dependent, the dynamics of the oxydo reduction potential is quite similar for all the cases.* This observation is the basic key enabling control of nitrogen removal systems by measurements of the redox potential.

The more stringent environmental regulation necessitates the optimization of nitrogen removal systems. These (complex, often cyclically operated) systems can only be optimally operated by advanced control systems, requiring *on-line measurements.* Besides the traditional measurements like oxygen concentration and pH, nowadays several direct measurements, such

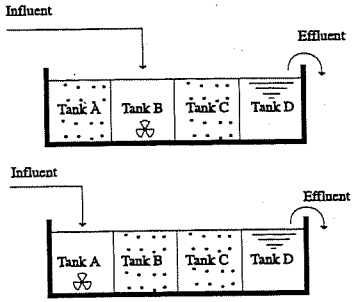


Figure 1.16: The subphases of the UNITANK® nitrogen removal system

as ammonium, nitrate and nitrite concentrations in the influent, effluent and treatment basins, are available. These measurements require expensive investments and maintenance costs.

An alternative approach is based on *oxydo reduction potential measurements.* This measurement is less expensive both from an investment and maintenance point of view. Although the state of the system is not completely accessible through the redox potential, this measurement can be used for reliable control of nitrogen removal systems. Control of a nitrogen removal system is based on the characteristic profile of the redox potential and not on the values of the potential.

Due to the consumption of nitrate during the denitrification the redox potential is decreasing. The profile becomes flatter when the nitrate is more and more consumed. When no nitrate is left, an abrupt change of the redox potential profile is observed. This knee is called the *nitrate knee.* This knee indicates the change of the system from anoxic conditions (no free oxygen but bounded oxygen) to anaerobic conditions (no oxygen available). The denitrification is considered to be complete. As such, the redox knee indicates that the aerator can be switched on to start the next nitrification phase.

Because the control strategy is based on the detection of the redox knee, reliable redox knee detection algorithm must be used (Chapter 6). In Chapter 4 it is shown that the estimation of the process state can be accelerated by using the redox potential.

1.8 Conclusions

Mathematical (low complexity) models, useful for design of on-line model based controllers (e.g., a nonlinear linearizing controller for the waste sludge rate) and dynamical optimization of the system design (e.g., the optimal

relative duration of the phases) have been developed and analyzed with *dynamical (state space) analysis* and *sensitivity studies*. Both unstructured and structured models have been considered for modeling of one stage and two stage UNITANK® systems.

The main goal was to obtain low complexity models, able to describe the main dynamics of the system. An *unstructured* model is sufficient for modeling the single stage system. The dynamical behavior of a cyclically operated wastewater treatment plant is difficult to analyze, due to the periodic switching of the phases. A *dynamical analysis* method based on equilibrium lines, is shown to be interesting for analysis purposes. This is illustrated in detail for the single stage system. A similar approach has been taken for the two stage system. From *dynamical analysis* and *sensitivity studies* one can conclude that an unstructured model is inadequate for accurate simulation of the two stage system. Therefore, a *structured* model has been proposed. The structured model is more appropriate for the two stage system because it incorporates the design philosophy of such a system, using the first stage for biodegradation of the rapidly biodegradable substrates and the second stage for biodegradation of the slowly biodegradable substrates. As a conclusion it can be stated that *dynamical (state space) analysis* and *sensitivity studies* can contribute in determining the optimal model complexity.

The identification of model parameters from both lab- and full-scale data is discussed. It has been illustrated that determination of the kinetic parameters (parameters of the Monod law) is extremely difficult due to an intrinsic identifiability problem. Model simplification can cure this and can be motivated in practice.

It is found that the respirometric parameters can be determined rather well. Respirometry can thus be used as basic concept for monitoring. By comparing the respiration in the plant with model simulations one can conclude that the model describes the main dynamics of the plant fairly well. It is also shown that partitioning of the influent into different fractions is necessary in practice.

Modeling of cyclically operated activated sludge wastewater treatment plants for carbon removal is shown to be feasible. Due to the low complexity the obtained models can be used further for optimization, monitoring and control of the plant.

Part II

Optimization of biotechnological processes

Chapter 2

Optimal control of fed-batch fermentation processes with multiple limiting substrates

2.1 Introduction

An interesting approach for applying model based control theory to biotechnological processes relies on a *two step procedure*. In a first step an *optimal control problem* [Bryson and Ho 1995], [Kirk 1970], [Pontryagin *et al.* 1962] is solved while in a second phase the resulting optimal control strategy is reformulated in the framework of advanced nonlinear control theory [Krstic *et al.* 1995], [Marino and Tomei 1995], [Isidori 1989].

This two step procedure, illustrated in detail in [Van Impe 1993a], [Van Impe and Bastin 1995a] combines the advantages of both optimal control and nonlinear control theory. The application of optimal control theory results in an optimal control strategy, while the embedding of this strategy in an advanced (adaptive) nonlinear controller guarantees good robust performance.

Recall that optimal control theory generally results in a model sensitive open loop control strategy, which can serve as a reference profile required by nonlinear control design methods. Notice that the disadvantages of optimal control theory are very critical for biotechnological processes due to the large model uncertainties. Thanks to the two step procedure the optimization of a biotechnological processes can still be formulated in the framework of optimal control theory, which is indeed the only appropriate setting for solving this type of problems.

The optimization of biotechnological processes has been discussed intensively in literature [Parulekar 1992], [Modak and Lim 1987; 1989], [Modak *et al.* 1986], [Cazzador 1987], [Lim *et al.* 1986], [Parulekar and Lim 1985].

The main goal of the chapter is to illustrate that the two step procedure, enabling the use of optimal control theory for bioprocess optimization, can be extended for fed-batch fermentation processes with multiple limiting substrates.

In this chapter a general state space model (Section 2.2.1) for biotechnological processes is used for calculation of the equations appearing in the framework of optimal control theory (Section 2.2.2). The dynamical equations for the costates (Lagrange multipliers) and the conditions for occurrence of a singular solution are derived. These formulas are then further refined for a model with multiple limiting substrates and one biomass (Section 2.3.1). The dynamics of the costates (Section 2.3.2) and the optimal control strategy (including the singular control conditions and a stop criterion) (Section 2.3.3) are derived without specifying a relation between the specific reaction velocities. A general equation for the singular control law of second order is derived and interpreted (Section 2.3.4). A linear relation between the specific biomass growth rate and the specific substrate consumption rates is assumed in this last derivation. The results are illustrated for a model with two limiting substrates and one biomass (Section 2.4). Depending on the qualitative knowledge of the reaction velocities in the model several cases can be distinguished. Initial work along the same lines has been reported in [Van Impe and Bastin 1993b].

The optimization of the remaining degrees of freedom is discussed in Section 2.5. In Section 2.6 simulation results are presented.

2.2 General framework

2.2.1 General state space model for biotechnological processes

A general model for biotechnological processes is given by equation (2.1).

$$\frac{d\mathbf{x}}{dt} = \varphi(\mathbf{x}, V) + \mathbf{r} \tag{2.1}$$

$$\varphi(\mathbf{x}, V) = \begin{pmatrix} \varphi_1 \\ \vdots \\ \varphi_n \end{pmatrix} \; ; \; \mathbf{r} = \begin{pmatrix} C_{X_1,in} \cdot u_1 \\ \vdots \\ C_{X_n,in} \cdot u_n \end{pmatrix} \tag{2.2}$$

$\mathbf{x}$ is a $n \times 1$ vector with as elements the absolute quantities of each reactant X_i [g], $i = 1 \ldots n$, φ is a vector of reaction-velocities [g/h], $i = 1 \ldots n$, while $\mathbf{r}$ is a $n \times 1$ vector with the inputs $C_{X_i,in} \cdot u_i$ [g/h], $i = 1 \ldots n$. The vector $\mathbf{r}$

can also be rewritten as $\mathbf{C_n} \cdot \mathbf{u}$ with $\mathbf{C_n}$ a $n \times n$ matrix with the reactant concentrations in the input stream i $C_{X_i,in}$ [g/L] on the diagonal and $\mathbf{u}$ a $n \times 1$ vector with inflow rate of the input stream i u_i [L/h] (2.3). The dynamic equation for the volume V [L] in the reactor can then be written as (2.4).

$$\mathbf{C_n} = \begin{pmatrix} C_{X_1,in} & 0 & \dots & 0 \\ 0 & C_{X_2,in} & \dots & 0 \\ \vdots & \vdots & \vdots & \vdots \\ 0 & 0 & \dots & C_{X_n,in} \end{pmatrix} \tag{2.3}$$

$$\frac{dV}{dt} = \mathbf{1_n^T} \cdot \mathbf{u} = \begin{pmatrix} 1 & \dots & 1 \end{pmatrix} \cdot \begin{pmatrix} u_1 \\ \vdots \\ u_n \end{pmatrix} \tag{2.4}$$

$\mathbf{1_n}$ is an $1 \times n$ vector. The nonlinearities of this model are introduced by the reaction velocities φ_i, which are non-linear functions of the concentrations of the reactants $C_{X_i} = \frac{X_i}{V}$ [g/L].

In [Bastin and Dochain 1990] linear combinations of reaction-velocities γ_j [g/h], $j = 1 \dots m$, are considered. $\mathbf{K}$ is a $n \times m$ matrix with yield parameters k_{ij}[-], $i = 1 \dots n$, $j = 1 \dots m$. When the reaction-velocities γ_j are gathered in the $m \times 1$ vector γ, then $\varphi = \mathbf{K} \cdot \gamma(\mathbf{x}, V)$.

$$\mathbf{K} = \begin{pmatrix} k_{11} & \dots & k_{1m} \\ \vdots & \vdots & \vdots \\ k_{n1} & \dots & k_{nm} \end{pmatrix} \; ; \; \gamma = \begin{pmatrix} \gamma_1 \\ \vdots \\ \gamma_m \end{pmatrix} \tag{2.5}$$

The general state space model for biotechnological processes is now reformulated in a standard model (2.6) used in systems and control theory. The standard model is affine in the control vector $\mathbf{u}$. This model consists of a drift term $\mathbf{f}(\xi)$ and a controlled part $\mathbf{B} \cdot \mathbf{u}$.

$$\frac{d\xi}{dt} = \mathbf{f}(\xi) + \mathbf{B} \cdot \mathbf{u} \tag{2.6}$$

The general biotechnological model is converted in a model of this form when the following notation is introduced. ξ is an $(n+1) \times 1$ vector with the first n elements the amount of reactants X_i [g], $i = 1 \dots n$, and the $(n+1)^{th}$ element is the volume V [L]. $\mathbf{u}$ is the n-dimensional vector of flow rates u_i, $i = 1 \dots n$. The drift vector $\mathbf{f}(\xi)$ is a $(n+1) \times 1$ vector with the first n rows defined by $\varphi(\mathbf{x}, V)$ $(= \mathbf{K} \cdot \gamma(\mathbf{x}, V))$ while the last row is zero. The $(n+1) \times n$ constant matrix $\mathbf{B}$ contains the matrix of reactant concentration in the input stream $\mathbf{C_n}$ (2.3) for the first n rows and $\mathbf{1_n^T}$ for the last row.

$\mathbf{O_n}$ is a n-dimensional zero vector. The structure of these matrices is given below.

$$\xi = \begin{pmatrix} X_1 \\ X_2 \\ \vdots \\ X_n \\ \hline V \end{pmatrix} \; ; \; \mathbf{f}(\xi) = \begin{pmatrix} \varphi \\ \hline \mathbf{O_n^T} \end{pmatrix} \; ; \; \mathbf{B} = \begin{pmatrix} \mathbf{C_n} \\ \hline \mathbf{1_n^T} \end{pmatrix} \tag{2.7}$$

2.2.2 Optimal control of biotechnological processes

The performance of the biotechnological processes (2.6), described by a cost criterion $\mathcal{J}[u_1, u_2, \dots, u_n]$ is optimized by applying optimal flow rates u_i^*, $i = 1 \dots n$. Throughout this chapter cost criteria of the following form are used.

$$\mathcal{J}[u_1, u_2, \dots, u_n] = -\sum_{i=1}^{n} \delta_i X_i(t_f) \tag{2.8}$$

A weighted sum of amounts of the different reactants obtained at the end of the process must be optimized. The minus sign appears because this optimization problem will be treated as a minimization problem. The weighting factors δ_i could be for instance a measure of the economical profit related to a certain amount of reactant X_i. The time t_f [h] is the final time of the process, which can be chosen to be free or fixed.

Due to practical limitations there are bounds (an upper bound u_i^{max} and a lower bound u_i^{min} (often zero)) on the control signals u_i. Also bounds on the state variables ξ are present. As an example the upperbound on the state variable $\xi_{(n+1)}$ (the volume V) V_{max}, which is the maximum reactor volume, is mentioned. Initial conditions $\xi(0)$ (initial amounts of the reactants $X_i(0)$ and the initial volume $V(0)$) are given for the vector ξ.

The optimization problem is only well posed if the amount of each reactant i, $i = 1 \dots n$, which is added to the process, is limited (maximum value α_i [g]). This constraint is described by relation (2.9) and contains a first term due to the initial condition and a second term, describing the addition by the flow rate u_i.

$$X_i(0) + \int_{t_0}^{t_f} C_{X_i,in} u_i dt \;\; \leq \;\; \alpha_i \tag{2.9}$$

Notice that when the optimal control problem (the determination of the structure of the optimal flow rate u_i) is solved (*first optimization problem*), the initial conditions $X_i(0)$ and the amounts of reactant to be added α_i are remaining degrees of freedom, which can be further optimized (*second optimization problem*). In this second optimization problem one should take into account the relation (2.10) between the volume V and the amounts of reactant α_i which can be added. V_* is the volume of the liquid phase when

no reactants are added.

$$V(t_f) = V_* + \sum_1^n \frac{\alpha_i}{C_{X_i,in}} \tag{2.10}$$

Optimal control theory and the Minimum Principle of Pontryagin in particular [Pontryagin *et al.* 1962] provide a procedure for determining the optimal flow rates $u_i^*(t)$.

A Hamiltonian function $\mathcal{H}$ is defined as the product of the right hand side of the model equation (2.6) and a vector $\boldsymbol{\lambda}$. The vector $\boldsymbol{\lambda}$ is a $(n+1) \times 1$ vector of costates λ_j with $j = 1 \ldots (n+1)$. The Hamiltonian $\mathcal{H}$ can be written as in Equation (2.11) with $\phi = \boldsymbol{\lambda}^{\mathbf{T}} \cdot \mathbf{f}(\boldsymbol{\xi})$ a function and Ψ is a n-dimensional vector of functions ψ_i, $i = 1 \ldots n$.

$$\mathcal{H} = \boldsymbol{\lambda}^{\mathbf{T}}(\mathbf{f}(\boldsymbol{\xi}) + \mathbf{B} \cdot \mathbf{u}) = \phi + \Psi^{\mathbf{T}} \cdot \mathbf{u} \tag{2.11}$$

The Minimum Principle states that $\mathcal{H}$ should be minimum for every time instant t. This can only be realized by using the following control strategy for the different control inputs u_i: (i) if $\psi_i < 0$ then $u_i = u_i^{max}$, (ii) if $\psi_i > 0$ then $u_i = u_i^{min}$. It is assumed that the control handles u_i can be modified independently. When $\psi_i = 0$ during a finite interval another approach for determining u_i is necessary because now the control input u_i is not appearing explicitly in the Hamiltonian $\mathcal{H}$.

The approach is discussed in detail in [Van Impe 1993a]. In a first step the time derivative of ψ_i is derived and set equal to zero. Unfortunately this time derivative is again independent of the control input u_i, so no extra information about the optimal control law u_i is found. In a second step the second time derivative of ψ_i is calculated and set equal to zero. When this derivative is an explicit function of u_i an expression for u_i is found. This expression is called the singular control law $u_i^s(t)$ of second order. When the second time derivative of ψ_i is still independent of u_i a singular control law can be found by taking higher order derivatives. This procedure does always lead to an explicit expression in the control handle u_i. This is not further discussed [Bryson and Ho 1975].

In general the singular control laws u_i^s are functions of the costates $\boldsymbol{\lambda}$. Optimal control theory states that the dynamical system of the costates can be derived by calculating the gradient of the Hamiltonian with respect to the state variables $\boldsymbol{\xi}$. This results in the following expression containing the jacobian of the drift vector $f(\boldsymbol{\xi})$ with respect to $\boldsymbol{\xi}$. It can be found that for the general model for biotechnological systems this equation turns out to be of the following form (2.12).

$$\frac{d\boldsymbol{\lambda}}{dt} = -\frac{\partial \mathcal{H}}{\partial \boldsymbol{\xi}} = -\frac{\partial \mathbf{f}(\boldsymbol{\xi})}{\partial \boldsymbol{\xi}}^{\mathbf{T}} \cdot \boldsymbol{\lambda} = -\mathbf{S}(\boldsymbol{\xi}) \cdot \boldsymbol{\lambda} (= -\bar{\mathbf{S}}(\boldsymbol{\xi}) \cdot \bar{\mathbf{K}} \cdot \boldsymbol{\lambda}) \tag{2.12}$$

The $(n+1) \times n$ matrix $\mathbf{S}(\boldsymbol{\xi})$ (the $(n+1) \times m$ matrix $\bar{\mathbf{S}}(\boldsymbol{\xi})$) contains the sensitivity functions of the reaction velocities φ_j [g/h] (respectively γ_j),

$j = 1 \ldots n$ with respect to the states $\boldsymbol{\xi}$. The $m \times (n+1)$ matrix $\bar{\mathbf{K}}$ consists of the transpose of the yield matrix $\mathbf{K}$ and a zero $(n+1)$-dimensional vector $\mathbf{O_{n+1}}$.

$$\mathbf{S}(\boldsymbol{\xi}) = \left(\frac{\partial \boldsymbol{\varphi}}{\partial \boldsymbol{\xi}}\right)^{\mathbf{T}} \quad ; \quad \bar{\mathbf{S}}(\boldsymbol{\xi}) = \left(\frac{\partial \boldsymbol{\gamma}}{\partial \boldsymbol{\xi}}\right)^{\mathbf{T}} \quad ; \quad \bar{\mathbf{K}} = \left(\mathbf{K}^{\mathbf{T}} \mid \mathbf{O_{n+1}} \right) \tag{2.13}$$

For the dynamical system of the costates $\boldsymbol{\lambda}$ terminal conditions are found by taking the derivative of the cost criterion $\mathcal{J}[\mathbf{u}]$ with respect to the states $\boldsymbol{\xi}$.

$$\lambda_i(t_f) = \frac{\partial \mathcal{J}}{\partial \xi_i} \tag{2.14}$$

For the costates $\lambda_i(t_f)$, $i = 1 \ldots n$ and the cost criterion under consideration this results in minus the weight factor δ_i while $\lambda_{n+1}(t_f)$ is undefined because a terminal condition on the state $\xi_{n+1} = V$ is given.

From the procedure for determining the extremal flow rates $u_i^*(t)$ it is clear that the singular control law $u_i^s(t)$ is a special part of the optimal control solution. In fact it is the part of the solution which is depending on the system equations. The numerical value of the other parts (maximal feeding u_i^{max} or no feeding u_i^{min}) are due to practical constraints and are in this sense arbitrary.

The extremal flow rate u_i^* is equal to the singular control solution u_i^s when a set of conditions is fulfilled. The first condition results out of the definition of a singular control law. This condition states that ψ_i is zero. When this condition is assumed to hold for all control signals u_i (under the assumption that the control handles u_i can be modified independently) the following matrix equality is found.

$$\Psi(\boldsymbol{\xi}) = (\mathbf{C_n} \mid \mathbf{1_n}) \cdot \boldsymbol{\lambda} = 0 \tag{2.15}$$

The second condition follows out of the procedure for determining the singular control law. The time derivative for ψ_i is found to be independent of the control input u_i. This is trivial because the costate dynamics are independent of the control signals. The singular control law is found by taking the second time derivative of ψ_i and setting it to zero under the constraint that the first time derivative of ψ_i is equal to zero, which is the second condition. When this condition is written for all control inputs, the following matrix equality is found.

$$\frac{d\Psi(\boldsymbol{\xi})}{dt} = \left(\mathbf{C_n} \mid \mathbf{1_n} \right) \cdot \mathbf{S}(\boldsymbol{\xi}) \cdot \boldsymbol{\lambda} (= \left(\mathbf{C_n} \mid \mathbf{1_n} \right) \cdot \bar{\mathbf{S}}(\boldsymbol{\xi}) \cdot \bar{\mathbf{K}} \cdot \boldsymbol{\lambda}) = 0 \tag{2.16}$$

When the cost criterion $\mathcal{J}[\mathbf{u}]$ and the Hamiltonian $\mathcal{H}$ are not explicitly dependent on time and the final time t_f is free, then the Hamiltonian is zero along an extremal trajectory. If every control input is singular the

additional condition (2.17) is found.

$$\phi(\xi) = \mathbf{f}^{\mathbf{T}}(\xi) \cdot \boldsymbol{\lambda} = \varphi(\xi)^{\mathbf{T}} \cdot \boldsymbol{\lambda} (= \gamma(\xi)^{\mathbf{T}} \cdot \bar{\mathbf{K}} \cdot \boldsymbol{\lambda}) = 0 \qquad (2.17)$$

2.3 Multiple limiting substrates

2.3.1 Model description

In the sequel a model with r limiting substrates and one biomass is used. S_j [g], $j = 1 \ldots r$, X [g DW] are respectively the amount of each substrate and the biomass in the reactor. The vector ξ of the standard model (2.6) is given as follows:

$$\begin{aligned} \xi &= \left(\begin{array}{cccc} S_1 & S_2 & \ldots & S_r \quad X|V \end{array} \right)^T \\ \varphi(\xi) &= \left(\begin{array}{cccc} -\sigma_1 & -\sigma_2 & \ldots & -\sigma_r \quad \mu \end{array} \right)^T \cdot X \end{aligned} \qquad (2.18)$$

The vector φ with the reaction velocities φ_i, $i = 1 \ldots m$, [g/h] is written as a product of a vector, containing minus the specific substrate consumption rate σ_j [1/h], $j = 1 \ldots r$, and the specific biomass growth rate μ [1/h] with the amount of biomass X. m is equal to the amount of reactants $r + 1$. It is assumed that no biomass is fed by the input stream. The matrix $\mathbf{C_n}$ is defined as before except that $C_{X_n,in}$ is zero. Also in the control vector $\mathbf{u}$ the input corresponding to the biomass X can be set to zero. In the sequel $C_{S_i,in}$ [g/L] denotes the substrate concentration in the input stream u_i. The amount of each substrate S_i available for the process is denoted α_i [g], $j = 1 \ldots r$.

The specific substrate consumption rates σ_j and the specific biomass growth rate μ are in general functions of the concentrations of the substrates $C_{S_j} \triangleq \frac{S_j}{V}$ [g/L], $j = 1 \ldots r$, and the biomass $C_X \triangleq \frac{X}{V}$ [g/L]. The derivatives of the kinetics of the reaction velocities φ_j, $j = 1 \ldots m$, with respect to the states ξ can be written in function of the derivatives of σ_j and μ with respect to the substrate and biomass concentrations. The derivative of σ_j and μ with respect to the substrate concentration C_{S_i} are denoted by $\sigma_j^{S_i}$ and μ^{S_i} respectively. The derivatives of these specific rates with respect to the biomass concentration C_X are written as σ_j^X and μ^X.

$$\frac{\partial \varphi_j}{\partial S_i} = -\sigma_j^{S_i} \frac{X}{V}, j = 1 \ldots r, i = 1 \ldots r \quad ; \quad \frac{\partial \varphi_m}{\partial S_i} = \mu^{S_i} \frac{X}{V} \qquad (2.19)$$

$$\frac{\partial \varphi_j}{\partial X} = -\sigma_j^X \frac{X}{V} - \sigma_j, j = 1 \ldots r \quad ; \quad \frac{\partial \varphi_m}{\partial X} = \mu^X \frac{X}{V} + \mu \qquad (2.20)$$

$$\frac{\partial \varphi_j}{\partial V} = \frac{X}{V^2} \left(\begin{array}{ccc} \sigma_j^{S_1} & .. & \sigma_j^{S_r} \quad \sigma_j^X \end{array} \right) \left(\begin{array}{c} S_1 \\ \vdots \\ S_r \\ X \end{array} \right) \qquad (2.21)$$

$$\frac{\partial \varphi_m}{\partial V} = -\frac{X}{V^2} \left(\begin{array}{ccc} \mu^{S_1} & .. & \mu^{S_r} \quad \mu^X \end{array} \right) \left(\begin{array}{c} S_1 \\ \vdots \\ S_r \\ X \end{array} \right) \qquad (2.22)$$

When a linear relation (2.26) between the specific substrate consumption rates σ_i and the specific biomass growth rate μ is assumed more explicit results can be obtained. Y_i [-] is the yield of biomass on substrate i. Let the overall specific energy demand m for maintenance of living biomass be written as a sum of maintenance terms m_i, each associated with the conversion from the substrate S_i to the biomass X. When using the concept, introduced by Van Impe (1993), of endogenous fraction f_i for each of the conversion reactions, the maintenance demand m_i can be decomposed in two terms (2.23). The first term represents the maintenance due to consumption of substrate (exogenous metabolism) while the second term is the maintenance due to combustion of the biomass X (endogenous metabolism).

$$m = \sum_1^r m_i \quad ; \quad m_i = (1 - f_i) m_i + f_i m_i \qquad (2.23)$$

The specific biomass growth rate μ [1/h] can then also be decomposed in a term μ_S, representing the specific growth rate of biomass on the substrates, neglecting the endogenous maintenance, and a second term, giving a measure of the overall endogenous maintenance.

$$\mu = \mu_S - \sum_1^r Y_i f_i m_i \qquad (2.24)$$

μ_S is a function of the substrate concentrations C_{S_j}, j=1 ...r and the biomass concentration C_X. With the definition of μ_i (2.25), representing the specific biomass growth rate of the biomass on the substrates, including the maintenance related to the reaction i, a linear relation (2.26) can be specified between μ_i and the specific substrate consumption rate σ_i (2.26).

$$\mu_i = \mu_S - Y_i f_i m_i \qquad (2.25)$$

$$\sigma_i = \frac{\mu_S}{Y_i} + (1 - f_i) m_i \quad ; \quad \sigma_i = \frac{\mu_i}{Y_i} + m_i \qquad (2.26)$$

With these definitions the following relations between the derivatives are found.

$$\frac{\partial \varphi_j}{\partial S_i} = -\frac{\mu_S^{S_i}}{Y_j} \frac{X}{V}, j = 1 \ldots r, i = 1 \ldots r \qquad (2.27)$$

$$\frac{\partial \varphi_j}{\partial X} = -\frac{\mu_S^X}{Y_j} \frac{X}{V} - \frac{\mu_j}{Y_j} - m_j, j = 1 \ldots r \qquad (2.28)$$

$$\frac{\partial \varphi_j}{\partial V} = \frac{X}{V^2} \frac{1}{Y_j} \left(\begin{array}{ccc} \mu_S^{S_1} & .. & \mu_S^{S_r} \quad \mu_S^X \end{array} \right) \left(\begin{array}{c} S_1 \\ \vdots \\ S_r \\ X \end{array} \right) \qquad (2.29)$$

The model of the process can also be written in terms of the substrate and biomass concentrations.

$$\begin{pmatrix} \frac{dC_{S_1}}{dt} \\ \vdots \\ \frac{dC_{S_r}}{dt} \\ \frac{dC_X}{dt} \end{pmatrix} = \begin{pmatrix} -\sigma_1 C_X \\ -\sigma_2 C_X \\ \vdots \\ -\sigma_r C_X \\ \mu C_X \end{pmatrix} - (-\mathbf{C_n} + \begin{pmatrix} C_{S_1} \\ C_{S_2} \\ \vdots \\ C_{S_r} \\ C_X \end{pmatrix} \mathbf{1_n^T}) \frac{\mathbf{u}}{V} \quad (2.30)$$

2.3.2 Dynamical costate equations

The costates can be divided in costates related to the differential equations of the substrates (vector $\boldsymbol{\lambda}_S$), the costate referring to the biomass λ_X and the costate λ_V associated to the volume V.

The matrix $\mathbf{S}$, which is the matrix of the sensitivities of the reaction velocities with respect to the states, can now be calculated more explicitly.

It can be seen that (i) the model assumption, stating that one biomass and multiple substrates are considered, and (ii) the linear relation between the substrate consumption rates σ_i and the biomass growth rate μ_S induce a special structure.

First the dynamics of the costates are derived without assuming the linear relation. The dynamics of the costate vector $\boldsymbol{\lambda}_S$ and the costates λ_X and λ_V are now given explicitly. Observe that (i) the costate λ_V is not involved in the dynamics of the costates, (ii) the dynamic equations of the costates $\boldsymbol{\lambda}_S$ and the costate λ_X are quite simular up to an extra matrix, (iii) the dynamics of the costate λ_V are given as a combination of the dynamics of the other costates and (iv) the dynamics of the costates can be fully expressed in terms of the concentrations of biomass C_X and the substrates C_{S_j}, j=1 ...r. This last property is due to the special function of the state V in the fermentation process.

$$\frac{d\,\boldsymbol{\lambda}_S}{dt} = \begin{pmatrix} \sigma_1^{S_1} & . & \sigma_r^{S_1} & \mu_S^{S_1} \\ \vdots & \vdots & \vdots & \vdots \\ \sigma_1^{S_r} & . & \sigma_r^{S_r} & \mu_S^{S_r} \end{pmatrix} \begin{pmatrix} \lambda_{S_1} \\ \vdots \\ \lambda_{S_r} \\ -\lambda_X \end{pmatrix} C_X \quad (2.31)$$

$$\frac{d\lambda_X}{dt} = \begin{pmatrix} \sigma_1^X & .. & \sigma_r^X & \mu_S^X \end{pmatrix} \begin{pmatrix} \lambda_{S_1} \\ \vdots \\ \lambda_{S_r} \\ -\lambda_X \end{pmatrix} + \begin{pmatrix} \sigma_1 & .. & \sigma_r & \mu \end{pmatrix} \begin{pmatrix} \lambda_{S_1} \\ \vdots \\ \lambda_{S_r} \\ -\lambda_X \end{pmatrix} \quad (2.32)$$

$$\frac{d\lambda_V}{dt} = -C_X \begin{pmatrix} C_{S_1} & .. & C_{S_r} & C_X \end{pmatrix} \begin{pmatrix} \sigma_1^{S_1} & .. & \sigma_r^{S_1} & \mu_S^{S_1} \\ \vdots & \vdots & \vdots & \vdots \\ \sigma_1^{S_r} & .. & \sigma_r^{S_r} & \mu_S^{S_r} \\ \sigma_1^X & .. & \sigma_r^X & \mu_S^X \end{pmatrix} \begin{pmatrix} \lambda_{S_1} \\ \vdots \\ \lambda_{S_r} \\ -\lambda_X \end{pmatrix} \quad (2.33)$$

When linear relations are assumed between the specific growth rate μ_S and the specific substrate consumpion rates σ_i, the matrix containing the sensitivities of the specific rates with respect to the substrate and biomass concentrations can be decomposed in a product of the matrix $\bar{Y}$ and the matrix $\bar{\mu}$.

$$\bar{Y} = \begin{pmatrix} \frac{1}{Y_1} & \dots & \frac{1}{Y_r} & 1 \end{pmatrix} \; ; \; \bar{\mu}^T = \begin{pmatrix} \mu_S^{S_1} & \dots & \mu_S^{S_r} & \mu^X \end{pmatrix} \quad (2.34)$$

2.3.3 Optimal control strategy

The optimal control strategy can be found by careful analysis of the conditions imposed by optimal control theory. First the singular control conditions are analyzed, revealing some interesting features of the control strategy. Secondly the dynamics of the system during the final phase of the process are studied, resulting in a stop criterion.

Singular control conditions Let u_i be the inflow rate of substrate S_i. The conditions, which must be fulfilled for u_i to be equal to a singular control law u_i^*, are analyzed first. The first condition (2.35) arises from the definition of the singular control problem, stating that the Hamiltonian $\mathcal{H}$ is not explicitly function of the control input u_i. The second condition (2.37) is due to the fact that the time derivative of ψ_i is also not explicitly dependent on u_i and that this time derivative must be set equal to zero.

$$\psi_i = C_{S_i,in} \cdot \lambda_{S_i} + \lambda_V = 0 \quad (2.35)$$

$$\bar{\mathbf{C}}_\mathbf{i} = \begin{pmatrix} C_{S_1} & .. & C_{S_i} - C_{S_i,in} & .. & C_{S_r} & C_X \end{pmatrix} \quad (2.36)$$

$$\frac{d\psi_i}{dt} = C_X \cdot \bar{\mathbf{C}}_\mathbf{i} \cdot \begin{pmatrix} \sigma_1^{S_1} & .. & \sigma_r^{S_1} & \mu_S^{S_1} \\ \vdots & \vdots & \vdots & \vdots \\ \sigma_1^{S_r} & .. & \sigma_r^{S_r} & \mu_S^{S_r} \\ \sigma_1^X & .. & \sigma_r^X & \mu_S^X \end{pmatrix} \begin{pmatrix} -\lambda_{S_1} \\ \vdots \\ -\lambda_{S_r} \\ \lambda_X \end{pmatrix} = 0 \quad (2.37)$$

When all inflow rates u_i, i=1 ...r, are singular then the following set of equations must be fulfilled. The biomass concentration C_X is assumed to be different from zero.

$$\bar{\mathbf{C}}_\mathbf{n} = -\mathbf{C_n} + \mathbf{1_n} \cdot \begin{pmatrix} C_{S_1} \\ C_{S_2} \\ \vdots \\ C_{S_r} \\ C_X \end{pmatrix}^T \quad (2.38)$$

$$\bar{\mathbf{C}}_\mathbf{n}\begin{pmatrix} \sigma_1^{S_1} & .. & \sigma_s^{S_1} & \mu_S^{S_1} \\ \vdots & \vdots & \vdots & \vdots \\ \sigma_1^{S_r} & .. & \sigma_r^{S_r} & \mu_S^{S_r} \\ \sigma_1^{X} & .. & \sigma_r^{X} & \mu_S^{X} \end{pmatrix}\begin{pmatrix} -\lambda_{S_1} \\ \vdots \\ -\lambda_{S_r} \\ \lambda_X \end{pmatrix} = 0 \qquad (2.39)$$

In the sequel the specific biomass growth rate μ_S is assumed to be independent of the biomass concentration, resulting in the following set of equations.

$$\bar{\mathbf{C}}_\mathbf{n}\begin{pmatrix} \sigma_1^{S_1} & .. & \sigma_r^{S_1} & \mu_S^{S_1} \\ \vdots & \vdots & \vdots & \vdots \\ \sigma_1^{S_r} & .. & \sigma_r^{S_r} & \mu_S^{S_r} \end{pmatrix}\begin{pmatrix} -\lambda_{S_1} \\ \vdots \\ -\lambda_{S_r} \\ \lambda_X \end{pmatrix} = 0 \qquad (2.40)$$

In matrix notation:

$$\mathbf{Q}\cdot\mathbf{P}\cdot\ \boldsymbol{\lambda}^* = 0 \qquad (2.41)$$

The $r \times r$ matrix $\mathbf{Q} = \bar{\mathbf{C}}_\mathbf{n}$ contains the substrate concentrations in the reactor C_{S_i} and in the feed streams $C_{S_i,in}$. The $r \times (r+1)$ matrix $\mathbf{P}$ is the sensitivity matrix of the specific substrate consumption rates σ_i and the specific growth rate of the biomass μ_S with respect to the substrate concentrations C_{S_i}. $\boldsymbol{\lambda}^*$ contains minus the costates associated to the substrate concentrations (costate vector $\boldsymbol{\lambda}_S$) and the biomass concentration (costate λ_X). The costate λ_V, associated to the volume V, is not appearing in this equation. Notice that this is a linear set of r equations in $r+1$ costates. Another interesting condition appears when all substrate feedrates u_i are given by a singular control law. The property of the Hamiltonian $\mathcal{H}$ stating that it is equal to zero on an optimal trajectory, results in this case in the equation $\phi = 0$.

$$\phi \;=\; \begin{pmatrix} \sigma_1 & \dots & \sigma_s & \mu \end{pmatrix}\begin{pmatrix} -\lambda_{S_1} \\ \dots \\ -\lambda_{S_r} \\ \lambda_X \end{pmatrix} X \;=\; 0 \qquad (2.42)$$

The $(r \times r)$ matrix $\mathbf{Q}$ is full rank so the set of equations (2.40) can be simplified to the following set of equations.

$$\begin{pmatrix} \sigma_1 & \dots & \sigma_r & \mu \\ \sigma_1^{S_1} & \dots & \sigma_r^{S_1} & \mu_S^{S_1} \\ \vdots & \vdots & \vdots & \vdots \\ \sigma_1^{S_r} & \dots & \sigma_r^{S_r} & \mu_S^{S_r} \end{pmatrix}\begin{pmatrix} -\lambda_{S_1} \\ \vdots \\ -\lambda_{S_r} \\ \lambda_X \end{pmatrix} \;=\; 0 \qquad (2.43)$$

Notice that the extra equation due to the special property of the Hamiltonian is added to the simplified matrix equation (2.40). It can be shown that a nontrivial solution of this set of equations must exist so the $(r+1)\times(r+1)$

matrix of equation (2.43) must be rank deficient or the determinant of this matrix (denoted $\mathbf{G}$) must be zero.

When the specific substrate consumption rates σ_i are related to the specific biomass growth rate μ_S by linear equations the following decomposition of the matrix $\mathbf{G}$ can be made:

$$\bar{\mathbf{M}}^\mathbf{T} \;=\; \begin{pmatrix} (1-f_1)m_1 \\ \vdots \\ (1-f_r)m_r \\ -\sum_{i=1}^{r} Y_i f_i m_i \end{pmatrix} \;;\; \mathbf{M} \;=\; \begin{pmatrix} \bar{\mathbf{M}} \\ \hline \mathbf{O_{r\times(r+1)}} \end{pmatrix} \qquad (2.44)$$

$$\mathbf{G} \;=\; \begin{pmatrix} \mu_S \\ \mu_S^{S_1} \\ \vdots \\ \mu_S^{S_r} \end{pmatrix}\bar{\mathbf{Y}} \;+\; \mathbf{M} \qquad (2.45)$$

Notice that in this case the matrix equation (2.43) can only have a nontrivial solution if the derivatives of the specific growth rate μ_S with respect to the substrate concentrations are zero. Notice that the first equation reveals no extra information. Recall that this last conclusion is based on two assumptions, which are proven further.

1. There exists a nontrivial solution $\boldsymbol{\lambda}^*$ to Equation (2.43).

2. The product of the yield vector $\bar{Y}$ with the costate vector λ^* is not equal to zero.

If all maintenance coefficients m_i are zero and the above used assumption (concerning the derivatives) holds then the matrix equation (2.43) has only a nontrivial solution if μ_S equal to zero. It is clear that this is not a feasible result so one can state that at least one maintenance coefficient m_i is different from zero. This result is in agreement with the results found by Van Impe (1993a). From equation (2.43) and (2.45) it follows that the specific biomass growth rate can be written as a function of the costates, the yield vector and the maintenance coefficients. Because the costates are constant during singular control the specific biomass growth rate μ_S is constant when all feed rates u_i, $i = 1 \dots r$, are singular.

Notice that when p flow rates u_i are not singular, from equation (2.37) and the decomposition of $\mathbf{G}$ (2.45) (and using the condition $\bar{Y}\lambda^* \neq 0$) still a set of n-p equations, defining a so-called singular manifold in the n-dimensional state space, can be found. This singular manifold can be used for detection of the main features of the optimal control strategy.

The final phase The final phase of the fermentation process starts when the reactor is full (the volume V of the liquid phase is equal to V_{max}) or equivalently the available amounts of substrate α_i, $i = 1 \dots r$ are added.

All control inputs u_i are equal to zero. Due to the special property of the Hamiltonian $\mathcal{H}$ the condition (2.42) must be fulfilled.

The costate λ_X related to the biomass is constant during the end phase due to condition (2.42) and the assumption that the specific growth rate of the biomass is not depending on the biomass concentration (2.32).

Suppose that the performance criterion $\mathcal{J}[\mathbf{u}] = -\delta_X X(t_f)$ must be optimized. δ_X is the profit per unit of biomass. When the boundary conditions (2.14) on the costates are used an interesting stop criterion (2.46) is found.

$$\begin{aligned} \delta_X \cdot \mu &= 0 \\ \mu_S(t_f) &= \textstyle\sum_{i=1}^{r} Y_i f_i m_i \end{aligned} \tag{2.46}$$

This stop criterion states that the fermentation is stopped when the netto biomass growth rate μ equals zero. An explicit value of the specific biomass growth rate at the final time t_f can be calculated when a linear relation between the specific consumption rates and the specific growth rate is assumed.

Notice that the fact that the costates have a final value (2.14) and the costate λ_X is constant during the final phase indicates that the assumption, that a nontrivial solution for the matrix equation (2.43) must exist, is fulfilled if it is assumed that all feed rates u_i are singular in the phase preceding the final phase.

The condition $\bar{Y}\lambda^* \neq 0$ is proven by contradiction. Suppose that this equality would hold during the singular interval (all feed rates u_i are singular), then it would hold also during the end phase (again if the singular phase is preceding the final phase), which can not be a generic result because there are terminal conditions given on the costates at the final time t_f.

2.3.4 A general singular control law

The singular control law u_i^s is now calculated by differentiating $\frac{d\psi_i}{dt}$ (2.37) with respect to time. The linear relation (2.26) between the specific biomass growth rate and the specific substrate consumption rates is used in the derivation. $\mu_S^{S_iS_j}$, $\mu_S^{S_jX}$ and μ_S^{XX} are respectively the second order partial derivative of the specific biomass growth rate μ_S with respect to the substrate concentration C_{S_i} and C_{S_j}, the second order partial derivative with respect to the biomass concentration C_X and the substrate concentration C_{S_j}, the second order partial derivative with respect to the biomass concentration C_X.

When condition (2.42) (all feed rates are singular) and assumption $\bar{Y}\lambda^*$ are fulfilled then the formula for the second order derivative of ψ_i can be simplified significantly and results in an expression without costates. By separating this formula in terms containing the feedrate u_i and the terms

without u_i an expression with the structure (2.47) appears.

$$\mathbf{v_i^T} \cdot \mathbf{w_i} \cdot \frac{u_i}{V} = \mathbf{v_i^T} \cdot \mathbf{z_i} \tag{2.47}$$

$\mathbf{w_i}$ is an $(r+1) \times 1$ vector containing the concentrations of the reactans (substrates and biomass) in the reactor and the substrate concentration in the input stream i.

$$\mathbf{w_i^T} = (C_{S_1}, \ldots, C_{S_i} - C_{S_i,in}, \ldots, C_X) \tag{2.48}$$

The vector $\mathbf{v_i}$ is a $(r+1)\times 1$ vector containing the first and second derivatives of the specific biomass growth rate μ_S with respect to the concentrations of the substrates and the biomass. For a nice representation of the vector $\mathbf{v_i}$ the vector notation (2.49) is introduced.

$$\mathbf{v_i} = \mathbf{l} + \mathbf{P} \cdot \mathbf{w_i} \tag{2.49}$$

$\mathbf{l}$ is a $(r+1) \times 1$ vector containing the first derivatives. The matrix $\mathbf{P}$ is a symmetric $(r+1) \times (r+1)$ matrix with the second derivatives.

$$\mathbf{l} = \begin{pmatrix} \mu_S^{S_1} \\ \cdots \\ \mu_S^{S_r} \\ \mu_S^{X} \end{pmatrix} \quad ; \quad \mathbf{P} = \begin{pmatrix} \mu_S^{S_1S_1} & \mu_S^{S_1S_2} & \cdots & \mu_S^{S_1X} \\ \mu_S^{S_1S_2} & \cdots & \cdots & \mu_S^{S_2X} \\ \vdots & \vdots & \vdots & \vdots \\ \mu_S^{XS_1} & \cdots & \cdots & \mu_S^{XX} \end{pmatrix} \tag{2.50}$$

The $(r+1) \times 1$ vector $\mathbf{z_i}$ contains the substrate degradation $\sigma_j C_X$ rates for all the substrates, the biomass growth rate μC_X and the transport terms, describing the feeding of the substrates (besides the substrate S_i) and the dilution due to the inputs (besides the input u_i). $\mathbf{u_i}$ is the vector of flow rates except the flow rate u_i.

$$\mathbf{z_i} = \frac{\varphi}{V} - (-\mathbf{C_n} + \begin{pmatrix} C_{S_1} \\ C_{S_2} \\ \vdots \\ C_{S_r} \\ C_X \end{pmatrix} \mathbf{1_n^T}) \frac{\mathbf{u_i}}{V} \tag{2.51}$$

The singular control law can be interpreted as a special sum of elementary control laws u_i^j. Each of these elementary control laws try to keep its corresponding substrate or biomass concentration at a constant value. These elementary control laws are added in a special way. The elementary control laws can be written as a quotient of a term a_i^j and a term b_i^j (2.52). The final singular control law u_i is then written as a quotient of a sum of terms a_i^j multiplied with a weighting factor d_i^j and a sum of terms b_i^j multiplied with the same weighting factor (2.52). The weighting factors are function

of the first and second derivatives of the specific biomass growth rate μ_S and the concentrations of substrates and biomass.

$$u_i^j = \frac{a_i^j}{b_i^j} \quad ; \quad u_i = \frac{\sum_{k=1}^{r+1} d_i^k a_i^k}{\sum_{i=k}^{r+1} d_i^k b_i^k} \tag{2.52}$$

Notice (1) that the feedrates u_j, $j = 1 \ldots r$, $i \neq j$, appear in the formula of the singular control u_i in an explicit way and (2) that the singular control law is independent of the costates. Recall that in this derivation all feedrates are supposed to be singular. So all control inputs have the same structure given by formula (2.47). A formula for the singular control input u_i independent from the other control inputs can be derived which results in the following equation.

$$\frac{u_i}{V} = \frac{\begin{vmatrix} (C_{S_1} - C_{S_1,in}) & .. - \sigma_1 C_X .. & C_{S_1} \\ C_{S_2} & .. - \sigma_2 C_X .. & C_{S_2} \\ \vdots & & \vdots \\ C_{S_r} & .. - \sigma_r C_X .. & (C_{S_r} - C_{S_r,in}) \end{vmatrix}}{\begin{vmatrix} (C_{S_1} - C_{S_1,in}) & ..C_{S_1}.. & C_{S_1} \\ C_{S_2} & ..C_{S_2}.. & C_{S_2} \\ \vdots & & \vdots \\ C_{S_r} & ..C_{S_r}.. & (C_{S_r} - C_{S_r,in}) \end{vmatrix}} \tag{2.53}$$

When these determinants are developed around the i^{th} column then it is clear that the singular controller u_i has the structure of a special sum (2.52). The elementary control laws (2.54) are setpoint controllers. The feedrate u_i^i keeps the substrate concentration C_{S_i} on a setpoint if there is no dilution due to other inputs. The feedrate $u_i^{j \neq i}$ tries to compensates for its dilution effect on the substrate concentration C_{S_j}

$$\frac{u_i^{e_i}}{V} = \frac{\sigma_i C_X}{C_{S_i,in} - C_{S_i}} \quad ; \quad \frac{u_i^{e_j \neq i}}{V} = \frac{\sigma_j C_X}{-C_{S_j}} \tag{2.54}$$

Notice that the dynamics of the substrate concentrations can be written in the matrix form (2.30). Combination of these equations with the definition equation of the singular control laws u_i (2.53) illustrates that the substrate concentrations are kept constant.

The general results are now illustrated with a detailed case study.

2.4 Case study

The optimal control strategy is now derived for a biotechnological process with one biomass X and two limiting substrates S_1 and S_2 which are fed by two separate input streams. The model of the process is given in concentrations (2.55). Equation (2.56) describes the dynamics of the volume V [L].

S_1 [g] and S_2 [g] are the absolute amount of the substrates in the reactor with volume V [L]. X [g] is the amount of biomass. $\mu(C_{S_1}, C_{S_2})$ [1/h] is the specific growth rate of the biomass and is assumed to be a function of only the substrate concentrations C_{S_1} and C_{S_2} [g/L]. The specific substrate consumption rates σ_i [1/h] are linearly dependent on μ. A maintenance metabolism (maintenance coefficients m_1 [1/h] and m_2 [1/h]) is assumed (endogenous fraction f_1 and f_2 are zero). Y_1 [-] and Y_2 [-] are the yields of biomass on substrate 1 and substrate 2 respectively. u_1 and u_2 [L/h] are the substrate feedrates for substrates 1 and 2 respectively.

$$\begin{pmatrix} \frac{dC_{S_1}}{dt} \\ \frac{dC_{S_2}}{dt} \\ \frac{dC_X}{dt} \end{pmatrix} = \begin{pmatrix} -1 & 0 & 0 \\ 0 & -1 & 0 \\ 0 & 0 & 1 \end{pmatrix} \begin{pmatrix} \sigma_1 C_X \\ \sigma_2 C_X \\ \mu C_X \end{pmatrix} + \begin{pmatrix} (C_{S_1,in} - C_{S_1})\frac{u_1}{V} - C_{S_1}\frac{u_2}{V} \\ (C_{S_2,in} - C_{S_2})\frac{u_2}{V} - C_{S_2}\frac{u_1}{V} \\ -C_X\frac{u_1+u_2}{V} \end{pmatrix} \tag{2.55}$$

$$\frac{dV}{dt} = u_1 + u_2 = \begin{pmatrix} 1 & 1 \end{pmatrix} \begin{pmatrix} u_1 \\ u_2 \end{pmatrix} \tag{2.56}$$

$$\sigma_1 = \frac{\mu}{Y_1} + m_1 \quad ; \quad \sigma_2 = \frac{\mu}{Y_2} + m_2 \tag{2.57}$$

The flow rates u_1 and u_2 are now determined such that the cost criterion $\mathcal{J}[u_1, u_2] = -X(t_f)$ (the amount of biomass at the end of the process) is optimized. α_1 and α_2 are respectively the available amount of substrate 1 and 2 which can be added during the process. This optimization problem will be discussed for three different structures of the specific biomass growth rate μ. The specific growth rate μ is modeled as a product of factors $\mu_{C_{S_i}}$ [-], with each factor function of only one of the substrates. It is assumed that the μ is independent from the biomass concentration C_X. μ_m [1/h] is a parameter.

$$\mu(C_{S_1}, C_{S_2}) = \mu_m \mu_{C_{S_1}}(C_{S_1}) \mu_{C_{S_2}}(C_{S_2}) \tag{2.58}$$

These factors can now be (1) a monotonic increasing function (Monod type (2.59) left) or (2) a non-monotonic function (Haldane type (2.59) right) of the concentration C_{S_1} or C_{S_2}. Three cases can be distinguished.

Case 1. Both factors $\mu_{C_{S_1}}$ and $\mu_{C_{S_2}}$ are non-monotonic functions.

Case 2. One of the factors is a monotonic function, while the other factor is non-monotonic.

Case 3. Both factors are monotonic functions.

$$\mu_{C_{S_i}}(C_{S_i}) = \frac{C_{S_i}}{K_{M_i} + C_{S_i}} \quad ; \quad \mu_{C_{S_i}}(C_{S_i}) = \frac{C_{S_i}}{K_{S_i} + C_{S_i} + \frac{C_{S_i}^2}{K_{I_i}}} \tag{2.59}$$

The optimal flow rates $u_1^\star$, $u_2^\star$ can principally be determined with optimal

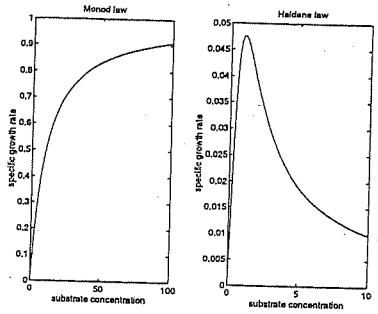


Figure 2.1: Left: Monod kinetic. Right: Haldane kinetic

control theory. From this theoretical framework the structure of the optimal flow rate $u_i^\star$ is clear. $u_i^\star$ is equal to the maximal feedrate, the minimal feedrate (zero) or the singular feedrate u_i^s. The selection between these three possibilities is made by evaluating a function of the costates $\boldsymbol{\lambda}$. Unfortunately the dynamics of the costates is unknown because of the two point boundary value problem. In general the singular feedrate is also function of the costates.

From the previous general analysis of the optimal control problem for a system with multiple substrates some general characteristics of the optimal control solution are found. More specific the final phase of the process, the conditions for having singular feedrates and the structure of the singular control laws are analyzed in detail.

2.4.1 Case 1: double Haldane kinetic

Suppose that the specific biomass growth rate μ is modelled as a double Haldane kinetic. From the general analysis it is found that a singular feedrate for both inputs u_1 and u_2 is only feasible when the first order derivatives of the specific biomass growth rate μ with respect to the substrate concentrations C_{S_1} and C_{S_2} are equal to zero.

$$\mu^{S_1} = 0 \quad ; \quad \mu^{S_2} = 0 \tag{2.60}$$

For the case considered here this set of equations has a unique solution. The optimal feedrate $u_1^\star$ and $u_2^\star$ can only be equal to the singular feedrate u_1^s

and u_2^s respectively when the substrate concentrations in the reactor C_{S_1} and C_{S_2} are equal to the substrate concentrations $C_{S_1}^*$ and $C_{S_2}^*$ respectively. These are the concentrations for which the Haldane kinetics are maximal. These are the substrate concentrations for which the equations (2.60) are fulfilled. The specific biomass growth rate μ is maximal for these substrate concentrations.

$$C_{S_1}^* = \sqrt{K_{S_1} K_{I_1}} \quad ; \quad C_{S_2}^* = \sqrt{K_{S_2} K_{I_2}} \tag{2.61}$$

When one of the feedrates is singular and the other one is equal to the maximal or minimal feedrate then the singular feedrate is given by Formula (2.47). For the feedrate u_1^s this results in the control law (2.63). A similar control law is found of u_2^s.

$$u_1^s = \frac{(-\sigma_1 C_X)A + (-\sigma_2 C_X)B}{(C_{S_1} - C_{S_1,in})A + C_{S_2}B} + \frac{(-C_{S_2}u_2)A + ((C_{S_2,in} - C_{S_2})u_2)B}{(C_{S_1} - C_{S_1,in})A + C_{S_2}B} \tag{2.62}$$

$$\begin{aligned} A(C_{S_1}, C_{S_2}) &= \mu^{S_1} + \mu^{S_1 S_1}(C_{S_1} - C_{S_1,in}) + \mu^{S_1 S_2}(C_{S_2}) \\ B(C_{S_1}, C_{S_2}) &= \mu^{S_2} + \mu^{S_2 S_1}(C_{S_1} - C_{S_1,in}) + \mu^{S_2 S_2}(C_{S_2}) \end{aligned} \tag{2.63}$$

From optimal control theory it follows that the first time derivative (2.37) of ψ_i must be zero for having a singular feedrate u_i^s. When the feedrate u_i is considered this results in equation (2.64).

$$(-C_{S_1,in} + C_{S_1})\mu^{S_1} + C_{S_2}\mu^{S_2} = 0 \tag{2.64}$$

When the double Haldane kinetic is used for μ the equation (2.64) can be rewritten as follows if assumption $\bar{Y}\lambda^\star$ is valid:

$$(C_{S_1} - C_{S_1,in})C_{S_2}\frac{K_{S_1} - \frac{C_{S_1}^2}{K_{I_1}}}{K_{S_1} + C_{S_1} + \frac{C_{S_1}^2}{K_{I_1}}} + (C_{S_2})C_{S_1}\frac{K_{S_2} - \frac{C_{S_2}^2}{K_{I_2}}}{K_{S_2} + C_{S_2} + \frac{C_{S_2}^2}{K_{I_2}}} = 0 \tag{2.65}$$

It is clear that this equation defines a manifold in the 2-dimensional space spanned by the substrate concentrations C_{S_1} and C_{S_2}. Figure 2.2 (left) shows part of the singular manifold for feedrate u_1. The optimal control strategy can now be determined easily. The feedrate u_i is selected (maximal, minimal or singular) as follows.

- If the substrate concentrations C_{S_1} and C_{S_2} are not on the singular manifold associated with the feedrate u_i then this feedrate is set to its maximal value if this drives the substrate concentrations towards the singular manifold.
- If the substrate concentrations C_{S_1} and C_{S_2} are not on the singular manifold associated with the feedrate u_i then this feedrate is set to its minimal value if this drives the substrate concentrations towards the singular manifold.

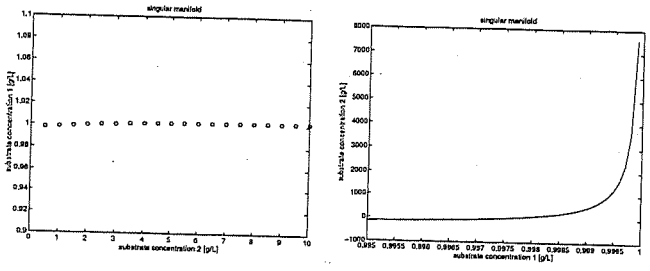


Figure 2.2: Singular manifold

- If the substrate concentration C_{S_1} and C_{S_2} are on the singular manifold associated with the feedrate u_i then this feedrate becomes singular. This feedrate will keep the substrate concentrations on this singular manifold.

Notice that now the selection of the feedrate is based on a comparison of the substrate concentrations with the singular manifold. The dynamics of the costates are not necessary anymore. In this way the two point boundary value problem is circumvented. From the analysis of the singular manifolds it is clear that the singular control laws u_i^s keep the substrate concentrations C_{S_i} near the setpoint $C_{S_i}^\star$. This observation results in the following simplified control strategy.

- If the substrate concentration C_{S_i} in the reactor is lower than the substrate concentration $C_{S_i}^\star$ then the feedrate u_i is set to its maximal value. The purpose is to bring the substrate concentration to the optimal value.
- If the substrate concentration C_{S_i} in the reactor is higher than the substrate concentration $C_{S_i}^\star$ then the feedrate u_i is set to zero (its minimal value), again with the same purpose.
- If the substrate concentration C_{S_i} equals the substrate concentration $C_i^\star$ then the feedrate u_i is singular.

The general formula (2.53) for the singular feedrates can be used when both feedrates u_1 and u_2 are singular. This results in the following singular feedrates:

$$\frac{u_1}{V} = \frac{(C_{S_2} - C_{S_2,in})(-\sigma_1 X) + (-C_{S_1})(-\sigma_2 X)}{(C_{S_2} - C_{S_2,in})(C_{S_1} - C_{S_1,in}) - C_{S_1} C_{S_2}} \tag{2.66}$$

$$\frac{u_2}{V} = \frac{(C_{S_1} - C_{S_1,in})(-\sigma_2 X) + (-C_{S_2})(-\sigma_1 X)}{(C_{S_1} - C_{S_1,in})(C_{S_2} - C_{S_2,in}) - C_{S_2} C_{S_1}} \tag{2.67}$$

The substrate concentrations are kept at a constant value when using these flow rates. This can easily be verified by using these flow rates in the equations (2.56). Notice that the structure of the feedrates is indeed of the form of the special sum (2.52). Each elementary part of the feedrates tries to keep the substrates at a constant value. The first term (the first product of the numerator divided by the first product of the denumerator) of the feedrate u_1 keeps the substrate concentration C_{S_1} at a constant value if there is no dilution effect due to feedrate u_2. The second term of u_1 (second product of the numerator divided by the second product of the denumerator) tries to compensate for its dilution effect on the dynamics of the substrate concentration C_{S_2}. The weight factors here are given in terms of the substrate concentrations C_{S_1} and C_{S_2}. Recall that Formula (2.66,2.67) for the singular feedrates is only valid when both feedrates are singular. When the simplified control strategy is used, and one of the feedrates is not singular, then a modified control control law can be used. When the feedrate u_2 is not singular, then the control law (2.68) for u_1^s can be used which keeps the substrate concentration C_{S_1} on the setpoint. A similar formula can be written for u_2^s.

$$\frac{u_1^s}{V} = \frac{-\sigma_1 C_X - C_{S_2} u_2}{C_{S_1} - C_{S_1,in}} \tag{2.68}$$

Notice that the feedrate u_i can be non singular because the substrate concentration C_{S_i} has not reached the setpoint $C_{S_i}^\star$ yet or because the available amount of substrate C_{S_i} is completely added. In this last case the feedrate is equal to zero. From the general analysis it follows that the process is stopped when the specific biomass growth rate is equal to zero or one of the substrate concentrations becomes zero.

2.4.2 Case 2: Haldane/Monod kinetic

When the specific biomass growth rate μ is modelled as a product of a non-monotonic function of the substrate concentration C_{S_1} and a monotonic function of the substrate concentration C_{S_2} then the set of equations (2.60) has no solution.

From Figure 2.1 it is clear that the Monod kinetic reaches its maximal value for a substrate concentration which is infinitely high. In fact the derivative of the Monod kinetic with respect to the substrate concentration becomes zero for an infinite substrate concentration. From this observation it is clear that substrate S_2 must be added as fast as possible. This can be realized by setting the feedrate u_2 equal to its maximal value. Another approach is to add the available amount of substrate S_2 initially and setting u_2 equal to zero during the process. This approach is now further discussed.

The singular control law u_1 is now given by Formula 2.47 and results in

the following equation.

$$\frac{u_1}{V} = \frac{(\sigma_1 C_X)A(C_{S_1}, C_{S_2}) + (\sigma_2 C_X)B(C_{S_1}, C_{S_2})}{(C_{S_1,in} - C_{S_1})A(C_{S_1}, C_{S_2}) - C_{S_2}B(C_{S_1}, C_{S_2})} \tag{2.69}$$

$$\begin{aligned} A(C_{S_1}, C_{S_2}) &= \mu^{S_1} + \mu^{S_1 S_1}(C_{S_1} - C_{S_1,in}) + \mu^{S_1 S_2}(C_{S_2}) \\ B(C_{S_1}, C_{S_2}) &= \mu^{S_2} + \mu^{S_2 S_1}(C_{S_1} - C_{S_1,in}) + \mu^{S_2 S_2}(C_{S_2}) \end{aligned} \tag{2.70}$$

Notice that the feedrate u_1 is independent from u_2. This singular feedrate has again the structure of a special sum (2.52) of elementary feedrates. The first term keeps the substrate concentration C_{S_1} at a constant value while the second term tries to compensate for its dilution effect in the dynamics of the substrate concentration C_{S_2}. The weighting factors are now determined by the first and second derivatives of the specific biomass growth rate μ and the substrate concentrations. If C_{S_2} is in the saturation range of the monotonic kinetic, then the singular feedrate can be approximated by the feedrate (2.71), which keeps the substrate concentration C_{S_1} constant.

$$\frac{u_1}{V} = \sigma_1 \frac{C_X V}{C_{S_1,in} - C_{S_1}} \tag{2.71}$$

Recall that in the case with the double Haldane kinetic the decision whether a feedrate is equal to its maximal, minimal value or singular, is made independently of the costate dynamics via a detailed analysis of the singular conditions.

From optimal control theory it follows that the first time derivative (2.37) of ψ_1 must be zero for having a singular feedrate u_1^s. For the case under consideration this results in Equation (2.72).

$$(-C_{S_1,in} + C_{S_1})\mu^{S_1} + C_{S_2}\mu^{S_2} = 0 \tag{2.72}$$

When the Haldane and Monod kinetics are used for $\mu_{C_{S_1}}$ and $\mu_{C_{S_2}}$ respectively, Equation (2.72) can be rewritten as follows:

$$(C_{S_1} - C_{S_1,in})\frac{K_{S_1} - \frac{C_{S_1}^2}{K_{I_1}}}{K_{S_1} + C_{S_1} + \frac{C_{S_1}^2}{K_{I_1}}} + \frac{C_{S_1} K_{M_2}}{K_{M_2} + C_{S_2}} = 0 \tag{2.73}$$

It is clear that this equation defines a manifold in the 2-dimensional space spanned by the substrate concentrations C_{S_1} and C_{S_2}. Figure 2.2 (right) shows part of this manifold. There exist only a limited range of substrate concentrations C_{S_1} with a corresponding physical relevant substrate concentration C_{S_2}. From the analysis above the following optimal control strategy is determined:

- The available amount of substrate S_2 is added initially and the feedrate u_2 is set equal to zero.

- The feedrate u_1 is chosen maximal or minimal such that the point (C_{S_1}, C_{S_2}) approaches the singular manifold.
- When the point (C_{S_1}, C_{S_2}) is on the singular manifold, then the feedrate u_1 is singular and given by Equation (2.70).
- The feedrate u_1 is equal to zero when all the available substrate S_1 is added.
- The process is terminated when one of the substrate concentrations becomes zero.

Notice that the substrate concentration C_{S_2} can only decrease during the process. The singular manifold indicates that for large values of the substrate concentration C_{S_2} the substrate concentration C_{S_1} is equal to the optimal value $C_{S_1}^*$. This observation allows a simplification of the optimal control strategy. The feedrate u_1 is chosen minimal or maximal such that the substrate concentration C_{S_1} is approaching the optimal value $C_{S_1}^*$. When the substrate concentration C_{S_1} is equal to the optimal value, then the singular feedrate (2.71) is used.

2.4.3 Case 3: double Monod kinetic

When the specific biomass growth rate is modelled as a double Monod kinetic, then the set of equations (2.60) has no solution. Figure 2.59 shows that the specific biomass growth rate μ becomes maximal for infinite high value of both substrate concentrations C_{S_1} and C_{S_2}. Notice that the first order derivative of μ with respect to the substrate concentrations becomes then equal to zero. From this observation it is clear that the optimal performance of the process is obtained by adding both substrates as fast as possible, thus by setting both u_1 and u_2 equal to their maximal value. Another approach is to add the available amount of both substrates initially.

2.5 Optimization

The optimization of the remaining degrees of freedom and the relation with the optimal control strategy is now discussed in detail. First the optimal control strategy is summarized.

- **Monod/Monod** The optimal performance of the process is obtained when a *batch operation* is used. The available amount of substrate for both S_1 and S_2 (α_1 and α_2) is added initially.
- **Haldane/Monod** Optimality with respect to the cost criterion (final amount of biomass) is obtained when the available amount of substrate S_2 (α_2) is added initially, which is again a *batch operation*, and the feedrate u_1 keeps the substrate concentrations C_{S_1} and C_{S_2}

on a *singular manifold.* Note that both concentrations are influenced by the feedrate u_1.

- **Haldane/Haldane** The optimal feedrate keep the substrate concentrations on setpoints, which can be determined from the kinetics. Thus the optimal control strategy can be described as *setpoint control.*

Notice that above only the main characteristics of the optimal control strategy are described. Often an initial phase will be necessary to get for instance (1) on the singular manifold in the case of a Haldane/Monod kinetic and (2) to reach the optimal setpoints when a double Haldane kinetic is considered. Notice that of course the question whether the singular manifold is reachable should be posed. If this is not the case degenerated situations (without a singular control part) will occur.

There will also be a terminal phase. This phase starts when the optimal strategy described above can not continue anymore. This happens for instance when the amount of available substrate α (α_1 for substrate S_1 when a Haldane/Monod kinetic is used (Figure 2.3, time instance t_1), α_1 and α_2 for substrates S_1 and S_2 respectively when a double Haldane kinetic is considered) is completely added (Figure 2.3, time instances t_2, t_1 respectively).

In the case of a Haldane/Monod kinetic the terminal phase is then a batch operation. The flow rate u_1 becomes zero. When a double Haldane kinetic is used the terminal phase is more complicated. When α_1 (respectively α_2) is completely added (and thus the feedrate u_1 (respectively u_2) must become zero) the optimal feedrate u_2 (respectively u_1) will keep the substrate concentrations on a singular manifold. When both α_1 and α_2 are added, then the feedrates u_1 and u_2 are set to zero (batch operation) (Figure 2.3, time instance t_2).

The process operation stops when the specific growth rate of the biomass becomes equal to zero. When only exogenous maintenance is considered this happens when at least one substrate concentration becomes zero. Note that besides the complete addition of the substrates this can be a second reason to stop the optimal feeding strategy described above.

In the case with a Haldane/Monod kinetic two situations can appear. In the first situation the optimal feeding strategy of u_1 is interrupted because the amount of available substrate α_1 is added. The feedrate u_1 is set to zero (Figure 2.3, time instance t_1). The process operation continues in batch till the stop criterion is fulfilled (Figure 2.3, time instance t_2). In the second situation the optimal feeding strategy is stopped because the substrate concentration of S_2 is zero (dashed-dotted line). There is no terminal phase. The process operation stops immediately.

In the case with a Haldane/Haldane kinetic generally there will be two different terminal phases. During the first phase one of the flow rates is set to zero (because the corresponding available substrate is completely added)(Figure 2.3, time instance t_1). In the second phase both flow rates

are set to zero (because for both substrates the available amount is added) (Figure 2.3, time instance t_2). and the process continues in batch until one of the substrate concentrations becomes zero (Figure 2.3, time instance t_3).

A special case is when the process stops after the first terminal phase when the substrate concentration (corresponding to the flow rate u_i which was set to zero first) becomes zero (Figure 2.3, time instance t_4). There is no second batch phase because one of the substrate concentrations is already zero (dashed-dotted line).

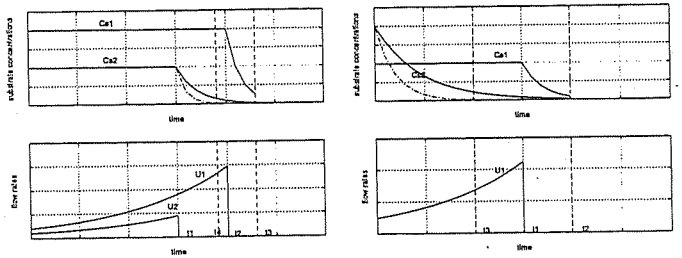


Figure 2.3: Structure of the optimal control solution for the Haldane/Haldane case (left) and the Haldane/Monod case (right).

From the previous analysis it follows that the main characteristics of the optimal feeding strategy can be determined from a qualitative knowledge of the kinetics μ [1/h]. For the analytical calculation of the singular manifold and the feedrates of course a quantitative description of the kinetics is necessary.

The following relationships can now be considered. Let u_1 and u_2 [L/h] be the feedrate of substrate S_1 and S_2 respectively.

$$S_1(0) + \int_{t_0}^{tf} C_{S_1,in} u_1 dt \;=\; \alpha_1 \;\;;\;\; S_2(0) + \int_{t_0}^{tf} C_{S_2,in} u_2 dt \;=\; \alpha_2 \tag{2.74}$$

$S_1(0)$ and $S_2(0)$ [mg] are respectively the initial amount of substrate S_1 and S_2 in the reactor. $C_{S_1,in}$ and $C_{S_2,in}$ [mg/L] are the substrate concentrations in the feedrates u_1 and u_2 respectively. α_1 [mg] and α_2 [mg] are respectively the total amount of substrate S_1 and S_2 available for the process. t_f and t_0 [h] are the final and initial time. Define V_* [L] as the volume of the liquid phase when no substrates are added. $V(t_f)$ [L] is the maximal volume of the reactor. Equation (2.75) states that the reactor is full when the sum of the volume of the initial liquid phase, the volume due to the addition of the initial substrates and the volume due to feeding are equal to the maximal volume.

$$V(t_f) \;=\; V_* + \frac{\alpha_1}{C_{S_1,in}} + \frac{\alpha_2}{C_{S_2,in}} \tag{2.75}$$

It can be concluded that α_1 and α_2 are two degrees of freedom which must be optimized under the constraint (2.75). In fact one ends up with a one-dimensional optimization problem. Depending on the qualitative knowledge of the kinetics the following cases are distinguished.

Monod/Monod Optimal control theory indicates that adding the substrates S_1 and S_2 as fast as possible results in an optimal control strategy. In the limit (when the feedstreams u_1 and u_2 are unbounded) this results in adding the available substrates α_1 and α_2 at the initial time. During the process the feedstreams u_1 and u_2 are zero. A one-dimensional optimization problem in $S_1(0) = \alpha_1$ is found. $S_2(0) = \alpha_2$ is found with relation (2.75).

Haldane/Monod It is found that substrate S_2 must be added as fast as possible. Again in the limit (when the feedstream u_2 is unbounded) this results in adding all the available substrate α_2 initiallly. During the process the feedstream u_2 is equal to zero. Substrate S_1 is added by the feedstream u_1 in such a way that the substrate concentrations C_{S_1} and C_{S_2} are on the singular manifold. In fact a one-dimensional optimization problem in $S_2(0) = \alpha_2$ is found with a constraint (2.75) on α_1.

Haldane/Haldane The optimal control strategy is to bring the substrate concentrations $C_{S_1}(0)$ and $C_{S_2}(0)$ to the substrate concentrations $C^*_{S_1}$ and $C^*_{S_2}$ (the substrate concentrations resulting in a maximum specific growth rate or the maximum of the two Haldane kinetics) and to keep the substrate concentrations on these setpoints as long as possible (till the available substrates α_1 and α_2 are fed). In fact a one-dimensional optimization problem in α_1 is found with a constraint on α_2.

Note that the above described optimization problem should not be confused with the following two problems.

Optimization of the initial conditions Consider the case where the kinetics is determined with *a double Haldane kinetic*. A one-dimensional optimization problem in α_1 (and a related α_2 is found). Additional degrees of freedom is this case are the initial substrate concentrations $C_{S_1}(0)$ and $C_{S_2}(0)$ (or the initial amount $S_1(0)$ and $S_2(0)$). Notice that this choice changes the amount of the substrates that can be added by the feedstreams. The solution of this two-dimensional optimization problem should however not be confused with the previous discussed problem because the solution is given by optimal control theory itself. The optimal initial substrate concentrations are the setpoints $C^*_{S_1}$ and $C^*_{S_2}$. The conclusion is that first the optimal control strategy including the optimal initial concentrations must be determined. The optimization of the amount of substrates α_1 and α_2 is done afterwards. For the case where the kinetics is determined with *a Haldane/Monod kinetic* the optimal process initialization is starting on the singular manifold (relating C_{S_1} and C_{S_2} and thus also connecting $C_{S_1}(0)$ and $C_{S_2}(0)$). In this case a one-dimensional optimization problem in $S_2(0)$ (or the distance to the singular manifold) is found. The corresponding optimal initial concentration $C_{S_1}(0)$ can be calculated with the formula of the singular manifold. The amount of substrate S_1 to be added by the feedrate

u_1 (α_1) must of course be adjusted. Only in the case where *a double Monod kinetic* is considered the optimal initialization problem is equal to the optimization problem of the available substrate α_1 and α_2 discussed above, because the degrees of freedom of both optimization problems are equal here.

Optimization of the control strategy The optimization of the available substrates α_1 and α_2 and the optimal initialization problem should not be confused with the determination of some degrees of freedom of the optimal control law. In the case of *a double Haldane kinetic* it is found that u_1 and u_2 are setpoint controllers, keeping the substrate concentrations C_{S_1} and C_{S_2} both on fixed optimal setpoints, given by optimal control theory. It can be shown that these setpoints are optimal by comparing the obtained performance (the resulting biomass X) with the results found if other setpoints are used. For the case where *a Haldane/Monod kinetic* is considered the distance to the singular manifold can be used to show that this singular manifold is indeed the optimal manifold (distance is zero). For the case where *a double Monod kinetic* no such analysis is relevant.

Comparison with suboptimal control strategies For the *double Monod kinetic* and the *double Haldane kinetic* an optimal control strategy is found with interesting properties from an implementation point of view. For the *Haldane/Monod* case a difficult singular control law is found. The singular manifold indicates that the optimal control strategy can be approximated by a control strategy keeping the substrate concentration C_{S_1} equal to a setpoint $C^*_{S_1}$ (almost equal to the substrate concentration for which a maximum specific growth rate is found). The determination of this setpoint is again another optimization problem.

Note that when maintenance is negligible (m_1 and m_2 zero) then the feeding strategy does not influence the obtained goal of the process which is the optimization of the amount of biomass. Thus the optimal control problem (determining the optimal feed rates u_1 and u_2) and the related optimal initialization (determining the optimal initial concentrations $C_{S_1}(0)$ and $C_{S_2}(0)$) are not relevant. The optimization of the available substrates α_1 and α_2 however is still important and even solvable analytically in this case.

The main conclusion of this section is that *two main optimization problems* can be distinguished. First the optimal control strategy is selected from qualitative knowledge of the kinetics. Then the optimal amount of available substrates α_1 and α_2 are determined.

2.6 Simulations

The optimization of the biotechnological process with one biomass and 2 substrates is now illustrated for the three cases. The dimensions and notation for the state variables, the parameters and the constraints used during simulations are given in Appendix D. The main features of the optimal con-

trol strategy for the different cases will be shown. The difference between the determination of the optimal control strategy (first optimization problem) and the optimization of the available amount of substrate α_1 and α_2 (second optimization problem) is illustrated.

2.6.1 Case 1: double Haldane kinetic

Figure 2.4 shows the dynamics of the substrate concentrations C_{S_1}, C_{S_2}, the amount of biomass X, the flow rates u_1, u_2 and the volume V of the liquid in the reactor when the simplified control strategy is applied. The initial substrate concencentrations are set equal to zero. The initial biomass concentration is 10 g/L. One can observe that initially the flow rates u_1 and u_2 are maximal until the optimal setpoints $C^*_{S_1}$ and $C^*_{S_2}$ are obtained. The flow rate u_2 is set equal to zero because the amount of available substrate α_2 is completely added. The fermentation process stops because the substrate concentration C_{S_2} becomes zero and the stop criterion is satisfied. Notice that at the end of the fermentation process the reactor is not completely filled. The reactor volume V at the final time differs from the maximal volume V_{max} or the amount of available substrate α_1 is not completely added. This does not indicate that the optimal control strategy is wrong (first optimization problem) but the determination of α_1 and α_2 is certainly not optimal.

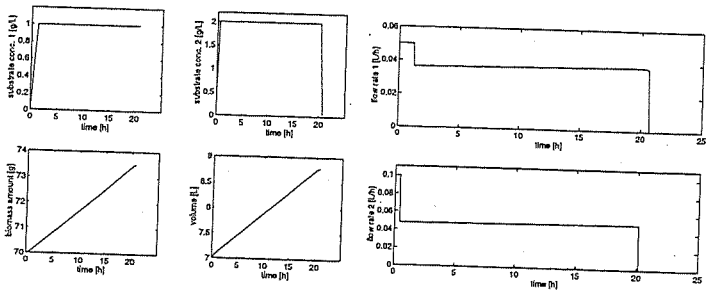


Figure 2.4: Process dynamics for a double Haldane kinetic with a simplified optimal control strategy

Table 2.1 shows the amount of biomass at the end of the process for various combinations of setpoints for the substrate concentration C_{S_1} and C_{S_2}. It is clear that the setpoints $C^*_{S_1}$ and $C^*_{S_2}$ obtained with optimal control theory are resulting in the optimal performance.

C^*_1 [g/L]	C^*_2 [g/L]	Obtained biomass [g]
1	**2**	**73.5238**
0.8	2	73.4748
1	1.8	73.5050
1.2	2	73.4746
1	2.2	73.5090

Table 2.1: Biomass yield as function of the setpoints

2.6.2 Case 2: Haldane/Monod kinetic

Figure 2.5 shows the dynamics of the substrate concentrations C_{S_1} and C_{S_2}, the biomass amount X and the volume V of the liquid in the reactor. The available amount of substrate S_2 α_2 is added initially. Notice that the substrate concentration C_{S_2} decreases during the process. The flow rate u_1 is set maximal untill the singular manifold is reached. The lower part of the figure is a measure of the distance to the singular manifold. Again one can observe that the reactor is not maximal filled at the end of the fermentation. This is not due to a wrong feeding strategy (first optimization problem) but the result of an unappropriate selection of α_1 and α_2. The fermentation process stops because the specific growth rate μ equals zero although not all the available substrate α_1 is added. Table 2.2 shows the obtained biomass

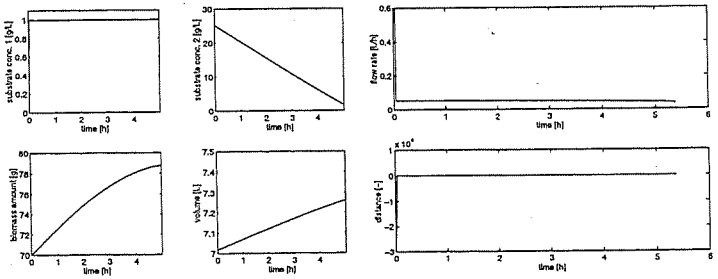


Figure 2.5: Dynamics of the state variables, flow rate and distance to the singular manifold

amount at the end of the fermentation process for 4 cases. In the first case the optimal control strategy is used. The deviation β from the singular manifold is zero. In the second and third case a deviation (-0.1 and 0.1) from the singular manifold is introduced. This illustrates that this manifold results in the optimal performance. In the fourth case the simplified control

Strategy	β	Obtained biomass [g]
Optimal	**0**	**71.70495103318**
Optimal	- 0.1	71.70495103314
Optimal	+ 0.1	71.70495103316
Heuristic	1.0	71.70462942821

Table 2.2: Biomass yield as function of the feeding

strategy, keeping the substrate concentration C_{S_1} on a setpoint (1 g/L), is used. One can observe a small decrease in performance. The simulations for this table have been performed with a large value (300 g/L) of the Monod parameter K_{M_2}. For this value the interaction between the dynamics of the two substrates is increased. Figure 2.6 shows the optimization of the available amounts of substrate α_1 and α_2 (second optimization problem). Again a high value of the Monod parameter is used. α_2 is used a degree of freedom. α_1 is calculated by using the volume constraint.

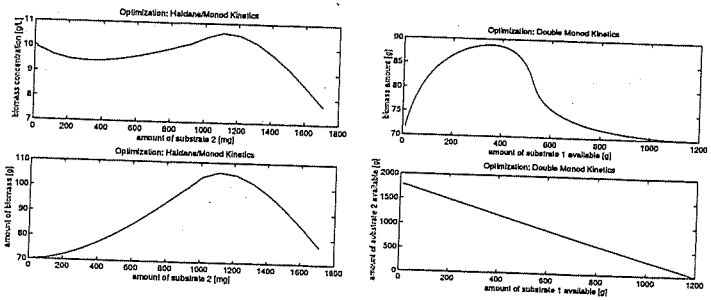


Figure 2.6: Left: Case 2. Upper part: Biomass concentration in function of α_2. Lower part: Biomass amount in function of α_2. Right: Case 3. Upper part: Biomass amount in function of α_1. Lower part: α_2 versus α_1

2.6.3 Case 3: double Monod kinetic

The optimal control strategy is in this case straightforward because the available amount of substrate α_1 and α_2 must be added initially. The process goes on in batch. Recall that the determination of the control strategy is the first optimization problem. A second optimization problem is to determine the optimal values of α_1 and α_2 such that an optimal amount of biomass will be obtained at the end of the fermentation. Figure 2.6 shows the biomass amount at the end of the fermentation in function of α_1. The initial biomass amount is 70 g.

2.7 Conclusions

The optimization of fed-batch fermentation processes with multiple limiting substrates by using optimal control theory is discussed in detail.

It is illustrated that from *qualitative* notion of the kinetics (monoticity or non-monoticity) of the process the optimal control strategy can be derived. Both analytical and simulation results are presented. The obtained results can be considered as an extension of the work described in [Van Impe 1993a].

Two main optimization problems ((i) selection of the optimal feeding strategy and (ii) determination of the optimal amounts of the substrates) are clearly distinguished. Some related optimization problems are also discussed.

Extension of the two step procedure towards fed-batch fermentation processes with multiple limiting substrates is presented. As such from the intrinsically model sensitive optimal control solutions practically implementable nearly optimal control strategies are extracted. It must be emphasized that the optimization problem is clearly separated from the control strategy implementation problem, which fits in the 'divide et impera' strategy used throughout the thesis. Also the optimization problem itself is decomposed into some subproblems.

Chapter 3

Optimization of cyclically operated activated sludge wastewater treatment plants

3.1 Introduction

More stringent environmental regulations require more adequate process control of existing wastewater treatment plants. By combining advanced process control and modern design procedures smaller systems with less investment and operational costs can be built.

The application of modern model based control techniques (e.g., adaptive, neural, fuzzy and predictive control) on carbon and nitrogen removal systems has already been described by several authors ([Busby and Andrews 1975, Beck 1986, Marsili-Libelli 1992, Youssef *et al.* 1995, Haarsma and Keesman 1995, Isaacs 1996]) However, these methods often need a so-called *reference behavior* which is usually not provided.

In this chapter it is illustrated that with *optimal control theory* [Bryson and Ho 1975, Kirk 1970] the reference dynamics can be determined. It must be emphasized that generically the optimal control strategy is model sensitive and as such is not suited for real life implementation. However, the obtained reference dynamics have properties which are model independent. By combining these properties with more robust control techniques a practically implementable control strategy is obtained [Van Impe and Bastin 1995a].

Optimization of multi tank cyclically operated wastewater treatment plants is discussed in this chapter. The following solution strategy is used.

Step 1. The optimal control problem of a ideal single tank system is solved (Section 3.2) for a cost criterion including both the aeration cost and the environmental constraints. The resulting optimal control strategy is presented and illustrated with simulations.

Step 2. It is analyzed which modifications to the resulting optimal control strategy must be made when a cyclically operated system is considered (Section 3.3).

Step 3. The optimal control problem for not cyclically operated multi tank system is formulated and compared with the solution for the ideal single tank system (Section 3.3).

Step 4. With the elements obtained from step 1 to 3 a heuristic, nearly optimal control strategy for two tank cyclically operated wastewater treatment systems is constructed (Section 3.4.1).

Step 5. An extension to three tank systems (UNITANK® systems) is formulated (Section 3.4.2). Some implementation aspects are discussed.

Besides the results obtained for the application under consideration, it is demonstrated how application of optimal control theory reveals important features of the optimal control strategy without explicitly solving the two-point boundary value problems typically encountered when applying the minimum principle of Pontryagin. Moreover, a method for solving optimal control problems for complex interconnected systems is presented. The basic idea of this method is to combine the solutions of simplified optimal control problems in a well motivated manner.

The heuristic nearly optimal control strategy for cyclically operated wastewater treatment is reported in [Ryckaert *et al.* 1996d]. *A detailed description of cyclically operated wastewater treatment systems is presented in Chapter 1. It is shown how the observer based estimator for the respiration rate, discussed in Chapter 6, can be used for on-line implementation of the optimal control strategy.*

The main goal of the chapter is to illustrate that optimal control theory can also be applied for optimization of multi tank cyclically operated systems.

3.2 Optimal control of a single tank system

In this section the optimization of a single tank system for carbon removal is considered in the framework of optimal control theory. In Section 3.2.1 the problem is formulated, in Section 3.2.2 the optimal control solution is derived while in Section 3.2.3 the optimal control solution is summarized.

3.2.1 Problem formulation

Consider a perfectly mixed aerated tank (Figure 3.1) with a constant volume V [L] containing a biomass X (biomass concentration C_X [gMLSS/L]) and a substrate S (substrate concentration C_S [mgCOD/L]) with dynamics described by Equation (3.1). In Chapter 1 this type of process model is found to be suited for simplified description of the biodegradation in wastewater treatment systems [Claes *et al.* 1996a], [Ryckaert *et al.* 1997a]. Notice that the dynamics of the oxygen concentration C_O [mgO_2/L] in the reactor is not modeled here. It is assumed that an appropriate aeration strategy is used such that sufficient oxygen is available for the biodegradation process.

$$\begin{aligned} \frac{dC_X}{dt} &= \mu(C_S)C_X - DC_X \\ \frac{dC_S}{dt} &= -\sigma(C_S)C_X + D(C_{S,in} - C_S) \end{aligned} \tag{3.1}$$

The specific growth rate of the biomass μ [1/h] and the specific substrate degradation rate σ [mgCOD/gMLSS h] are functions of the substrate concentration C_S. The dilution D [1/h] is defined as the flow rate F [L/h] divided by the volume V [L].
An amount of wastewater ξ [L] with substrate concentration $C_{S,in}$ [mgCOD/L] must be degraded in the tank. The question arises whether a clever selection of the wastewater flow rate F (or, equivalently, the dilution rate D) can be found such that the total aeration cost, the amount of substrate in the effluent, and the amount of residual substrate in the tank at the end of the operation ($t = T$) [denoted $C_S(T)$] can be minimized. This can be represented by the following cost criterion:

$$\mathcal{J}[D] = \alpha \int_0^T DC_S dt + \beta \int_0^T (\frac{\mu}{Y_{X/O}} + m)C_X dt + \alpha C_S(T) \tag{3.2}$$

α[\$ L/mgCOD] and β [\$ L/mg O_2] are the unit costs related to the effluent wasted into the environment and to the aeration respectively. T [h] is the duration of the biological degradation. The aeration cost is expressed as the time integral of the total respiration rate OUR [mgO_2/L h], consisting of the endogenous respiration OUR_{end} [mgO_2/L h] and the exogenous respiration OUR_{ex} [mgO_2/L h]. The parameter m [mgO_2/gMLSS h] models the endogenous respiration proportional to the amount of biomass, while the exogenous respiration is proportional to the growth rate μC_X of the biomass with $Y_{X/O}$ [mgO_2/gMLSS] the yield of biomass on oxygen. A model for the oxygen concentration dynamics is given in Chapter 1.

An isoperimetric constraint (3.3) on the dilution rate must be fulfilled stating that the total amount of wastewater ξ [L] must be treated.

$$\int_0^T V \cdot D(t) \cdot dt = \xi \tag{3.3}$$

Notice that here it is assumed that the biomass and substrate in the effluent can be separated. That this separation is realized in a real plant by an additional sedimentation tank is not considered at the moment.

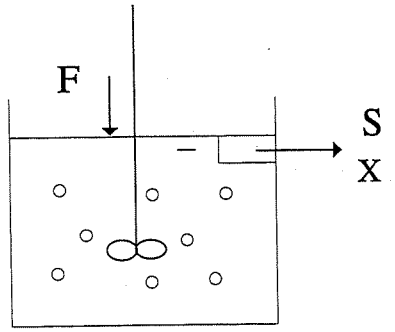


Figure 3.1: Ideal single tank system

3.2.2 Derivation of the optimal control solution

The optimization problem stated above can be solved with optimal control theory. An auxiliary variable κ [L] is introduced which represents the amount of wastewater added in the basin. The dynamics of κ is given below.

$$\frac{d\kappa}{dt} = D(t)V \tag{3.4}$$

Initially κ is equal to zero ($\kappa(0) = 0$). The isoperimetric constraint (3.3) can be rewritten as a terminal constraint on the variable κ ($\kappa(T) = \xi$).

A Hamiltonian function $\mathcal{H}$ is written for this system. The Hamitonian is given by the right-hand side of the dynamic equations of the system multiplied with a costate vector $\boldsymbol{\lambda}$ and the integrand of the cost criterion. With λ_1, λ_2 and λ_3 respectively the costates related to the substrate, biomass and auxiliary variable dynamics, the Hamiltonian $\mathcal{H} = \phi + \psi \cdot D$ is obtained.

$$\phi = -\sigma C_X \lambda_1 + \mu C_X \lambda_2 + \beta(\frac{\mu}{Y_{X/O}} + m)C_X \tag{3.5}$$

$$\psi = (C_{S,in} - C_S)\lambda_1 - C_X \lambda_2 + \lambda_3 V + \alpha C_S \tag{3.6}$$

An important property of optimal control theory states that the Hamiltonian is zero along an optimal trajectory if the final time T is free and the Hamiltonian and the final cost are not explicitly dependent on time. The dynamics of the costate $\boldsymbol{\lambda}$ is given by minus the Jacobian of the Hamiltonian with respect to the state vector $\mathbf{x}$, consisting of the substrate concentration

C_S, biomass concentration C_X and the auxiliary variable κ. σ^{C_S} and μ^{C_S} are respectively the derivative of the specific substrate consumption rate and the specific biomass growth rate with respect to the substrate concentration C_S.

$$\begin{aligned}
\frac{d\lambda_1}{dt} &= \sigma^{C_S} C_X \lambda_1 - \mu^{C_S} C_X \lambda_2 - \beta(\frac{\mu^{C_S}}{Y_{X/O}}) C_X + D \cdot (-\alpha + \lambda_1) \\
\frac{d\lambda_2}{dt} &= \sigma \lambda_1 - \mu \lambda_2 - \beta(\frac{\mu}{Y_{X/O}} + m) + D \cdot \lambda_2 \\
\frac{d\lambda_3}{dt} &= 0
\end{aligned} \tag{3.7}$$

From optimal control theory terminal conditions for the costates λ_1 ($\lambda_1(T) = \alpha$)and λ_2 ($\lambda_2(T) = 0$) are found. Notice that for λ_3 no terminal condition is given because the state variable κ has both an initial and terminal condition.

With the optimal control framework important features of the optimal control trajectory can be deduced.

Stop criterion and the final phase. When the amount of wastewater ξ that must be treated is completely added in the basin, the dilution rate D is set to zero. From the property of the Hamiltonian $\mathcal{H} = 0$ it follows that ϕ (3.5) must be equal to zero. When the terminal conditions on the costates λ_1 and λ_2 are used in the equation $\phi = 0$ the following stop criterion is found.

$$\alpha \cdot \sigma = \beta(\frac{\mu}{Y_{X/O}} + m) \tag{3.8}$$

The degradation is stopped when the aeration cost is equal to the wastewater degradation cost. Notice that during the final phase the dilution rate D and ϕ are zero. From the dynamic equation of λ_2 (3.7) and the terminal condition one can conclude that λ_2 is constant and equal to zero during this phase.

Singular control solution. With optimal control theory one can determine whether the control input D must be set to its minimal value (here zero) or its maximal value D_{max}. This is decided by evaluating the sign of the function ψ. If $\psi < 0$ the control input $D = D_{max}$ is used. If $\psi > 0$ the control input D is set to zero. When ψ equals zero this procedure fails. The following approach is then used. The time derivative of ψ is calculated. It is found that this derivative is independent of the control input D. The second time derivative of ψ is then calculated and set to zero under the constraint that the first time derivative is set equal to zero. From the second time derivative an expression for D is found, which is called the singular control law. The singular control law can only be applied when ϕ (3.5), ψ (3.6) and the first time derivative of ψ are equal to zero.

$$\begin{aligned}
\frac{d\psi}{dt} &= \lambda_1 \sigma^{C_S} C_X (C_{S,in} - C_S) - \lambda_2 (C_{S,in} - C_S) \mu^{C_S} C_X \\
&\quad -\beta(C_{S,in} - C_S) \frac{\mu^{C_S}}{Y_{X/S}} C_X + \beta(\frac{\mu}{Y_{X/S}} + m) C_X - \alpha\sigma C_X
\end{aligned} \tag{3.9}$$

When it is assumed that the final phase is preceded with a singular control phase, then it is clear that the costate λ_2 is constant and equal to zero. The costate λ_1 can be found from the equation ϕ equals zero. When λ_1 and λ_2 are used in the expression for the first time derivative of ψ and the biomass concentration C_X is assumed to be different from zero, the following expression is obtained.

$$\frac{\sigma^{C_S}}{\sigma} \beta(\frac{\mu}{Y_{X/O}} + m) = \beta(\frac{\mu^{C_S}}{Y_{X/O}}) + \frac{-\beta(\frac{\mu}{Y_{X/O}} + m) + \alpha\sigma}{C_{S,in} - C_S} \tag{3.10}$$

From this formula, which is a nonlinear function of the substrate concentration C_S, it can be concluded that the singular control law will keep the substrate concentration C_S on a setpoint C_S^*. This setpoint C_S^* is the solution of Equation (3.10) with respect to the substrate concentration C_S. When the aeration cost is negligible (β zero) this substrate concentration setpoint is zero. All the substrate in the wastewater must be consumed. When the effluent cost is not important (α zero) then a positive substrate concentration is found. When the singular control law is calculated with the procedure stated above via the second time derivative of ψ the following result is found.

$$D = \frac{\sigma C_X}{C_{S,in} - C_S} \tag{3.11}$$

When this control law is used in the dynamic equation for the substrate concentration C_S (3.1) it is clear that this concentration is kept constant. As such one can conclude that the control law (3.11) is indeed a substrate setpoint control law.

Two-point boundary value problems. As stated before with optimal control theory one can decide whether the control input D must be set to its minimal value (zero), its maximal value (D_{max}) or D given by the singular control law, by evaluating the sign of ψ. Notice that ψ is a function of both the state vector $\mathbf{x}$ and the costate vector $\boldsymbol{\lambda}$. For the substrate and biomass concentration only initial conditions are given while for the auxiliary variable κ both an initial and terminal condition is given. For the costates λ_1 and λ_2 only terminal conditions are given while for the costate λ_3 no condition is specified. This problem is known as the two-point boundary value problem, which can be solved numerically. It must be emphasized that a numerical approach is rejected here because this results in model sensitive results.

Although the two-point boundary value problem is not solved for the problem under consideration it is clear that optimal control theory provides two important features (stop criterion and the singular control law) of the optimal control strategy. In fact optimal control provides the key elements for building the optimal control strategy. This indicates that the optimal control framework is indeed a powerful tool in the optimization of processes

although its intrinsic implementation problems. It constrains the solution space considerably. The actual solution is then found by combining the key elements with process knowledge.

3.2.3 Optimal control solution

The application of optimal control theory to the problem formulated above results in the following control strategy.

- **Step 1.** Bring the substrate concentration to the setpoint, calculated with Equation (3.10), by using the maximal or minimal flow rate F, depending on the initial substrate concentration $C_S(0)$. If $C_S(0)$ is smaller then C_S^*, then $F = F_{max}$. If $C_S(0)$ is larger then C_S^*, then $F = 0$.
- **Step 2.** Keep the substrate concentration constant at the setpoint by using the control law (3.11).
- **Step 3.** When the total dose ξ is injected, continue the biodegradation until the substrate concentration, solution of Equation (3.8), is obtained. Equation (3.8) states that the biodegradation is stopped when the unit cost for aeration is equal to the unit cost related to the amount of remaining substrate in the tank.

As a conclusion, it can be stated that optimal control theory provides an expression for (i) the optimal substrate concentration setpoint and (ii) the substrate concentration at the end of the biodegradation process. As such the key elements for construction of the complete optimal control strategy are obtained.

It must be emphasized that the suggested control strategy is only feasible when the substrate concentration setpoint C^* is lower than the constraints given by environmental legislation. However, when this is the case still substrate setpoint control is the optimal solution.

3.2.4 Simulations

Figure 3.2 shows the dynamics of the process state $\mathbf{x}$ (the substrate and biomass concentration and the amount of wastewater added in the basin), the evolution of the different contributions of the cost (aeration cost and the cost due to effluent disposal), the total cost (including the cost related to the substrate amount in the basin), the dilution rate D and the specific dilution rate (dilution rate divided by the biomass concentration) when the control strategy, keeping the substrate concentration constant at a certain setpoint, is used. The model parameters, used for the simulation, are given in Appendix D. The specific biomass growth $\mu(C_S)$ rate is described by the Monod law while the specific substrate consumption rate $\sigma(C_S)$ is assumed to be linearly related to the specific growth rate. Maintenance is neglected.

It must be emphasized that these assumptions are only specified because they are used for simulation. During derivation of the optimal control strategy no kinetic model is used. The substrate concentration setpoint for C_S, used in the simulation, is 1 kg/m^3. This arbitrary value is chosen for reasons of presentation.

This value differs from the optimal value, which is equal to 0.1504 kg/m^3. The maximal value for the flow rate F_{max} is taken high enough such that the substrate setpoint is reached within an acceptable time.

In Figure 3.3 the total cost, the aeration cost, the effluent cost and the optimal degradation time in function of the substrate concentration setpoint are indicated. It can be observed that indeed an optimal substrate concentration C_S^* is found. This optimal value is the one which can be found with Formula (3.10).

In Figure 3.4 the comparison is made between an optimal feeding pattern (full line) and a constant feeding rate (dashed-dotted line). The constant feeding rate is chosen such that the total doses is added at the same time as in the optimal case. One can notice that the aeration cost looks quite similar (the optimal feeding pattern has a greater aeration cost), while the effluent cost is significantly lower with the optimal control law. When the total cost (including the residual substrate in the basin) is evaluated it can be observed, that a (slightly) lower cost is obtained with the optimal control strategy. Notice that the amount of performance improvement depends on the model parameters. Notice that in simulation indeed the optimal setpoint can be determined. Practically due to the uncertainty on the kinetics this is not feasible. However, the most important conclusion of the optimal control analysis is that optimal performance is obtained with substrate setpoint control. With trial and error an appropriate setpoint can be obtained. When model knowledge is available, the substrate concentration setpoint C_S^* obtained with Formula (3.10), can serve as initial guess.

3.3 Optimal control of complex systems

The optimal control strategy for the single tank system (Section 3.2) serves as a starting point for the development of a control strategy for cyclically operated wastewater treatment systems. In this section the optimal control strategies for more complex configurations are presented, which will motivate the control strategy for the full scale cyclically operated treatment plant. In Section 3.3.1 the impact of a constraint on one of the state variables is examined. The constraint is due to the condition that a cyclic operation of the single tank system (and later of the full scale system) must be considered. In Section 3.3.2 the optimal control problem of a cascade of an aeration and a sedimentation tank is considered while in Section 3.3.3 the cascade of two aeration tanks is discussed.

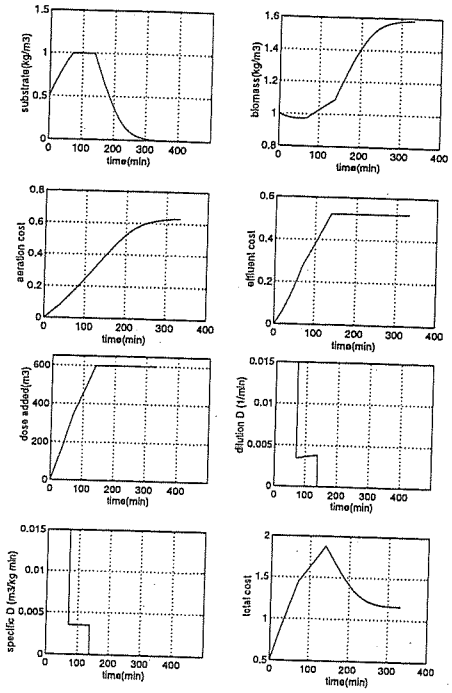


Figure 3.2: Optimal control evolution. Dynamics of the substrate and biomass concentration C_S, C_X, the aeration and effluent cost (without final cost), the dose of substrate added κ, the dilution rate D, the specific dilution rate and the total cost $\mathcal{J}$

3.3.1 Optimal control solution for a single tank system with partially fixed state

The previous result gives the optimal control strategy and the optimal time for degradation of a certain dose of wastewater ξ. A cyclic operation of the process in this single tank system (Figure 3.1) can now be considered. When the dose ξ is degraded, a next dose can be processed. Suppose that after the degradation, the aeration and stirring are switched off for a certain time such that the biomass can settle in the basin. Suppose that a perfect separation of biomass and substrate takes place. The biomass concentration can then be brought back to the initial biomass concentration by wasting some sludge without altering the substrate concentration. Notice that here it is assumed

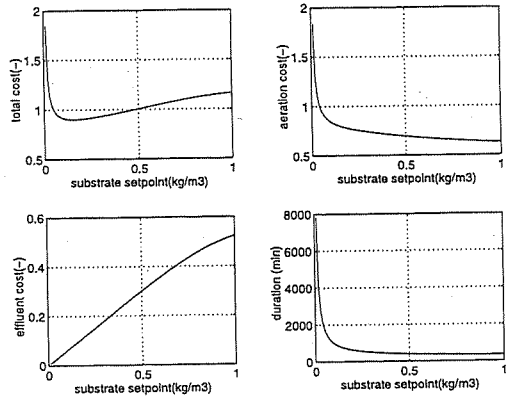


Figure 3.3: Optimization of the substrate concentration setpoint C_S^*. Total, aeration and effluent cost and the duration of the biodegradation T as function of the substrate concentration setpoint C_S^*

that the biomass concentration is increasing during the operation.

A cyclic operation is only feasible when the terminal substrate concentration is equal to the initial substrate concentration. This constraint modifies the end phase of the degradation process. Notice that the initial (terminal) substrate concentration can never be higher than the substrate setpoint, used during the singular phase. The singular phase is not altered by adding the conditions on the initial and terminal substrate concentration. The initial biomass and substrate concentration can now be optimized such that a minimal cost is obtained.

Due to the periodic setting it makes no sense to add a terminal cost in the cost criterion. It is found that in this case the singular substrate concentration is the optimal value for the optimal initial (terminal) substrate concentration. This indicates that the treatment process stops when the dose ξ is added. Notice that this approach is the only feasible solution, which is satisfying the relation ϕ equal to zero. Recall that in this case both λ_1 and λ_2 are equal to zero. The terminal condition states that the aeration cost must be made zero. There is no substrate concentration for which this condition can be fulfilled, so the only solution is to stop the process by switching the aeration off (β zero).

Figure 3.5 shows that the cost criterion (without terminal cost) is minimized when the initial (terminal) substrate concentration equals the substrate concentration setpoint C_S^* found with Formula (3.10) is used. The same parameters values as in the previous section are used (Appendix D).

It is proven below that the cost criterion (without terminal cost) is in-

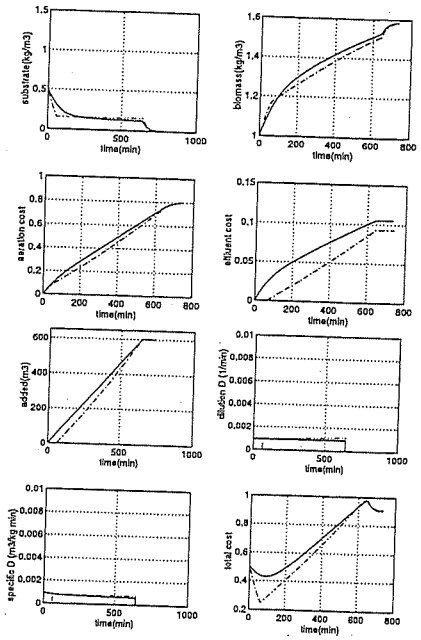


Figure 3.4: Comparison optimal control strategy (dashed-dotted line) and constant feed rate (full line). Dynamics of the substrate and biomass concentration C_S, C_X, the aeration and effluent disposal cost (without the final cost), the dose of substrate added κ, dilution D and specific dilution rate and the total cost (including final cost) $\mathcal{J}$

dependent of the initial biomass concentration. The cost criterion (3.12) is proportional with the time integral of the biomass concentration evolution. The proportionality constant k_1 and k_2 are independent from the initial biomass concentration. From the condition (3.13) that the dose ξ must be treated, it follows that the time integral of the biomass concentration is constant and independent of the initial biomass concentration.

$$\begin{aligned} \mathcal{J}(C_X(0)) &= \int_0^T (DC_S + \beta(\frac{\mu(C_S)}{Y_{X/O}} + m)C_X)dt \\ &= \int_0^T (\frac{\sigma(C_S^*)C_X}{C_{S,in} - C_S^*}C_S^* + \beta(\frac{\mu(C_S^*)}{Y_{X/O}} + m)C_X)dt \qquad (3.12) \\ &= \int_0^T k_1 C_X dt \end{aligned}$$

$$\int_0^T D(t)V dt = \int_0^T \frac{\sigma(C_S^*)C_X}{C_{S,in} - C_S^*}V dt = \int_0^T k_2 C_X dt = \xi \qquad (3.13)$$

Combination of these equations shows that the cost criterion is indeed independent of the biomass concentration evolution and thus independent of the initial biomass concentration, which is confirmed by simulations. From the

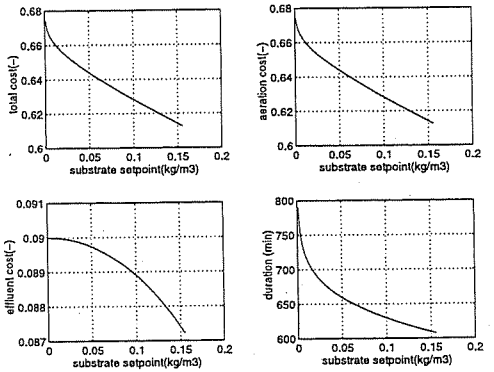


Figure 3.5: Optimization of the initial state in a cyclically operated ideal single tank system. Total, aeration and effluent disposal cost and duration of the biodegradation T as function of the initial substrate concentration $C_S(0)$.

facts deduced above some remarks on the design (selection of the constant volume V [L]) of the tank can be made. The optimal substrate setpoint C_S^* can be determined if the parameters of the kinetic model (for instance μ_{max}, K_S when the Monod law is used), the yield coefficient $Y_{X/S}$, the parameters related to the aeration model $Y_{X/O}$, m and the unit costs for aeration and effluent disposal α, β are known.

This setpoint is independent of the volume V. Suppose that the degradation time T is fixed due to external conditions. When the initial biomass concentration is given, the dilution rate D (or the flow rate F) is known. In the problem formulation the treatment of a dose ξ [L] is discussed. In practice however the constraint (3.15) must be fulfilled which states that the amount of wastewater treated in one cycle with duration T must be equal to the amount of wastewater provided to the treatment system during this time. The duration of sedimentation process is considered to be negligible here. Extension of the formulas for non-zero duration of the sedimentation process are however straightforward.

Consider the configuration of Figure 3.6. F_{in} [L/h] is the flow rate of wastewater entering a buffer tank. $\Gamma(C_S^*)$ is a nonlinear function of the substrate concentration setpoint C_S^* and independent of the volume V.

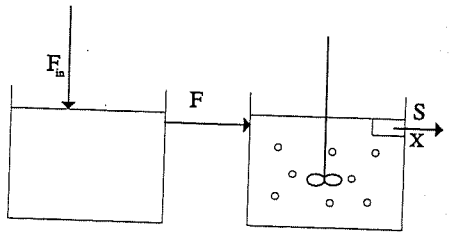


Figure 3.6: Cascade of a buffer tank with an ideal single tank system

$$\Gamma(C_S^*) = \frac{\sigma(C_S^*)}{C_{S,in} - C_S^*} \tag{3.14}$$

$$V \int_0^T D(C_X(0))dt = V\Gamma(C_S^*) \int_0^T C_X(t)dt = F_{in} \cdot T \tag{3.15}$$

Recall that the purpose of the optimization problem under consideration is to determine the dilution rate D (or equivalently the flow rate F) of the wastewater from the buffer tank into the treatment system such that the cost criterion $\mathcal{J}$ is minimized. In practice often F_{in}, the flow rate of the receiving wastewater, is used. Of course the constraint (3.15) must be fulfilled. In fact the results of the optimization problem indicate that process performance can be optimized when the buffer tank is used as additional dynamical unit. The volume of the liquid in the buffertank is assumed to be time-varying. By using the capacity of the buffer tank the flow rate F_{in} is shaped into an optimal profile F. The constraint (3.15) can be used as design formula. When the constraint is not fulfilled, the biomass load can be adapted or the volume V of the basin must be changed. The adaptation of the biomass load is of course limited. On the other hand this option can be changed during operation while the volume V is determined during the design phase and remains fixed.

One can conclude that the following design procedure can be used. From the parameters of the model and the unit costs for aeration and effluent disposal the optimal substrate setpoint C_S^* (and the corresponding parameter $\Gamma(C_S^*)$) is determined. The volume V is determined with the following formula.

$$V = \frac{F_{in}}{\Gamma(C_S^*)\dfrac{\int_0^T C_X(t)dt}{T}} \tag{3.16}$$

In the formula for the volume V the maximal allowable average biomass concentration is used. If during the course of the operation the load of the system is lowered (lower F_{in}), then the average biomass concentration can be modified. This formula can be compared with a standard steady state design formula. With this formula the volume is calculated under the assumption that the substrate degradation takes place at the highest

possible rate. η [-] is a correction factor which (i) takes into account that the degradation does not go on at the maximal degradation rate and (ii) is used for introducing some safety margins.

$$V = \eta \frac{F_{in} C_{S,in}}{\sigma_{max} \dfrac{\int_0^T C_X(t)dt}{T}} = \eta \frac{F_{in}}{\dfrac{\sigma_{max}}{C_{S,in}} \dfrac{\int_0^T C_X(t)dt}{T}} \tag{3.17}$$

One can observe that the optimal volume (3.16) has a similar structure as the volume calculated with the standard steady state formula (3.17). The factor $\Gamma(C_S^*)$ takes into account the dependency of the substrate degradation rate σ on the substrate concentration and the effect of transport. Note that the substrate concentration must not be reduced till zero but till the substrate concentration C_S^* is obtained. Moreover via the substrate concentration setpoint C_S^* the optimization of the cost criterion $\mathcal{J}$ is explicitly taken into account.

3.3.2 Optimal control solution for a combined aerator and sedimentation tank

In the ideal single tank system the separation of the biomass and substrate in the effluent is assumed. In a wastewater treatment plant the aeration basins are placed in cascade with a sedimentation tank, in which the separation of the biomass and the effluent takes place (Figure 3.7). This fact introduces additional dynamics (the dynamics of the sedimentation tank) into the problem formulation and requires a formulation of the cost criterion in terms of the substrate concentration of the sedimentation tank. The combined system is described by model (3.18). Notice that the effluent contains no biomass when the sedimentation process is perfect. A buffer tank, although not explicitly drawn, is assumed to be available.

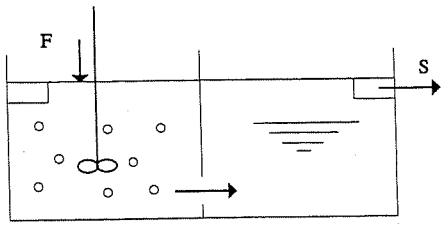


Figure 3.7: Cascade of an aeration and sedimentation tank

$$\begin{aligned}
\frac{dC_{S_1}}{dt} &= -\sigma(C_{S_1})C_{X_1} + D(C_{S,in} - C_{S_1}) \\
\frac{dC_{X_1}}{dt} &= \mu(C_{S_1})C_{X_1} - DC_{X_1} \\
\frac{dC_{S_2}}{dt} &= D(C_{S_1} - C_{S_2}) \\
\frac{dC_{X_2}}{dt} &= DC_{X_1}
\end{aligned} \tag{3.18}$$

C_{S_1} and C_{S_2} [mgCOD/L] are respectively the substrate concentrations in the aeration and sedimentation tank while C_{X_1} and C_{X_2} [gMLSS/L] are the biomass concentrations in these basins. The sedimentation tank is modeled as a perfect settler. There is no biomass in the effluent stream. The biomass is accumulating in the sedimentation tank.

The cost criterion is given by Equation (3.19) with T the (free) duration of the process.

$$\mathcal{J}[D] = \alpha \int_0^T DC_{S_2}dt + \beta \int_0^T (\frac{\mu(C_{S_1})}{Y_{X/O}} + m)C_{X_1} + \alpha(C_{S_1}(T) + C_{S_2}(T)) \tag{3.19}$$

Notice that the cost due to the effluent is now expressed in terms of the substrate concentration of the sedimentation tank. The substrate concentrations at the end of the process of both tanks is taken into consideration.

The optimal control strategy can be derived in a similar way as in Section 3.2.1. The same stop criterion (3.8) and the same Formula (3.10) for the optimal substrate concentration setpoint C_S^* are found.

It can be concluded that although additional dynamics are added and a modified cost criterion is used the same results as for a single tank system are obtained.

3.3.3 Optimal control solution for a combination of two aerators

In this section the optimal control problem for a combination of two aerators in cascade is analyzed. A theorem is presented which enables a well-motivated reduction of the complexity of the optimal control problem.

The system, consisting of two aeration tanks in cascade, is described with the model (3:20) given below. Consider the configuration depicted in Figure 3.8. Notice that (i) the second tank is now stirred and aerated, (ii) there is biomass outflow via the effluent and (iii) there is direct influent addition in both tanks. A buffertank, although not explicitly drawn, is

assumed to be available.

$$\begin{aligned}
\frac{dC_{S_1}}{dt} &= -\sigma(C_{S_1})C_{X_1} + D_1(C_{S,in} - C_{S_1}) \\
\frac{dC_{X_1}}{dt} &= \mu(C_{S_1})C_{X_1} - D_1C_{X_1} \\
\frac{dC_{S_2}}{dt} &= -\sigma(C_{S_2})C_{X_2} + D_2C_{S,in} + D_1C_{S_1} - (D_1 + D_2)C_{S_2} \\
&= -\sigma(C_{S_2})C_{X_2} + D_2(C_{S,in} - C_{S_2}) + D_1(C_{S_1} - C_{S_2}) \\
\frac{dC_{X_2}}{dt} &= \mu(C_{S_2})C_{X_2} + D_1C_{X_1} - (D_1 + D_2)C_{X_2} \\
&= \mu(C_{S_2})C_{X_2} - D_2C_{X_2} + D_1(C_{X_1} - C_{X_2})
\end{aligned} \tag{3.20}$$

C_{S_1} and C_{S_2} [mgCOD/L] are respectively the substrate concentrations in the first and second tank of the cascade. C_{X_1} and C_{X_2} [gMLSS/L] are respectively the biomass concentrations in the first and second tank of the cascade. μ [1/h] and σ [1/h] are the specific biomass growth rate and specific substrate consumption rate. It is assumed that these rates are modeled with the same nonlinear functions for both tanks. Notice that this is a reasonable assumption because in both tanks the same biomass and substrate is used. D_1 (F_1) and D_2 (F_2) [1/h] ([m^3/h]) are the dilution (flow) rates for the first and second tank respectively. Suppose that the following cost criterion must be optimized:

$$\begin{aligned}
\mathcal{J}[D_1, D_2] &= \alpha \int_0^T (D_1 + D_2)C_{S_2}dt + \alpha(C_{S_1}(T) + C_{S_2}(T)) \\
&+ \beta \int_0^T ((\frac{\mu(C_{S_1})}{Y_{X/O}} + m)C_{X_1} + (\frac{\mu(C_{S_2})}{Y_{X/O}} + m)C_{X_2})dt
\end{aligned} \tag{3.21}$$

The total cost is due to the substrate C_{S_2} in the effluent of tank 2, the aeration of both basins and the amount of substrate in both tanks at the end of the biodegradation process. Suppose that first the optimization of the first tank of the cascade with respect to the cost criterion $\mathcal{J}_1[D_1]$ (3.22) is considered. The model for this first tank is given by the first two equations of the model (3.20).

$$\mathcal{J}_1[D_1] = \alpha \int_0^T D_1C_{S_1}dt + \beta \int_0^T (\frac{\mu(C_{S_1})}{Y_{X/O}} + m)C_{X_1} + \alpha C_{S_1}(T) \tag{3.22}$$

In Section 3.2 it is shown that optimal performance is obtained when the substrate concentration C_{S_1} is kept constant at a setpoint C_S^*. Let D_1^* be the control law which achieves this objective.

Suppose that for the optimization of the second tank of the cascade the influence of the first tank is neglected. The dynamics in the second tank is then described with the same model as for the first tank with a similar cost criterion (3.22) (only the subscripts must be altered). It is trivial that in this case the same optimal control strategy is found, thus, keeping the

substrate concentration C_{S_2} constant at the setpoint C_S^*. Let D_2^s be the control law which realized this objective. The following theorem can then be formulated.

> When (i) the initial biomass concentrations $C_{X_1}(0)$ and $C_{X_2}(0)$ are equal for both tanks, (ii) the initial substrate concentration $C_{S_1}(0)$ and $C_{S_2}(0)$ are optimized (and thus equal to the optimal substrate setpoint C_S^*) and (iii) the optimal control laws D_1^s and D_2^s are used then the optimization of both tanks separately with respect to their cost criterion and neglecting interactions is equal to the combined optimization of the cascade without neglecting interactions.

This is proven as follows. When the initial biomass concentrations are equal then the biomass concentrations $C_{X_1}(t)$ and $C_{X_2}(t)$ and the applied dilution rates $D_1(t)$ and $D_2(t)$ are equal for all time instances. The sum of the two cost criteria $\mathcal{J}_1$ and $\mathcal{J}_2$ is then equal to the cost criterion $\mathcal{J}[D_1, D_2]$. When now these two controlled tanks are placed in cascade, physically the dynamics will not change because the interactions due to transport are zero.

From this theorem it can be concluded that under the constraint that the same strategy must be used for both tanks it follows that the same strategy as for a single tank system can be used. This theorem does not indicate that this control strategy is optimal for the cascade of the two aeration tanks.

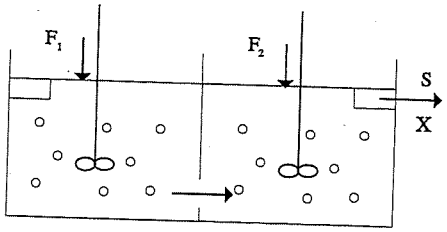


Figure 3.8: Cascade of two aeration tanks

3.4 Optimization of cyclically operated multi tank systems

Nearly optimal control strategies for cyclically operated wastewater treatment systems with multiple tanks, discussed in Chapter 1, are now determined. Notice that an exact optimal control solution for these configurations can only be found numerically as two-point boundary value problems must be solved. Because the resulting optimal control solution is model sensitive, this approach is rejected.

Combination of the optimal control solutions for (i) the ideal single tank system (including the cyclically operated case), and (ii) the cascade of aeration and sedimentation tank, results in an optimal control solution for a two tank cyclically operated treatment plant (Section 3.4.1).

A nearly optimal control strategy for a three tank cyclically operated treatment plant and the on-line implementation are shortly presented in Section 3.4.2.

3.4.1 Two tank systems

In Section 3.3.1 the single tank treatment system is made cyclically in a rather artificial way. Notice that in this system the separation of the effluent and the sludge is not realized. Moreover it is assumed that the biomass concentration can be brought back to its initial concentration by wasting some sludge. This is only feasible if during the treatment process the biomass concentration increases. In Section 3.3.2 it is shown that the use of a sedimentation tank in series with an aeration tank does not change the optimal control solution. In Section 3.3.2 cyclic operation of this configuration is not discussed.

From the results obtained in Section 3.3.1 and 3.3.2 an optimal control strategy for a two tank cyclically operated system can be determined (Figure 3.9). The system consists of two tanks. The function of each tank can

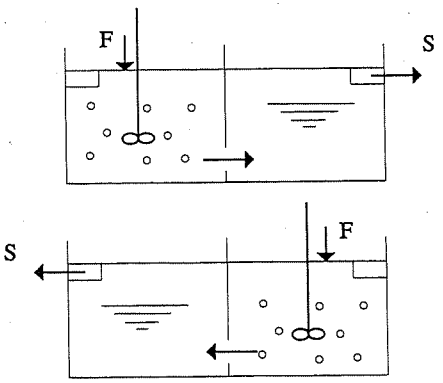


Figure 3.9: Cyclically operated two tank system

switch between *aeration* and *sedimentation mode*. During the first main phase (Figure 3.9, top) the first tank is fed with influent and is in aeration mode. The second tank is used as sedimentation tank. During the second main phase (Figure 3.9, bottom) the operation of the tanks is reversed. The influent is then fed in the second tank. Between the main phases there is a

short intermediate phase, preparing the appropriate tank for sedimentation. A buffertank is assumed to be available.

The optimal control strategy for this configuration is now determined.

Main phases. It is clear that when one main phase is considered the problem formulation is exactly the one treated in Section 3.3.2. The influent flow rate F or the dilution rate D keeps the substrate concentration in the aeration tank on the substrate concentration setpoint C_S^*, obtained with Formula (3.10). When the substrate concentration in the sedimentation tank and the aeration tank are initially equal to this setpoint, then the substrate concentrations in both tanks remain equal and constant during the main phase.

Cyclic operation. Suppose that the biomass concentration in the aeration tank and sedimentation tank are initially equal to some value C_X^*.

Notice that in this configuration indeed a separation between the effluent and the sludge is realized. From the dynamical equation of the biomass concentration in the sedimentation tank one can conclude that the biomass accumulates in this basin. After a certain time T the main phase must be stopped because the biomass concentration in the sedimentation tank is too high, resulting in a failure of the sedimentation process.

During the intermediate phase the aeration tank is prepared for sedimentation. The aerator and stirrer are switched off. The biomass is settling. The biomass concentration in the sedimentation tank can be brought to the value C_X^* by wasting some sludge. Notice that this is feasible due to the biomass accumulation in this tank. When the settling operation is perfect, the substrate concentration is not changed.

The function of the two tanks is now reversed. The influent flow in the second tank keeps the substrate concentration on the setpoint C_S^*. Because the substrate concentration in the first tank is already equal to this setpoint, the concentration in this tank is also constant. The biomass is now accumulated in the first tank.

It is clear that after a transient a cyclic operation of this two tank configuration is obtained. The substrate concentrations in both tanks remain constant and equal to optimal setpoint C_S^* during the operation. The biomass concentration of each tank is after two main phases set equal to the value C_X^*.

3.4.2 Three tank systems

A nearly optimal control strategy for three tank systems and some implementation aspects are now discussed.

Nearly optimal control strategy. A straightforward extension of the optimal control solution for two tank systems to three tank systems, discussed in Chapter 1, is based on the Theorem of Section 3.3.3. The substrate concentration in each aeration basin is kept constant. The controlled inputs are the influent flow rates F_1, F_2 to each aeration tank (Figure 3.8). The

buffertank is exploited as dynamical unit. Recall that in the original process description (Chapter 1) only the first tank is fed. Practical implementation of this control strategy is now shortly discussed. Because advanced model based control of a biological wastewater treatment plant is only possible when measurements of the actual biological state are available on-line, or can be estimated out of on-line measurements, an advanced monitoring system is constructed.

Advanced monitoring system. The monitoring and sampling system is designed to provide both fast and slow measurements in a cost effective way. An oxygen probe is installed in a fastloop, connected to all the tanks of the wastewater treatment system. In this way on-line information is available with a limited set of hardware sensors. In addition to the fastloop, two extra reactors, one equipped with an oxygen probe, are provided. These reactors can be filled with sludge and wastewater of the system. In this way the exogenous and endogenous respiration of the installation can be measured. Methods for determination of the substrate concentration in the influent and in the tanks are implemented. Also influent toxicity tests can be performed. These tests are slower than the measurements provided by the fastloop. The data obtained here are useful for correction of estimation and control algorithms.

Implementation of the control strategy. Direct implementation of the control law (3.11) would require on-line measurements of the substrate and biomass concentration and full knowledge of the kinetics (structure and parameters). The control goal can however be reformulated in terms of respiration. The optimal control strategy keeps the specific exogenous respiration on a constant level. For the outer biodegradation tanks of UNITANK® systems the control law is approximated by (3.23). For the middle biodegradation tank some additional transport terms are required.

$$D = \frac{\sigma C_X}{C_{S,in} - C_S} \approx K \frac{OUR_{ex}}{C_{S,in}} \tag{3.23}$$

OUR_{ex} is the exogenous respiration in the tank. $C_{S,in}$ is the influent substrate concentration. K is a proportionality constant, which is a function of yield parameters. The monitoring and sampling system provides the required measurements. Out of the oxygen measurements in the fast-loop the total respiration OUR in the tanks can be estimated by observer based estimation algorithms [Ryckaert *et al.* 1995] (Chapter 6). When the endogenous respiration OUR_{end} is known, the exogenous respiration can be found. The dynamics of the endogenous respiration can be predicted by the model and periodically be updated by a measurement provided by the measurement system. An extra measurement of the total respiration, also obtained with the sampling and monitoring system, can be used to check the values, estimated by the observers. Also the substrate concentration in the biodegradation tanks and the influent concentration $C_{S,in}$ can be determined by the measurement system and gives indications whether the overall

control system is performing appropriately, thus keeping the substrate concentration around the setpoint.

Detailed model based analysis of the UNITANK® systems in [Ryckaert *et al.* 1997a] (Chapter 1) reveals that the load in the tanks of these systems is quite time-varying when a constant feed rate is applied. The model based control law, obtained with optimal control theory, keeps the load constant by shaping the given influent feed rate and exploiting the dynamics of the buffer tank. This enables a more critical, optimal (but still safe) loading of the installation.

3.5 Conclusions

It is illustrated how *optimal control theory* provides the *reference behavior*, essential for other nonlinear controller design techniques.

A nearly optimal control strategy for cyclically operated wastewater treatment systems for carbon removal is determined. A rather straightforward on-line implementation of the optimal control strategy with an advanced sampling and monitoring system and observer based estimators is presented.

The optimal control problem of these complex systems is decomposed into simplified optimal control problems in a well motivated way.

Determining first the optimal control strategy for an ideal single tank system is the key idea of the approach. It is then evaluated how an increase in complexity of the configuration affects the optimal control solution. Such an evaluation is only feasible as long as the optimal control solution is analytically tractable. When this is not the case for a certain degree of complexity, a well motivated approximation of the optimal control strategy is determined.

Optimization of a multi tank cyclically operated wastewater treatment system with optimal control theory is presented. It must be emphasized that the approach results in a nearly optimal control strategy and does not require detailed knowledge of the process model. The determination of the control strategy is clearly separated from the implementation aspects (divide et impera strategy). The solution of the optimization problem is also found by using a well motivated problem decomposition.

Part III

Monitoring of biotechnological processes

Chapter 4

State and parameter estimation of bioprocess models

4.1 Introduction

The application of modern model based control techniques to biotechnological processes -such as biological wastewater treatment and fermentation processes- is hampered due to the lack of reliable, accurate and cheap on-line sensors. This problem can be relaxed by using *software sensors*.

A software sensor is a (parameter and/or state) estimation algorithm, based on (i) a *model* of the process, and (ii) available *on-line measurements*. The following question can then be stated.

Given a measurement set (hardware sensors) and additional knowledge about the system (model structure and some model parameters), which unmeasured state variables and model parameters can be extracted?

Analysis of the *observability* of the unmeasured states and the *identifiability* of the unknown model parameters is the first step one must consider when designing software sensors.

In Appendix A a general dynamical model for biotechnological processes, software sensors based on this model, reparameterizations and model transformations are introduced. These methods are adopted from the work of Bastin and Dochain (1990).

In Section 4.2 the observability and identifiability analysis of the prototype model of Chapter 0, is performed for the class of estimation algorithms, discussed in Appendix A. The analysis is performed in the context of activated sludge wastewater treatment plants for carbon removal.

In Section 4.3 the observability of the states of a nitrogen removal activated sludge wastewater treatment plant when using the *oxydo reduction potential* as on-line measurement is discussed.

Notice that in Section 4.2 a general analysis (different measurement sets and assumed a priori knowledge) of the prototype model is considered while in Section 4.3 a particular problem (on-line redox potential measurement and full model knowledge available) is discussed.

Some general conclusions on the observability and identifiability analysis are drawn in Section 4.4.

The observability and identifiability analysis of the prototype model is reported in [Ryckaert and Van Impe 1997b].

Modeling of activated sludge wastewater treatment plants for carbon removal is discussed in Chapter 1. Also the nitrogen removal process is shortly introduced. Observability and identifiability analysis, discussed here, is a first step in software sensor design. Chapter 5 and 6 deal with performance analysis of software sensors and methods for optimal tuning of these algorithms respectively.

The main goal of the chapter is to illustrate that observability and identifiability analysis is not just an evaluation of some mathematical properties but provides a framework for data interpretation with direct practical use. The minimum modeling concept, stating that the model must not be completely specified, makes the analysis feasible also for bioprocesses.

4.2 Observability and identifiability analysis of the prototype model

In Section 4.2.1 the (state) observability and (parameter) identifiability problem is formulated for the prototype model, introduced in Chapter 0.

In Section 4.2.2 the transformations in Appendix A are applied on the prototype model. State observation, observer based parameter and least squares estimation are presented in Sections 4.2.3, 4.2.4 and 4.2.5 respectively. Design of estimators based on reparameterizations of the prototype model is discussed in Section 4.2.6.

The results have been summarized and interpreted in the context of (cyclically operated) activated sludge wastewater treatment systems in Section 4.2.7.

4.2.1 Problem statement

The prototype model of Chapter 0 describes the basic dynamics of an aerobic carbon removal wastewater treatment system. For analysis of the observ-

ability and identifiability the prototype model is reformulated and simplified. This results in the following model.

$$\begin{array}{rcl} \frac{dC_S}{dt} &=& k_1 \cdot \mu C_X + D \cdot (C_{S,in} - C_S) \\ \frac{dC_X}{dt} &=& \mu C_X + D \cdot (C_{X,in} - C_X) \\ \frac{dC_O}{dt} &=& k_3 \cdot \mu C_X + k_L a \cdot (C_{SAT} - C_O) \end{array} \tag{4.1}$$

k_1 [mgCOD/gMLSS] and k_3 [mgO_2/gMLSS] are minus the inverse of the yield of biomass on substrate and biomass on oxygen respectively.

The inflow of biomass in the tank models (i) the recycle stream often encountered in a classical treatment plant, or (ii) transport between a cascade of biodegradation tanks.

Notice that in the model only exogenous metabolism and exogenous respiration is assumed to be relevant.

Outflow of oxygen is neglected, which can be motivated for the cyclically operated treatment plants under consideration because due to non-complete mixing of the tanks the oxygen concentration at the outlet of the tank is approximately zero.

The general (state) observability and (parameter) identifiability problem of Section 4.1 is now reformulated for this model.

Which states (C_S, C_X, C_O) and which parameters (k_1, k_2 and μ) can be estimated if a certain state, or a combination of states, and additional parameters are known?

Notice that in certain cases $\mu(C_S)$ is considered to be a (time varying unknown) parameter. This follows from a *minimal modeling principle* [Bastin and Dochain 1990] which states that parts of the system with high uncertainty (the kinetics) are treated as parameters.

4.2.2 Transformations

The prototype model used here can be rewritten in the matrix form of the general dynamical model for biotechnological processes (Appendix A).

For the model under consideration the rank of $\mathbf{K}$ is equal to one, so the state ξ_a is one state variable. Three possibilities can be considered. For the observability and identifiability analysis performed here, the model must be rewritten in terms of the state z (dynamics independent of the kinetics) and the measurable state ξ_m. This is illustrated below when the oxygen concentration C_O is considered to be measurable on-line. By a detailed analysis of the several transformations and the resulting process models, conclusions about the measurability of the system can be drawn under various assumptions concerning the knowledge of the parameters and

availability of on-line measurements.

$$\xi = \begin{pmatrix} C_S \\ C_X \\ C_O \end{pmatrix} \quad \mathbf{K} = \begin{pmatrix} k1 \\ 1 \\ k3 \end{pmatrix} \quad \varphi = \mu C_X \tag{4.2}$$

$$\mathbf{f} = \begin{pmatrix} DC_{S,in} \\ DC_{X,in} \\ k_L a C_{SAT} \end{pmatrix} \quad \mathbf{D} = \begin{pmatrix} D & 0 & 0 \\ 0 & D & 0 \\ 0 & 0 & k_L a \end{pmatrix} \tag{4.3}$$

Three possible transformations can be considered depending whether the substrate, biomass or oxygen concentration is assumed to be on-line measured.

A two step approach is used. First the model is transformed to a model, involving ξ_a and second to a model, involving the measured state ξ_m. Recall that these models are discussed in Appendix A. Only the result for the three cases are stated.

- Transformation with ξ_a equal to the substrate concentration C_S.

$$Z_1 \triangleq -\frac{1}{k_1} C_S + C_X \qquad Z_2 \triangleq -\frac{k_3}{k_1} C_S + C_O \tag{4.4}$$

$$\begin{array}{rcl} \frac{dC_O}{dt} &=& k_3 \mu (Z_1 + \frac{1}{k_3}(C_O - Z_2)) \\ && + k_L a \cdot C_{SAT} - k_L a \cdot C_O \\ \frac{dZ_1}{dt} &=& -DZ_1 - \frac{1}{k_1} DC_{S,in} + DC_{X,in} \\ \frac{dZ_2}{dt} &=& -DZ_2 + k_L a \cdot C_{SAT} - \frac{k_3}{k_1} DC_{S,in} + (D - k_L a) C_O \end{array} \tag{4.5}$$

- Transformation with ξ_a equal to the biomass concentration C_X.

$$Z_1 \triangleq -k_1 C_X + C_S \qquad Z_2 \triangleq -k_3 C_X + C_O \tag{4.6}$$

$$\begin{array}{rcl} \frac{dC_O}{dt} &=& \mu(C_O - Z_2) + k_L a \cdot C_{SAT} - k_L a \cdot C_O \\ \frac{dZ_1}{dt} &=& -DZ_1 + DC_{S,in} - k_1 DC_{X,in} \\ \frac{dZ_2}{dt} &=& -DZ_2 + k_L a \cdot C_{SAT} - k_3 DC_{X,in} + (D - k_L a) C_O \end{array} \tag{4.7}$$

- Transformation with ξ_a equal to the oxygen concentration C_O.

$$Z_1 \triangleq -\frac{k_1}{k_3}C_O + C_S \qquad Z_2 \triangleq -\frac{1}{k_3}C_O + C_X \tag{4.8}$$

$$\begin{aligned}
\frac{dC_O}{dt} &= k_3\mu(Z_2 + \frac{1}{k_3}C_O) + k_La \cdot C_{SAT} - k_La \cdot C_O \\
\frac{dZ_1}{dt} &= -DZ_1 + (k_La - D)\frac{k_1}{k_3}C_O + DC_{S,in} - \frac{k_1}{k_3}k_La \cdot C_{SAT} \\
\frac{dZ_2}{dt} &= -DZ_2 + DC_{X,in} + \frac{1}{k_3}(k_La - D)C_O - \frac{1}{k_3}k_La \cdot C_{SAT}
\end{aligned} \tag{4.9}$$

The obtained models will be used for solving various estimation problems.

4.2.3 State observers

The state estimation problem is now considered for different cases, depending on which states are measured on-line and whether a model for the reaction rates is available or not.

- **Case 1. State estimation from oxygen measurements with knowledge of the reaction rates.**

  The matrix $\mathbf{A}(\boldsymbol{\xi})$ (4.10) is calculated below. $\bar{\mu}$ is the partial derivative of the specific biomass growth rate with respect to the substrate concentration C_S. It is assumed that the specific biomass growth rate is independent from the biomass concentration C_X and the oxygen concentration C_O.

$$\mathbf{A}(\boldsymbol{\xi}) = \begin{pmatrix} k_1\bar{\mu}C_X - D & k_1\mu & 0 \\ \bar{\mu}C_X & \mu - D & 0 \\ k_3\bar{\mu}C_X & k_3\mu & -k_La \end{pmatrix} \tag{4.10}$$

  The observability matrix $\mathcal{O}$ is then determined. The variable $r = k_1\bar{\mu}C_X - D + \mu - k_La$ is introduced for ease of notation.

$$\begin{pmatrix} 0 & 0 & 1 \\ k_3\bar{\mu}C_X & k_3\mu & -k_La \\ k_3\bar{\mu}C_Xr & k_3\mu r & k_L^2a \end{pmatrix} \tag{4.11}$$

  The observability matrix $\mathcal{O}$ (4.11) is not full rank. From this observation one can conclude that from on-line oxygen measurements the biomass and substrate concentration can not be estimated at an arbitrary speed. The model is not exponentially observable if only on-line oxygen measurements are available. Consider the following state observer with $\widehat{C_S}$, $\widehat{C_X}$ and $\widehat{C_O}$ the estimates of the substrate, biomass

and oxygen concentration respectively. Ω_1, Ω_2 and Ω_3 are the tuning functions. $\widehat{\mu}$ is the model for the kinetics evaluated for the estimated substrate concentration.

$$\begin{aligned}
\frac{d\widehat{C_S}}{dt} &= k_1 \cdot \widehat{\mu} \cdot \widehat{C_X} + D \cdot (C_{S,in} - \widehat{C_S}) \quad -\Omega_1(C_O - \widehat{C_O}) \\
\frac{d\widehat{C_X}}{dt} &= \widehat{\mu} \cdot \widehat{C_X} + D \cdot (C_{X,in} - \widehat{C_X}) \quad -\Omega_2(C_O - \widehat{C_O}) \\
\frac{d\widehat{C_O}}{dt} &= k_3 \cdot \widehat{\mu} \cdot \widehat{C_X} + k_La \cdot (C_{SAT} - \widehat{C_O}) \quad -\Omega_3(C_O - \widehat{C_O})
\end{aligned} \tag{4.12}$$

The eigenvalues of the error system are given below.

$$\begin{aligned}
\lambda_1 &= -D \\
\lambda_{2,3} &= -D - k_La + \mu + C_Xk_1\bar{\mu} - \Omega_3 \pm \sqrt{\Delta} \\
\Delta &= D^2 - 2Dk_La + k_L^2a - 2D\mu + 2k_La + \mu^2 - 4k_3\mu\Omega_2 \\
&\quad -2D\Omega_3 + 2k_La\Omega_3 + 2\mu\Omega_3 + \Omega_3^2 - 2C_XDk_1\bar{\mu} \\
&\quad +2C_Xk_La k_1\bar{\mu} + 2C_Xk_1\mu\bar{\mu} - 4C_Xk_3\bar{\mu}\Omega_3 \\
&\quad +2C_Xk_1\Omega_3\bar{\mu} + C_X^2k_1^2\bar{\mu}^2
\end{aligned} \tag{4.13}$$

The eigenvalue λ_1 is only determined by the dilution rate D, which illustrates that this model is not exponentially observable for oxygen concentration measurements. This does not mean that the observer (4.12) can not be useful. By a proper selection of the tuning functions all eigenvalues can be chosen to be strictly negative. The resulting observer is an asymptotic observer. Notice that the tuning functions can be chosen such that part of the dynamics can be assigned.

- **Case 2. State estimation from oxygen measurements without knowledge of reaction rates.**

  When the state transformation (4.4) is used, the dynamical model (4.5) of $\mathbf{z}$ is obtained which is independent of the specific growth rate μ. Notice that this model is function of the measured state C_O. With this model the state observer (4.14) is designed. The dynamics of this observer can easily be understood when the error dynamics is analyzed. It follows that the error system has an eigenvalue $-D$ with double multiplicity.

$$\begin{aligned}
\frac{d\widehat{Z_1}}{dt} &= -D \cdot \widehat{Z_1} + D \cdot C_{X,in} - \frac{1}{k_1} \cdot D \cdot C_{S,in} \\
\frac{d\widehat{Z_2}}{dt} &= -D \cdot \widehat{Z_2} + k_La \cdot C_{SAT} - \frac{k_3}{k_1} \cdot D \cdot C_{S,in} + (D - k_La)C_O
\end{aligned} \tag{4.14}$$

  The substrate and biomass concentration C_S and C_X are found by using the inverse of transformation (4.4). It is clear that also the other transformations (4.6), (4.8) can be used for the design of the state observers. This approach results in asymptotic observers. Recall that asymptotic observability is the best that can be obtained

when only oxygen concentration measurements are on-line available. In comparison with the type of observers discussed in the first case these observers do not require knowledge of the kinetic model. This is an important advantage because often the kinetic part of the model is not well known.

- **Case 3. State estimation from oxygen and biomass measurements with knowledge of reaction rates.**

  Again the observability matrix $\mathcal{O}$ is determined.

$$\mathcal{O} = \begin{pmatrix} 0 & 1 & 0 \\ 0 & 0 & 1 \\ \bar{\mu}C_X & \mu - D & 0 \\ k_3\bar{\mu}C_X & k_3\mu & -k_La \\ \star & \star & \star \\ \star & \star & \star \end{pmatrix} \tag{4.15}$$

This observability matrix is full rank. One can conclude that with the observer (4.16) exponential estimation of the substrate concentration is obtained.

$$\begin{aligned} \frac{d\widehat{C_S}}{dt} &= k_1 \cdot \widehat{\mu} \cdot \widehat{C_X} + D \cdot (C_{S,in} - \widehat{C_S}) \\ &- \Omega_1(C_X - \widehat{C_X}) - \Phi_1(C_O - \widehat{C_O}) \\ \frac{d\widehat{C_X}}{dt} &= \widehat{\mu} \cdot \widehat{C_X} + D \cdot (C_{X,in} - \widehat{C_X}) \\ &- \Omega_2(C_X - \widehat{C_X}) - \Phi_2(C_O - \widehat{C_O}) \\ \frac{d\widehat{C_O}}{dt} &= k_3 \cdot \widehat{\mu} \cdot \widehat{C_X} + k_La \cdot (C_{SAT} - \widehat{C_O}) \\ &- \Omega_3(C_X - \widehat{C_X}) - \Phi_3(C_O - \widehat{C_O}) \end{aligned} \tag{4.16}$$

Ω_1, Ω_2, Ω_3, Φ_1, Φ_2 and Φ_3 are the tuning functions of the observer.

- **Case 4: State estimation from oxygen and biomass measurements without knowledge of reaction rates.**

For the estimation of the substrate concentration $\widehat{C_S}$ from oxygen and biomass concentration measurements without knowledge of the reaction rate μ, the above discussed method, based on the dynamics of $\mathbf{z}$, is still valid. The main difference is that the state ξ_a can now be replaced by a combination of both measured states, which will alter the eigenvalues of the state observer. Nevertheless only asymptotic observability is obtained.

4.2.4 Observer based estimators

Estimation of the growth rate

The biomass growth rate $\alpha = \mu C_X$ can be estimated with an observer based parameter estimator. When the tuning functions Ω and Γ are selected to be strictly negative and strictly positive respectively, the convergence of the observer based estimator is guaranteed. Notice that $\Phi = k_3$ is persistently exciting.

$$\begin{aligned} \frac{d\widehat{C_O}}{dt} &= k_3 \cdot \widehat{\alpha} + k_La \cdot (C_{SAT} - C_O) - \Omega \cdot (C_O - \widehat{C_O}) \\ \frac{d\widehat{\alpha}}{dt} &= -k_3 \cdot \Gamma \cdot (C_O - \widehat{C_O}) \end{aligned} \tag{4.17}$$

All parameters of the oxygen mass balance must be known.

Estimation of the specific growth rate

The specific biomass growth rate can be determined, e.g. from on-line biomass concentration measurements. The condition of persistently excitation of $\Phi = C_X$ is fulfilled because the biomass concentration is different from zero.

$$\begin{aligned} \frac{d\widehat{C_X}}{dt} &= \widehat{\mu} \cdot C_X + D \cdot C_{X,in} - D \cdot C_X - \Omega \cdot (C_X - \widehat{C_X}) \\ \frac{d\widehat{\mu}}{dt} &= -C_X \cdot \Gamma \cdot (C_X - \widehat{C_X}) \end{aligned} \tag{4.18}$$

All parameters of the biomass mass balance must be known. Remark the fact that no yield coefficients must be known in this case. Alternative estimation schemes based on combined measurements of biomass and substrate concentration or biomass and oxygen concentration can be used. The main difference between these estimation schemes is that other parameter sets must be known for implementation of these algorithms.

4.2.5 Least squares estimation

The general method of least squares estimation of the yield coefficients, independently of the specific growth rate μ, described in Appendix A, is illustrated here. The matrix $\mathbf{K}$ has rank one. The following auxiliary quantities are introduced.

$$\begin{aligned} \eta_a &= C_S(t) - C_S(0) + \int_0^t (DC_S - DC_{S,in})d\tau \\ \eta_{b_1} &= C_X(t) - C_X(0) + \int_0^t (DC_X - DC_{X,in})d\tau \\ \eta_{b_2} &= C_O(t) - C_O(0) + \int_0^t (k_LaC_O - k_LaC_{SAT})d\tau \end{aligned} \tag{4.19}$$

The relation (4.20) between these new variables can be written. By using a reparameterization a relation linear in the unknown parameter vector θ is obtained. Based on this relation different least squares estimation methods can be designed. The determination of the yield coefficient k_1 and k_3 from the parameter vector θ is trivial.

$$\begin{pmatrix} \eta_{b_1} \\ \eta_{b_2} \end{pmatrix} = \begin{pmatrix} \frac{1}{k_1} \\ \frac{k_3}{k_1} \end{pmatrix} \cdot \eta_a = \begin{pmatrix} \theta_1 \\ \theta_2 \end{pmatrix} \cdot \eta_a \qquad (4.20)$$

4.2.6 Reparameterizations

Joint estimation of yield coefficients and the specific growth rate

Full state measurements. The combined estimation of the yield coefficients and the specific growth rate is based on the reparameterization (4.21). It is clear that this reparameterization is invertible.

$$a = k_1 \cdot \mu \quad ; \quad b = \mu \quad ; \quad c = k_3 \cdot \mu \qquad (4.21)$$

The following observer based estimator can then be written. Notice that here diagonal matrices $\mathbf{\Gamma}$ and $\mathbf{\Omega}$ are used for easy of notation. However, more general matrices can be used. The convergence of this type of observer based estimators is guaranteed if (i) the matrix $\mathbf{\Gamma}$ is stable (negative diagonal elements), (ii) $\mathbf{\Omega}$ positive definite (positive diagonal elements) and (iii) the matrix $\mathbf{\Phi}$ is persistently exciting. It can easily be checked that this condition is fulfilled when the biomass concentration is different from zero.

$$\begin{aligned}
\frac{d\widehat{C_S}}{dt} &= \widehat{a} \cdot C_X + D \cdot (C_{S,in} - \widehat{C_S}) && -\Omega_1(C_S - \widehat{C_S}) \\
\frac{d\widehat{C_X}}{dt} &= \widehat{b} \cdot C_X + D \cdot (C_{X,in} - \widehat{C_X}) && -\Omega_2(C_X - \widehat{C_X}) \\
\frac{d\widehat{C_O}}{dt} &= \widehat{c} \cdot C_X + k_L a \cdot (C_{SAT} - \widehat{C_O}) && -\Omega_3(C_O - \widehat{C_O}) \\
\frac{d\widehat{a}}{dt} &= && C_X \Gamma_4 (C_S - \widehat{C_S}) \\
\frac{d\widehat{b}}{dt} &= && C_X \Gamma_5 (C_X - \widehat{C_X}) \\
\frac{d\widehat{c}}{dt} &= && C_X \Gamma_6 (C_O - \widehat{C_O})
\end{aligned} \qquad (4.22)$$

Oxygen concentration measurements. The model obtained via ξ_a equal to the substrate concentration C_S is used. The following reparameterization is used.

$$\theta = \begin{pmatrix} a \\ b \end{pmatrix} = \begin{pmatrix} k_3 \mu \\ \mu \end{pmatrix} \qquad (4.23)$$

$$\begin{aligned}
\frac{d\widehat{C_O}}{dt} &= \begin{pmatrix} \widehat{Z_1} & (\widehat{C_O} - \widehat{Z_2}) \end{pmatrix} \begin{pmatrix} \widehat{a} \\ \widehat{b} \end{pmatrix} + k_L a C_{Sat} - k_L a C_O \\
&- \Omega_1 (C_O - \widehat{C_O}) \\
\frac{d\widehat{Z_1}}{dt} &= -D\widehat{Z_1} - \frac{1}{k_1} D C_{S,in} + D C_{X,in} \\
&- \Omega_2 (C_O - \widehat{C_O}) \\
\frac{d\widehat{Z_2}}{dt} &= -D\widehat{Z_2} + k_L a C_{SAT} - \frac{k_3}{k_1} D C_{S,in} + (D - k_L a) C_O \\
&- \Omega_3 (C_O - \widehat{C_O}) \\
\frac{d\widehat{a}}{dt} &= \widehat{Z_1} \cdot \Gamma_1 \cdot (C_O - \widehat{C_O}) \\
\frac{d\widehat{b}}{dt} &= (C_O - \widehat{Z_2}) \cdot \Gamma_2 \cdot (C_O - \widehat{C_O})
\end{aligned} \qquad (4.24)$$

Notice that the dynamics of the state $\mathbf{z}$ is only independent from the yield coefficients if $C_{S,in}$ equals zero. From the estimation of a and b the yield coefficient k_3 and the specific growth rate μ can be calculated because the reparameterization (4.23) is invertible. The dynamical model obtained by using the biomass or the oxygen concentration as the state ξ_a could not be used for combined estimation of some of the yield coefficients and the specific growth rate μ because independence of the dynamics of $\mathbf{z}$ could not be obtained and no suitable reparameterization can be found.

The tuning parameters Ω_1, Ω_2 and Ω_3 are chosen negative while the parameters Γ_1 and Γ_2 are strictly positive. The convergence of the observer based estimator is guaranteed if $\mathbf{\Phi}$ is persistently exciting. It can easily be checked that this condition is fulfilled when the substrate concentration C_S is different from zero.

Estimation of the specific growth rate independently of the yield coefficients

For the prototype model two interesting cases can be distinguished.

Case 1. Yield coefficient k_3 known. Condition $C_{S,in} = 0$. If the yield coefficient k_3 is known, and the influent substrate concentration $C_{S,in}$ equals zero, then the model (4.5) of Section 4.2.2 is independent from the yield coefficient k_1. From this observation an observer based estimator for the specific growth rate can be built. The tuning parameters Ω_1, Ω_2 and Ω_3 are chosen to be negative while the parameter Γ is a positive constant. The convergence of this observer based estimator is guaranteed if Φ is persistently exciting. It can easily be checked that

this is fulfilled if the biomass concentration C_X is different from zero.

$$\Phi = k_3(\widehat{Z_1} + \frac{1}{k_3}(C_O - \widehat{Z_2})) \tag{4.25}$$

$$\begin{aligned}
\frac{d\widehat{C_O}}{dt} &= k_3\widehat{\mu}(\widehat{Z_1} + \frac{1}{k_3}(C_O - \widehat{Z_2})) + k_La \cdot C_{SAT} - k_La \cdot C_O \\
&- \Omega_1 \cdot (C_O - \widehat{C_O}) \\
\frac{d\widehat{Z_1}}{dt} &= -D\widehat{Z_1} - \frac{1}{k_1}DC_{S,in} + DC_{X,in} \\
&- \Omega_2 \cdot (C_O - \widehat{C_O}) \\
\frac{d\widehat{Z_2}}{dt} &= -D\widehat{Z_2} + k_La \cdot C_{SAT} - \frac{k_3}{k_1}DC_{S,in} + (D - k_La)C_O \\
&- \Omega_3 \cdot (C_O - \widehat{C_O}) \\
\frac{d\widehat{\mu}}{dt} &= -k3(\widehat{Z_1} + \frac{1}{k_3}(C_O - \widehat{Z_2})) \cdot \Gamma \cdot (C_O - \widehat{C_O})
\end{aligned} \tag{4.26}$$

Notice that estimation of the specific biomass growth from only on-line oxygen concentration measurements is possible in this case. However, the obtained observer is from the asymptotic type.

Condition $C_{X,in} = 0$. Model (4.7) from Section 4.2.2 is independent of the yield coefficients if the biomass concentration $C_{X,in}$ in the influent stream is zero. The convergence of the observer based estimator is guaranteed if Φ is persistently exciting and the same tuning parameters as described above are used. It can easily be checked that the persistently excitation condition is fulfilled if the biomass concentration is different from zero.

$$\Phi = (C_O - \widehat{Z_2}) \tag{4.27}$$

$$\begin{aligned}
\frac{d\widehat{C_O}}{dt} &= \widehat{\mu}(C_O - \widehat{Z_2}) + k_La \cdot C_{SAT} - k_La \cdot C_O \\
&+ \Omega_1 \cdot (C_O - \widehat{C_O}) \\
\frac{d\widehat{Z_1}}{dt} &= -D\widehat{Z_1} + DC_{S,in} - k_1DC_{X,in} \\
&+ \Omega_2 \cdot (C_O - \widehat{C_O}) \\
\frac{d\widehat{Z_2}}{dt} &= -D\widehat{Z_2} + k_La \cdot C_{SAT} - k_3DC_{X,in} + (D - k_La)C_O \\
&+ \Omega_3 \cdot (C_O - \widehat{C_O}) \\
\frac{d\widehat{\mu}}{dt} &= -(C_O - \widehat{Z_2}) \cdot \Gamma \cdot (C_O - \widehat{C_O})
\end{aligned} \tag{4.28}$$

Again an asymptotic observer is obtained.

4.2.7 Summary

The results are summarized in three tables: Table 1 describes the case where only on-line oxygen measurements are assumed to be available. Table 2 summarizes the results for the case where both biomass and oxygen concentration are measured, while Table 3 contains the results for the case where full state measurements are available.

Notice that the analysis has been limited to on-line measurements of oxygen and biomass (except when full state measurements are assumed). This can be motivated because (i) oxygen measurements are relative cheap and (ii) biomass can be measured for instance with a biomass monitor or respirometric experiments. Moreover, the biomass concentration is not varying fast. As such a larger sampling time can be allowed.

Each table lists which yield coefficients, transport and input parameters are assumed to be known. It is also indicated whether explicit knowledge of the growth rate model is necessary or not and whether additional constraints (on the input) must be satisfied. In the table can be found which states and/or parameters can be estimated. It is also indicated whether the convergence of the estimator is *asymptotic* (determined only by the process conditions, often the transport terms) or *exponential* (chosen by the designer of the algorithm).

On-line measurements of oxygen concentration. Out of the oxygen concentration measurement the biomass and substrate concentration can be estimated even without knowledge of the growth rate. However, the convergence is asymptotic and determined by the transport terms.

Exponential estimation of the growth rate is possible when complete knowledge of the oxygen balance is available.

Estimation of the specific growth rate, independently from (some) yield coefficients, and even simultaneous estimation of the growth rate and some yield coefficients, is only possible in asymptotic way if some conditions on the inputs are fulfilled. These conditions must be examined for the particular system under study.

On-line measurements of oxygen and biomass concentration. Exponential estimation of the substrate concentration C_S is possible when the growth rate model is explicitly known. The substrate concentration C_S can still be estimated without the growth rate model but only in an asymptotic manner.

Exponential estimation of the growth rate, independently from (some) yield coefficients, is possible. The estimation of the yield k_3 independently from the growth rate model from the available on-line measurements is trivial.

On-line measurements of oxygen, biomass and substrate concentration. The specific growth rate can be exponentially estimated independently from the yield coefficients while the yield coefficients can be determined independently from the growth rate model.

Also the simultaneous estimation of the yield coefficients and specific growth rate is possible.

Notice that the substrate and biomass concentration can be estimated when only on-line oxygen concentration measurements are available. However, this is only possible in an asymptotic way. On the other hand there is no need to use an explicit model for the kinetics. This would only introduce additional uncertainty and does not result in faster estimation.

When both oxygen and biomass concentration are on-line available, exponential estimation of the substrate concentration is possible. When no explicit model for the kinetics is available the substrate concentration can still be estimated, but only asymptotically.

From full state measurements the yield coefficients can be determined independent from the kinetics. In some particular situations the specific growth rate can be determined independently of the yield coefficients. An alternative approach is the joint estimation of the yield and the specific growth rate.

The results of the observability and identifiability properties of the prototype model can now be interpreted in the context of carbon removal activated sludge wastewater treatment plants. In wastewater treatment systems on-line oxygen concentration measurements are often available for control of the aerators. These measurements are quite reliable and cheap. More expensive (and thus hardly available in reality) alternatives are (i) on-line biomass measurements, obtained via a biomass monitor (using capacitance measurements) or a suspended solids sensor (using turbidity measurements) and (ii) respirometric measurements, resulting in on-line measurements of substrate and biomass concentration.

Plant design and measurability. The analysis illustrates that quite often the convergence speed is asymptotic and determined by the transport terms. In a wastewater treatment system the obtained convergence speed is often quite low due to the oversizing of the installations. Notice that here an explicit link between the design of the installation and the measurability of the process is made.

Plant configuration and measurability. The estimation of states and parameters is often only possible when certain conditions on the input parameters are fulfilled. This depends strongly on the system under study. The condition on the biomass concentration of the input stream is for instance not fulfilled in a classical wastewater treatment system due to the biomass recycle flow. For the cyclically operated systems discussed in Chapter 1 this condition is satisfied for the first tank of each stage.

Sensor investment policy. This study indicates that an important investment in on-line measurements is needed. However, the systematic analysis of the estimation problem can be used to determine an optimal investment policy.

Online measurement of oxygen Co						
Yield	**Transp.**	**Inputs**	**Kinetics**	**Constr.**	**Estimate**	**Converg.**
k1,k3	D kLa,Csat	Cxin Csin	Growth rate		Cs,Cx	Asympt.
k1,k3	D kLa,Csat	Cxin Csin			Cs,Cx Indep. μ	Asympt.
k3	kLa,Csat				Growth rate	Expon.
k3	D	Cxin		Csin=0	Growth rate Indep. K	Asympt.
	kLa,Csat	Csin		Cxin=0		
	D kLa,Csat	Cxin		Csin=0	Growth rate k3	Asympt.

Table 4.1: Estimation based on oxygen concentration measurements

Online measurements of oxygen Co and biomass Cx						
Yield	**Transp.**	**Inputs**	**Kinetics**	**Constr.**	**Estimate**	**Converg.**
k1, k3	D kLa, Csat	Cxin Csin	Growth rate		Cs	Expon.
	D	Cxin			Growth rate Indep. K	Expon.
k3	D kLa, Csat					
k1, k3	D kLa, Csat	Cxin Csin			Cs Indep. μ	Asympt.
	D kLa, Csat	Cxin Csin			k3	

Table 4.2: Estimation based on oxygen and biomass concentration measurements

Online measurements of oxygen Co, biomass Cx and substrate Cs						
Yield	**Transp.**	**Inputs**	**Kinetics**	**Constr.**	**Estimate**	**Converg.**
k1	D	Csin			Growth rate Indep.K	Expon.
k3	kLa, Csat					
	D	Cxin				
	D kLa, Csat	Csin Cxin			k1,k3 Indep. μ	RLS
	D kLa, Csat	Csin Cxin			Growth rate k1,k3	Expon.

Table 4.3: Estimation based on full state measurements

4.3 State estimation and the redox sensor

A basic model, describing the nitrogen removal process in activated sludge wastewater treatment plants and the related state estimation problem is introduced in Section 4.3.1. A more detailed description is found in Chapter 1. In Section 4.3.2 state estimation based on the on-line measurement of the oxydo reduction potential is presented as an interesting approach to tackle the state estimation problem and illustrated with simulations.

4.3.1 Problem statement

A single tank system is considered. The operation mode of the tank is switched between *nitrification* and *denitrification* by setting the aerator on or off.

The basic model describes the evolution of the ammonium (and organic nitrogen) concentration C_{NH_4} [kg/m^3] nitrate (and nitrite) concentration C_{NO_X} [kg/m^3], heterotrophic biomass concentration C_{X_H} [kg/m^3] and autotrophic biomass concentration C_{X_A} [kg/m^3].

Notice that the dynamics of the oxygen concentration is not modeled. It is assumed that due to an adequate aeration process oxygen is not limiting for the nitrification process and sufficiently low during denitrification. Also the carbon concentration dynamics is not modeled. It is assumed that the carbon concentration in the effluent is low and that carbon is removed fast during nitrification. During denitrification the carbon concentration is assumed to be controlled at a setpoint by an extra inflow.

Nitrification model.

$$\begin{aligned}
\frac{dC_{NH_4}}{dt} &= -\sigma_{NH}C_{X_A} \quad -DC_{NH_4} \quad +DC_{NH_4,in} \\
\frac{dC_{NO_X}}{dt} &= \pi_{NO}C_{X_A} \quad -DC_{NO_X} \\
\frac{dC_{X_A}}{dt} &= \mu_A C_{X_A} \quad -DC_{X_A} \\
\frac{dC_{X_H}}{dt} &= 0 \quad -DC_{X_H}
\end{aligned} \tag{4.29}$$

σ_{NH} [1/h] is the specific ammonium consumption rate. $D = \frac{F_{in}}{V}$ [1/h] is the dilution rate with F_{in} [m^3/h] the influent flow rate and V[m^3] the volume of the tank. $C_{NH_4,in}$ is the influent ammonium concentration. μ_A [1/h] is the specific growth rate of the autotrophic biomass while π_{NO} [1/h] is the specific production rate of nitrate (and nitrite).

Denitrification model.

$$\begin{aligned}
\frac{dC_{NH_4}}{dt} &= \quad -(D+U)C_{NH_4} \quad +DC_{NH_4,in} \\
\frac{dC_{NO_X}}{dt} &= -\sigma_{NO}C_{X_H} \quad -(D+U)C_{NO_X} \\
\frac{dC_{X_H}}{dt} &= \mu_H C_{X_H} \quad -(D+U)C_{X_H} \\
\frac{dC_{X_A}}{dt} &= 0 \quad -(D+U)C_{X_A}
\end{aligned} \tag{4.30}$$

σ_{NO} [1/h] is the specific nitrate (and nitrite) consumption rate. μ_H [1/h] is the specific growth rate of the heterotrophic biomass. $U = \frac{F_C}{V}$ [1/h] models the carbon dosage flow with F_C [m^3/h] the flow rate and V the volume of the tank. U is used for controlling the carbon substrate concentration at a specified setpoint.

The modeling of the specific rates as function of the concentrations is based on the IAWQ model, reported in [Henze *et al.* 1995] and is not further discussed here.

The *oxydo reduction potential* measurements are frequently used in nitrogen removal wastewater treatment systems for detection of the end of the denitrification phase. Notice that in this sense the redox potential is only useful at that particular time instance where the nitrate concentration becomes zero, such that the denitrification stops. This is observed as a knee in the redox potential curve. Redox knee detection with observer based estimators is discussed in Chapter 6. The following question can now be posed.

Which process states can be estimated by using the redox potential as on-line measurement?

Notice that in this case the redox potential is used for monitoring of the process during the whole process rather than just for detection of the end of the denitrification process. As such, more benefit of an in practice frequently used measurement can be expected without major additional investments.

4.3.2 State estimation of ammonium and nitrate concentration

In the sequel an adaptive state estimation scheme is suggested as a possible approach for tackling the state estimation problem by using on-line redox potential measurements.

More precisely, the state estimation of ammonium and nitrate concentration from on-line redox potential measurements is solved. Adaptation is suggested as an approach tackling the time variability in the relation

between the redox potential and the process state. This relation is the corner stone of the state estimation algorithm. The adaptive state estimation problem itself is not solved because the involved parameter updating problem depends heavily on the measurement setup available on the treatment plant. Adaptive state estimation is shortly introduced in Appendix A.

First the relation $h(\mathbf{x})$ between the measurement of the redox potential y and the process state $\mathbf{x}$ is discussed. This relation is a key element for exponential state estimation.

Then an exponential state observer for estimation of the ammonium and nitrate concentration during the denitrification phase is discussed.

Relation between the redox potential and the states of the system

The state estimation based on the redox potential is based on a mathematical relation between this potential and the internal process states of the system under consideration.

In [Héduit and Thévenot 1989, 1992] and [Koch and Oldham 1985] partial descriptions of the influences of the process states on the redox potential are given. Based on this information the mathematical relation (4.31) between the redox potential y and the process states is proposed here. $\mathbf{p}(t)$ is a time-varying parameter vector which can be decomposed in two parts $\mathbf{p}_1(t) = (p_1, p_2, p_3, p_4)$ and $\mathbf{p}_2(t)$. C_O [mgO_2/L] and C_C [mgCOD/L] are the oxygen and carbon concentration in the reactor respectively.

$$\begin{aligned} y &= h(\mathbf{x}, \mathbf{p}) \\ &= \mathbf{p}_1 \cdot k(\mathbf{x}, \mathbf{p}_2) \\ &= \begin{pmatrix} p_1 & p_2 & p_3 & p_4 \end{pmatrix} \cdot \begin{pmatrix} \log(10^3 C_{NH_4} + 1) \\ \log(10^3 C_{NO_X} + 1) \\ \log(10^3 C_C + 1) \\ \log(10^3 C_O + 1) \end{pmatrix} \end{aligned} \tag{4.31}$$

The parameters in the quantitative relation described above must be determined from full scale data. Further refinements of this relation must be based on biochemical knowledge (Nernst law), dedicated lab experiments and *full scale* validation. This is not further discussed. Recall that the main purpose is to illustrate which information can be extracted from an *on-line* redox potential measurement when a sufficiently accurate mathematical relation is available.

Notice that the relation described above has a structure comparable with the Nernst law. The influences of the several components are assumed to be additive. The switching function in the logarithmic parts are introduced to describe the fact that a component has no influence when its concentrations drops below a critical value.

It must be emphasized that the interpretation of the relation (4.31) is of no importance for the state estimation scheme. The relation (4.31) can just be considered as a fit between the process state and the corresponding redox

potential. The fact that such a relation can be time varying, is compensated by parameter adaptation. One can conclude that the interpretation of the relation is just a tool for selection of an appropriate structure for the relation.

Exponential state estimation

The concentration of ammonium and nitrate is estimated with an exponential observer by using on-line measurements of the oxydo-reduction potential during the denitrification phase. The observer has the following structure.

$$\begin{aligned} \frac{d\widehat{C_{NH_4}}}{dt} &= -(D+U)\widehat{C_{NH_4}} + DC_{NH_4,in} + \phi_1 \cdot (y - \bar{h}(\widehat{C_{NH_4}}, \widehat{C_{NO_X}})) \\ \frac{d\widehat{C_{NO_X}}}{dt} &= -\widehat{\sigma_{NO}} C_{X_H} - (D+U)\widehat{C_{NO_X}} + \phi_2 \cdot (y - \bar{h}(\widehat{C_{NH_4}}, \widehat{C_{NO_X}})) \end{aligned} \tag{4.32}$$

$\widehat{C_{NH_4}}$ and $\widehat{C_{NO_X}}$ are the estimates of the ammonium and nitrate concentration respectively. $\widehat{\sigma_{NO}}$ is the estimate of the specific nitrate consumption rate, obtained by evaluating the relation of the specific reaction rate as function of the nitrate concentration for the estimated nitrate concentration. Notice that it is assumed that a kinetic model is given. The heterotrophic biomass concentration C_{X_H} in the tank is assumed to be known (for instance from a respirometric experiment) and rather constant. This last condition is fulfilled in practice. ϕ_1 and ϕ_2 are the tuning functions of the observer. These functions can be depending on the ammonium and the nitrate concentration estimates. In Chapter 5 it is illustrated that the tuning functions are functions of the state estimates. $\bar{h}(\widehat{C_{NH_4}}, \widehat{C_{NO_X}})$ equals the formula (4.31) evaluated for a zero oxygen concentration and a carbon concentration setpoint C_C^*.

The oxygen concentration in this relation is zero because the denitrification process is anaerobic while the carbon concentration C_C^* is assumed to be fixed by using an appropriate carbon feed rate. As such, the error matrix (4.33) is found with σ_{NO}^{NO} the derivative of σ_{NO} with respect to the nitrate concentration C_{NO_X}.

$$\begin{pmatrix} -\phi_1 \dfrac{\partial \bar{h}}{\partial C_{NO_X}} & -(D+U) - \phi_1 \dfrac{\partial \bar{h}}{\partial C_{NH_4}} \\ -\sigma_{NO}^{NO} C_{X_H} - (D+U) - \phi_2 \dfrac{\partial \bar{h}}{\partial C_{NO_X}} & -\phi_2 \dfrac{\partial \bar{h}}{\partial C_{NH_4}} \end{pmatrix} \tag{4.33}$$

Notice that the eigenvalues of the error matrix can be influenced by using the redox potential measurements. The convergence speed of the observer can be chosen by selecting the tuning functions ϕ_1 and ϕ_2. The design of the tuning functions is not discussed here. It is the fact that redox potential

measurements can speed up the estimator that is the main point of the discussion here.

The exponential state observer relies on the relation (4.31). The effects of uncertainty on this relations must be examined. It is known that with careful selection of the tuning functions and the convergence rate a certain robustness against uncertainty can be obtained. It is often claimed that the relation (4.31) is time-varying. On the other hand, measurements of the process state are often available at certain time instances. These measurements are taken for evaluation of the plant performance and can be used to adapt the parameters of the relation (4.31). Whether this is possible or not (parameter identifiability) depends on the measurement set available and is not further discussed here. A possible approach is to perform dedicated experiments regularly in a separate reactor to determine the parameters.

Simulations

The use of the exponential observer for estimation of the ammonium and nitrate concentration is illustrated with simulations. The parameter values used are given in Appendix D. The kinetic models (and the related parameter values), presented by [Henze *et al.* 1995], are used.

First the dynamics of the process states and the related dynamics of the redox potential is simulated. Figure 4.1 shows the evolution of the oxygen concentration C_O, carbon concentration C_C, autotrophic and heterotrophic biomass C_{X_A}, C_{X_H}, ammonium concentration C_{NH_4} and nitrate concentration C_{NO_x} in function of time during the nitrification (0-20 min.) and the denitrification phase (20-130 min.).

Notice that the oxygen concentration is high during the nitrification (aerobic process) and low during the denitrification (anaerobic process). The carbon concentration drops to zero fast during the nitrification and is kept constant by an appropriate control action during the denitrification. The feed rate D is constant during the first 70 minutes of the process and then set equal to zero, because it is assumed that the amount of wastewater that must be treated is completely fed into the system.

Figure 4.1 illustrates that the biomass concentration variations are indeed small. Notice that the relative duration of the nitrification and denitrification, the carbon concentration setpoint and the duration of the feeding are degrees of freedom which can be used for process optimization.

The redox potential dynamics is shown in Figure 4.2. The increase of the redox potential during the nitrification phase is mainly due to the oxygen concentration dynamics. The fast change of the redox potential at 20 minutes is due to the fast increase of the carbon concentration. The redox potential is then further decreasing because the oxygen concentration decreases to zero. When the oxygen concentration becomes zero, the further dynamics of the redox potential is mainly due to the evolution of the ammonium and nitrate concentration.

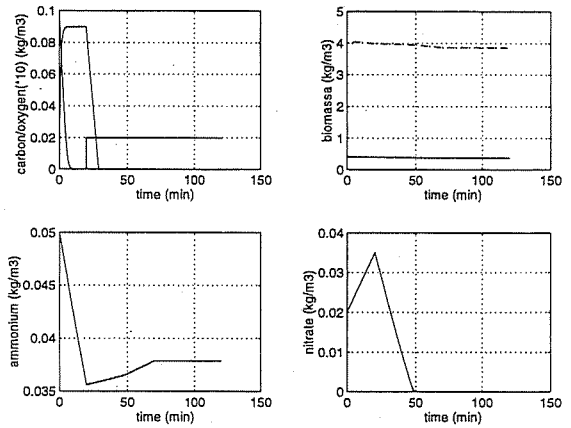


Figure 4.1: Dynamics of the state variables. Top left: oxygen and carbon concentration. Top right: biomass concentrations. Bottom left: ammonium concentration. Bottom right: nitrate concentration

Figure 4.3 shows the evolution of the ammonium- and nitrate concentration in the installation and the estimates of these concentrations obtained with an asymptotic estimator (tuning functions zero) and the exponential estimator. The estimated redox potential is indicated in Figure 4.2. During the nitrification an asymptotic observer (just a copy of the model) is used. In Figure 4.3 also the dynamics of the estimation error for both the asymptotic and the exponential observer is shown. This figure illustrates that the estimation error of the asymptotic observer goes to zero slowly. By using the redox potential as additional correction signal the convergence rate can be increased significantly. Notice that in the beginning of the denitrification phase the error on the ammonium concentration estimate is increasing. This is due the oxygen concentration dynamics which is assumed to be constant in the observer design.

4.3.3 Summary

On-line redox potential measurements can be used for the estimation of the ammonium and nitrate concentration in the denitrification process. An estimation scheme, based on a mathematical relation between the process state and the redox potential, is used. The approach shows that more information can be extracted from the redox potential measurements than just detection of the end of the denitrification phase.

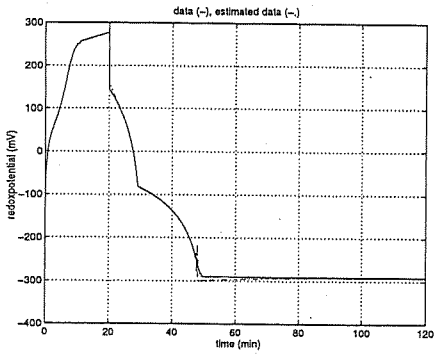


Figure 4.2: Dynamics of the redox potential (full line) and its estimate (dashed-dotted line)

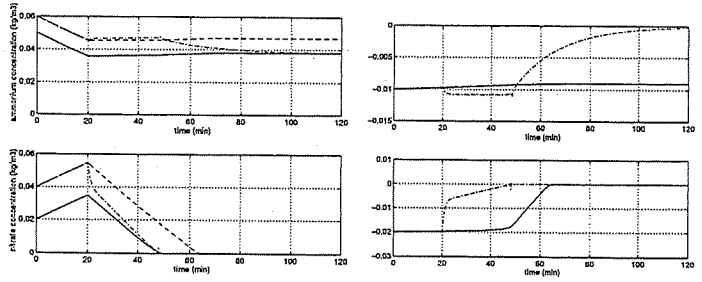


Figure 4.3: Dynamics of the state estimator. Left. Ammonium concentration (full line) and its estimate, nitrate concentration and its estimate (asymptotic observer: dashed, exponential observer: dashed-dotted) Right. Error on the ammonium concentration estimate, error on the nitrate concentration estimate (asymptotic observer: full line, exponential observer: dashed-dotted line)

4.4 Conclusions

Observability and identifiability analysis is the first step that must be performed while designing software sensors. From such an analysis one can determine whether for particular choices of on-line measurements and additional model knowledge non-measured states and parameters can be estimated.

The method can be used for (i) analysis of existing situations, e.g. for the available hardware sensors and (ii) for examining the potential of new sensors. As such it serves as a tool for determining an optimal sensor investment policy.

The analysis performed here also indicates a clear link between the measurability of the plant and its design. The asymptotic convergence rate of several estimation algorithms is mainly determined by the transport terms of the plants under consideration. Oversizing of the treatment plants results in a loss of measurability. Moreover the applicability of some type of estimators is quite depending on the type of plant considered. From this one can conclude that measurability is a criterion that must be taken into account during design of a plant.

The (adaptive) state estimation scheme based on the redox potential shows that from in practice frequently used on-line measurements more information about the process can be extracted than what is expected at first sight. Creative combinations of models, measurements and process knowledge improve the return of investments in on-line sensor equipment.

Observability and identifiability analysis is a first step in the design of software sensors. The analysis can be performed without selecting a priori the observer or parameter estimator design methodology. As such it fits in the 'divide et impera' strategy. However, it is illustrated that the plant design does influence the measurability of the system. This observation is not in contradiction with the decomposition approach as the measurability can be taken easily into account in the design for instance as a constraint on the volume of the plant.

Chapter 5

Performance analysis of nonlinear observers

5.1 Introduction

In biotechnological applications, such as wastewater treatment plants and fermentation processes, the application of modern model based control algorithms is hampered by the lack of accurate and cheap on-line sensors.

The design of state observers, which reconstruct states out of a limited set of measurements, is a possible approach for dealing with the measurement problem. Due to the (time varying) nonlinear behavior of biological systems, the measurement problem can only be attacked properly by designing nonlinear observers.

In linear controller and observer design eigenvalue assignment [Kailath 1980] is the preferred method. This approach is also attractive for nonlinear observer design.

A *first class* of design methodologies transform the nonlinear system globally to a linear observer canonical form, up to an output injection. Then an observer can be designed with linear error dynamics. In this case the eigenvalue assignment method is applicable. In [Isidori 1989] this is shown for systems without input, while in [Keller 1987] also inputs are considered. In this methods partial differential equations must be solved analytically. Other references are [Xia and Wei-bin 1989] and [Krener and Respondek 1985].

A *second class* of design methodologies also rely upon the method of eigenvalue assignment. The transformation of the error system to a linear system is done by local linearization. The linearization can be applied in the original coordinate system [Bastin and Dochain 1990] or in observer coordinates [Bestle and Zeitz 1983] (*pseudo linearization*). The obtained observers are called extended Luenberger observers.

A *third class* of methods does not apply eigenvalue assignment but guarantees exponential convergence [Gauthier *et al.* 1992]. This method is based on a high gain approach.

In this chapter four *nonlinear observer design methodologies* are reviewed and illustrated for a prototype model for biotechnological processes. The results of an extensive *performance analysis* (convergence region, speed of convergence, noise sensitivity, robustness against uncertainty and discretization) of the different observers are presented.
Besides the evaluation of the applicability of the above described algorithms for the prototype model, the main goal of this study is to provide the concepts needed for performance analysis. As such the case study is used as a vehicle for illustrating the *performance analysis tools*.
The performance analysis is considered to be an interesting tool for selection of an appropriate observer for process engineers.

Some other methods, not further described here are cited below. A first interesting alternative is the method described in [Hunt and Madanpal 1994]. In this approach the combined design of state feedback and observer is considered. In the particular case of feedback linearizable systems, the method is also straightforward.

A method, which introduces statistics in the problem formulation, is the extended Kalman observer [Emara-Shabiak and Leondes 1981]. Another approach in observer design is to reformulate the estimation problem in a setting such that equation solving methods can be used. This results in, for instance, a Newton observer [Moraal and Grizzle 1995]. This approach can be reformulated as a Kalman observer.

In the approaches mentioned above, the original system is transformed (exactly or approximately) to a linear system modulo an output injection. An alternative approach is to transform the system to a bilinear system or linear time varying system [Hammouri *et al.* 1988, 1992, 1994]. Observer design for bilinear systems has been described, for instance, in [Derese and Noldus 1980].

A discussion about general exponential observers is given in [Banks 1981]. An interesting theoretical discussion on observers can be found in [Vanderschaft 1985].

In the design methods transformations must be calculated. Most often, these are very hard to calculate in an analytical way. However, one can try to find the transformation in a numerical way. An interesting parametrization can be provided, for instance, with neural networks [Levin 1992].

Application of nonlinear observers for biotechnological applications has been studied in [Moubaraki *et al.* 1993] and [Williamson 1997].

Part of the performance analysis has been reported in [Ryckaert and Van Impe 1996c] while the concepts used in the robustness analysis are presented in [Ryckaert and Van Impe 1997c]. *The prototype model is introduced in Chapter 0. In Chapter 4 observability and identiability analysis of bioprocesses, which is the first step to consider when designing estimation algorithms, is discussed. In Chapter 6 performance analysis is introduced as a tool for optimal tuning of estimation algorithms while here it is used for structure selection.*

In Appendix C canonical forms used throughout this chapter are shortly reviewed. Also the observer design based on exact linearization, introduced here from a differential algebraic point of view, is reformulated in the differential geometry framework in this appendix.

The chapter is organized as follows. In Section 5.2 the case study and a general form for the nonlinear observers discussed here are presented. In the Sections 5.3, 5.4 and 5.5 the observer design methodologies are reviewed and illustrated for the case study. Simulation results are shown in Section 5.6. The different aspects of the performance analysis are introduced in Section 5.7. Each aspect of this analysis is discussed in detail in the Sections 5.8, 5.9, 5.10 and 5.11. Finally conclusions about nonlinear observer design, the observer performance and the applicability to bioprocesses are drawn in Section 5.12.

In this chapter an overview of various observer design techniques and performance analysis tools, inspired from a process engineering point of view are presented. Robustness analysis is performed to illustrate that although the large model uncertainty, which is typical for bioprocesses, still acceptable performance is obtained.

5.2 Prototype model and observers

State estimators are constructed for the prototype model, introduced in Chapter 0. The model is reformulated as follows.

$$\begin{aligned} \frac{dC_X}{dt} &= f_1(C_X, C_S) - UC_X \\ \frac{dC_S}{dt} &= f_2(C_X, C_S) - UC_S + UC_{S,in} \end{aligned} \tag{5.1}$$

The concentrations of biomass C_X [g/L] and substrate C_S [g/L] are the *states* of the system. The estimation of the biomass (substrate) concentration from *on-line* substrate (biomass) concentration measurements is considered. Continuous operation of the bioreactor is assumed. The volume of the liquid phase in the stirred tank is V [L]. There is an influent stream with substrate concentration $C_{S,in}$ [g/L] and without biomass ($C_{X,in} = 0$). F [L/h] is the volumetric flow rate through the system. $U = F/V$ [1/h] is the so-called dilution rate and is considered as a constant *input variable* of

the system. f_1 [g/L h] and f_2 [g/L h] represent the biomass growth rate and the substrate consumption rate respectively, and are in general nonlinear functions of the concentrations C_X and C_S.

Throughout this chapter, the first order model (5.2) is used as prototype kinetic model, although results for other kinetic models are shortly stated. The Monod model is used in the robustness analysis.

$$\begin{aligned} f_1(C_X, C_S) &= \mu(C_S) \cdot C_X = aC_SC_X \\ f_2(C_X, C_S) &= -\sigma(C_S) \cdot C_X = bC_SC_X \end{aligned} \tag{5.2}$$

The state observers considered here consist of a copy of the nonlinear system and a sum of correction terms. Each correction term is given as a product of a nonlinear tuning function k_{ij} multiplied with the error between the measured state and its estimate. The measured state and its estimate may be transformed by a function t_{ij}. For the class of biological models (5.1) the following general forms with the states $\widehat{C_X}$ and $\widehat{C_S}$ as estimates can be written.

Case 1: measurements of substrate C_S.

$$\begin{aligned} \frac{d\widehat{C_X}}{dt} &= f_1(\widehat{C_X}, \widehat{C_S}) - U\widehat{C_X} + \textstyle\sum_j k_{1j}(\widehat{C_X}, \widehat{C_S}) \cdot (t_{1j}(\widehat{C_S}) - t_{1j}(C_S)) \\ \frac{d\widehat{C_S}}{dt} &= f_2(\widehat{C_X}, \widehat{C_S}) - U\widehat{C_S} + UC_{S,in} + \textstyle\sum_j k_{2j}(\widehat{C_X}, \widehat{C_S}) \cdot (t_{2j}(\widehat{C_S}) - t_{2j}(C_S)) \end{aligned} \tag{5.3}$$

Case 2: measurements of biomass C_X.

$$\begin{aligned} \frac{d\widehat{C_X}}{dt} &= f_1(\widehat{C_X}, \widehat{C_S}) - U\widehat{C_X} + \textstyle\sum_j k_{1j}(\widehat{C_X}, \widehat{C_S}) \cdot (t_{1j}(\widehat{C_X}) - t_{1j}(C_X)) \\ \frac{d\widehat{C_S}}{dt} &= f_2(\widehat{C_X}, \widehat{C_S}) - U\widehat{C_S} + UC_{S,in} + \textstyle\sum_j k_{2j}(\widehat{C_X}, \widehat{C_S}) \cdot (t_{2j}(\widehat{C_X}) - t_{2j}(C_X)) \end{aligned} \tag{5.4}$$

5.3 Method 1: Exact linearization

Observers for linear systems are designed with the eigenvalue assignment method. When the nonlinear system can be linearized exactly modulo output injection, the linear observer design methodology is applicable. Two approaches are possible. The method of Keller is inspired by *differential algebra* techniques, while the method of Isidori is based on *differential geometry*.

The first approach is considered here. In the approach of Keller the inputs of the model are explicitly considered. The transformation to the linear canonical form is a two step procedure.

Step 1. Transformation to the *generalized observability canonical form.* Conditions (based on the characteristic equation for nonlinear systems) can then be formulated for solvability of the problem.
Step 2. Transformation to the *generalized observer canonical form.* First, the method is illustrated for the model prototype (5.1)(5.2) in the case of measurements of C_S. Second, the results with C_X as measured state are summarized.

Case 1: measurements of substrate C_S. The output equation is:

$$Y = h(C_S, C_X, U) = C_S \tag{5.5}$$

The input U is considered to be constant in order to simplify the analytical computations. However, time varying inputs can be considered as well.
Step 1: transformation to the GOBCF. The system is transformed to the GOBCF (Appendic C) by the following transformation (and its inverse) [Keller 1987].

$$\begin{aligned} Z_1 &= C_S \\ Z_2 &= bC_X C_S - UC_S + UC_{S,in} \end{aligned} \tag{5.6}$$

$$\begin{aligned} \frac{dZ_1}{dt} &= Z_2 \\ \frac{dZ_2}{dt} &= \frac{Z_2^2}{Z_1} + Z_2(-U + aZ_1 - \frac{UC_{S,in}}{Z_1}) \\ &+ aUZ_1^2 - aUC_{S,in}Z_1 - (UZ_1)^2 + U^2C_{S,in} \end{aligned} \tag{5.7}$$

The existence of the transformation is an observability condition.
Step 2: transformation to the GOCF. In order to proceed with the second step, the right hand side of the last equation (denoted $-a_{nl}$) of the canonical form (5.7) should have the following form [Keller 1987]:

$$a_{nl} = K_2(Y,U)Z_2^2 + K_1(Y,U)Z_2 + K_0(Y,U) \tag{5.8}$$

When this structural condition is fulfilled, there exists a solution ($a_0(Y,U)$, $a_1(Y,U)$, $c(Y,U)$) [see the GOCF (Appendix C)] of the following set of differential equations:

$$\begin{aligned} K_2(Y,U)\frac{\partial c(Y,U)}{\partial Y} &= \frac{\partial^2 c(Y,U)}{\partial Y^2} \\ \frac{\partial a_1(Y,U)}{\partial Y} &= K_1(Y,U)\frac{\partial c(Y,U)}{\partial Y} \\ a_0(Y,U) &= K_0(Y,U)\frac{\partial c(Y,U)}{\partial Y} \end{aligned} \tag{5.9}$$

The transformation (for the general formulas reference is made to [Keller 1987]) and its inverse are given below. Note that W_1 and W_2 are used to denote the transformed states, in order to avoid confusion with the states Z_1 and Z_2 used in Step 1.

$$\begin{aligned} W_1 &= bC_X - U - aC_S + U\ln(C_S) \\ W_2 &= \ln(C_S) \end{aligned} \tag{5.10}$$

The resulting canonical form is then:

$$\begin{aligned} \frac{dW_1}{dt} &= U(aY - U) + \frac{U^2C_{S,in}}{Y} - aUC_{S,in} \\ \frac{dW_2}{dt} &= W_1 + (aY - U\ln(Y)) + \frac{UC_{S,in}}{Y} \\ W_2 &= \ln(Y) \end{aligned} \tag{5.11}$$

The observer design becomes then trivial, because the resulting system (5.11) is now linear up to output injection. The observer in observer canonical form is given by a copy of the system added with a correction term proportional to the error between the measurement and the estimated state, multiplied with tuning parameters l_i. The tuning parameters are chosen with eigenvalue assignment.

When transforming the system back to the original coordinates, the observer is again a copy of the original system with a correction term. The total correction term consists of a sum of correction terms. Each correction term is a product of a nonlinear function with the error between the (transformed) estimated state and the measured state. It is important to notice that these functions consist of a part proportional with l_i and a part due to the output injection. The total correction terms are given as:

$$\begin{aligned} \textstyle\sum_j k_{1j}(\widehat{C_X},\widehat{C_S})\cdot(t_{1j}(\widehat{C_S}) - t_{1j}(C_S)) &= -\frac{1}{b}(a^2\widehat{C_S})\cdot(\widehat{C_S} - C_S) \\ &-\frac{1}{b}(l_1 + U^2 - l_2U + l_2a\widehat{C_S} - Ua\widehat{C_S})\cdot(\ln(\widehat{C_S}) - \ln(C_S)) \\ &-\frac{1}{b}(aUC_{S,in})\widehat{C_S}\cdot(\frac{1}{\widehat{C_S}} - \frac{1}{C_S}) \\ \textstyle\sum_j k_{2j}(\widehat{C_X},\widehat{C_S})\cdot(t_{2j}(\widehat{C_S}) - t_{2j}(C_S)) &= (-l_2 + U)\widehat{C_S}\cdot(\ln(\widehat{C_S}) - \ln(C_S)) \\ &-a\widehat{C_S}\cdot(\widehat{C_S} - C_S) \\ &-UC_{S,in}\widehat{C_S}\cdot(\frac{1}{\widehat{C_S}} - \frac{1}{C_S}) \end{aligned}$$

Case 2: measurements of biomass C_X.
The same method can be applied to the case where biomass is measured and substrate is to be reconstructed. The correction functions are then given as follows:

$$\begin{aligned} \textstyle\sum_j k_{1j}(\widehat{C_X},\widehat{C_S})\cdot(t_{1j}(\widehat{C_X}) - t_{1j}(C_S)) &= -\frac{b}{a}\widehat{C_X}\cdot(\widehat{C_X} - C_X) \\ &-\frac{1}{a}(l_1 + l_2b\widehat{C_X} - l_2U + U^2 - bU\widehat{C_S})\cdot(\ln(\widehat{C_X}) - \ln(C_X)) \\ &-b^2\widehat{C_X}\cdot(\widehat{C_X} - C_X) \\ \textstyle\sum_j k_{2j}(\widehat{C_X},\widehat{C_S})\cdot(t_{2j}(\widehat{C_X}) - t_{2j}(C_X)) &= -(l_2 - U)\widehat{C_X}\cdot(\ln(\widehat{C_X}) - \ln(C_X)) \end{aligned}$$

Extendibility.
The applicability of the exact linearization method has been examined for the Monod and Volterra model. The results are summarized below.

- Case 1: measurements of substrate C_S.
  The exact linearization approach can be applied to all these kinetic models, since the structural condition (5.8) is satisfied.

- Case 2: measurements of biomass C_X.
  The method is only applicable to the model prototype (5.2). For the Monod and Volterra model, the structural condition (5.8) is not satisfied.

5.4 Local linearization

5.4.1 Method 2: Local linearization in original coordinates

Case 1: measurements of biomass C_X.
The method, presented in [Bastin and Dochain 1990], is based on a local linearization around the estimate. The observer with C_X as measured state is given as:

$$\begin{aligned}\frac{d\widehat{C_X}}{dt} &= \mu(\widehat{C_S})\widehat{C_X} - U\widehat{C_X} + k_1(\widehat{C_X},\widehat{C_S})\cdot(\widehat{C_X}-C_X)\\ \frac{d\widehat{C_S}}{dt} &= -\sigma(\widehat{C_S})\widehat{C_X} - U\widehat{C_S} + UC_{S,in} + k_2(\widehat{C_X},\widehat{C_S})\cdot(\widehat{C_X}-C_X)\end{aligned} \tag{5.12}$$

The tuning functions k_1, k_2 are chosen such that the error system given below, converges to zero. The errors are defined as $E_1 = C_X - \widehat{C_X}$ and $E_2 = C_S - \widehat{C_S}$. Notice that here only one correction term appears and that the estimate and the measurement are not transformed.

$$\begin{pmatrix}\frac{dE_1}{dt}\\ \frac{dE_2}{dt}\end{pmatrix} = \begin{pmatrix}\mu(\widehat{C_S}) - U + k_1(\widehat{C_X},\widehat{C_S}) & \frac{\partial\mu}{\partial C_S}(\widehat{C_S})\widehat{C_X}\\ -\sigma(\widehat{C_S}) + k_2(\widehat{C_X},\widehat{C_S}) & -\frac{\partial\sigma}{\partial C_S}(\widehat{C_S})\widehat{C_X} - U\end{pmatrix}\begin{pmatrix}E_1\\ E_2\end{pmatrix} \tag{5.13}$$

A possible way for designing the tuning function is to calculate the eigenvalues of the linear time varying error system as functions of the tuning functions and construct the tuning functions such that the eigenvalues are constant and negative. An additional requirement is that the time derivative of the error matrix is bounded. As indicated in Appendix A on estimation theory it is sufficient to assure boundedness of the tuning functions in the region of interest.

For instance, for an eigenvalue $\lambda = -5$ (with double multiplicity), the following result is obtained for the correction terms.

$$\begin{aligned}k_1(\widehat{C_X},\widehat{C_S}) &= -(-2U + a\widehat{C_S} + b\widehat{C_X} + 10)\\ k_2(\widehat{C_X},\widehat{C_S}) &= -\frac{1}{a\widehat{C_X}}(25 + U^2 - 10U - 2Ub\widehat{C_X} + ab\widehat{C_S}\widehat{C_X} + b^2\widehat{C_X^2} + 10b\widehat{C_X})\end{aligned} \tag{5.14}$$

Case 2: measurements of substrate C_S.
For the same (double) eigenvalue $\lambda = -5$, we obtain:

$$\begin{aligned}k_1(\widehat{C_X},\widehat{C_S}) &= -\frac{1}{b\widehat{C_S}}(25 + U^2 - 10U - 2Ua\widehat{C_S} + ab\widehat{C_S}\widehat{C_X} + a^2\widehat{C_S^2} + 10a\widehat{C_S})\\ k_2(\widehat{C_X},\widehat{C_S}) &= -(-2U + a\widehat{C_S} + b\widehat{C_X} + 10)\end{aligned} \tag{5.15}$$

Extendibility.
The method is also applicable to the Monod and Maynard-Smith (Volterra) models.
The method has two major drawbacks.

1. The result is only locally valid. The method of Keller and Isidori is certainly better in this respect.

2. The construction of the tuning functions k_i can be very hard. The method of Bestle and Zeitz tries to relax this problem by transforming the system to a canonical form. However, their method is also only locally valid.

5.4.2 Method 3: Local linearization in observer coordinates

Bestle and Zeitz show in their work that the use of a canonical form obtained by linearization and output injection is very interesting because the error dynamics are then represented by a linear time invariant model.

As it was already the case for the methodology of Isidori and Keller (Section 5.3), the corresponding transformation may be very hard to find analytically or does not even exist. However, Bestle and Zeitz show that the *derivatives* (with respect to the state vector) *of the transformation* to the canonical form can be easily found. By taking a local approximation of the error system in canonical coordinates, these derivatives can be used directly in the observer design without explicit need for the transformation itself. Of course, this result is again only locally valid. However, at least the selection of the observer tuning parameters is simplified a lot.

The actual implementation of the method is rather straightforward. It is not even necessary to go to the canonical form. The tuning functions are given by straightforward calculations.

The method of Bestle and Zeitz is also applicable to time varying systems. Here the application of this design method is limited to time invariant systems. In the following procedure, g is the vector containing the right hand sides of the state differential equations while h is the right hand side of the output equation.

1. Define the following operator:

$$N_1(\frac{\partial h}{\partial x})^T \triangleq g^T(\frac{\partial}{\partial x}(\frac{\partial h}{\partial x})^T) + (\frac{\partial h}{\partial x})^T \frac{\partial g}{\partial x} \tag{5.16}$$

2. Check the following observability condition:

$$rank \begin{pmatrix} (\frac{\partial h}{\partial x})^T \\ N_1(\frac{\partial h}{\partial x})^T \end{pmatrix} \stackrel{?}{=} 2 \tag{5.17}$$

3. If this condition is satisfied, calculate the vector $q(x)$ which is the last column of the inverse of the above observability matrix.

4. Define the following operator:

$$N_2(r) \triangleq -(\frac{\partial r}{\partial x})g + (\frac{\partial g}{\partial x})r \tag{5.18}$$

5. Select the coefficients p_0 and p_1 such that the following equation has solutions for λ in the open left half plane:

$$\lambda^2 + p_1\lambda + p_0 = 0$$

6. The tuning function vector is then given as (I_2 is the identity matrix of dimension 2):

$$k(\hat{x}) = (p_0 I_2 + p_1 N_2 + N_2^2)q(\hat{x}) \tag{5.19}$$

Case 1: measurements of biomass C_X. The output equation is:

$$Y = h(X) = C_X \tag{5.20}$$

For the model prototype (5.2) the observability matrix is:

$$\begin{pmatrix} 1 & 0 \\ aC_S - UC_X & aC_X \end{pmatrix} \tag{5.21}$$

The rank condition is fulfilled if $C_X \neq 0$. The tuning functions are given now by:

$$\begin{aligned} k_1 &= p_1 + 3a\widehat{C_S} - 4U + b\widehat{C_X} \\ k_2 &= \frac{p_0}{a\widehat{C_S}} - \frac{3Up_1}{a\widehat{C_S}} + \frac{bp_1}{a} + \frac{2\widehat{C_X}p_1}{\widehat{C_S}} \\ &\quad - \frac{8U\widehat{C_X}}{\widehat{C_S}} + \frac{9U^2}{a\widehat{C_S}} + \frac{4a\widehat{C_X}^2}{\widehat{C_S}} - b\widehat{C_X} - \frac{4UC_{S,in}}{\widehat{C_S}} - \frac{4bU}{a} + \frac{b^2\widehat{C_S}}{a} \end{aligned} \tag{5.22}$$

Case 2: measurements of substrate C_S.
The tuning functions for substrate measurements are:

$$\begin{aligned} k_1 &= \frac{p_0}{b\widehat{C_X}} + \frac{-3Up_1}{b\widehat{C_X}} + \frac{ap_1}{b} + \frac{2\widehat{C_S}p_1}{\widehat{C_X}} + \frac{2p_1UC_{S,in}}{b\widehat{C_X}^2} - a\widehat{X_1} - \frac{8U\widehat{C_S}}{\widehat{C_X}} + \\ &\quad \frac{12UC_{S,in}\widehat{C_S}}{\widehat{C_X}^2} - \frac{8U^2C_{S,in}}{b\widehat{C_X}^2} + \frac{8U^2C_{S,in}^2}{b\widehat{C_X}^3} + \frac{9U^2}{b\widehat{C_X}} - \frac{8U^2C_{S,in}}{b\widehat{C_X}^2} + \frac{4b\widehat{C_S}^2}{\widehat{C_X}} + \\ &\quad \frac{2aUC_{S,in}}{b\widehat{C_X}} - \frac{4aU}{b} + \frac{a^2\widehat{C_X}}{b} \\ k_2 &= p_1 + \frac{2UC_{S,in}}{\widehat{C_X}} - 4U + a\widehat{C_X} + 3b\widehat{C_S} \end{aligned} \tag{5.23}$$

Extendibility.
As this method only consist of straightforward calculations, it can be used for all the biotransformation models.

5.5 Method 4: High gain observers

The methodology by [Gauthier *et al.* 1992] can be summarized as follows.

1. Transform the original system to a canonical form (Appendix C). It can be shown that this transformation is possible for the biotechnological model class (5.1), independently of the biotransformation model.

2. The following observer based on the canonical form can then be used:

$$\begin{aligned} \frac{d\widehat{Z_1}}{dt} &= \widehat{Z_2} + G_1(\widehat{Z_1})U + s_1 \cdot (\widehat{Z_1} - Z_1) \\ \frac{d\widehat{Z_2}}{dt} &= -a(\widehat{Z_1}, \widehat{Z_2}) + G_2(\widehat{Z_1}, \widehat{Z_2})U + s_2 \cdot (\widehat{Z_1} - Z_1) \end{aligned} \tag{5.24}$$

The correction terms are given by the following equation with $Y = Z_1$ the measured state:

$$\begin{pmatrix} s_1 \cdot (\widehat{Z_1} - Z_1) \\ s_2 \cdot (\widehat{Z_1} - Z_1) \end{pmatrix} = S^{-1}(\infty) \cdot \begin{pmatrix} \widehat{Z_1} - Y \\ 0 \end{pmatrix} \tag{5.25}$$

The matrix $S(\infty)$ is the solution of the following equation with A the anti-shift operator and C the output matrix in the transformed coordinate system (here $C = (1\ 0)$). $\theta = -3\lambda$ is the only tuning parameter with λ the convergence rate of the observer.

$$-\theta S(\infty) - A^T S(\infty) - S(\infty)A + C^T C = 0 \tag{5.26}$$

3. Transform back to the original coordinate system.

The existence of such a transformation is guaranteed if the condition of uniform observability for any input is satisfied [Gauthier and Bornard 1981]. However, a method for calculation of the transformation for a general system is not available. The exponential convergence of this observer can be proven for θ large enough. In [Gauthier *et al.* 1992] an underbound is given.

Case 1: measurements of biomass C_X.
For our model prototype (5.1)(5.2), the following observer is designed:

- State transformation:

$$\begin{aligned} Z_1 &= C_X \\ Z_2 &= aC_XC_S \end{aligned} \tag{5.27}$$

- The dynamical equations for the new states are:

$$\begin{aligned} \frac{dZ_1}{dt} &= Z_2 - Z_1\,U \\ \frac{dZ_2}{dt} &= bZ_1Z_2 + \frac{Z_2^2}{Z_1} + (-2Z_2 + aC_{S,in}Z_1)\,U \end{aligned} \tag{5.28}$$

- The observer in the new coordinate system is given below:

$$\begin{aligned} \frac{d\widehat{Z_1}}{dt} &= \widehat{Z_2} - U\widehat{Z_1} - 2\theta\cdot(\widehat{Z_1} - Z_1) \\ \frac{d\widehat{Z_2}}{dt} &= b\widehat{Z_1}\widehat{Z_2} + \frac{\widehat{Z_2^2}}{\widehat{Z_1}} + U(-2\widehat{Z_2} + aC_{S,in}\widehat{Z_1}) - \theta^2\cdot(\widehat{Z_1} - Z_1) \end{aligned} \tag{5.29}$$

- In the original coordinates the observer consists of the original system with the following correction terms:

$$\begin{aligned} k_1(\widehat{C_X},\widehat{C_S}) &= 6\lambda \\ k_2(\widehat{C_X},\widehat{C_S}) &= -\frac{1}{\widehat{C_X}}\left(\frac{9\lambda^2}{a} + 6\lambda\widehat{C_S}\right) \end{aligned} \tag{5.30}$$

Case 2: measurements of substrate C_S.
A quite similar result is found when substrate is considered to be measurable. The correction terms look as follows:

$$\begin{aligned} k_1(\widehat{C_X},\widehat{C_S}) &= -\frac{1}{\widehat{C_S}}\left(\frac{9\lambda^2}{b} + 6\lambda\widehat{C_X}\right) \\ k_2(\widehat{C_X},\widehat{C_S}) &= 6\lambda \end{aligned} \tag{5.31}$$

Extendibility.
This method is again applicable to all biotransformation models.

5.6 Simulation results

The dynamical behavior of the different observers is illustrated on simulation data, generated by using a dilution rate $U = 1$ 1/h and input substrate concentration $C_{S,in} = 500$ g/L as operational conditions and $a = 0.05$ L/g h, $b = -0.1$ L/g h the parameters in the prototype model (5.1) (5.2). The initial conditions of the system are $(C_X(0), C_S(0)) = (150g/L, 30g/L)$.

Performance of the algorithms based on (i) exact linearization, (ii) local linearization in observer coordinates or (iii) in original coordinates, and (iv) high gain approach for *biomass measurements* is shown.

In Figure 5.1 a plot of the evolution of the error in the biomass-substrate space is given for the four algorithms, starting from several initial values. In Figure 5.2 a plot of the evolution of the estimated state, the real state and the error versus time is given for the four algorithms, for a particular initial value $((\widehat{C_X(0)}, \widehat{C_S(0)}) = (155g/L, 30g/L)$. The parameters for the several observers are: (i) exact linearization: $l_1 = 25, l_2 = 10$, corresponding with an eigenvalue $\lambda = -5$ with double multiplicity, (ii) local linearization in observer coordinates: $p_0 = 25, p_1 = 10$, resulting in the same eigenvalues as in the first algorithm, (iii) local linearization in original coordinates with the tuning functions constructed such that the eigenvalues of the local linear system are equal to the eigenvalues of the previous algorithms and (iv) finally high gain observer: $\theta = 0.1$. Notice that the eigenvalues indicate the convergence speed of the algorithms, but expressed in another coordinate system, which makes comparing difficult. Chosing the eigenvalues of the different algorithms, such that the same convergence speed is obtained in the original coordinate system, is however difficult as the result is depending on the state of the observer.

5.7 Performance analysis

Due to the existence of several quite different design methodologies there exists an observer selection problem for the process engineer, who wants to use the observer concept to relax the measurement problem. Besides the applicability of the methods for the considered process the selection must be based on performance measures of the observers. The performance of an observer can be characterized by (i) the convergence region (Section 5.8), (ii) the noise sensitivity (Section 5.9), (iii) the speed of convergence (Section 5.9), (iv) the robustness against uncertainty (Section 5.10), and (v) the robustness against discretization (Section 5.11).

Performance analysis is introduced as an interesting tool to tackle *the observer selection problem.*

In Sections 5.8, 5.9, 5.10 and 5.11 these performance criteria are evaluated for a prototype model (5.2) for bioprocesses and the related observers, orig-

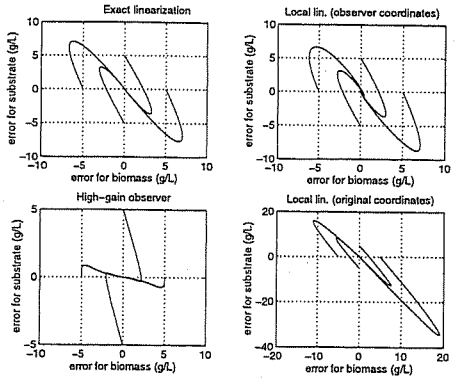


Figure 5.1: Measurements of biomass. Error dynamics in the biomass-substrate space

inating from the different design methodologies. The performance analysis is illustrated for the case with *biomass* and *substrate* measurements.

Recall that the main goals of the analysis are (i) introduction of the performance criteria, (ii) presentation of the (general) concepts used for analysis and (iii) illustration how the results must be interpreted. As such the case study presented here must first be considered as a vehicle for presenting the performance analysis tools.

From the particular results obtained for the prototype model, although quite depending on the particular parameters used in the calculations, some conclusions about observer design in general and the methodologies studied in particular can be formulated. Obtaining such conclusions can be considered to be the second goal of the case study.

5.8 Convergence region

An important characteristic of an observer is its *convergence region* or its domain of attraction defined below.

Definition. *$\Omega(C_X(0), C_S(0))$ is the convergence region of the observer if and only if the observer converges to the real state $C_X(t), C_S(t)$ of the system (with initial state $C_X(0)$, $C_S(0)$) for any initial estimate $\widehat{C_X}(0)$, $\widehat{C_S}(0)$ belonging to $\Omega(C_X(0), C_S(0))$.*

Notice that the convergence region is function of the initial state of the system. Below the convergence region of the different observers is plotted for the initial state of the system given in Section 5.6. The domain of attraction

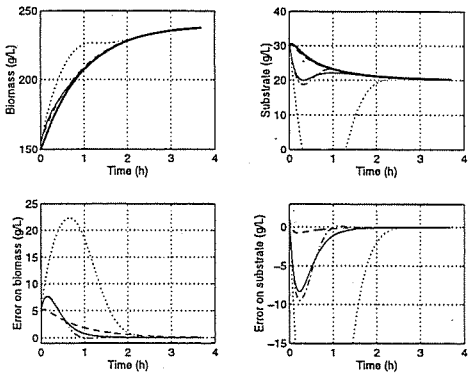


Figure 5.2: Measurements of biomass. Time evolution of the state estimates and the errors. Exact linearization (—), Local linearization (in original coordinates ($\cdots$), in observer coordinates ($-\cdot-$)), High gain observer ($--$)

is shown in error coordinates. The plots (Figure 5.3, 5.4) indicate which initial errors (E_1, E_2) on the biomass $\widehat{C}_X$ and substrate $\widehat{C}_S$ concentration estimates are allowed to guarantee convergence of the estimates to the real state. The allowable errors are indicated by $+$. The points, marked with a $\star$, are leading to divergence.

From a theoretical point of view the convergence area should be the full 2-dimensional state space. In practice a limited convergence area is sufficient. The maximum initial error has been limited here to 100 % for both the biomass C_X and the substrate C_S concentration. This prevents occurence of zero and negative states.

The following conclusions can be stated.

Exact linearization and high-gain methods.

The convergence region covers the 2-dimensional state space, spanned by the positive concentrations.

Local linearization techniques.

The convergence region is for most cases quite limited.

Recall that the construction of the tuning functions is based on a transformation to a certain canonical form. Notice that limitation of the convergence region can appear due to the local approximation property used in the method (local linearization in observer and original coordinates) or because the transformation to the canonical form is not a diffeomorphism.

As a conclusion it can be stated that both the high-gain and the exact linearization method have excellent performance when the convergence region is considered as a measure of performance.

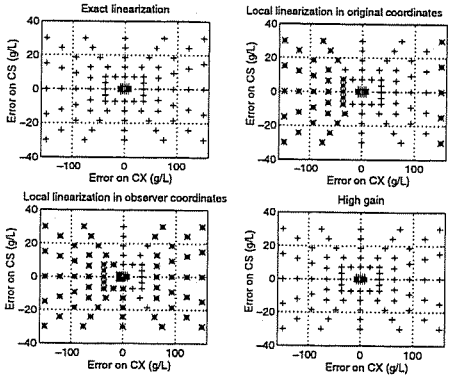


Figure 5.3: Measurements of biomass. Domain of attraction. Divergence (*) or convergence (+)

5.9 Noise sensitivity and speed of convergence

The tuning of the observer parameters is generally based on the trade-off between *speed of convergence* and *noise sensitivity*.

In the observers studied here, the selection of the tuning parameters is reduced to the selection of the eigenvalue of the error system in a certain coordinate system. The value of the eigenvalue indicates the speed of convergence.

The noise sensitivity is determined by the magnitude of the tuning functions. This can be seen easily when it is assumed that (i) the real system has converged to its equilibrium point, (ii) the estimate of the state has converged to the real state and (iii) the noise is modeled as a white noise source $W(t)$ added to the measurement (the biomass or substrate concentration). Then the observer dynamics are written (except for the exact linearization approach) as follows.

$$\begin{aligned} \frac{d\widehat{C_X}}{dt} &= k_1(\widehat{C_X},\widehat{C_S})\cdot(W(t)) \\ \frac{d\widehat{C_S}}{dt} &= k_2(\widehat{C_X},\widehat{C_S})\cdot(W(t)) \end{aligned} \qquad (5.32)$$

Notice that the influence of the noise term on the dynamics of the observer is given by the tuning functions. Different measures for the noise sensitivity of an observer can be defined. One possible choice is to determine the maximum absolute value of the tuning functions over the (limited) convergence

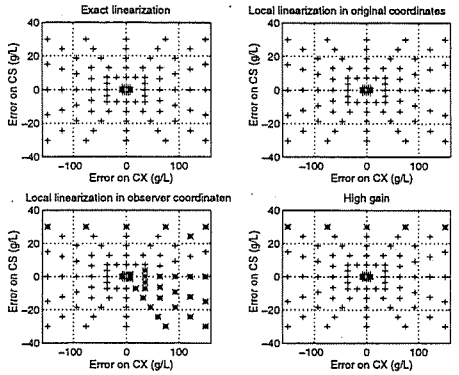


Figure 5.4: Measurements of substrate. Domain of attraction. Divergence (*) or convergence (+)

region for a certain design eigenvalue λ. It is clear that this measure represents the worst-case situation. This measure is useful for determining an operating region of the observer. Such an operating region can be defined as the set of state estimates for which the noise sensitivity remains acceptable. It is clear that singularities of the tuning functions must be excluded from this operating region. These values obtained with this definition are quite high because the tuning functions generally reaches their maximum at the boundary of the (limited) convergence region. As such this measure is not representative for the overall noise sensitivity.

An alternative measure of the noise sensitivity is the absolute value of the evaluation of the tuning function for a certain state.

$$R_1(\lambda) = |\,k_1(C_X,C_S)\,| \;\;;\;\; R_2(\lambda) = |\,k_2(C_X,C_S)\,| \qquad (5.33)$$

This measure is then assumed to be a good estimate of the overall noise sensitivity. It is clear that the quality of this measure is depending on the point for which the sensitivities are evaluated. In this sense it is an arbitrary measure. Careful selection, for instance by avoiding singularities of the tuning functions, will result however in a good approximation of the overall noise sensitivity. In the sequel the noise sensivity is evaluated in the equilibrium state of the system.

The Figures 5.5 and 5.6 show the results obtained in the case with biomass concentration measurements. Similar figures are determined in the case of substrate concentration measurements.

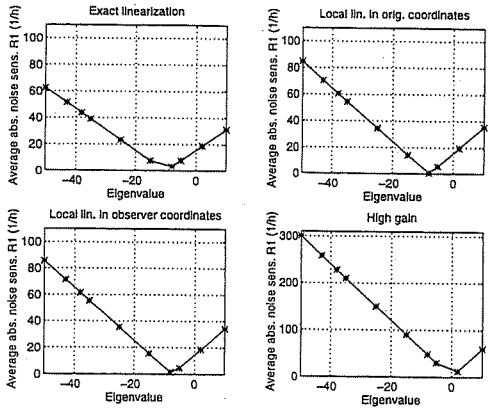


Figure 5.5: Measurements of biomass. Noise sensitivity of the measured state (biomass)

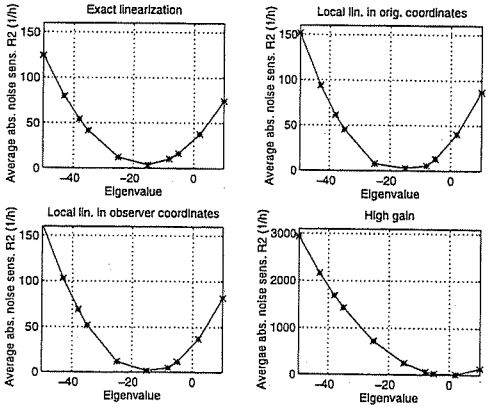


Figure 5.6: Measurements of biomass. Noise sensitivity of the estimated state (substrate)

From the analysis it can be concluded that the noise sensitivity measure confirms the fact (described in literature) that the high-gain observer is the most noise sensitive method (factor 10 in comparison with the other methods), although the noise sensitivity of these methods is still quite high (when compared to the absolute value of the states).

Exact linearization. The noise sensitivity norms are based on the tuning functions $k_1(\widehat{C_X}, \widehat{C_S}), k_2(\widehat{C_X}, \widehat{C_S})$. Due to the transformations of the data and the estimates found in the exact linearization case a fair comparison can only be done by defining new tuning functions $\bar{k}_1(\widehat{C_X}, \widehat{C_S}), \bar{k}_2(\widehat{C_X}, \widehat{C_S})$. Because the estimate and the state are equal (when the observer converge) these functions are defined by taking a limit. This is shown below for biomass measurements. A similar approach can be used for substrate concentration measurements.

$$\begin{aligned} \bar{k}_1(\widehat{C_X}, \widehat{C_S}) &= \lim_{\widehat{C_X} \to C_X} \frac{\sum_j k_{1j}(\widehat{C_X}, \widehat{C_S}) \cdot (t_{1j}(\widehat{C_X}) - t_{1j}(C_X))}{(\widehat{C_X} - C_X)} \\ \bar{k}_2(\widehat{C_X}, \widehat{C_S}) &= \lim_{\widehat{C_X} \to C_X} \frac{\sum_j k_{2j}(\widehat{C_X}, \widehat{C_S}) \cdot (t_{2j}(\widehat{C_X}) - t_{2j}(C_X))}{(\widehat{C_X} - C_X)} \end{aligned} \tag{5.34}$$

5.10 Robustness analysis

The effect of (parametric and structural) uncertainty on the estimation error and the stability of the estimator is discussed. The concepts and terminology used in the analysis of the estimation error and the stability analysis of the nonlinear observers are introduced in general.

The robustness analysis is illustrated for the prototype model (5.2) for biological processes and the related observers, originating from the different design methodologies, for both measurements of *biomass* and *substrate* concentration. The results obtained for the case study are presented. The parameters of Section 5.6 are used.

More general conclusions on robustness of nonlinear observers are given at the end of the chapter. The following notation is used in the sequel.

The model of the system. It is assumed that this model exactly describes the dynamics of the system under consideration. In this sense the model will be referred to as the *perfect* or *exact* model. The input of the system is not explicitly mentioned as it is assumed to be constant.

$$\frac{d\mathbf{x}(t)}{dt} = \mathbf{f}(\mathbf{x}(t)) \tag{5.35}$$

The model of the system with uncertainty. This is the model of the system used in the observer design. This model does not describe the dynamics of the system under consideration because (i) the parameters of this model differ from the one used in (5.35) (due to parametric uncertainty) or (ii) even the structure of the models (5.36) and (5.35) do not match (due to structural uncertainty). For the reason discussed above this model will be referred to as the *wrong* model.

$$\frac{d\mathbf{x}(t)}{dt} = \tilde{\mathbf{f}}(\mathbf{x}) \tag{5.36}$$

The observer equations. The observer equation consists of a copy of the so-called wrong model (5.36) and a correction term. The correction term is a product of the tuning functions $\widetilde{\mathbf{k}}(\widehat{\mathbf{x}})$ and the error between the measured state and its estimate. The notation of the tuning functions indicates that their design is based on the wrong model. The selection matrix $\mathbf{L}$ is used to select the measured state and its estimate.

$$\frac{d\widehat{\mathbf{x}}(t)}{dt} = \widetilde{\mathbf{p}}(\widehat{\mathbf{x}}) = \widetilde{\mathbf{f}}(\widehat{\mathbf{x}}) + \widetilde{\mathbf{k}}(\widehat{\mathbf{x}}) \cdot \mathbf{L} \cdot (\mathbf{x} - \widehat{\mathbf{x}}) \tag{5.37}$$

This general notation of the observer equations is suited for all observers studied except for the observers based on exact linearization. The extension for this type of observers is however straightforward.

5.10.1 Equilibrium analysis

Concepts

In the equilibrium analysis the steady state error on the estimate (non-measured state) is taken as a measure of robustness. It is assumed that the state of the system under study has converged to its steady state value. Note that an observer can also be used as filter for the measured state. The steady state error on this variable can in this case be taken as robustness measure. Recall that in the case that a perfect model of the system under consideration is used for the observer design these steady state errors are zero by design. One must be aware that due to the steady state assumption the robustness measure obtained in this way is only locally valid. The following calculations must be performed.

Determination of the equilibrium point $\mathbf{x_e}$ of the system. This equilibrium point is found by solving the set of nonlinear equations, obtained by setting the perfect model equations (5.35) equal to zero.

Determination of the equilibrium point $\widehat{\mathbf{x_e}}$ of the observer. This equilibrium point is found by solving the set of nonlinear equations, obtained by setting the observer equations (5.37) equal to zero. Notice that in the observer equations the wrong model (denoted $\widetilde{\mathbf{f}}(\mathbf{x}(t))$) is used.

The equilibrium point $\widehat{\mathbf{x_e}}$ of the observer is calculated as function of a measure of the uncertainty on the model. These calculations requires repeated solving of a set of nonlinear equations. Two methods are used in the analysis.

Method 1. The nonlinear equations are solved numerically. Notice that for the case study this results in a 2-dimensional problem. It has been observed in the case study that (i) this problem can be numerical badly conditioned, (ii) the solution obtained depends on the initial starting point (indicating that there is no unique result), (iii) it may appear that no solution exists in the region of interest. From these observations one must conclude that the obtained results must be interpreted very cautiously. The main advantage is that this method is generally applicable.

Method 2. The structure of the nonlinear equations has been exploited when possible. When one of the unknowns can be written explicitly as a nonlinear function of the other unknown, the complexity of the problem can be reduced. For the 2-dimensional case, a nonlinear equation in one variable (part of the state $\widehat{\mathbf{x_e}}$) is then obtained, which can be solved. The other part of the state $\widehat{\mathbf{x_e}}$ is then obtained by using the explicit relation.

For the case study often one variable can be written as a ratio of two polynomials of the other variable. This relation is obtained from one of the nonlinear equations. By substitution of this relation into the other equation a polynomial in one variable (part of the state $\widehat{\mathbf{x_e}}$) is obtained, which is then solved. The other part of the state is then obtained via this relation. Notice that besides the complexity reduction obtained, the polynomial formulation of the problem has additional advantages. A dedicated solver for polynomials can be used. Such a solver provides all the possible solutions and does not require initial starting points. Moreover it will be shown that the polynomial formulation gives better insight in the robustness analysis because it provides also complex solutions. It is important to mention that the reformulation with polynomials can results in extra solutions (not satisfying the nonlinear equations) or not physically relevant solutions (negative, complex). Some additional tests must be performed to select the appropriate solution. The main drawback of this method is that it is not generally applicable.

The error due to uncertainty consists of two contributions. When the steady state value of the exact model (5.35), the wrong model (5.36) (used in the observer design) and the observer (5.37) are denoted respectively $\mathbf{x_e}$, $\widetilde{\mathbf{x_e}}$ and $\widehat{\mathbf{x_e}}$ the relation (5.38) can be written by applying Schwarz inequality.

$$|\widehat{\mathbf{x_e}} - \mathbf{x_e}| \leq |\widehat{\mathbf{x_e}} - \widetilde{\mathbf{x_e}}| + |\widetilde{\mathbf{x_e}} - \mathbf{x_e}| \tag{5.38}$$

From equation (5.38) one can conclude that the estimation error due to the uncertainty on the model consists of two contributions.

1. The first contribution is the error between the estimate $\widehat{\mathbf{x_e}}$ obtained with the observer and the steady state value $\widetilde{\mathbf{x_e}}$ for the wrong model. It is clear that this error is dependent on the tuning functions and thus different for the observers originating from different design methodologies.

2. The second contribution is the error between the steady state value $\mathbf{x_e}$ of the perfect model and the wrong model $\widetilde{\mathbf{x_e}}$. This part of the robustness measure is independent of the tuning functions and as such independent of the observer design methodology.

In the case study both contributions (o total error $|\widehat{\mathbf{x_e}} - \mathbf{x_e}|$, $+$ error due to model part $|\widetilde{\mathbf{x_e}} - \mathbf{x_e}|$ and $*$ error due to the tuning functions $|\widehat{\mathbf{x_e}} - \widetilde{\mathbf{x_e}}|$) of the estimation error will be indicated. In this way one can easily determine which contribution dominates. From this observation one can con-

clude whether the robustness can be improved by considering another design methodology or is intrinsically related to the model under consideration.

Robustness against parametric uncertainty

For the case study, it is assumed that the parameter a of the model (5.1)(5.2) is not perfectly known. The parametric uncertainty on a is denoted Δa. It is assumed that the parametric uncertainty on the parameter b (denoted Δb) is proportional with the parameter uncertainty on a. The proportionality constant is the yield coefficient $Y_{X/S}$ of biomass on substrate.

The exact model has two equilibrium points. The one with a non-zero biomass concentration is $(C_{X,e}, C_{S,e}) = (20, 240)$ [g/L]. The equilibrium point (with non-zero biomass concentration) of the wrong model is found with equation (5.39).

$$\widetilde{C_{S,e}} = \frac{U}{(a+\Delta a)} \quad ; \quad \widetilde{C_{X,e}} = \frac{U-(a+\Delta a)C_{S,in}}{(b+\Delta b)} \tag{5.39}$$

In the sequel the equilibrium analysis is performed for the different observers for both *biomass* and *substrate* concentration measurements. The results are shown in Figure 5.7. Some comments on the calculations and the results are presented below.

Exact linearization up to an output injection

Due to the nonlinear transformations in the correction terms of this type of observers, their steady state values as function of the uncertainty on the parameter a (and the related change of the parameter b) are found by solving the observer equations simultaneously.

Measurements of the biomass concentration

The steady state values are obtained by solving the observer equation, consisting of the model (5.1), with the first order kinetics (5.2) and the correction term (5.3). The parameters a and b are replaced by $a+\Delta a$ and $b+\Delta b$. No numerical problems are detected during solving the equations.

In Figure 5.7 the two contributions of, and the total relative error on the estimates (compared with the steady state obtained with the exact model) are shown for both the biomass and the substrate concentration.

Measurements of the substrate concentration

When compared with the previous case only the correction term in the observer equation is different. The correction term is given by equation (5.3). The results are shown in Figure 5.7.

Local linearization in original coordinates

Measurements of the biomass concentration

The observer consists here of the model (5.1) with the first order model and the correction terms (5.14). The steady state values for the observer are found by setting these equations equal to zero. From the equation describing the dynamics of the biomass concentration estimate, the substrate concentration estimate can be written explicitly as a function (second order

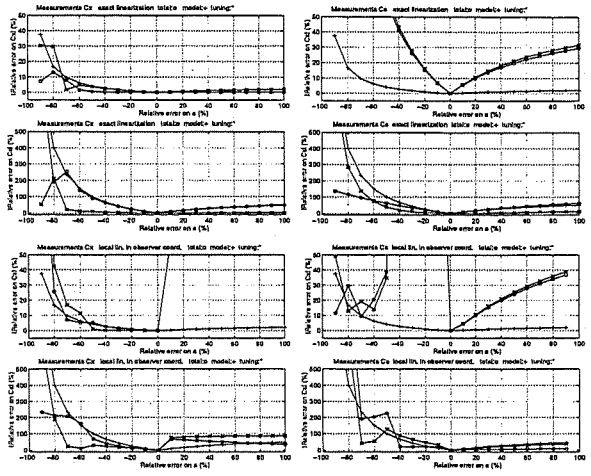


Figure 5.7: Equilibrium analysis. Relative estimation error on the biomass and substrate concentration as function of the relative uncertainty on the parameter a

polynomial) of the biomass concentration estimate. When this relation is used in the equations describing the dynamics of the substrate concentration estimate, a third order polynomial in the biomass concentration estimate is obtained, which can be solved. The results for this case are not shown.

Measurements of the substrate concentration

The polynomial method is used for solving the observer equations, consisting of the model and the correction terms (5.15). The biomass concentration estimate can written as an explicit function (second order polynomial) of the substrate concentration estimate. This relation is obtained from the dynamic equation of the substrate concentration estimate. A third order polynomial in the substrate concentration estimate is found by combining this relation with the biomass concentration estimates dynamic equation. The results for this case are not shown.

Local linearization in observer coordinates

Measurements of the biomass concentration

The polynomial method is used here. The observer consists of the model and the tuning function (5.22). The substrate concentration estimate can be written as a ratio of two polynomials in the biomass concentration estimate (numerator order 2, denominator order 3). This relation is obtained from the dynamic equation for the biomass concentration estimate. Using this relation in combination with the substrate concentration estimates dy-

$\frac{\Delta a}{a}$ (%)	C_X ($\times 10^{-2}$)					Selected
-30	2.463	2.362	1.829	1.367	-0.645	2.3627
-20	2.451	2.378	1.838	1.240	-0.614	2.3785
-10	2.440	2.389	1.846	1.141	-0.587	2.3899
0	2.430	2.400	1.852	1.060	-0.564	2.4000
10	2.414 - 0.005i	2.414 + 0.005i	1.858	0.994	-0.544	0.9942
20	2.414 - 0.014i	2.414 + 0.014i	1.862	0.937	-0.526	0.9378
30	2.413 - 0.018i	2.413 + 0.018i	1.866	0.889	-0.509	0.8893
40	2.413 - 0.020i	2.413 + 0.020i	1.870	0.847	-0.495	0.8471

Table 5.1: Local linearization in observer coordinates. Solutions of the fifth order polynomial in the biomass concentration estimate in function of the relative parametric uncertainty on the parameter a. Measurements of the biomass concentration

namic equation, a fifth order dynamic equation in the biomass concentration estimate is obtained.

The results (Figure 5.7) show a discontinuous jump in the error on both the biomass and substrate concentration estimate. This strange result is due to the selection procedure and is discussed now in detail.

Table (5.1) shows the results of the fifth order polynomial in the biomass concentration estimate in function of the relative parametric uncertainty on the parameter a. The solver for the polynomial gives five results. As discussed before, not all the solutions are valid and physically relevant. In the table it is visualized that for underestimates of the parameter a the solution of column two is selected as the final solution. The selection criteria are: (i) the resulting estimate must be real and positive, (ii) satisfy the original equilibrium equations and (iii) result in the smallest estimation error. From the table it is clear that for overestimates of the parameter a the solutions are indeed continuously varying as function of the parametric uncertainty but the solution of column two becomes complex and as such can not be selected as a valid solution. This example illustrates that the polynomial method provides better insight in the robustness properties. When the determination of the equilibrium point is done by simultaneously solving the observer equations, a badly conditioned problem is obtained, resulting in unreliable results.

Measurements of the substrate concentration

The equilibrium points of the observer equations with tuning functions (5.23) are obtained with the polynomial method. From the substrate concentration estimate dynamical equation the biomass concentration estimate can be written as a ratio of a third order polynomial and a second order polynomial in the substrate concentration estimate. Combining this relation with the other dynamic equation of the observer, results in a seventh

order polynomial in the substrate concentration estimate.

The results (Figure 5.7) show again discontinuities in the error as function of the parametric uncertainties for underestimates of the parameter a. A similar explanation as for the biomass concentration measurements case can be given.

High gain observer

Measurements of the biomass concentration

The equilibrium points of the observer with tuning functions (5.30) are determined with the polynomial method. From the biomass concentration estimate dynamical equation the substrate concentration estimate can be written as a ratio of two first order polynomial of the biomass concentration estimate. Combining this relation with the substrate concentration estimate dynamical equation results in a third order polynomial in the biomass concentration. The results for this case are not shown.

Measurements of the substrate concentration

The tuning functions are given by Equation (5.31). From the substrate concentration estimate dynamical equation the biomass concentration estimate can be written as a ratio of a two first order polynomial of the substrate concentration estimate. Combining this relation with the biomass concentration estimate dynamical equation results in a third order polynomial in the substrate concentration. The results for this case are not shown.

Robustness against structural uncertainty

For the case study, it is assumed that the system under consideration is not modeled with the first order model (5.2) but with the Monod model although the observer equations are based on the first order model. The parameter of the first order model and the Monod model are related by Equation (5.40). This equation states that the first order model and the Monod model results in the same value for the specific biomass growth rate for some arbitrary substrate concentration C_S^*. In the case study the initial substrate concentration $C_S(0)$ used in the simulations has been used. From a process point of view one can assume that the identification of the parameters a and b is performed for the operating point with substrate concentration $C_S(0)$ while during the operation of the observer the operating point has changed. Notice that the yield coefficient $Y_{X/S}(= \frac{a}{b})$ can be determined without specifying the kinetics [Bastin and Dochain 1990].

$$a \triangleq \mu_{max} \cdot \frac{1}{K_S + C_S^*} \quad ; \quad b \triangleq \frac{-a}{Y_{X/S}} \tag{5.40}$$

In the case study the values for a and b are fixed. The Monod constant K_S is varied and the maximum specific biomass growth rate μ_{max} is adapted using relation (5.40). Notice that due to this approach the steady state value for the system (obtained with the exact model) and the observer (obtained

with the wrong model and the wrong tuning functions) varies as function of the Monod constant while the steady value of the wrong model remains fixed ($(C_{X,e}, C_{S,e}) = (240, 20)$ [g/L]). The equilibrium point for the exact model are found with relation (5.41).

$$\begin{aligned} C_{S,e} &= \frac{UK_S}{\mu_{max} - U} \\ C_{X,e} &= \frac{-Y_{X/S}}{\mu_{max}} \cdot \left(\frac{U^2 K_S}{\mu_{max} - U} - UC_{S,in} \right) \cdot \left(\frac{K_S + \frac{UK_S}{\mu_{max} - U}}{\frac{UK_S}{\mu_{max} - U}} \right) \end{aligned} \tag{5.41}$$

Only the results for the observer based on exact linearization are shown in Figure 5.8.

Notice that the approximation of the Monod model by the first order model becomes more valid for large values of the Monod parameter K_S. It is expected that the performance of the observers will degrade for small values of this parameter because the model on which the observer is designed shows larger differences when compared to the real process dynamics.

The calculations performed for the robustness analysis against structural uncertainty can principally be done with the same equations as for the parametric robustness analysis. Notice that the observer equations have not changed with respect to the previous analysis. The main difference is the varying of the steady state of the system as function of the Monod parameter K_S, which is used (i) as input to the observer equations and (ii) serves as reference value for determining the error.

Below some comments on the calculations are presented for the different observers for both *biomass* and *substrate* concentration measurements.

These results for the observer based on exact linearization are obtained by simultaneously solving the equilibrium equations of the respective observers. The robustness analysis results of the observer based on linearization in original coordinates can be found with both simultaneously solving of the equations or the polynomial method.

For robustness analysis of the observer based on linearization in observer coordinates for both *biomass* and *substrate* concentration measurements the polynomial method is preferred. The method based on simultaneously solving of the equations is badly conditioned.

For the robustness analysis of the high-gain observer both calculation methods are feasible for the two cases.

5.10.2 Dynamical analysis

In the dynamical analysis it is investigated how the stability of the error system changes due to parametric and structural uncertainty. The eigenvalues of a local linear approximation of the error system are calculated in the equilibrium point of the estimator.

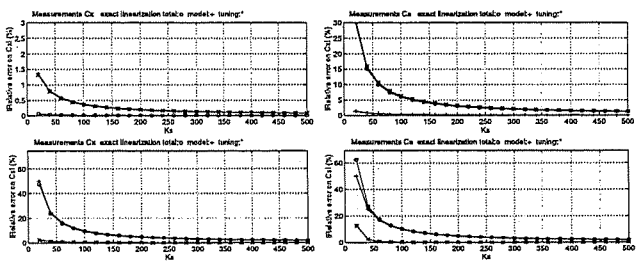


Figure 5.8: Equilibrium analysis. Relative estimation error on the biomass and substrate concentration as function of the Monod constant K_S

Recall that when a perfect model of the system under study is used in the observer design methods based on eigenvalue assignment then the eigenvalues are chosen to be time invariant and with a double multiplicity. One must be however aware of the fact that the design eigenvalues are generally not determined in the original coordinate system.

Concepts

First the dynamics of the estimation error and the estimated state is analyzed under the assumption that perfect model knowledge is available while secondly it is indicated how the uncertainty affects the dynamics of the error system and the estimator.

Dynamical analysis in the perfect model case

Assume that the model (5.35) perfectly describes the dynamics of the system under consideration. The state observer (5.42) can then be designed.

$$\frac{d\widehat{\mathbf{x}}(t)}{dt} = \mathbf{p}(\widehat{\mathbf{x}}) = \mathbf{f}(\widehat{\mathbf{x}}) + \mathbf{k}(\widehat{\mathbf{x}}) \cdot \mathbf{L} \cdot (\mathbf{x} - \widehat{\mathbf{x}}) \tag{5.42}$$

Notice that it is assumed here that the correction terms are proportional with the estimation error, defined as the difference between the state of the system $\mathbf{x}$ and the estimate of this state $\widehat{\mathbf{x}}$. Because the full state $\mathbf{x}$ is not available, the matrix $\mathbf{L}$ is used to select these states which are measured.

With this general form for the observer both observers based on local linearization and the high-gain observer can be described. The extension of the results obtained here towards observers based on exact linearization is however straightforward.

The observer (5.42) will be called the *correct* observer because its design is based on the model (5.35) which described the system perfectly. The dynamics of the estimation error $\mathbf{e} = \mathbf{x} - \widehat{\mathbf{x}}$ are described by Equation

(5.43).

$$\frac{de(t)}{dt} = \mathbf{f}(\mathbf{x}) - \mathbf{p}(\widehat{\mathbf{x}}(t)) = \mathbf{f}(\mathbf{x}) - \mathbf{f}(\widehat{\mathbf{x}}) - \mathbf{k}(\widehat{\mathbf{x}}) \cdot \mathbf{L} \cdot (\mathbf{x} - \widehat{\mathbf{x}}) \quad (5.43)$$

The stability of the error system (5.43) can be analyzed by evaluating the eigenvalues of a local linearizing approximation of the error system. The local approximation is obtained by linearizing the model part in Equation (5.43) around the state estimate $\widehat{\mathbf{x}}$. The robustness analysis will be performed in the equilibrium point of the observer, denoted by $\widehat{\mathbf{xe}}$.

$$\frac{de(t)}{dt} \approx \mathbf{f}(\widehat{\mathbf{xe}}) + \left.\frac{\partial \mathbf{f}(\mathbf{x})}{\partial \mathbf{x}}\right|_{\widehat{\mathbf{xe}}} \cdot (\mathbf{x} - \widehat{\mathbf{xe}}) - \mathbf{f}(\widehat{\mathbf{xe}}) - \mathbf{k}(\widehat{\mathbf{xe}}) \cdot \mathbf{L} \cdot (\mathbf{x} - \widehat{\mathbf{xe}}) \quad (5.44)$$

The error dynamics around the equilibrium point $\widehat{\mathbf{xe}}$ of the observer are approximately described by the linear system (5.45).

$$\frac{de(t)}{dt} \approx \left(\left.\frac{\partial \mathbf{f}(\mathbf{x})}{\partial \mathbf{x}}\right|_{\widehat{\mathbf{xe}}} - \mathbf{k}(\widehat{\mathbf{xe}}) \cdot \mathbf{L} \right) \cdot \mathbf{e} \quad (5.45)$$

The local linearization used here is exactly the local linearization used in the observer design method based on local linearization in original coordinates. In fact the observer design used for this observer guarantees that the local approximation is stable. Notice that from a design point of view it is not feasible to linearize around another point, for instance, the state of the system $\mathbf{x}$, because this state is not completely available.

This local linearization will also be used for robustness analysis of the estimation error dynamics for the other observers although their design is not based on this local approximation.

With Equation (5.45) the stability of the estimation error dynamics is analyzed. The estimator (5.42) must however also be stable. This is again analyzed by evaluating the eigenvalues of a local linearizing approximation of the estimator around the observers equilibrium point $\widehat{\mathbf{xe}}$. $\mathbf{x_e}$ denotes the equilibrium of the system.

$$\begin{aligned}\frac{d\widehat{\mathbf{x}}(t)}{dt} &\approx \mathbf{f}(\widehat{\mathbf{xe}}) + \mathbf{k}(\widehat{\mathbf{xe}}) \cdot \mathbf{L} \cdot (\mathbf{x_e} - \widehat{\mathbf{xe}}) \\ &+ \left(\left.\frac{\partial \mathbf{f}(\widehat{\mathbf{x}})}{\partial \widehat{\mathbf{x}}}\right|_{\widehat{\mathbf{xe}}} + \left.\frac{\partial \mathbf{k}(\widehat{\mathbf{x}})}{\partial \widehat{\mathbf{x}}}\right|_{\widehat{\mathbf{xe}}} \cdot \mathbf{L} \cdot (\mathbf{xe} - \widehat{\mathbf{xe}}) - \mathbf{k}(\widehat{\mathbf{xe}}) \cdot \mathbf{L} \right) \cdot (\widehat{\mathbf{x}} - \widehat{\mathbf{xe}})\end{aligned} \quad (5.46)$$

Because the observer is designed such that the equilibrium point of the system $\mathbf{x_e}$ is equal to the equilibrium point of the observer $\widehat{\mathbf{xe}}$, the dynamics of the observer are approximated by the linear system (5.47).

$$\frac{d\widehat{\mathbf{x}}(t)}{dt} \approx \left(\left.\frac{\partial \mathbf{f}(\widehat{\mathbf{x}})}{\partial \widehat{\mathbf{x}}}\right|_{\widehat{\mathbf{xe}}} - \mathbf{k}(\widehat{\mathbf{xe}}) \cdot \mathbf{L} \right) \cdot (\widehat{\mathbf{x}} - \widehat{\mathbf{xe}}) \quad (5.47)$$

It can be concluded that the dynamics of the approximation of the estimation error system (5.45) and the observer (5.47) are described by the same matrix.

Dynamical analysis with uncertainty on the model

Suppose that the dynamics of the system under consideration are described perfectly with the model (5.35) but that the design of the observer is based on the model (5.36). The model (5.36) will be referred to as the *design* or the *wrong* model. The dynamics of the estimation error are now analyzed by using the observer (5.37).

$$\frac{de(t)}{dt} = \mathbf{f}(\mathbf{x}) - \tilde{\mathbf{p}}(\widehat{\mathbf{x}}(t)) = \mathbf{f}(\mathbf{x}) - \tilde{\mathbf{f}}(\widehat{\mathbf{x}}) - \tilde{\mathbf{k}}(\widehat{\mathbf{x}}) \cdot \mathbf{L} \cdot (\mathbf{x} - \widehat{\mathbf{x}}) \quad (5.48)$$

Notice that the dynamics of the estimation error are described by both the perfect model of the system and the observer. A local approximation of these dynamics is now derived based on a local approximation of the model of the system around the estimate, obtained with the observer. The equilibrium point of the observer is denoted $\widehat{\mathbf{xe}}$.

$$\frac{de(t)}{dt} \approx \mathbf{f}(\widehat{\mathbf{xe}}) + \left.\frac{\partial \mathbf{f}(\mathbf{x})}{\partial \mathbf{x}}\right|_{\widehat{\mathbf{xe}}} \cdot (\mathbf{x} - \widehat{\mathbf{xe}}) - \tilde{\mathbf{f}}(\widehat{\mathbf{xe}}) - \tilde{\mathbf{k}}(\widehat{\mathbf{xe}}) \cdot \mathbf{L} \cdot (\mathbf{x} - \widehat{\mathbf{xe}}) \quad (5.49)$$

With this approach the following linear approximation of the estimation error dynamics is obtained.

$$\frac{de(t)}{dt} \approx \left(\left.\frac{\partial \mathbf{f}(\mathbf{x})}{\partial \mathbf{x}}\right|_{\widehat{\mathbf{xe}}} - \tilde{\mathbf{k}}(\widehat{\mathbf{xe}}) \cdot \mathbf{L} \right) \cdot \mathbf{e} + \mathbf{f}(\widehat{\mathbf{x}}) + \tilde{\mathbf{f}}(\widehat{\mathbf{x}}) \quad (5.50)$$

One can observe that this approximation consists of a linear part in $\mathbf{e}$, which is function of the model of the system and the tuning functions (designed on basis of the design model) and a function of the state estimate. This function is depending both on the model of the system and the design model. As discussed before, the dynamical robustness analysis can also be performed by analyzing the stability of the observer itself. Again a local linear approximation of the observer dynamics is determined.

$$\begin{aligned}\frac{d\widehat{\mathbf{x}}(t)}{dt} &\approx \tilde{\mathbf{f}}(\widehat{\mathbf{xe}}) + \tilde{\mathbf{k}}(\widehat{\mathbf{xe}}) \cdot \mathbf{L} \cdot (\mathbf{xe} - \widehat{\mathbf{xe}}) \\ &+ \left(\left.\frac{\partial \tilde{\mathbf{f}}(\widehat{\mathbf{x}})}{\partial \widehat{\mathbf{x}}}\right|_{\widehat{\mathbf{xe}}} + \left.\frac{\partial \tilde{\mathbf{k}}(\widehat{\mathbf{x}})}{\partial \widehat{\mathbf{x}}}\right|_{\widehat{\mathbf{xe}}} \cdot \mathbf{L} \cdot (\mathbf{xe} - \widehat{\mathbf{xe}}) - \tilde{\mathbf{k}}(\widehat{\mathbf{xe}}) \cdot \mathbf{L} \right) \cdot (\widehat{\mathbf{x}} - \widehat{\mathbf{xe}})\end{aligned} \quad (5.51)$$

Notice that the resulting local linear approximation of the dynamics of the observer (5.51) is different from the local linear approximation of the dynamics of the estimation error (5.50). From this one could conclude that the dynamical robustness analysis would result in different conclusions dependent on the local linear approximation used.

It can be shown that the local linear approximation of the dynamics of the estimation error given by Equation (5.50) is not suited for analysis

of the stability of the error system. This is due to the additional driving term, which is function of the estimate and thus also dependent on the estimation error. Another local linear approximation of the dynamics of the estimation error is now derived. The basic idea of this derivation is that not the model part of the error dynamics must be linearized but the part due to the observer. This part must be linearized around the equilibrium error $\mathbf{e_e}$.

$$\frac{d\mathbf{e}(t)}{dt} = \mathbf{f}(\mathbf{x}) - \widetilde{\mathbf{p}}(\widehat{\mathbf{x}}(t)) = \mathbf{f}(\mathbf{x}) - \widetilde{\mathbf{f}}(\widehat{\mathbf{x}}) - \widetilde{\mathbf{k}}(\widehat{\mathbf{x}}) \cdot \mathbf{L} \cdot (\mathbf{x} - \widehat{\mathbf{x}}) \quad (5.52)$$

Let $\bar{\mathbf{e}}$ be the difference between the estimated state $\widehat{\mathbf{x}}$ and its steady state value $\widehat{\mathbf{x}}_\mathbf{e}$. The following relation can then be written:

$$\mathbf{e} = \mathbf{x} - \widehat{\mathbf{x}} = \mathbf{x_e} - \widehat{\mathbf{x}}_\mathbf{e} - \bar{\mathbf{e}} = \mathbf{e_e} - \bar{\mathbf{e}} \quad (5.53)$$

$$\begin{aligned} \widetilde{\mathbf{f}}(\widehat{\mathbf{x}}) &= \widetilde{\mathbf{f}}(\mathbf{x} - \mathbf{e}) \approx \widetilde{\mathbf{f}}(\mathbf{x_e} - \mathbf{e_e}) + \left.\frac{\partial \widetilde{\mathbf{f}}(\widehat{\mathbf{x}})}{\partial \widehat{\mathbf{x}}}\right|_{\mathbf{x_e}-\mathbf{e_e}} \cdot \bar{\mathbf{e}} \\ \widetilde{\mathbf{k}}(\widehat{\mathbf{x}}) &= \widetilde{\mathbf{k}}(\mathbf{x} - \mathbf{e}) \approx \widetilde{\mathbf{k}}(\mathbf{x_e} - \mathbf{e_e}) + \left.\frac{\partial \widetilde{\mathbf{k}}(\widehat{\mathbf{x}})}{\partial \widehat{\mathbf{x}}}\right|_{\mathbf{x_e}-\mathbf{e_e}} \cdot \bar{\mathbf{e}} \end{aligned} \quad (5.54)$$

The resulting local linear approximation for the estimation error dynamics is described by the same matrix as the local linear approximation found for the observer.

$$\frac{d\mathbf{e}(t)}{dt} \approx \left(\left.\frac{\partial \widetilde{\mathbf{f}}(\widehat{\mathbf{x}})}{\partial \widehat{\mathbf{x}}}\right|_{\widehat{\mathbf{x_e}}} - \widetilde{\mathbf{k}}(\widehat{\mathbf{x_e}}) \cdot \mathbf{L} + \left.\frac{\partial \widetilde{\mathbf{k}}(\widehat{\mathbf{x}})}{\partial \widehat{\mathbf{x}}}\right|_{\widehat{\mathbf{x_e}}} \cdot \mathbf{L} \cdot \mathbf{e_e} \right) \mathbf{e} + (\ldots) \quad (5.55)$$

Robustness against parametric uncertainty

From the discussion above it is clear that the effect of the parametric uncertainty on the stability of the error system can be determined by analyzing the eigenvalues of the Jacobian of the observer equations. The Jacobian is evaluated in the equilibrium point $\widehat{\mathbf{x_e}}$ of the observer, found in the equilibrium analysis. It is clear that this is only a measure of the robustness which is locally valid.

The dynamical robustness analysis is performed for the different observers for both measurements of the *biomass* and *substrate* concentration. In the Figures the real part of the eigenvalues of the Jacobian are shown as function of the uncertainty, represented by the relative error on the parameter a.

Only the results of the dynamical robustness analysis for the observer based on exact linearization and local linearization in original coordinates are visualized in Figure 5.9.

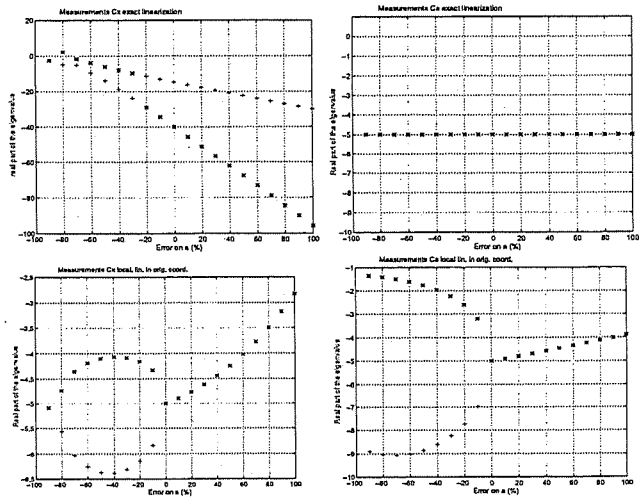


Figure 5.9: Dynamical analysis. Eigenvalues of the error system in function of the relative error on the parameter a. Design eigenvalue $\lambda_{design} = -5$

Robustness against structural uncertainty

The dynamical analysis is performed for the four observer for both measurements of biomass and substrate concentrations. The results for the observer based on exact linearization and the observer based on local linearization in original coordinates are visualized in Figure 5.10.

5.10.3 Conclusions

The robustness analysis problem of nonlinear observers is discussed in general and illustrated for observers, originating from different design methodologies. The main contribution is the introduction of the terminology and analysis concepts. As the results are *case sensitive* (function of the system (structure and parameters) under consideration) the case study just serves as an example.

Both for *parametric* and *structural uncertainty* are studied. A *first classification* of nonlinear observers is based on the static error on the estimated state. A *second classification* of nonlinear observers is based on the dynamical robustness of the observers. A first measure of the dynamical robustness of observers is the deviation between the obtained eigenvalues and the design eigenvalues. Recall that the eigenvalues are here calculated in the original state space and as such can deviate from the design eigenvalues. The dy-

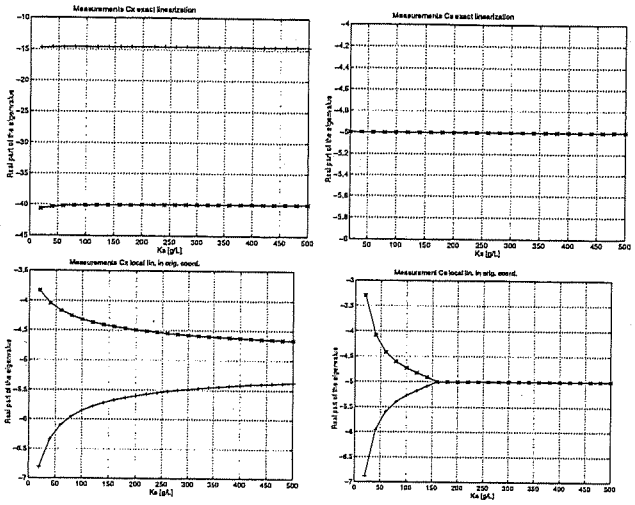


Figure 5.10: Dynamical analysis. Eigenvalues of the error system in function of the Monod parameter K_S. Design eigenvalue $\lambda_{design} = -5$

namical robustness of the observers can also be quantified by evaluating the change of the eigenvalues over the region of parametric error under consideration and the distance from zero of the eigenvalues. The results of the case study are now presented.

Robustness against parametric uncertainty. The robustness is evaluated for an error of -50% and 50% on the parameter a.

On-line measurements of the biomass concentration. The robustness of the observers is mainly determined by the model part in the observer equations and as such quite independent of the observer design methodologies. Notice that this result is not known a priori.

When these observers are classified with respect to their *static robustness*, the high-gain observer is found to have the best performance, followed by the observer based on exact linearization and the observer based on linearization in original coordinates. The performance of these observers is however quite comparable. The observer based on linearization in observer coordinates is generally non-robust.

When these observers are classified with respect to their *dynamical robustness*, the observer based on linearization in original coordinates is found to have the best performance. The change of the eigenvalues is rather small. Notice that the eigenvalue for a zero error on the parameter is here indeed the design eigenvalue. The second best observer is the high-gain observer.

The observer based on exact linearization shows a large variation of the eigenvalues over the region of parametric errors considered and is even not stable for all parametric errors. This can however be cured by using a more negative design eigenvalue. The observer based on linearization in observer coordinates has a bad dynamical robustness, as could be expected from the static analysis.

On-line measurements of the substrate concentration. The robustness of the observers is mainly determined by the tuning functions. Larger difference between the different observers is expected.

When these observers are classified with respect to their *static robustness*, the observer based on exact linearization and the observer based on linearization in original coordinates are found to have the best performance. These observers have a comparable performance. The high-gain observer performance is slightly less than for the previous two observers but is still acceptable. The observer based on linearization in observer coordinates has generally a bad performance.

When these observers are compared with respect to their *dynamical robustness* it is found that the observer based on exact linearization has the best performance. The eigenvalues remains almost constant. The observer based on linearization in original coordinates and the high-gain observer have also a good performance. The change of the eigenvalues of the region of parametric errors under consideration is limited. The dynamical robustness of the observer based on linearization in observer coordinates is bad as could be expected from the static analysis.

Robustness against structural uncertainty. The worst-case situation (low values of K_S) is taken as criterion.

On-line measurements of the biomass concentration. The robustness of the observers is mainly determined by the model part of the observer equations and as such quite independent of the observer design methodology.

When these observers are classified with respect to the worst-case static error (a measure of the *static robustness*) on the substrate concentration it is found that the observer based on linearization in observer coordinates has the best performance. This good performance is due to the fact that the tuning functions are compensating the error originating from the model part in the observer equations. The performance of the observer based on exact linearization and the high-gain observer are comparable and considered to be sufficiently good. The observer based on linearization in original coordinates has the worst performance.

From analysis of the *dynamical robustness* of these observers it can be concluded that the observer based on linearization in original coordinates has a good performance. The eigenvalues are almost equal to the design eigenvalue and the change of the eigenvalues as function of the Monod parameter K_S is limited. The observer based on exact linearization has the second best performance. Although its eigenvalues are considerable different from the design eigenvalue, the eigenvalues are quite constant as function

of the Monod parameter K_S and strongly negative. The high-gain observer has a performance which is comparable with the previous observer. There is only some more variation in the eigenvalues as function of the Monod parameter K_S. The observer based on linearization in observer coordinates has a bad dynamical robustness because the resulting eigenvalues are close to zero. Using a more negative design eigenvalue does not improve the dynamical robustness of this observer.

On-line measurements of the substrate concentration. The robustness of the observers, is mainly determined by the tuning functions in the observer equations. Larger differences between the observers is expected.

When these observers are classified with respect to the static worst-case error (a measure of the *static robustness*) on the biomass concentration estimate it is found that the observer based on exact linearization and the observer based on linearization in original coordinates have the best performance. The observer based on linearization in observer coordinates has a slightly larger static error while the high-gain observer has the worst performance.

When examining the *dynamic robustness* of these observers it can be concluded that the observer based on exact linearization has the best performance. The obtained eigenvalues are almost equal to the design eigenvalues over the whole range of values of the Monod parameter K_S considered in the analysis. The observer based on linearization in original coordinates has the second best performance. For a large range of values of the Monod parameter K_S the obtained eigenvalues are almost equal to the design eigenvalue. Even on the full range of the Monod parameter the change of the eigenvalues is quite limited. Also the dynamical robustness of the high-gain observer is quite good. Although the obtained eigenvalues differ from the design eigenvalues and the variation as function of the Monod parameter is a bit larger, one can observe that the resulting eigenvalues are strongly negative. The observer based on linearization in observer coordinates has the worst dynamical robustness.

It can be concluded that the high-gain observer has robust performance against parametric uncertainty when on-line measurements of the biomass concentration are available. The observer based on exact linearization is shown to have the best robust performance against both parametric and structural uncertainty when on-line measurements of the substrate concentration are available and against structural uncertainty when the case with on-line measurements of the biomass concentration is considered.

5.11 Discretization

In this section the effects of time discretization on the observer stability is analyzed. A general expression for the stability matrix of the discrete observer is presented. The results of the discretization analysis for the four

observers for both on-line measurements of *biomass* and *substrate* concentrations are summarized and some general conclusions are drawn.

The discrete version (5.56) of a continuous time observer (5.42) obtained with a forward Euler approximation of the first order time derivative of the state estimate is given below.

$$\widehat{\mathbf{x}}(k+1) \;=\; \widehat{\mathbf{x}}(k) + T\mathbf{p}(\widehat{\mathbf{x}}(k)) \tag{5.56}$$

The stability of the nonlinear discrete time system (5.56) is now analyzed by analyzing the stability of a local linear approximation of the system (5.57).

$$\widehat{\mathbf{x}}(k+1) \;=\; \left(\mathbf{I} + T\,\frac{\partial \mathbf{p}(\widehat{\mathbf{x}}(k))}{\partial \widehat{\mathbf{x}}(k)}\bigg|_{\widehat{\mathbf{x}_e}}\right)\cdot \widehat{\mathbf{x}}(k) \tag{5.57}$$

The discretization analysis reduces now to analysis of the eigenvalues of the matrix involved in Equation (5.57) as function of the discretization step T. Having eigenvalues within the unit circle in the complex plane is a necessary (but not sufficient) condition for having local stability of the discrete version of the observer. Sufficientness is obtained by guaranteeing boundedness of the matrix and its time derivative. It must be emphasized that this result is only valid locally around the equilibrium point. Nevertheless it provides an indication on the maximum allowable discretization time for the particular observer under study.

The discretization analysis has been performed for the observers resulting from the four different methodologies. This is done for the case where on-line measurements of the biomass concentrations is assumed and the case with measurements of the substrate concentration.

The stability matrix (5.57) is derived for the different observers for the different cases. The discretization step for which the amplitude of the eigenvalues exceeds one is taken as the maximum allowable discretization time. Notice that in the derivation of the stability matrix the Jacobian of the observers must be determined such as in the robustness analysis against parametric uncertainty performed before. In the case here the error on the parameters must be set to zero.

The results of the analysis for the prototype model are summarized in Table 5.2. When different observers are compared one must be aware that in Table 5.2 the maximum allowable discretization step is indicated as a function of the design eigenvalue (constant over the state space and with double multiplicity). This eigenvalue represents the convergence rate but not necessary in the original coordinate system. This fact has been mentioned in the robustness analysis. From this observation one could decide to take the eigenvalues in the original coordinates system as a representative measure of the convergence rate. Notice that generally this will results in two time-varying eigenvalues, which is a drawback of this approach. By taking the eigenvalue with the smallest amplitude (representing the slowest dynamics of the observer) obtained in the original coordinate system and

	λ_{design}	$maxT$ [h] Measurements C_X	Measurements C_S
Exact linearization	-1	0.035	2
	-5	0.05	0.4
	-10	0.07	0.2
Local lin. orig. coord.	-1	2	2
	-5	0.4	0.4
	-10	0.2	0.2
Local lin. observer coord.	-1	0.04	0.04
	-5	0.05	0.05
	-10	0.0	0.0
High-gain	-1	0.085	0.085
	-5	0.055	0.055
	-10	0.035	0.035

Table 5.2: Maximum allowable discretization step T as function of the design eigenvalue λ_{design}

	Measurements C_X	Measurements C_S
Exact linearization	≈ 1	≈ 2
Local lin. orig. coord.	2	2
Local lin. observer coord.	≈ 0	≈ 0
High-gain	≈ 1.7	≈ 0.3

Table 5.3: Robustness against discretization. Design eigenvalue $\lambda_{design} = -5$

multiplying it with the maximum allowable discretization step a more representative measure of the robustness of the observers against discretization is obtained. This measure is presented in Table 5.3. From this table it follows that for the observer based on local linearization in original coordinates the proportionality constant relating the maximum allowable discretization step and the convergence rate is 2, which is the value also found for linear observers. This observer has the best robustness property with respect to discretization.

It is found that the observer based on exact linearization has a similar robustness against discretization when the case with on-line substrate concentration measurements is considered. The high-gain observer has only a slightly lower performance (compared with the best observer) with respect to discretization in the case of on-line biomass measurements.

In the case study the observer based on exact linearization for the case with on-line biomass measurements still has a reasonable performance while the high-gain observer with substrate measurements does not cope very well

with discretization.

In Table 5.2 it is indicated that the discrete version of the nonlinear observer based on local linearization in observer coordinates with measurements of the biomass concentration has a maximum allowable discretization step zero for a design eigenvalue -10. Recall however the corresponding continuous time observer is not stable for this eigenvalue. No conclusion can be drawn from the discretization analysis.

The following conclusions can be drawn. For linear systems the maximum allowable discretization step is known to be proportional with the inverse of the convergence rate. The main conclusion of the discretization analysis performed here is that the relation between the maximum allowable discretization step and the convergence rate is much more complex. For the observers based on local linearization, both in original and observer coordinates and the high-gain observer an increase in the convergence speed reduces the maximum allowable discretization step as would be expected intuitively. For the observer based on exact linearization it is found that by increasing the convergence speed the maximum allowable discretization time becomes larger.

It is indicated that one must be careful in analyzing the obtained results because the design eigenvalue indicates the convergence rate in different coordinate spaces.

It is found that the observer based on local linearization in original coordinates has the best performance for both biomass and substrate concentration measurements although the performance of the observer based on exact linearization and high-gain is comparable for some cases.

It is emphasized that the discretization analysis must only be performed in cases where the corresponding continuous time version of the observer is stable.

5.12 Conclusions

Four observer design methodologies for nonlinear observers are reviewed and illustrated for a prototype model for biotechnological processes. *Performance analysis measures* are introduced and illustrated for the case study. The results of the performance analysis are presented. The following conclusion can be drawn.

Convergence region.
A formal definition for the convergence region is given. The obtained convergence region for an observers is depending on the initial state of the system under consideration and the criterion used for evaluation whether convergence is obtained. *For the prototype model, the convergence region of the observer based on exact linearization and the high gain observer equals the positive quadrant of the state space. The convergence region of the local linearization techniques is rather small.*

Noise sensitivity and convergence speed.
Measures of the noise sensitivity are defined. One of the measures provides a worst-case evaluation of the performance. With this measure particular artifacts of a method (such as singularities in the tuning functions) can be detected. The second measure provides a more realistic view on the noise sensitivity but is quite dependent on the point in which it is evaluated. It is therefore necessary to evaluate this measure in several points. *For the prototype model, it is found that the noise sensitivity of the high gain observer is worse than for the other observers, which have a comparable noise sensitivity performance.* From this observation one should not conclude that the noise sensitivity of the other observers must not be considered. While comparing the noise sensitivity of the observers versus the speed of convergence one must be aware that the design eigenvalue indicates the convergence rate in different coordinate spaces.

Robustness against uncertainty.
The robustness against both parametric and structural uncertainty are examined. An equilibrium and dynamical analysis are performed.

It is shown that the equilibrium error on the estimated state consists of two contributions. Two methods for calculation of this equilibrium error are introduced. Advantages and disadvantages of both methods are indicated. It is indicated that these calculations can be ill-conditioned and must be interpreted cautiously.

For the dynamical analysis it is shown that the Jacobian of the local linear approximation of the observer and the Jacobian of the local linear approximation of the error system remains the same even with uncertainty on the design model. The Jacobian of the error system must however be determined in a particular way.

For the prototype model, the observer based on exact linearization and the high gain observer are found to have the best robust performance. This result is in contradiction with what is expected from a theoretical point of view.

Discretization.
The relation between the maximum allowable discretization step and the convergence rate of the nonlinear observer is complex when compared with the linear case.

For the prototype model, the observer based on local linearization in original coordinates has the best performance for both biomass and substrate concentration measurements although the performance of the observer based on exact linearization and high-gain are for some cases quite comparable.

From the obtained results one can conclude that the performance of the observers is *case sensitive* and sometimes in contradiction with what is expected from theoretical point of view. The observer design and the related performance analysis requires a lot of *symbolic* and *numerical calculations* and must be performed cautiously. The performance measure are often only locally valid, requiring evaluation in several states. The numerical

calculations can be ill-conditioned and lead to erroneous conclusions.

From these observation one must conclude that general rules for the selection of an observer design methodology for process engineers do not exist. The introduction of nonlinear observers in process industry to circumvent partially the lack of measurement is only feasible when a tool for fast design and analysis of the observers is available, allowing fast decision making. Such a tool should combine both symbolic and numerical methods. Because the analysis must be performed cautiously such a tool must be considered as a support for the process engineer rather than as a full problem solving program. Knowledge of the different design methodologies and analysis methods incorporated in the tool remains necessary.

As a general conclusion it can be stated that due to the *case sensitivity* of the performance of nonlinear observers no general observer selection rules can be formulated. However, it is shown that *performance analysis tools*, possibly incorporated in an appropriate software environment, can assist the process engineer in *observer selection.*

In the chapter a variety of observer design methodologies and evaluation techniques are presented. The global convergence property of the exact linearization based observers is extremely important for bioprocess monitoring due to the large uncertainty. The restricted applicability of this type of design methodology is a motivation for using low complexity models. Robustness analysis shows that good performance is obtained although simplified models are used.

Chapter 6

Optimal tuning of observers and observer based estimators

6.1 Introduction

The nonlinear time varying dynamics encountered in biotechnological processes and the lack of cheap and accurate biosensors, makes the analysis of these processes and the synthesis of advanced supervisory systems very hard [Van Impe *et al.* 1992, 1995].

Recent developments in measurement techniques (new types of hardware sensors) and nonlinear systems and control theory have initiated a lot of scientific research in bioprocess control.

Nonlinear state and parameter estimators can relax the measurement problems. These algorithms can reconstruct an unmeasurable state or parameter out of on-line measurements by using a model of the process. In this way extra useful information of the process is obtained.

In this chapter the *tuning* (selection of degrees of freedom) of the estimation algorithms is discussed. Two approaches (*performance analysis* and *trade-off analysis*) are compared and illustrated for observer based parameter estimators and nonlinear state observers. Both methods are basically inspired on [Bastin and Dochain 1990]. The main contributions are (i) the application of the methods to a larger class of systems and (ii) the emphasis on the interplay between both tuning methods. The use of an observer based parameter estimator for control of carbon removal and nitrogen removal activated sludge wastewater treatment systems is reported in [Ryckaert *et al.* 1995, 1996a]. *This chapter is organized as follows. In Section 6.2 the general problem statement is presented. The two approaches (performance and trade-off analysis) are first illustrated for observer based parameter estimators for two cases in Section 6.3. Secondly the tuning of a nonlinear state estimator (observer) is discussed in Section 6.4. The use of the observer based parameter estimators is demonstrated on data obtained from full-scale wastewater treatment systems for carbon and nitrogen removal, a yeast fermentation process and a germination process in Sections 6.3.5, 6.3.6, 6.3.7 and 6.3.8 respectively. The tuning of nonlinear observers is illustrated with simulations in the context of fed-batch fermentation. In Chapter 0 the basic models used in this chapter are presented. In Chapter 4 the observability of states and identifiability of model parameters is discussed. While in Chapter 5 the performance analysis of nonlinear state observers is used for selection of an appropriate structure of the estimator, here the performance analysis is presented as a tool for tuning (selection of the parameters) of the algorithms.*

In this chapter two tuning methods are presented. It is illustrated that even with simple models significant insight in the tuning problem can be obtained.

6.2 General problem statement

In the application of (nonlinear) estimation techniques typically two basic steps are found.

Step 1. The *structure* of the (nonlinear) algorithm is determined (Chapter 4 and 5).

Step 2. Second the tuning parameters are selected. The *tuning* of the parameters can be done with two approaches.

Approach 1: Performance analysis. The influence of the tuning parameters on performance criteria such as *noise sensitivity, convergence speed* and *the maximum allowable discretization time* is analyzed. Although this approach results (both for linear and nonlinear techniques) in analytical (approximate) expressions of the performance criteria as function of the tuning parameters, the actual selection of the parameters is still difficult because no overall view on the tuning problem is obtained and possible interactions are also neglected. The main advantage of the performance analysis is that it reveals some structural dependencies of the performance criteria on parameter values and process conditions.

Approach 2: Trade-off analysis. The influence of the tuning parameters on an *objective function*, describing the goal of the algorithm under study, is analyzed by *dynamic simulation*. This cost criterion is in fact an implicit function of performance criteria such as convergence speed, noise sensitivity and discretization time. The tuning parameters, for which a minimum value of the costcriterion is obtained, are selected. The advantage of this method is that the trade-off between the various performance criteria is now made

explicit. Also possible interactions are included. The disadvantage is that the simulation, performed for the analysis, must be representative for reality. An estimate of the expected (initial) errors and noise, appearing in the real case, should be available. With the trade-off analysis optimal tuning parameters are obtained but the method does not provide insight in the tuning problem.

With the case studies it is demonstrated that *trade-off analysis* is an easy procedure for fast tuning of the algorithm under study. The *performance analysis method* reveals some important facts about the tuning problem under consideration. This information can be used in the construction of the representative simulations, necessary in the trade-off analysis and indicate how certain lack of performance of the algorithm can be cured.

It must be emphasized that the main goal of this contribution is to discuss the tuning problem of observer based estimators and observers. The applications illustrate the potential of the estimation algorithms.

6.3 Case study 1: Observer based estimators

Optimal tuning of observer based estimators is illustrated with different case studies. An estimator for the oxygen uptake rate, independent of the oxygen transfer rate, is analyzed in Section 6.3.2. An estimator for the oxygen transfer rate in combination with an oxygen uptake rate estimator is studied in Section 6.3.3. The estimation of the oxygen uptake rate, dependent on the oxygen transfer rate, is examined in Section 6.3.4. Application of these estimators is described in the subsequent sections.

The basic model for the oxygen dynamics is introduced in Chapter 0. Throughout this chapter outflow of oxygen by transport is considered to be negligible, which is motivated in the context of wastewater treatment systems in Chapter 3.

6.3.1 Introduction

In Section 6.3.2 the estimation of the oxygen consumption rate OUR is discussed when the aerator is switched off. The estimation is of course independent of the oxygen transfer part due to the condition on the aerator. In Section 6.3.3 the estimation of the oxygen transfer rate k_La is considered. It is assumed that the aerator is on. In this case the oxygen consumption rate OUR appears explicitly in the dynamics of the oxygen concentration. This indicates that the estimation of the oxygen transfer rate can not be performed independently from the oxygen consumption rate. The on-off control strategy, used for the aerator, enables the estimation of the oxygen uptake rate OUR and the oxygen transfer coefficient k_La in an alternating way. When the aerator operation is switched regularly, then the following

approach can be used: The oxygen uptake rate OUR is estimated, independently of the oxygen transfer coefficient, when the aerator is off. The oxygen transfer coefficient k_La is estimated, using the oxygen uptake rate obtained from the previous estimation, when the aerator is on.

This approach relies on the fact that the dynamics of the oxygen uptake rate OUR are rather slow, in comparison with the dynamics of the oxygen concentration. When no on-off control strategy for the oxygen concentration is used, the previous approach is not suitable. The oxygen uptake rate can then only be estimated when the oxygen transport part of the dynamic equation of the oxygen concentration is exactly known. This is further discussed in Section 6.3.4.

Estimation of the oxygen uptake rate OUR and k_La from on-line oxygen concentrations is discussed by many authors. Some references are [Holmberg 1982], [de Prada *et al.* 1991] and [Vanrolleghem 1994]. Different measurement set ups (steady state conditions, step response experiments, ...), estimation schemes (recursive parameter estimators, dead-beat estimators, ...), assumptions (relations oxygen uptake rate and oxygen flow rate, ...) are evaluated. Recall that in this contribution the emphasis is on the tuning of estimation algorithms.

6.3.2 Oxygen uptake rate estimator, independent of the oxygen transfer rate

Problem statement

The oxygen uptake rate is equal to minus the slope of the oxygen concentration profile. A straightforward approach in the estimation of the uptake rate from oxygen concentration measurements would be the calculation of the slope between consecutive points. This approach is however noise sensitive.

Another approach, which incorporates model knowledge, is to use an observer based parameter estimator. Such an estimator consists of two coupled dynamic equations (6.1), which are integrated in time. The first equation expresses the dynamics of the estimated oxygen concentration $\widehat{C_O}$ and consists of the oxygen model and a correction term, proportional with the error between the measured C_O and estimated oxygen concentration $\widehat{C_O}$. The second equation describes the dynamics of the estimated oxygen uptake rate $\widehat{OUR}$ and is also proportional with the error between the measured and the estimated oxygen concentration. The proportionality constants a [1/h] and b [1/h^2] are *tuning parameters* of the algorithm.

$$\begin{aligned} \frac{d\widehat{C_O}}{dt} &= -\widehat{OUR} + a\cdot(C_O - \widehat{C_O}) \\ \frac{d\widehat{OUR}}{dt} &= b\cdot(C_O - \widehat{C_O}) \end{aligned} \tag{6.1}$$

The dynamics of the error system ($E_1 = C_O - \widehat{C_O}$ and $P_1 = OUR - \widehat{OUR}$) are:

$$\begin{pmatrix} \frac{dE_1}{dt} \\ \frac{dP_1}{dt} \end{pmatrix} = \begin{pmatrix} -a & -1 \\ -b & 0 \end{pmatrix} \cdot \begin{pmatrix} E_1 \\ P_1 \end{pmatrix} + \begin{pmatrix} 0 \\ \frac{dOUR}{dt} \end{pmatrix} \quad (6.2)$$

The tuning parameters a and b are chosen such that the unforced error system converges to the zero state. This can be done easily with eigenvalue assignment.

Notice that principally the oxygen consumption rate OUR is treated here as a (slowly time varying) parameter. The error system is unforced when the oxygen consumption rate is constant. The approach relies on the fact that the dynamics of the oxygen uptake rate OUR (and thus the dynamics of the biological state) are rather slow, in comparison with the dynamics of the oxygen concentration C_O. The oxygen concentration dynamics, which is considered as the state variable here, is mainly determined by the on-off control strategy of the aerator.

First the analysis of performance criteria as function of the tuning parameters is discussed while second the trade-off analysis method is presented.

Performance analysis

The analysis is here simple because the systems under consideration are linear. The performance criteria are the convergence speed, the noise sensitivity and the maximum allowable discretization time.

Convergence. The tuning parameters a and b are chosen such that the error system has a real negative eigenvalue λ [1/h] with a double multiplicity. A second order system with damping factor 1 is obtained which is an often used rule of thumb in engineering. In fact, the parameter λ can be considered as the tuning parameter of the algorithm. This parameter directly indicates the convergence speed of the algorithm. The tuning parameters $a = -2\lambda$ and $b = -\lambda^2$ are used.

When the time derivative of the OUR is zero, the errors will converge to the zero state or the oxygen uptake rate and the oxygen concentration are estimated perfectly. When the time derivative of the OUR is not zero, estimation errors appear. An upper bound on these estimation errors can then be determined by applying Technical Lemma (1), found in Appendix B.

$$| C_O - \widehat{C_O} | = \frac{| \frac{dOUR}{dt} |}{\lambda^2} \quad , \quad | OUR - \widehat{OUR} | = 2\frac{| \frac{dOUR}{dt} |}{| \lambda |} \quad (6.3)$$

Notice that the estimation errors can be reduced by increasing the convergence speed (i.e., selecting a more negative eigenvalue λ).

Discretization. In practice the observer based parameter estimator must be implemented in discrete time because the measurements are provided at discrete time instances. The time derivative in the continuous observer is approximated with the forward Euler formula. The following discrete estimator is obtained with T [h] the discretization time.

$$\begin{pmatrix} \widehat{C_O}(k+1) \\ \widehat{OUR}(k+1) \end{pmatrix} = \begin{pmatrix} 1-aT & -T \\ -bT & 1 \end{pmatrix} \cdot \begin{pmatrix} \widehat{C_O}(k) \\ \widehat{OUR}(k) \end{pmatrix} + \begin{pmatrix} aT \cdot C_O \\ bT \cdot C_O \end{pmatrix} \quad (6.4)$$

It can easily be shown that the discrete system has also one real eigenvalue λ_T with double multiplicity. The eigendynamics of this system must be stable or the eigenvalue λ_T must lie in the unit circle or because of the realness of the eigenvalue it must lie in the interval]-1,1[. This results in an upper bound on the discretization time T.

$$0 \leq T \leq \frac{2}{| \lambda |} = T_{max} \quad (6.5)$$

The maximum discretization T_{max} can be considered as a performance criterion of the algorithm, which is function of the tuning parameter λ. It can be concluded that the convergence speed can only be increased by selecting a more negative λ when faster sampling is possible by the measurement equipment. Notice also that the estimation error will increase when a large discretization time T is used because the Euler approximation becomes worse.

Noise sensitivity. In practice the on-line measurements of the oxygen concentration C_O are corrupted by noise. This can be described theoretically by adding noise signal $r(t)$ to the measurements. It is clear from the equations (6.1) for the continuous estimator (or the equations (6.4) for the discrete estimator) that the noise signal $r(t)$ will be amplified with a and b (or aT and bT). For the algorithm two noise sensitivity functions $\mathcal{R}^I_{C_O}$, $\mathcal{R}^I_{OUR}$ are defined, which are function of the tuning parameter λ.

$$\mathcal{R}^I_{C_O} = | 2\lambda | \quad ; \quad \mathcal{R}^I_{OUR} = \lambda^2 \quad (6.6)$$

It can be concluded that increasing the convergence speed by selecting a more negative eigenvalue λ will also increase the noise sensitivity. The functions $\mathcal{R}^I_{C_O}$ and $\mathcal{R}^I_{OUR}$ indicate the instantaneous influence of the noise on the estimates. An upper bound on the estimation error due to the measurement noise can be obtained again with Technical Lemma (1), found in Appendix B. This upper bound quantifies the asymptotic accuracy under noisy circumstances and includes besides the instantaneous amplification of the noise also the influence of the dynamics of the estimator on the noise. $\mathcal{R}^A_{C_O}$ and $\mathcal{R}^A_{OUR}$ are the asymptotic noise sensitivity functions. $| r(t) |$ is a

bound on the noise signal $r(t)$.

$$\begin{array}{rcl} |\, C_O - \widehat{C_O}\,| & = & \mathcal{R}^A_{C_O}\,|\, r(t)\,| \;=\; (\frac{4}{e}+1)\,|\, r(t)\,| \\ |\, OUR - \widehat{OUR}\,| & = & \mathcal{R}^A_{OUR}\,|\, r(t)\,| \;=\; 4\,|\,\lambda\,|\,|\, r(t)\,| \end{array} \tag{6.7}$$

From the previous analysis it becomes clear how the performance criteria (convergence speed, the maximum discretization time and the noise sensitivity) are influenced by the selection of the tuning parameter. Two trade-offs are found. A first trade-off exists between speed of convergence and maximum discretization while the second trade-off is between speed of convergence and the noise sensitivity. The first trade-off has another nature that the second one. The fact whether the discrete implementation works is determined by the data acquisition hardware under consideration and is a hard constraint. Notice that the convergence speed determines both the transient behavior of the system as the asymptotic accuracy. Although these trade-offs are found and an explicit relation between the tuning parameter and the performance criteria are found, it is still difficult to decide which value of the tuning parameter must be chosen because the analysis discusses each criterion separately but does not provide a global view on the tuning problem. One possible approach is to choose the parameter λ such that the trade-off between asymptotic accuracy and the asymptotic noise sensitivity is optimal.

$$\lambda^* \;=\; \arg\min_\lambda(4\,|\,\lambda\,|\,|\, r(t)\,| + \frac{2}{|\,\lambda\,|}\,|\,\frac{dOUR}{dt}\,|) \;=\; \sqrt{\frac{|\,\frac{dOUR}{dt}\,|}{2\,|\, r(t)\,|}} \tag{6.8}$$

The above described approach does not take into account the transient behaviour of the estimator and requires an estimate of the rate of change of the oxygen uptake rate. It is also not clear how the estimators performance will degraded due to discretization errors.

Trade-off analysis

The trade-off analysis is based on an objective function, which must be minimized with respect to the tuning parameter λ. Recall that the estimation of the oxygen uptake rate is the objective of the estimator under consideration. The following optimization problem can then be formulated with T_r [h] the reference time.

$$\lambda^* \;=\; \arg\min_\lambda(\textstyle\int_o^{T_r} |\, OUR - \widehat{OUR}\,|\, dt) \tag{6.9}$$

The estimation error, used in the objective function above, consists of two contributions, which can be separated. Let $\overline{OUR}$ be the oxygen uptake rate estimate obtained with the estimator in noise free conditions. The following

relation can then be written:

$$|\, OUR - \widehat{OUR}\,| \;\leq\; |\, OUR - \overline{OUR}\,| + |\, \overline{OUR} - \widehat{OUR}\,| \tag{6.10}$$

Transient behavior of the estimator. The first contribution to the objective function is due to the transient dynamics of the estimator. Let $(OUR - \overline{OUR})(0)$ be the initial estimation error (the uncertainty on the oxygen uptake rate), then a relation between the integral of the error and the tuning parameter λ can be written explicitly. It is assumed that there is no initial error on the oxygen concentration estimate.

$$\textstyle\int_o^{T_r} |\, OUR - \overline{OUR}\,|\, dt = |\, (OUR - \overline{OUR})(o)\,|\,|\, \frac{2}{\lambda}(e^{\lambda T_r} - 1) - T_r e^{\lambda T_r}\,| \tag{6.11}$$

Notice that when the reference time T_r is large when compared with the convergence time (the inverse of $|\,\lambda\,|$) then the approximation formula (6.12) of the error is found indicating that the contribution due to the initial error is inversely proportional with the tuning parameter λ. Recall that here the effect of the initial estimation error is studied. Notice that a similar formula for the asymptotic accuracy which describes the effect of a time varying oxygen uptake rate, is found.

$$\textstyle\int_o^{T_r} |\, OUR - \overline{OUR}\,|\, dt \;\approx\; |\, (OUR - \overline{OUR})(o)\,|\, \frac{2}{|\,\lambda\,|} \tag{6.12}$$

When the convergence speed becomes zero, the integral of the error equals the reference time T_r multiplied with the initial error on the oxygen uptake rate.

Noise sensitivity of the estimator. The second contribution to the objective function is due to the noise on the measurements. When the convergence speed is sufficiently large, the approximations found with Technical Lemma (1) in Appendix B, can be used and result in a similar formula as found in the analysis performed previously. When the convergence speed becomes zero, there is no contribution of the noise because the instantaneous noise sensitivities are zero. Notice that the noise contribution is proportional with the reference time T_r.

$$\textstyle\int_o^{T_r} |\, OUR - \overline{OUR}\,|\, dt \;=\; 4\,|\,\lambda\,|\,|\, r(t)\,|\, T_r \tag{6.13}$$

Although above the effect of the transient behavior and the noise on the measurements are discussed separately, the trade-off analysis based on the objective function provides a global view on the tuning problem. The following approach is used. In a first step a reference situation is constructed. This includes selection of the reference time T_r, noise level $|\, r(t)\,|$ and the initial error. The value of the objective function is then determined for various values of the tuning parameter λ. The value of the tuning parameter, minimizing the objective function, is chosen as the optimal value. The objective function provides a global view on the performance of the estimation

algorithm and implicitly weights the several error contributions. Moreover, besides the transient behavior and the noise effects, also the errors due to discretization (for a discretization time T lower then the maximum discretization time T_m) are included. The main disadvantage is that of course the reference time, the noise level and the initial error, must be representative for the situation for which the estimator is constructed.

When only the asymptotic noise contribution and the transient behavior of the estimator is taken into account, then an explicit value λ^* of the optimal tuning parameter is found as follows:

$$\begin{aligned} \lambda^* &= \arg\min_\lambda (4 \mid \lambda \mid\mid r(t) \mid T_r + \frac{2}{\mid \lambda \mid} \mid (OUR - \widehat{OUR})(o) \mid) \\ &= \sqrt{\frac{\mid (OUR - \widehat{OUR})(o) \mid}{2T_r \mid r(t) \mid}} \end{aligned} \tag{6.14}$$

Simulations

The trade-off analysis with the objective function is illustrated below with simulations.

It is assumed that the oxygen concentration C_O [mg/L] is controlled with an on-off control of the aerator between 1 and 4 mg/L. A flag is indicating whether the aerator is on (1) or off (0). The oxygen uptake rate OUR [mg O_2/L h] is constant and equal to 5 mg O_2/L h. The oxygen measurements are corrupted with random noise with a uniform distribution and quantified with its maximum value $\mid r(t) \mid$. The oxygen uptake rate is only estimated when the aerator is off. The discretization time T is 36 sec. The reference time T_r [h] is here 10 h. The initial error on the oxygen uptake rate estimate is 2 mg O_2/L h. The dynamics of the oxygen uptake rate, its estimate, the oxygen concentration and its estimate are shown in Figure 6.1, for a noise level of 0.5.

In Figure 6.2 the tuning of the oxygen uptake rate estimator with the objective function method is shown. The integral of the estimation error is shown as a function of the tuning parameter λ [1/h] for three different noise levels (indicated by the maximum value of the noise)

From a qualitative view point Figure 6.2 shows that influence of the tuning parameter $\mid \lambda \mid$ on the integral of the estimation error can be described by the formulas derived in the analysis. For low values of $\mid \lambda \mid$ indeed an error due to the transient behavior of the estimator is observed which is inversely proportional with $\mid \lambda \mid$ and rather well approximated by the formulas derived above. Notice that for $\mid \lambda \mid$ equal to zero indeed a value is obtained which is equal to the initial error multiplied with the duration of the reference period. One can also notice that for larger values of $\mid \lambda \mid$ the contribution to the error is approximately linearly increasing with $\mid \lambda \mid$ and the noise level $\mid r(t) \mid$. The proportionality constant is however much lower than the value predicted by analysis. Differences between the values

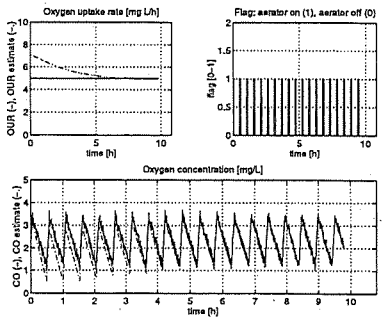


Figure 6.1: Dynamics of the oxygen uptake rate estimator for a noise level 0.5 mg/L. Upperleft plot: Time plot of the oxygen uptake rate and its estimate. Upperright plot: Time plot of the oxygen concentration and its estimate. Bottom left plot: Flag indicating whether the aerator is switched on (1) or off (0)

obtained with the analysis and the objective function method can be due to the following reasons.

Conservative bounds. In the analysis an upper bound on the noise contribution is derived which leads to a serious overestimation of the influence of noise on the estimator.

Alternating estimation. The oxygen uptake rate is only estimated when the aerator is off. Notice that this is only part of the duration of the reference time T_r.

Discretization. Discretization errors, for which no analytic expressions are derived, are implicitly contributing to the objective function.

6.3.3 Oxygen transfer rate estimator

Problem statement

The observer based parameter estimation scheme can be used now for estimation of the oxygen transfer coefficient k_La [1/h]. The estimation algorithm contains again an equation for the dynamics of the estimated oxygen concentration $\widehat{C_O}$, which consists of the oxygen model and a correction term, and an adaptation equation for the estimated oxygen transfer coefficient $\widehat{k_La}$. Notice that in the estimator the estimated oxygen uptake rate is used explicitly and assumed to be constant. This can be motivated because an alternating estimation scheme is considered here. The dilution of oxygen

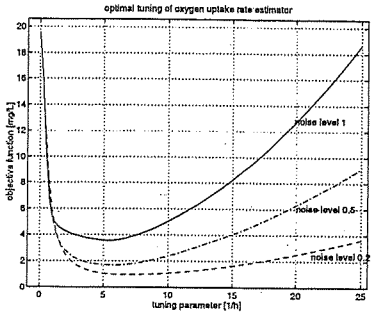


Figure 6.2: Optimal tuning of the oxygen uptake rate estimator with trade-off analysis. Integrated estimation error in function of the tuning parameter λ for three different noise levels

due to transport is neglected.

$$\begin{aligned} \frac{d\widehat{C_O}}{dt} &= -\widehat{OUR} + \widehat{k_La}(C_{SAT}-C_O) + c\cdot(C_O-\widehat{C_O}) \\ \frac{d\widehat{k_La}}{dt} &= d\cdot(C_{SAT}-C_O)(C_O-\widehat{C_O}) \end{aligned} \tag{6.15}$$

The error system ($E_2 = C_O - \widehat{C_O}$ and $P_2 = k_La - \widehat{k_La}$) is:

$$\begin{pmatrix} \frac{dE_2}{dt} \\ \frac{dP_2}{dt} \end{pmatrix} = \begin{pmatrix} -c & (C_{SAT}-C_O) & -1 \\ -d\cdot(C_{SAT}-C_O) & 0 & 0 \end{pmatrix} \cdot \begin{pmatrix} E_2 \\ P_2 \\ P_1 \end{pmatrix} \tag{6.16}$$

From a steady state analysis of the system (6.16) Equation (6.17) is obtained. Notice that the error on the oxygen uptake rate P_1 results in an error on the oxygen transfer coefficient estimate. The independent estimation of the oxygen uptake rate guarantees that the error on both the oxygen uptake rate and the oxygen transfer rate will eventually converge to zero.

$$k_La - \widehat{k_La} = \frac{OUR - \widehat{OUR}}{(C_{SAT}-C_O)} \tag{6.17}$$

A better estimation of the oxygen transfer rate is obtained for the same error on the oxygen uptake rate for lower oxygen concentrations.

Performance analysis

Convergence. The *tuning parameters* c and d must be chosen properly. Convergence of the estimation errors to zero (when the oxygen uptake rate

OUR is perfectly estimated) is guaranteed when the parameters c and d are positive and $(C_{SAT}-C_O)$ is different from zero. This is a standard result of adaptive system theory and is based on a persistently excitation argument [Bastin and Dochain 1990]. The condition on the oxygen concentration just indicates that the oxygen dynamics may not become independent of the oxygen transfer coefficient during a finite time interval. The tuning parameters are now selected such that again a negative eigenvalue λ with a double multiplicity is obtained.

$$c = -2\lambda \quad , \quad d = \left(\frac{\lambda}{C_{SAT}-C_O}\right)^2 \tag{6.18}$$

Notice that d is now a function of C_O and not constant. Recall that the alternating estimation of k_La and OUR is based on the fact that there are periods of no aeration (then the oxygen uptake rate is estimated) and that the OUR is assumed to be constant during the period used for estimation of the oxygen transfer rate (when the aeration is switched on). The implication of this second assumption is now analyzed. Suppose that the uncertainty on the estimate of the oxygen uptake rate is upper bounded by $M \geq 0$. The error on the oxygen uptake rate is considered as an input of the error system. The matrix (6.19) is the matrix of the error system with the selection of the tuning parameters (6.18).

$$\begin{pmatrix} 2\lambda & (C_{SAT}-C_O) \\ -\lambda^2\dfrac{1}{(C_{SAT}-C_O)} & 0 \end{pmatrix} \tag{6.19}$$

An upper bound on the error on the estimates of the oxygen concentration and the oxygen transfer rate is then found with Technical Lemma (1) in Appendix B. Notice that here the Lemma is applied on a linear but time-varying system while the Lemma is only valid for linear time invariant systems. In fact the Lemma is used here on a local approximation of the time-varying system with a time invariant system. The oxygen concentration determines the local process condition for which the result is valid. The approximation can be motivated because the oxygen concentration is controlled between two bounds and can be considered fixed when the distance between these bounds is small.

$$|\, C_O - \widehat{C_O}\,| \leq \frac{2}{e\lambda}M \quad , \quad |\, k_La - \widehat{k_La}\,| \leq \frac{1}{C_{SAT}-C_O}M \tag{6.20}$$

Notice that the asymptotic error on the oxygen transfer rate estimate can not be reduced by increasing the convergence speed. Good estimation of k_La is only possible when a good estimation of the OUR is performed. This result is also obtained with the steady state analysis (Equation (6.17)).

Robustness analysis. Above the robustness of the observer based estimator against violation of one of the assumptions, here assuming that the

estimated respiration rate $\widehat{OUR}$ equals the actual respiration rate OUR, is analyzed and results in an upper bound on the estimation error on the oxygen transfer coefficient k_La.

The robustness analysis can also be performed by (i) calculation of the equilibrium points of the error system as function of the errors on some parameters of the algorithm (equilibrium analysis) and (ii) determining how the eigenvalues differ from the design eigenvalues due to these errors (dynamical analysis).

This approach is illustrated for the analysis of the combined effect of an error on the oxygen saturation coefficient C_{SAT} and the oxygen uptake rate OUR. Let $\overline{C_{sat}}$ denote the oxygen saturation coefficient used in the observer, then the following observer is used:

$$\begin{aligned} \frac{d\widehat{C_O}}{dt} &= -\widehat{OUR} + \widehat{k_La}\cdot(\overline{C_{sat}} - C_0) + c\cdot(C_O - \widehat{C_O}) \\ \frac{d\widehat{k_La}}{dt} &= d\cdot(\overline{C_{sat}} - C_O)\cdot(C_O - \widehat{C_O}) \end{aligned} \tag{6.21}$$

With $\Delta C_{SAT} = \overline{C_{sat}} - C_{SAT}$ the difference between the oxygen saturation concentration used in the observer and the actual oxygen saturation coefficient and $\Delta OUR = OUR - \widehat{OUR}$ the error between the actual and the estimated oxygen uptake rate, the following error system is obtained.

$$\begin{pmatrix} \frac{dE_2}{dt} \\ \frac{dP_2}{dt} \end{pmatrix} = \begin{pmatrix} -c & (\overline{C_{sat}} - C_O) \\ -d\cdot(\overline{C_{sat}} - C_O) & 0 \end{pmatrix}\cdot\begin{pmatrix} E_2 \\ P_2 \end{pmatrix} + \begin{pmatrix} -P_1 - k_La\Delta C_{SAT} \\ 0 \end{pmatrix} \tag{6.22}$$

Equilibrium analysis. When the observer is in steady state, the estimated and measured oxygen concentration are equal. The following relation between the error on the estimated oxygen transfer coefficient and the errors on the oxygen uptake rate and the oxygen saturation concentration is found.

$$k_La - \widehat{k_La} = \frac{\Delta OUR + k_La\Delta C_{SAT}}{\overline{C_{sat}} - C_O} \tag{6.23}$$

From this relation one can conclude that the robustness of the observer is improved when the system under consideration operates at oxygen concentrations considerably lower than the oxygen saturation concentration. The error on the oxygen saturation concentration is amplified with the oxygen transfer coefficient. The error on the oxygen saturation coefficient will have less severe effects on the observer performance when an aeration system with low oxygen transfer capabilities is considered. Naturally the oxygen concentration should be

sufficient for the biological process under consideration and the economical impact of using an aeration system with small k_La must be examined.

Dynamical analysis. The eigenvalues λ of the dynamic matrix of the error system (6.22) can now be determined and compared with the design eigenvalues λ_c.

$$\lambda = \lambda_c \pm \lambda_c\sqrt{1-(1+\frac{\Delta C_{SAT}}{C_{SAT}-C_O})^2} \tag{6.24}$$

It can be concluded that the eigenvalues are altered due to the error on the oxygen saturation concentration. The error on the oxygen uptake rate estimate is of no importance here.

Discretization. The oxygen transfer rate estimator is implemented in a discrete way. This results again in an upper bound on the discretization time. The system matrix of the discrete of observer is given below.

$$\begin{pmatrix} 1-cT & T(C_{SAT}-C_O) \\ -d(C_{SAT}-C_O)T & 1 \end{pmatrix} \tag{6.25}$$

$$0 \leq T \leq \frac{2}{|\lambda|} \tag{6.26}$$

Noise sensitivity. The influence of noise on the on-line measurements of the oxygen concentration C_O can be analyzed in a similar way as for the oxygen uptake rate estimator. The instantaneous noise sensitivities of the k_La-estimator are given below.

$$\mathcal{R}^I_{C_O} = |2\lambda| \quad ; \quad \mathcal{R}^I_{k_La} = \lambda^2\frac{1}{C_{SAT}-C_O} \tag{6.27}$$

The asymptotic noise sensitivity functions $\mathcal{R}^A_{C_O}$ and $\mathcal{R}^A_{k_La}$ are determined with Technical Lemma (2) found in Appendix B.

$$\begin{aligned} |C_O - \hat{C_O}| &= \mathcal{R}^A_{C_O}|r(t)| = (\tfrac{4}{e}+1)|r(t)| \\ |k_La - \hat{k_La}| &= \mathcal{R}^A_{k_La}|r(t)| = 4|\lambda|\frac{1}{C_{SAT}-C_O}|r(t)| \end{aligned} \tag{6.28}$$

It is clear now how the performance criteria (convergence speed, the maximum discretization time and the noise sensitivity) of the oxygen transfer rate estimator are influenced by the selection of the tuning parameter. The trade-off between speed of convergence and maximum discretization, found for the oxygen uptake rate estimator, appears here also. There is also a trade-off is between speed of convergence and the noise sensitivity. Notice that the convergence speed determines here only the transient behavior of the system and not the asymptotic accuracy. The first approach for selection of the tuning parameter λ used for the oxygen uptake rate estimator

is thus not applicable here. The analysis does not provide insight how the estimators performance will degrade due to discretization errors nor does it indicate which value for the tuning parameter should be taken finally, but it reveals how the actual oxygen concentration C_O affects the noise sensitivity and the robustness.

Trade-off analysis

The objective of the estimator under consideration is to estimate the oxygen transfer rate, resulting in the following objective function.

$$\lambda^* = \arg\min \int_o^{T_r} \mid k_La - \widehat{k_La} \mid dt \tag{6.29}$$

The contribution of the transient behavior of the estimator and the noise can be analyzed separately.

Transient behavior of the estimator. Let $(k_La - \widehat{k_La})(o)$ be the initial estimation error (the uncertainty on the oxygen transfer rate), then the following relation can be written under the assumption that there is no initial error on the oxygen concentration and the oxygen uptake rate is known perfectly. T_r is the reference time and is assumed to be large with respect to the inverse of the $\mid \lambda \mid$.

$$\int_o^{T_r} \mid k_La - \widehat{k_La} \mid dt \approx \mid (k_La - \widehat{k_La})(o) \mid \frac{2}{\mid \lambda \mid} \tag{6.30}$$

Notice that this formula is the same as the relation found for the oxygen uptake rate estimator. When the convergence speed becomes zero, the integral of the error is equal to the product of the initial error with the reference time T_r.

Noise sensitivity of the estimator. The noise contribution to the objective function can be approximated as follows.

$$\int_o^{T_r} \mid (k_La - \widehat{k_La}) \mid dt = 4 \mid \frac{\lambda}{C_{SAT} - C_O} \mid\mid r(t) \mid T_r \tag{6.31}$$

When only the asymptotic noise contribution and the transient behavior of the estimator are taken into account, then an explicit value of the optimal tuning parameter is found as follows:

$$\begin{aligned} \lambda^* &= \arg\min_\lambda (4 \mid \frac{\lambda}{C_{SAT} - C_O} \mid\mid r(t) \mid T_r + \frac{2}{\mid \lambda \mid} \mid (k_La - \widehat{k_La})(o) \mid) \\ &= \sqrt{\frac{\mid (k_La - \widehat{k_La})(o) \mid (C_{SAT} - C_O)}{2T_r \mid r(t) \mid}} \end{aligned} \tag{6.32}$$

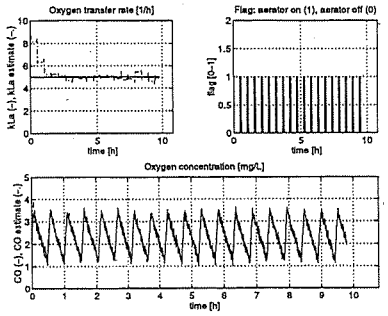


Figure 6.3: Dynamics of the estimator for a noise level 0.5 mg/L. Upperleft plot: Time plot of the oxygen transfer rate and its estimate. Upperright plot: Oxygen concentration and its estimate. Bottom left plot: Flag indicating whether the aerator is switched on (1) or off (0)

Simulations

The trade-off analysis with the objective function is illustrated below with simulations.

It is assumed that the oxygen concentration C_O [mg/L] is controlled with an on-off control of the aerator between 1 and 4 mg/L. A flag is indicating whether the aerator is on (1) or off (0). The oxygen uptake rate [mg O_2/L h] is constant and equal to 5 mg O_2/L h. The oxygen transfer rate [1/h] is constant and equal to 5 1/h. The oxygen measurements are corrupted with random noise with a uniform distribution and quantified with its maximum value $\mid r(t) \mid$. The oxygen uptake rate is estimated when the aerator is off with an optimal tuned estimator ($\lambda = 5$). The oxygen transfer rate is estimated when the aerator is on. The discretization time is 36 sec or 0.01 h. The reference time T_r [h] is here 10 h. The initial error on the oxygen uptake rate estimate is 2 mg O_2/L h. The initial error on the oxygen transfer coefficient is 5 1/h. The dynamics of the oxygen transfer rate, its estimate, the oxygen concentration and its estimate are shown in Figure 6.3.

In Figure 6.4 the tuning of the oxygen transfer rate estimator with trade-off analysis is shown. The integral of the estimation error is shown as a function of the tuning parameter λ [1/h] for three different noise levels (indicated by the maximum value of the noise)

Qualitatively the relations found by performance analysis are confirmed by the trade-off analysis. In the analysis an upper bound on the discretization time of both the oxygen uptake rate and oxygen transfer rate estimator is derived. Recall that this upper bound is just a hard constraint but it does not indicate how discretization affects the estimation error. An alternative trade-off analysis can be used to analyze this. Figure 6.5 shows the integral

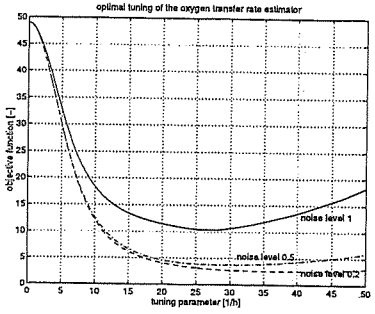


Figure 6.4: Optimal tuning of the oxygen transfer rate estimator with trade-off analysis. Integrated estimation error in function of the tuning parameter λ for three different noise levels

of the estimation error of the oxygen uptake rate and the oxygen transfer coefficient as function of the discretization time. The noise level is chosen to be 0.5. The λ for the oxygen uptake rate estimator is 5. The λ for the oxygen transfer rate is 30. These values are determined from the trade-off analysis. It is clear that the discretization error increases with a larger discretization time T. The discretization error increases drastically when the discretization time exceeds $0.033h$. Notice that this bound is twice lower than the constraint calculated in the analysis. An explanation is found in the alternating estimation.

6.3.4 Oxygen uptake rate estimator, dependent on the oxygen transfer rate

Another approach for estimation of the oxygen uptake rate is based on explicit knowledge of the oxygen transfer rate. Recall that in the previous cases the estimation of the oxygen uptake rate relies on the on-off control of the aerator, such that the estimation of the oxygen uptake rate could be performed without knowing the oxygen transfer rate. When the aerator is on during the whole process the estimation scheme discussed here is the only alternative.

It must be emphasized that the oxygen transfer rate is function of the operating conditions such as the air flow used for aeration, the stirring speed and so on. When the oxygen transfer rate is exactly known then the

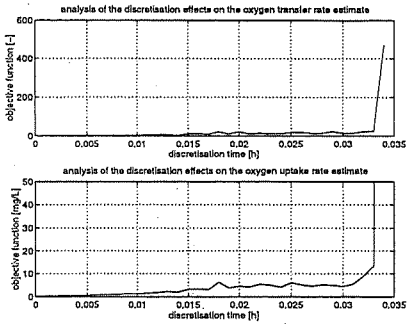


Figure 6.5: Analysis of discretization effects. Estimation error in function of the discretization time T

following observer based estimator for the oxygen uptake rate can be used.

$$\begin{array}{rcl} \frac{d\widehat{C_O}}{dt} & = & -\widehat{OUR} + k_La(C_{SAT} - C_O) \quad + \quad a \cdot (C_O - \widehat{C_O}) \\ \frac{d\widehat{OUR}}{dt} & = & b \cdot (C_O - \widehat{C_O}) \end{array} \tag{6.33}$$

This observer looks similar to the one discussed before for estimation of the oxygen uptake rate. The only difference is now the appearance of the oxygen transfer part in the dynamic equation of the estimate of the oxygen concentration. Notice that the oxygen transfer part is evaluated for the measured oxygen concentration and not in the estimate of this concentration. When the error system is written, the same system is obtained as in Section 6.3.2 because an exact cancellation of the oxygen transfer part is obtained. The same tuning procedure can be used.

The observer designed above relies on perfect knowledge of the oxygen transfer part of the oxygen concentration dynamics. The robustness against errors on the oxygen transfer coefficient k_La and the oxygen saturation coefficient C_{SAT} is analyzed. Both an equilibrium and a dynamical analysis is performed.

Robustness analysis against uncertainty on k_La. When in the observer $\overline{k_La}$ is used instead of k_La then the following error system is obtained:

$$\begin{pmatrix} \frac{dE_1}{dt} \\ \frac{dP_1}{dt} \end{pmatrix} = \begin{pmatrix} -a & -1 \\ -b & 0 \end{pmatrix} \cdot \begin{pmatrix} E_1 \\ P_1 \end{pmatrix} + \begin{pmatrix} -\Delta k_La(C_{SAT} - C_O) \\ \frac{dOUR}{dt} \end{pmatrix} \tag{6.34}$$

Δk_La denotes the difference between the value of the oxygen transfer coefficient used in the observer and the actual oxygen transfer coefficient.

The error on the oxygen uptake rate estimate can now be written as function of the error on the oxygen transfer coefficient as follows:

$$OUR - \widehat{OUR} = \Delta k_L a (C_{SAT} - C_O) \tag{6.35}$$

It can be concluded that the robustness of the observer based estimator can be improved by operating close to the oxygen saturation concentration. Notice that the error on the oxygen transfer coefficient has no effect on the dynamics of the estimator.

Robustness analysis against uncertainty on C_{SAT}. When in the observer $\overline{C_{SAT}}$ is used instead of C_{SAT} then the following error system is obtained:

$$\begin{pmatrix} \frac{dE_1}{dt} \\ \frac{dP_1}{dt} \end{pmatrix} = \begin{pmatrix} -a & -1 \\ -b & 0 \end{pmatrix} \cdot \begin{pmatrix} E_1 \\ P_1 \end{pmatrix} + \begin{pmatrix} -k_L a \Delta C_{SAT} \\ \frac{dOUR}{dt} \end{pmatrix} \tag{6.36}$$

ΔC_{SAT} denotes the difference between the value of the oxygen saturation concentration used in the observer and the actual oxygen saturation concentration. The error on the oxygen uptake rate estimate can now be written as function of the error on the oxygen saturation concentration as follows:

$$OUR - \widehat{OUR} = -k_L a \Delta C_{SAT} \tag{6.37}$$

It can be concluded that the effect of the error on the oxygen saturation concentration can be minimized by using an aerator with a low oxygen transfer coefficient. Notice that the dynamics of the observer based estimator is not altered by the mismatch of the oxygen saturation concentration.

6.3.5 Case study: carbon removal wastewater treatment systems

The application of observer based estimation of the oxygen uptake rate in activated sludge wastewater treatment systems for carbon removal is now illustrated.

As discussed before, the oxygen uptake rate is closely related to the biotransformation process in a wastewater treatment process. Reliable estimation of this process parameter from available on-line oxygen concentration measurements results in additional monitoring capabilities which can be used for on-line control of the overall plant (Chapter 3).

In the treatment plant under consideration an on-off control strategy of the oxygen concentration is used. The oxygen concentration is kept between a lower- and upper bound. The alternating estimation scheme for the oxygen uptake rate and oxygen transfer coefficient discussed before is used.

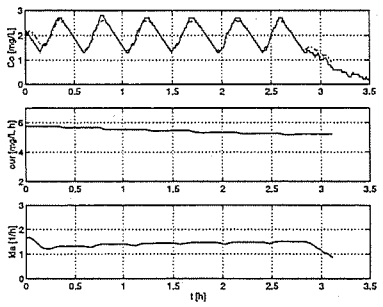


Figure 6.6: Observer based estimation of the oxygen uptake rate and oxygen transfer coefficient. Dynamics of the oxygen concentration (full line) and its estimate (dashed line) (top), oxygen uptake rate (middle) and the oxygen transfer coefficient estimate (bottom)

In Figure 6.6 the dynamics of the oxygen concentration measurements, its estimate, the estimated oxygen uptake rate and the estimated oxygen transfer coefficient are presented. The oxygen concentration is logged every 10 seconds. A reliable estimate of both the oxygen uptake rate and the oxygen transfer coefficient is obtained. The oxygen uptake rate estimator has been used on on-line oxygen concentration data obtained from four tanks of a two-stage cyclically operated wastewater treatment plant over a period of 60 hours. The obtained results are presented and discussed in Chapter 1. The main conclusion is that the dynamics observed in the oxygen uptake rate obtained with the observer is due to the dynamics of the underlying activated sludge process. With the observer the dynamics of the plant can thus be monitored in a reliable way.

6.3.6 Case study: nitrogen removal wastewater treatment systems

Application of observer based estimation on *on-line oxydo reduction potential measurements* in the context of the *two step nitrogen removal process*, introduced in Chapter 1, is now considered.

Nitrogen removal can be obtained in activated sludge processes by a two step *nitrification-denitrification* process (Chapter 1). One can switch between *nitrification* and *denitrification* by control of the oxygen concentration. It is clear that the operation must be switched from denitrification to nitrification when the available nitrate becomes zero. Unfortunately on-line measurements of the nitrate concentration are most often not available.

The oxydo reduction potential is measure of the oxidative or reductive capacity of a mixture which is relatively easily on-line measurable. When

the nitrate concentration is zero (or small) a knee in the redox potential profile is visible. The detection of this so-called *redox* knee can be used to detect the end of the denitrification phase and as such can be used to control the nitrification/denitrification process.

An algorithm, based on an *observer based parameter estimator*, for optimal reliable detection of a redox knee is discussed here.

First the redox knee detection algorithm is presented. Second results obtained both from simulations and on full scale data are shown.

Observer based parameter estimation scheme for redox detection. Suppose that the redox potential r [mV] can be related to the biochemical state of the system by a mathematical relation $h(\mathbf{x})$. The state vector $\mathbf{x}$ consists of the concentrations [mg/L] of the components in the reactor (autotrophic and heterotrophic biomass concentrations C_{X_A}, C_{X_H}, ammonium concentration C_{NH_4}, nitrate and nitrite concentration C_{NO_X}, carbon and oxygen concentration C_C, C_O). The following formal relation between (minus) the time derivative (the slope) of the redox potential r_d and the state of the system $\mathbf{x}$ can be written.

$$\frac{dr}{dt} = -r_d(C_{X_A}, C_{X_H}, C_{NH_4}, C_{NO_X}, C_C, C_O) \quad ; \quad \frac{dr_d}{dt} = 0 \qquad (6.38)$$

Not the absolute value of the redox potential is of importance but the change of the derivative of the redox potential (second order time derivative). The change of this variable indicates a redox knee in the oxydo reduction potential signal. This model does not indicate that the change of the slope of the redox potential is zero but that the change of the slope is assumed to be smaller than the change of the redox potential itself. From a system theoretic point of view the redox potential is assumed to be a state variable (a variable fast varying with time) and its time derivative is a parameter (a variable varying slowly with time). The estimation of the slope of the redox potential r_d can be done with the same observer based parameter estimator used for the oxygen uptake rate. The same comments can be made concerning convergence speed, noise sensitivity and discretisation. Notice that a kind of filtered derivative is obtained here.

The parameter estimator exist of two parts: (i) the copy of the model (6.38), expressed in $\widehat{r}$ and $\widehat{r_d}$, and (ii) correction terms $(a(r) \cdot (r - \widehat{r}), b(r) \cdot (r - \widehat{r}))$. r is the actual measured redox potential in the system. $\widehat{r}$ is the estimated redox potential and $\widehat{r_d}$ the estimated slope of the oxydo reduction potential. The parameters a and b are the *tuning functions* of the estimation scheme. A convergence time τ of the estimator (reduction of the estimation error of 37% or e^{-1} of the initial error within a time span τ) is obtained when the following tuning functions $a = \frac{2}{\tau}$ and $b = -\frac{1}{\tau^2}$ are used.

Filtering. The trade-off between convergence speed and noise sensitivity is discussed before. An alternative way of reducting the influence of noise is the application of a low pass filter on the measured signal. In the particular

application considered here the use of low pass filters is limited. Recall that the purpose of the estimator is the detection of a redox knee. Such a redox knee will introduce high frequent modes. The application of a low pass filter will result in a higher signal to noise ratio (and allowing a larger convergence speed) but the redox knee will be flattened. Notice that the parameter estimator is also a low pass filter of a specific type, allowing to include a priori knowledge of the system.

Some simulation results illustrate the importance of tuning and filtering. The application of the estimation scheme on real data, measured in a *full scale* installation, is shown.

Simulation results. Figure 6.7 (top left) shows the results of the estimation algorithm when noise free data of the oxydo reduction potential is assumed. It is shown that the estimate of the slope of the redox potential converges towards the actual value of the slope although there is an initial error, and unrealisticly fast changes of the slope. This represents in fact the worst case situation for the redox knee detector. Figure 6.7 (top right) shows the results of the same estimation algorithm, again on noise free data, but now with a higher convergence rate. One can hardly distinguish the redox potential and its estimate. In Figure 6.7 (bottom left) the impact of noise on the measurement of the oxydo reduction potential on the estimation results is illustrated. It is clear that algorithm still converges although a considerable noise component is present in the data. Figure 6.7 (bottom right) illustrates the trade off between the rate of convergence and the noise sensitivity. The algorithm considered here has a high convergence rate but does not provide a good estimate of the slope of the redox potential due to the noise on the data. Figure 6.8 illustrates that after prefiltering of the measurements with a fifth order Butterworth filter the algorithm with the high convergence rate provides good estimates of the redox potential slope. A combined backward and forward filter is used to prevent delays. This figure shows that prefiltering allows a higher convergence rate for the estimation algorithm. Recall that filtering of the measurements results in smoothing the signals, which is not practical in the context of knee detection discussed here. Notice the Gibbs effect in the estimated redox slope.

Application on full scale data. Figure 6.9 (left) shows the dynamics of the redox potential as function of time, measured in a cyclically operated wastewater treatment plant for nitrogen removal for a complete nitrification and denitrification cycle.

Figure 6.9 (right) shows the same redox potential in the time interval [340-420]. The top figure shows the filtered data r and the estimated redox potential $\widehat{r}$ while in the bottom figure the estimate of the slope of the oxydo reduction potential $\widehat{r_d}$ is shown.

A redox knee in the redox potential measurements can now be detected if a certain change of the slope r_d (or its estimate $\widehat{r_d}$) can be observed within a certain time interval. In Figure 6.9 the slope of the redox potential varies from $-0.1mV/s$ to $-0.3mV/s$ in a time interval of approximately 3 minutes.

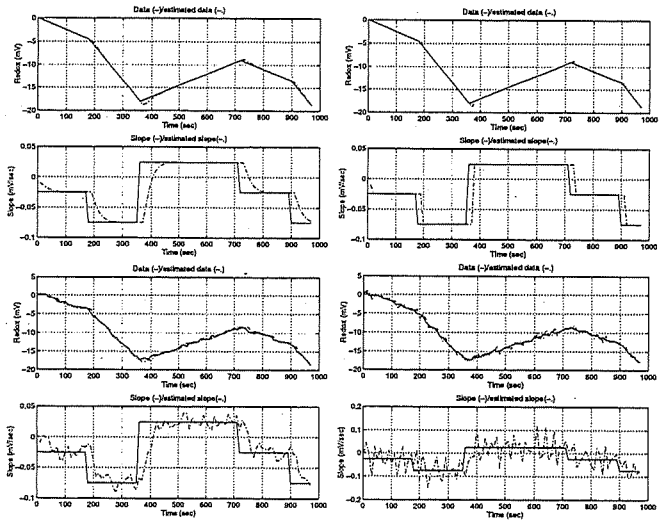


Figure 6.7: Observer based estimation of the redox knee. Dynamics of the redox potential, its estimate, the redox potential slope and its estimate. Top left: Slow convergence on noise free data. Top right: Fast convergence on noise free data. Bottom left: Slow convergence on unfiltered noisy data. Bottom right: Fast convergence on filtered noisy data

Notice that the actual detection of the redox knee depends on the definition of what a redox knee is. The algorithm presented here only guarantees that the signal on which the definition is applied is noise insensitive.

6.3.7 Case study: fermentation processes

The application of observer based estimators in fed-batch fermentation processes is now illustrated. A fed-batch fermentation of *Saccharomyces cerevisiae* is considered [Keulers 1993][Axelsson 1989]. The baker's yeast transforms substrate (glucose) into new biomass and specific metabolites (ethanol).

On-line oxygen concentration measurements are basically only used for testing whether enough oxygen is available for the aerobic fermentation process and for determining an appropriate control action of the aerator. As shown before from on-line oxygen concentration measurements information about the respiration rate can be extracted in a reliable way with an observer based estimator. In such a way the biotransformation process itself can be monitored on-line.

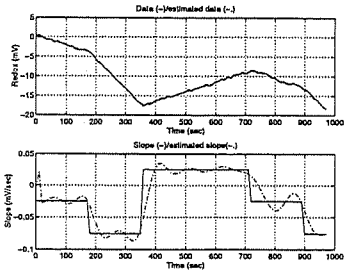


Figure 6.8: Observer based estimation of the redox knee. Dynamics of the redox potential, its estimate, the redox potential slope and its estimate. Fast convergence on filtered noisy data

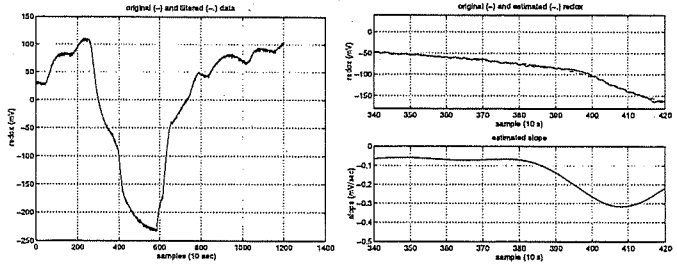


Figure 6.9: Left: Original and pre-filtered data. Right: Redox knee detection

The first data set used here for illustration of observer based estimation of the oxygen uptake rate OUR [mg/L min], depending on the oxygen transfer coefficient, is obtained from reactor with a 5 L working volume. Aeration is obtained by an oxygen flow F_O [L/min] into the reactor. There is continuous stirring in the reactor which stimulates the oxygen transfer to the liquid phase. The oxygen concentration in the reactor is controlled between 60 and 80 % of the oxygen saturation concentration by adaptation of the speed of the stirrer r [rpm] and if necessary the oxygen flow rate F_O. It is assumed that the relation between the oxygen transfer coefficient k_La [1/min] and the speed of the stirrer r is a linear relation (6.39). The coefficients of these relation are determined for the reactor with a priori experiments. These coefficients depend on the oxygen flow rate used. The

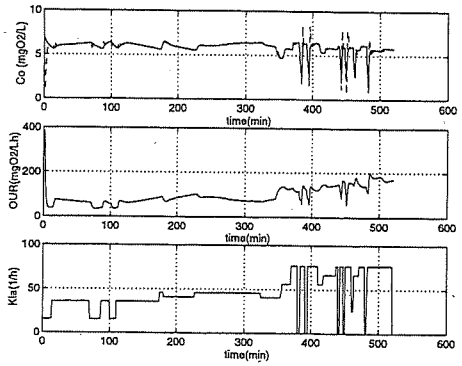


Figure 6.10: Observer based estimation of the oxygen uptake rate. Dynamics of the oxygen concentration and its estimate (top), oxygen uptake rate (middle) and the oxygen transfer coefficient (bottom)

oxygen concentration is logged every minute.

$$k_L a = 0.023 \cdot r - 0.1731 \quad F_O = 1 \quad k_L a = 0.034 \cdot r - 0.2537 \quad F_O = 2 \tag{6.39}$$

Figure 6.10 shows the dynamics of the oxygen concentration, its estimate, the estimated oxygen uptake rate and the oxygen transfer coefficient determined with relation (6.39). Roughly spoken the figure indicates an increase of the oxygen uptake rate as function of time. This is probably due to the increase of the biomass during the fermentation. The oxygen uptake rate profile is not smooth. The variation of the oxygen transfer coefficient corrupts the actual oxygen uptake rate profile. Notice that at the end of the fermentation process the aerator is switched off at certain time instances, which affects the estimation considerably. From this observation one should not conclude that the estimator can not cope with time variations of the oxygen transfer coefficient. It just indicates that one should be aware of the transient dynamics of the estimator. The capabilities of the estimator would become more clear when a better presentation of the estimation results, for instance, omitting results obtained some time (depending on the time constant of the estimator) after an abrupt change of the oxygen transfer coefficient, is used. Of course this coefficient is then expected not to switch to frequently. As indicated in the robustness analysis of the algorithm previously, the error on the oxygen transfer rate coefficient and the oxygen saturation concentration results in an error on the oxygen uptake rate. A determination of these parameters in experimental conditions which are similar to those used for the experiment will improve the accuracy of

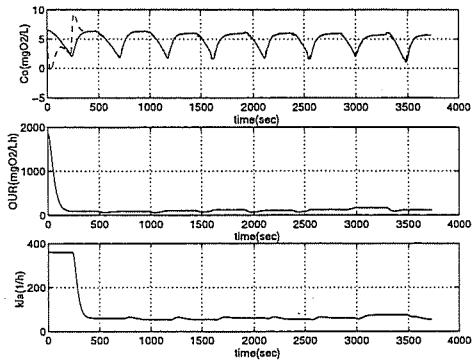


Figure 6.11: Observer based estimation of the oxygen uptake rate. Dynamics of the oxygen concentration (full line) and its estimate (dashed line) (top), the estimated oxygen uptake rate (middle) and the estimated oxygen transfer coefficient (bottom)

the observer based estimator.

The second data set used here for illustration of alternating estimating of the oxygen uptake and the oxygen transfer coefficient with observer based parameter estimators, is obtained at the end of the fed batch fermentation considered previously. The aeration is switched on and off by controlling the oxygen flow rate F_O. Figure 6.11 shows the dynamics of the oxygen concentration, its estimate and the estimated oxygen uptake and transfer coefficient. The oxygen concentration is logged every 5 seconds. A smooth profile for both the oxygen uptake rate and the oxygen transfer coefficient is obtained. From the application discussed before one can conclude that the observer based estimators are indeed valuable algorithms for extracting extra information from already available on-line measurements. The alternating estimation scheme for oxygen uptake rate and oxygen transfer coefficient shows excellent performance. The estimation of the oxygen uptake rate, depending on the oxygen transfer coefficient, is more critical.

6.3.8 Case study: germination processes

Germination is one of the basic processes of the malting process. The respiratory activity of barley (and its natural microflora) during the germination process is a key process parameter revealing basic information about the biotransformation [Van Campenhout and Iserentant 1996]. The estimation of the oxygen uptake rate and the carbon dioxide production rate from on-line measurements of oxygen and carbon dioxide concentration with observer

based estimators is illustrated here.

The data is obtained from a solid state reactor. In the reactor a layer of barley grain is fixed. There is in- and out-flow of air. The inflow air has a fixed concentration of oxygen and carbon dioxide. The composition of the outgoing air is changed due to the biotransformation process. The following mass balance can be written.

$$\begin{aligned} \frac{dC_O}{dt} &= -OUR + k_1 \frac{Q}{V} \cdot (C_{O,in} - C_O) \\ \frac{dC_C}{dt} &= Q_C + k_2 \frac{Q}{V} \cdot (C_{C,in} - C_C) \end{aligned} \tag{6.40}$$

C_O [%] and C_C [ppm] are respectively the oxygen and carbon dioxide concentration of the outgoing air. OUR [%/h] represents the oxygen consumption rate while Q_C [ppm/h] is the carbon dioxide production rate. Q is the flow rate through the reactor and V the reactor volume. $C_{O,in}$ and $C_{C,in}$ are respectively the oxygen and carbon dioxide concentration in the input flow. In the derivation of the mass balance above it is assumed that the reactor can be considered as a completely mixed reactor. Due to the fixed bed of grain this assumption is violated. By introducing the parameters $k_1(= 1.5)$ and $k_2(= 0.7)$ the mass balances can be adjusted. These parameters are determined experimentally. The ingoing air is first transported through a liquid phase. The difference in solubility of oxygen and carbon dioxide explains the difference between the adjustment parameters k_1, k_2. Recall that the objective is to estimate the oxygen uptake and carbon dioxide production rate from the on-line measurements. The main goal is to view the global trend of these quantities rather than determining their absolute values. This explains why the above given mass balances which represents only a rough description of the overall dynamics of the reactor, are sufficient for estimation of the rates.

It is clear from the structure of the mass balances (6.40) that an estimator of a similar structure as the one discussed in Section 6.3.4 can be used for both rates. This is illustrated in Figure 6.12. The tuning parameters are determined with trade-off analysis.

6.4 Case study 2: Nonlinear observers

6.4.1 Problem statement

The application of *performance analysis* and *trade-off analysis* for tuning of nonlinear state estimators or observers is discussed now.

Fed-batch fermentation is used as prototype biotechnological process. The basic model of Chapter 0 is used. Only the dynamics of the biomass concentration C_X [g/L] and the substrate concentration C_S [g/L] are considered. The specific biomass growth rate is described with Haldane kinetics. There is no biomass in the influent stream ($C_{X,in} = 0$). Assume that

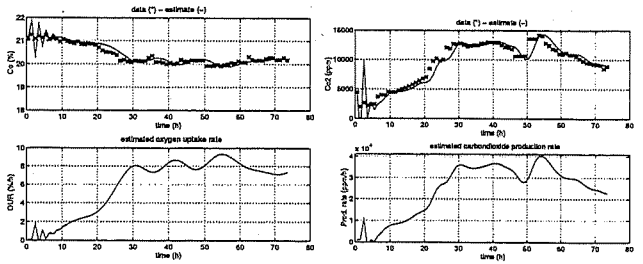


Figure 6.12: Left: Observer based estimation of the oxygen uptake rate in germination processes. Dynamics of the oxygen concentration (∗), its estimate (full line) (top) and the oxygen uptake rate (middle). Right: Observer based estimation of the carbon dioxide production rate in germination processes. Dynamics of the carbon dioxide concentration (∗), its estimate (full line) (top) and carbon dioxide production rate (middle)

on-line measurements of the substrate concentration are available. The biomass concentration is then estimated with a state estimator or observer. The tuning of an extended Luenberger observer for biomass concentration estimation is now discussed.

The extended Luenberger state estimator (observer) consists of a copy of the model and a correction term [Bastin and Dochain 1990]. $\widehat{C_X}$ and $\widehat{C_S}$ are the estimates of the biomass concentration and the substrate concentration. C_S is the *on-line* measurement of the substrate concentration. The correction term is proportional with the error between the estimate of the substrate concentration $\widehat{C_S}$ and the actual concentration in the reactor C_S. $k_1(\widehat{C_X}, \widehat{C_S})$ and $k_2(\widehat{C_X}, \widehat{C_S})$ are the tuning functions of the observer. It is assumed that the model of the growth rate is known. $\widehat{\mu}$ and $\widehat{\sigma}$ are respectively the specific biomass growth rate and the specific substrate consumption rate evaluated in the estimated state.

$$\begin{aligned} \frac{d\widehat{C_X}}{dt} &= \widehat{\mu}\widehat{C_X} - D\widehat{C_X} + k_1(\widehat{C_X}, \widehat{C_S})(C_S - \widehat{C_S}) \\ \frac{d\widehat{C_S}}{dt} &= -\widehat{\sigma}\widehat{C_X} - D\widehat{C_S} + DC_{S,in} + k_2(\widehat{C_X}, \widehat{C_S})(C_S - \widehat{C_S}) \end{aligned} \tag{6.41}$$

In Section 6.4.2 the local linearization approach is used for the design of the tuning functions k_1 and k_2. These functions are parametrized with a tuning parameter λ. The *performance analysis* is first illustrated. The relation between the tuning parameter and performance criteria such as convergence speed, noise sensitivity and maximum allowable discretization time is analyzed. Second the optimal selection of λ with *trade-off analysis*

is discussed.

6.4.2 Performance analysis

Convergence. The behavior of the estimator can be understood by analyzing the dynamics of the estimation error. Let $\mathbf{e}$ be the vector containing the error E_X on the biomass concentration estimate and the error E_S on the substrate concentration estimate. The design rule for Luenberger observers is to choose the tuning functions k_1 and k_2 in such a way that $\mathbf{e} = 0$ is an asymptotically stable equilibrium point of the linear tangent error model (6.42).

$$\frac{d\mathbf{e}}{dt} = \begin{bmatrix} \widehat{\mu} - D & f_S - k_1 \\ -\widehat{\sigma} & -\dfrac{f_S}{Y_{XS}} - D - k_2 \end{bmatrix} \mathbf{e} \tag{6.42}$$

$$f_S = \left.\frac{\partial \mu C_X}{\partial C_S}\right|_{(\widehat{C_X},\widehat{C_S})} = \mu_{max} \frac{K_S - \dfrac{\widehat{C_S}^2}{K_I}}{\left(K_S + \widehat{C_S} + \dfrac{\widehat{C_S}^2}{K_I}\right)^2} \widehat{C_X} \tag{6.43}$$

The tuning functions k_1 and k_2 are selected such that the matrix of the error system has a (negative) eigenvalue λ with a double multiplicity. Technical Lemma (3) stated in Appendix B is used.

$$\begin{aligned} k_1 &= \frac{(\lambda - \widehat{\mu} + D)^2}{-\widehat{\sigma}} + \left.\frac{\partial \mu C_X}{\partial C_S}\right|_{(\widehat{C_X},\widehat{C_S})} \\ k_2 &= -2\lambda - 2D + \widehat{\mu} - \frac{1}{Y_{XS}} \left.\frac{\partial \mu C_X}{\partial C_S}\right|_{(\widehat{C_X},\widehat{C_S})} \end{aligned} \tag{6.44}$$

Discretization. The state estimator can be implemented in discrete time by using a first order forward Euler approximation. The system matrix of the linear approximation (around the state estimate) of the discrete time estimator with discretization time T is presented below with $k_1^{C_S}$ and $k_2^{C_S}$ respectively the partial derivative of the tuning function k_1 and k_2 with respect to the substrate concentration and evaluated in the state estimate (Technical Lemma (3)).

$$\begin{aligned} k_1^{C_S} &= \frac{2\widehat{\sigma}(\lambda - \widehat{\mu} + D) \left.\dfrac{\partial \mu}{\partial C_S}\right|_{\widehat{C_S}} + (\lambda - \widehat{\mu} + D)^2 \left.\dfrac{\partial \sigma}{\partial C_S}\right|_{\widehat{C_S}}}{\widehat{\sigma}^2} + \left.\frac{\partial^2 \mu}{\partial C_S^2}\right|_{\widehat{C_S}} \widehat{C_X} \\ k_2^{C_S} &= \left.\frac{\partial \mu}{\partial C_S}\right|_{\widehat{C_S}} - \frac{1}{Y_{X/S}} \left.\frac{\partial^2 \mu}{\partial C_S^2}\right|_{\widehat{C_S}} \widehat{C_X} \end{aligned} \tag{6.45}$$

$$\begin{pmatrix} 1 + T(\widehat{\mu} - D - \left.\dfrac{\partial \mu}{\partial C_S}\right|_{\widehat{C_S}} \widehat{C_S}) & T(\dfrac{(\lambda - \widehat{\mu} + D)^2}{\widehat{\sigma}} - k_1^{C_S} \widehat{C_S}) \\ T(-\widehat{\sigma} + \dfrac{1}{Y_{X/S}} \left.\dfrac{\partial \mu}{\partial C_S}\right|_{\widehat{C_S}} \widehat{C_S}) & 1 + T(+D + 2\lambda - \widehat{\mu} - k_2^{C_S} \widehat{C_S}) \end{pmatrix} \tag{6.46}$$

The maximum allowable discretization time is a complicated function of the substrate and biomass concentration C_S and C_X and the tuning parameter λ. From Technical Lemma (3) one can conclude that the relation found between the maximum allowable discretization time and the convergence speed for the observer based estimators is part of the relation obtained in the case of nonlinear estimators. The inverse proportionality between the maximum allowable discretization time and the convergence speed still holds when the nonlinearities (the kinetics) are sufficiently smooth, thus resulting in small derivatives. Analysis of maximum allowable discretization time as function of the biomass and substrate concentration reveals under which processconditions the discretization of the estimator becomes more critical. Numerical evaluation of the eigenvalues of the discrete observer as function of the tuning parameter is performed in Chapter 5.

Noise sensitivity. The behavior of the state estimator when noise is added to the *on-line* measurement of the substrate concentration is examined in two steps. First the instantaneous noise sensitivity is analyzed. Secondly the asymptotic noise sensitivity is considered. The instantaneous noise sensitivity functions $\mathcal{R}^I_{C_X}$ and $\mathcal{R}^I_{C_S}$ are equal to the absolute value of the tuning functions k_1, k_2.

Notice that the instantaneous noise sensitivity for the state which must be estimated is a quadratic function of the tuning parameter λ while the sensitivity function of the measured state is proportional with λ.

The asymptotic noise sensitivity functions are found with Technical Lemma (2) in Appendix B. When the tuning functions k_1 and k_2 are chosen such that the linear tangent approximation of the error system has a negative eigenvalue λ with double multiplicity, then the matrix of the error system looks as follows:

$$\begin{bmatrix} \widehat{\mu} - D & \dfrac{(\lambda - \widehat{\mu} + D)^2}{\widehat{\sigma}} \\ -\widehat{\sigma} & 2\lambda - \widehat{\mu} + D \end{bmatrix} \tag{6.47}$$

With the elements on the diagonal of the matrix of the error system denoted a and b, upper bounds on $\mid C_X(t) - \widehat{C_X(t)} \mid$ and $\mid C_S(t) - \widehat{C_S(t)} \mid$ can then be calculated. The result for the biomass concentration is presented below.

Equations (6.48) and (6.49) show the result for $\lambda \leq a$ and $\lambda \geq a$ respectively.

$$\begin{aligned} & \mid -\frac{1}{\lambda} + \frac{1}{\lambda^2}(a-\lambda) \mid\mid \frac{(\lambda - \widehat{\mu} + D)^2}{-\widehat{\sigma}} + \left.\frac{\partial \mu}{\partial C_S}\right|_{\widehat{C_S}} C_X \mid\mid r(t) \mid \\ & + \\ & \mid \frac{(\lambda - \widehat{\mu} + D)^2}{\widehat{\sigma}} \mid \frac{1}{\lambda^2} \mid -2\lambda - 2D + \widehat{\mu} - \frac{1}{Y_{X/S}} \left.\frac{\partial \mu}{\partial C_s}\right|_{\widehat{C_S}} \widehat{C_X} \mid\mid r(t) \mid \end{aligned} \tag{6.48}$$

$$\begin{aligned} & \mid -\frac{1}{\lambda} - \frac{(a-\lambda)}{\lambda^2}(2e^{\frac{\lambda}{\lambda - a}} - 1) \mid\mid \frac{(\lambda - \widehat{\mu} + D)^2}{-\widehat{\sigma}} + \left.\frac{\partial \mu}{\partial C_S}\right|_{\widehat{C_S}} \widehat{C_X} \mid\mid r(t) \mid \\ & + \\ & \mid \frac{(\lambda - \widehat{\mu} + D)^2}{\widehat{\sigma}} \mid \frac{1}{\lambda^2} \mid -2\lambda - 2D + \widehat{\mu} - \frac{1}{Y_{X/S}} \left.\frac{\partial \mu}{\partial C_s}\right|_{\widehat{C_S}} \widehat{C_X} \mid\mid r(t) \mid \end{aligned} \tag{6.49}$$

The following conclusions can be drawn from these complicated relations: (i) The contribution to the biomass estimate (which is the objective here) due to noise increases when the substrate consumption rate decreases. This is because it is the biodegradation term which links the dynamics of both the substrate and biomass concentration. (ii) Although the noise sensitivity of the biomass estimate is a complicated function of the tuning parameter λ, for large absolute value of λ, the noise sensitivity is proportional with λ. (iii) The noise sensitivity is not zero when the tuning parameter λ approximates zero.

6.4.3 Trade-off analysis

The trade-off analysis with the objective function provides a global view on the tuning problem. The objective function is here the integral of a norm of the error on the biomass estimate. The optimal value of the tuning parameter λ is the value which minimizes the objective function (6.50). Notice that p can be equal to 1, indicating that the absolute value of the error is used, or equal to 2, indicating that a quadratic cost function is considered. The choice of the parameter p is an extra degree of freedom for the process engineer. T_r is the reference time.

$$\lambda^* \quad = \quad \arg\min_\lambda \int_0^{T_r} (\mid C_X - \widehat{C_X} \mid)^p dt \tag{6.50}$$

With the objective function the trade-off between the contribution to the error due to the transient behavior of the estimator and the noise contribution can be analyzed.

Transient behavior of the estimator. When it is assumed that initially the estimate of the substrate concentration is equal to the actual substrate concentration, then with Technical Lemma (2) the relation between the tuning parameter λ and the objective function can be made explicit. The

parameter a is equal to $\widehat{\mu} - D$. $E_X(0)$ is the initial error on the biomass concentration estimate. It is assumed that the reference period T_r is sufficiently large with respect to the convergence speed.

$$\begin{aligned} \int_0^{T_r} \mid C_X - \widehat{C_X} \mid \quad \leq \quad & (-\frac{1}{\lambda} + \frac{1}{\lambda^2}(a-\lambda)) \mid E_X(0) \mid (a \geq \lambda) \\ \text{or} \quad & (-\frac{1}{\lambda} - \frac{(a-\lambda)}{\lambda^2} 2e^{\frac{\lambda}{\lambda - a}} - 1) \mid E_X(0) \mid (a \leq \lambda) \end{aligned} \tag{6.51}$$

This analysis shows that for sufficiently large $\mid \lambda \mid$ the influence on the objective function of the initial error is inversely proportional with the convergence speed.

Noise sensitivity of the estimator. From the noise performance analysis above it is clear that the dependence of the objective function on the noise is of the following form with P a positive parameter.

$$\int_0^{T_r} \mid C_X - \widehat{C_X} \mid \quad \leq \quad P T_r \mid \lambda \mid\mid r(t) \mid \tag{6.52}$$

The performance analysis indicates how P is related to the process conditions.

Robustness of the estimator. The robustness of the nonlinear state observer against parametric and structural uncertainty in the model can also be examined (Chapter 5). Note that although above explicit relations between the tuning parameter and (certain parts of) the objective function are obtained, the trade-off analysis does not rely on this. The objective function is obtained with simulations and as such provides a global view on both the transient behavior, the noise sensitivity, possible interactions and discretization effects.

6.4.4 Simulations

The parameters K_S and K_I of the Haldane kinetics are chosen 0.4 and 10 g/L. The initial biomass concentration in the reactor is 1.5 g/L. The yield coefficient is equal to 0.5. The feedrate is 0.3 L/h and the initial volume is 7 L. The reference time T_r is 8 h.

The effect of discretization is illustrated in Figure 6.13 (left). The integral of the squared error ($p = 2$) on the biomass concentration estimate is shown as a function of the tuning parameter λ for 3 different discretization times. The initial error on the biomass concentration equals 0.5 g/L. This figure indicates that a lower bound for the tuning parameter exists. This lower bound increases for higher values of the discretization time.

For the noise sensitivity analysis Gaussian noise is used. The mean value of the noise signal is used as a norm ($\mid r(t) \mid$) for the noise signal. Figure 6.13 (right) shows the mean square error on the biomass concentration estimate as function of the tuning parameter λ for two noise levels. The first noise signal has a mean value of 0.1 g/L while the second noise signal has a mean

value of 0.2 g/L. To avoid discretization effects a low discretization time of 0.5 minutes is used. The figure clearly illustrates the trade-off between transient behavior and noise sensitivity. The noise contribution is proportional with λ^2 because here the squared error is considered. When the noise level increases the optimal value of the tuning parameter increases. The global

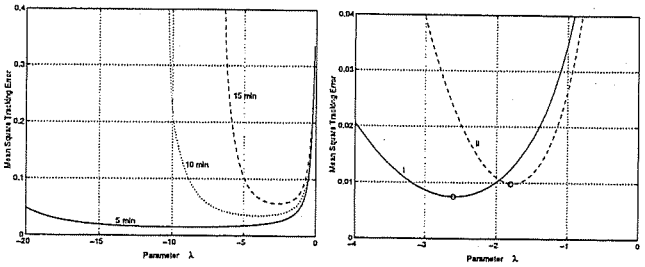


Figure 6.13: Optimal tuning of the biomass concentration observer with trade-off analysis. The mean square error on the biomass concentration estimate as function of the tuning parameter λ. Left: three different discretization times T. Noise level 0. Right: two different noise levels $\mid r(t) \mid$. Discretization step 0.5 [min]

tuning problem is shown in Figure 6.14. The mean square estimation error is evaluated for different values of the tuning parameter for different (realistic) discretization times T and a noise level of 0.1 g/L. Comparing Figure 6.13 (left) with Figure 6.14 clearly illustrates the interaction between noise sensitivity, transient dynamics and discretization effects.

6.5 Conclusions

The optimal tuning of observer based parameter estimators and nonlinear state observers is discussed. *Performance analysis* and *trade-off analysis* are presented as tools for optimal tuning of these estimation algorithms. It is shown that *performance analysis* reveals important relations between the tuning parameter, the process conditions and the performance. The analysis does not result in actual selection of an optimal parameter set because (i) the different aspects of the tuning problem are analyzed separately, (ii) not all facets can be treated and (iii) interaction between the different aspects is considered. The performance analysis method becomes also quite complicated in the nonlinear case. With *trade-off analysis* an optimal parameter set can be selected. The trade-off analysis relies on the quality of the simulations used for calculation of the objective function. The method does not indicate how the performance can be improved. From this observation the

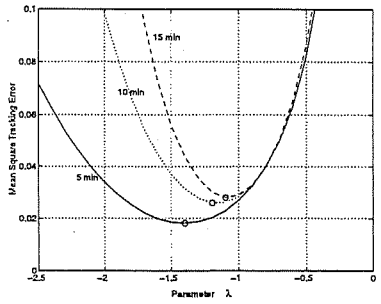


Figure 6.14: Optimal tuning of the biomass concentration observer with trade-off analysis. The mean square error on the biomass concentration estimate as function of the tuning parameter λ for different discretization times T and noise level 0.1

following main conclusion can be drawn.

Performance analysis and trade-off analysis are complementary tools for optimal estimator tuning. Combined use of these techniques results in optimal selection of tuning parameters. With the insight in the relation between performance of the algorithm under study and the process conditions, re-engineering of the process, the measurement setup and the control objective can be performed.

The observer based parameter estimators are sucessfully applied on real data obtained from various applications. This indicates that the framework discussed here is application independent. From the different applications one can conclude that with estimators additional information can be extracted in a reliable way from already available on-line measurements. Application of the optimal tuning tools in process industry can only be enhanced by providing a suitable software environment enabling (i) fast evaluation of the performance measures and (ii) easy set-up of dynamical simulations. The availability of such a toolbox shall however not change the fact that optimal tuning requires a creative input from the process engineer.

Optimal tuning is the third and last step in the design of software sensors. As such it fits into the 'divide et impera strategy' of the thesis. On the other hand it is shown that the performance depends on the procesconditions. This is not in contradiction with the decomposition strategy as this can be taken into account in the process design easily, for instance as a constraint on the state variables.

Part IV

Control of biotechnological processes

Chapter 7

Nonlinear control of bioprocesses

7.1 Introduction

Due to the intrinsic nonlinearities of bioprocesses, the implementation of nearly optimal heuristic control strategies with *nonlinear controllers* must be considered.

Several nonlinear controller design methodologies exist. In Section 7.2 *robustness analysis* of two nonlinear controllers (input-output feedback linearization and input-state feedback linearization) is presented. This analysis can be considered as a part of *performance analysis*, enabling selection of an appropriate design method. Due to the lack of cheap, reliable and accurate on-line sensors encountered when dealing with bioprocesses, the state feedback controllers, obtained in Section 7.2, must be combined with nonlinear observers. In Section 7.3 *combined observers-controllers* are analyzed. *Optimal tuning* of the parameters of the nonlinear control algorithms is considered in Section 7.4.

The biotechnological prototype model of Chapter 0 is used. Only the dynamics of the substrate and biomass concentration are considered. It is assumed that there is no biomass in the influent stream ($C_{X,in} = 0$). The dilution rate is denoted U [1/h]. In Sections 7.2 and 7.3 the biotransformation is modeled with a first order model for the specific rates and maintenance is neglected ($m = 0$). A continuous operation is assumed. In Chapter 5 the same model has been used. In Section 7.4 the biotransformation is modeled with a Haldane kinetic for the specific rates. A fed-batch operation is assumed. The parameter values used are given in Appendix D.

Derivation of nearly optimal heuristic control strategies is discussed in Chapters 2 and 3. Performance analysis tools for nonlinear observers are presented in Chapter 5. Performance and trade-off analysis of estimation algorithms is illustrated in Chapter 6. In Appendix C basic concepts of differential geometry, the two nonlinear controller design methodologies and two nonlinear observer design methods are described.

In this chapter first two nonlinear controller design techniques and robustness analysis are presented. Second the combination of estimators and controllers is discussed. Finally two techniques for tuning of the algorithms are presented briefly.

7.2 Robustness analysis

7.2.1 Problem statement

Nonlinear controller (and observer) design methods, based on global linearization techniques, incorporate the process model without approximations. These techniques reveal the main structure that must be incorporated in the controller. Also the fact that the performance of these algorithms is global over the state space motivates their use.

However, the use of linearization techniques is often criticized due to their lack of robustness against parametric and structural uncertainty on the process model. These techniques are considered to be sensitive because they rely often on cancellation of nonlinearities. Therefore, the robustness of the obtained controller must be checked.

Two nonlinear controller design methods are applied on the prototype model for biotechnological processes. Robustness against parametric uncertainty is determined. Both equilibrium and dynamical robustness analysis is performed, in a similar way as for observers (Chapter 5).
In Section 7.2.2 the two nonlinear controllers obtained for the prototype model are presented. The robustness analysis is discussed in Section 7.2.3. In Section 7.2.4 conclusions are presented.

7.2.2 Nonlinear controller design techniques

The robustness of two nonlinear controllers, originating from two quite different design techniques, is discussed. The control objective is substrate setpoint regulation. Such a control objective can be motivated for both fermentation processes (Chapter 2) and wastewater treatment plants (Chapter 3). First *input-output linearization* is applied to the prototype model. Secondly a controller is constructed with *input-state linearization*.

Input-output linearization

As output of the system the substrate concentration C_S is taken. The output in the context of controller design should not be confused with the

available on-line measurement. The output means here the variable that must be controlled. The input-output linearization theorem in Appendix C states that the relative degree of the output must be less than or equal to 2 in order to design an input-output linearizing controller. The relative degree is here 1 because the dynamics of the substrate concentration is directly influenced by the control input U. The error $E_S = C_S - C_S^*$ between the substrate concentration C_S and the setpoint C_S^* is defined. It is stated that the dynamics of the error E_S must be described by the first order stable linear reference dynamics defined below. λ is a positive constant and represents the convergence rate. This is the tuning parameter of the controller.

$$\frac{dE_S}{dt} = -\lambda E_S \tag{7.1}$$

By combining Equation (7.1) and the dynamic equation for the substrate concentration C_S an expression for the input U is obtained.

$$U = \frac{-\lambda(C_S - C_S^*) - bC_X C_S}{C_{S,in} - C_S} \tag{7.2}$$

When the controller U is applied, it is clear that the following equilibria are obtained.

$$\begin{array}{lllllll} (1) C_{S,e} & = & C_S^* & ; & C_{X,e} & = & -\frac{a}{b}(C_{S,in} - C_S^*) \\ (2) C_{S,e} & = & C_S^* & ; & C_{X,e} & = & 0 \end{array} \tag{7.3}$$

The control objective, setpoint control of the substrate concentration, is obtained. Only the equilibrium point (1) with non-zero biomass concentration is interesting. The biomass concentration reaches an equilibrium value, depending on the substrate concentration setpoint. The dynamics of the biomass concentration (the zero dynamics) are stable. It is sufficient to prove the stability of the biomass concentration dynamics under the assumption that the substrate concentration has reached its equilibrium point C^* and the control law U is used, for proving the local asymptotical stability of the complete system ([Isidori 1989, Proposition 4.2]). An explicit stable solution of the biomass concentration dynamics can easily be obtained. Also from a local linear approximation of the zero dynamics one can conclude that the equilibrium point (1) is stable (eigenvalue equals $-aC_S^*$) and the equilibrium point (2) is unstable.

Input-state linearization

It can easily be verified that the conditions of the input-state linearizing theorem in Appendix C are fulfilled for the whole state space, except for (i) a substrate concentration equal to $C_{S,in}$, (ii) a zero biomass concentration and (iii) the equilibrium point of the system. Because the equilibrium point is only reached asymptotically, the system never comes into a forbidden

state. From a theoretical point of view one can conclude that the theorem is applicable. In practice one must verify whether no singularities in the control law $U(t)$ appear.

The first condition (7.4) is a rank condition while the second condition states that the distribution spanned by transport terms is involutive. Notice that this second condition is fulfilled here because a 1-dimensional distribution is always involutive.

$$Rank\left[\begin{array}{cc} \mathrm{g} & ad_{\mathbf{f}}\mathrm{g} \end{array}\right] = Rank\left[\begin{array}{cc} -C_X & -aC_X(C_{S,in} - C_S) \\ -C_S + C_{S,in} & -bC_X(C_{S,in} - C_S) \end{array}\right] = 2 \tag{7.4}$$

An output $p(\mathbf{x})$ is selected by solving the partial differential equations (7.5).

$$< \mathbf{dp}, \mathbf{g} > = \frac{\partial p(\mathbf{x})}{\partial C_X}(-C_X) + \frac{\partial p(\mathbf{x})}{\partial C_S}(C_{S,in} - C_S) = 0 \tag{7.5}$$

From the output function $p(\mathbf{x})$ the state diffeomorphism $\mathbf{z} = \mathbf{t}(\mathbf{x})$ can be found.

$$\begin{array}{lllll} Z_1 & = & p(\mathbf{x}) & = & \frac{C_X}{C_S - C_{S,in}} \\ Z_2 & = & L_{\mathbf{f}}p(\mathbf{x}) & = & \frac{aC_X C_S}{C_S - C_{S,in}} - \frac{bC_X^2 C_S}{(C_S - C_{S,in})^2} \end{array} \tag{7.6}$$

In the state space, spanned by Z_1 and Z_2, the prototype system is described by the Brunovsky controller form (see Appendix C) with V a new input defined as follows.

$$\begin{gathered} V = g_2(C_X, C_S) \cdot U + g_1(C_X, C_S) \\ g_1 = (a + b\frac{C_X}{C_{S,in} - C_S})\frac{C_X C_S}{C_{S,in} - C_S}(\frac{C_X b C_{S,in}}{C_{S,in} - C_S} + C_S(a + b\frac{C_X}{C_{S,in} - C_S})) \\ g_2 = (a + b\frac{C_X}{C_{S,in} - C_S})C_X \end{gathered} \tag{7.7}$$

Notice that because g_1 becomes zero in the equilibrium point U can not be determined from V. Fortunately also g_2 vanishes in the equilibrium point, which explains why the control law U no singularities appear.

Because the controller design is now performed in the new coordinate system, the control objective must be reformulated in the state space, spanned by Z_1 and Z_2. The substrate concentration setpoint control objective is equivalent with the objective that Z_1 and Z_2 satisfy the equation stated below. Notice that Equation (7.8) with parameters $A = aC_S^*$ and $B = -bC_S^*$ defines a manifold in the new coordinate system.

$$Z_2 = Z_1 C_S^*(a + bZ_1) = AZ_1 + BZ_1^2 \tag{7.8}$$

The controller is now designed in two steps. First a reference controller is defined, which keeps the state of the system on the manifold when the state

of the system is on the manifold. The reference controller is obtained by taking the time derivative of the state Z_2 along the manifold. This time derivative must be equal to the control input V_{ref}.

$$\frac{dZ_2}{dt} = AZ_2 + 2BZ_1Z_2 = V_{ref} \tag{7.9}$$

$$V_{ref} = (a + b\frac{C_X}{C_{S,in} - C_S})\frac{C_XC_S}{C_{S,in} - C_S}(aC_S^* + 2bC_S^*\frac{C_X}{C_{S,in} - C_S}) \tag{7.10}$$

In a second step an error variable indicating the distance between the actual state and the manifold is defined. A stable linear reference model is defined for this error. λ is a positive tuning parameter, representing the convergence rate. Combining the time derivative of the error variable with the reference model results in an equation for the control input V.

$$E = Z_2 - AZ_1 - BZ_1^2 \quad ; \quad \frac{dE}{dt} = V - AZ_2 - 2BZ_1Z_2 = -\lambda E \tag{7.11}$$

There are two equibrium points: (1) $(Z_1, Z_2) = (0, 0)$ and (2) $(Z_1, Z_2) = (-A^{-1} \cdot B, 0)$. The latter equilibrium is the interesting one. The stability of the dynamics of the system *along the manifold* is trivial from the dynamic equations. The correction term $-\lambda E$ forces the state towards the stable manifold. This can easily be proven by using as Lyapunov function E^2 [Khalil 1992, Theorem 4.8]. Finally the control input U in the original coordinate space can then be determined. Notice that the control law consists of a part proportional with λ, which forces the system towards the control objective, and another part which results from the reference controller.

$$\begin{aligned} U(t) &= \frac{-bC_XC_S(C_{S,in} - C_S^*)}{(C_{S,in} - C_S)^2} \\ &+ (C_S^* - C_S)\frac{C_S(a(C_{S,in} - C_S) + bC_X)}{(C_{S,in} - C_S)^2} \\ &- \lambda\frac{C_S - C_S^*}{C_{S,in} - C_S} \end{aligned} \tag{7.12}$$

7.2.3 Robustness against parametric uncertainty

The robustness analysis consists of two parts.

Equilibrium analysis. The effect of uncertainty on the control objective is analyzed.

Dynamical analysis. The effect of uncertainty on the closed loop stability is examined.

The robustness analysis is now performed for the input-output linearizing controller and the input-state linearizing controller. Robustness against parametric uncertainty on the parameter b is examined. It is assumed that a is perfectly known.

First some notes on the determination of the equilibria and their stability is given for both controllers and then illustrated with simulations.

Analysis of the input-output linearizing controller

Let $\widehat{b}$ be the estimate of the parameter b and Δb is the estimation error $\widehat{b} - b$. The control law U (7.13) is then implemented.

$$U = \frac{-\lambda(C_S - C_S^*) - \widehat{b}C_XC_S}{C_{S,in} - C_S} \tag{7.13}$$

Equilibrium analysis. The equilibrium point is now determined. The following equations are obtained by setting the dynamic equations of the substrate and biomass concentration equal to zero respectively. $C_{X,e}$ and $C_{S,e}$ are the biomass and substrate equilibruim concentrations. It is assumed that Δb is different from zero.

$$C_{X,e} = \lambda\frac{C_S^* - C_{S,e}}{\Delta bC_{S,e}} = \frac{aC_{S,e}(C_{S,in} - C_{S,e}) + \lambda(C_{S,e} - C_{S,e}^*)}{-\widehat{b}C_{S,e}} \tag{7.14}$$

Combination of these equations results in a second order polynomial in $C_{S,e}$, if $C_{S,e}$ is not equal to zero. With the second order polynomial two equilibrium substrate concentrations $C_{S,e}$ are found. The corresponding biomass concentration can then be found with one of the relations (7.14).

Notice that $(C_{X,e}, C_{S,e}) = (0, C_S^*)$ is an equilibrium point of the closed loop system, not found with the polynomial approach.

One must also be aware that the polynomial method can provide solutions which are not equilibrium points, or which are not feasible, for instance, negative or complex concentrations. So when the equilibria are obtained with the polynomial method additional tests must be performed. This is illustrated further in the simulations.

It must be emphasized that a numerical determination of the equilibria points is chosen here because this is more general. In Chapter 5, Subsection 5.10 on robustness of nonlinear observer, a more detailed explanation of the determination of equilibria can be found.

Dynamical analysis. The local stability of an equilibrium point is analyzed by determining the eigenvalues of the linearized system, using the controller. The matrix of the linearized system is then given as follows.

$$r = a + \lambda\frac{C_{S,in} - C_S^*}{(C_{S,in} - C_{S,e})^2} + \frac{C_{S,in}\widehat{b}C_{X,e}}{(C_{S,in} - C_{S,e})^2} \tag{7.15}$$

$$\begin{pmatrix} aC_{S,e} + 2\dfrac{\widehat{b}C_{X,e}C_{S,e}}{C_{S,in} - C_{S,e}} + \lambda\dfrac{C_{S,e} - C_S^*}{C_{S,in} - C_{S,e}} & C_{X,e}r \\ -\Delta bC_{S,e} & -\Delta bC_{X,e} - \lambda \end{pmatrix} \tag{7.16}$$

The following conclusions can be drawn:

- The point $(0, C_S^*)$ has eigenvalues aC_S^* and $-\lambda$. Notice that the matrix becomes a lower diagonal matrix. The first eigenvalue describes the dynamics of the biomass. The dynamics of the substrate is given by both eigenvalues. This indicates that this point is never stable.

- For the point $(C_{X,e}, C_{S,e})$ in the case $\Delta b = 0$ the eigenvalues $-aC_S^*$ and $-\lambda$ are obtained. This indicates that the equilibrium point is stable. This is of course the purpose of the controller. Notice that here an upper diagonal matrix is found. The second eigenvalue describes the dynamics of the substrate, which is intrinsic for this design method. The dynamics of the biomass is now depending on both eigenvalues.

Analysis of the input-state linearizing controller

The input-state linearizing controller is explicitly function of the parameter a. Obviously one can conclude that the input-state linearizing controller is sensitive towards errors on the parameter a, while this is not the case for the input-output linearizing approach. In the sequel the robustness against uncertainty on the parameter b is examined. It is assumed that a is perfectly known.

Equilibrium analysis. The equilibrium point of the closed loop system (combination of the system with the correct parameter b and the controller with the estimated parameter $\widehat{b}$) is calculated by combining the two equations, obtained by setting both time derivatives of the states (biomass and substrate concentration) to zero.

The equation, based on the substrate mass balance, is a third order polynomial in $C_{S,e}$, but with a dependence on $C_{X,e}$. The equation, based on the biomass mass balance, results in a rational function for $C_{X,e}$, with a second order polynomial in $C_{S,e}$ as numerator and a second order polynomial in $C_{S,e}$ as denumerator. Substitution of this equation into the third order polynomial results in a fifth order polynomial in $C_{S,e}$. From the fifth order polynomial the equilibrium substrate concentrations $C_{S,e}$ are obtained. The corresponding equilibrium biomass concentrations $C_{X,e}$ are found with the rational function. Recall that with the polynomial method solutions can be obtained which are not equilibrium points of the closed loop system, so additional tests are necessary. This is illustrated in the simulations further. Notice that only numerical determination of the equilibria is possible here.

Dynamical analysis. Examination of the eigenvalues of the system matrix of the linearized model indicates whether the equilibrium points are stable or not. Because the Jacobian is not informative (conclusions about the eigenvalues can not be drawn directly), it is not shown here. The eigenvalues in function of the uncertainty on the parameter a are calculated in the next section.

Simulation results

The robustness of both controllers is now analyzed by performing simulations for a substrate concentration setpoint $C_S^* = 1.2$ [g/L].

In Figures 7.1 and 7.2 the relative error on the control objective (deviation of the equilibrium substrate concentration $C_{S,e}$ from the setpoint C_S^*)

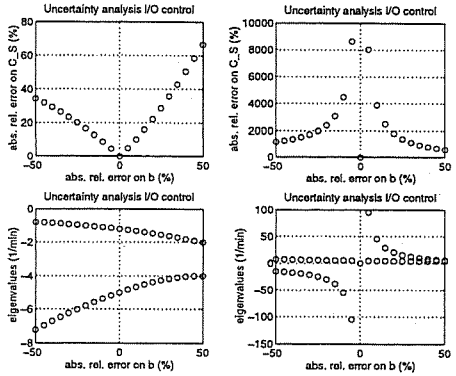


Figure 7.1: Robustness analysis of the input-output linearizing controller. Equilibruim and dynamical analysis. Design eigenvalue $\lambda_c = -5$.

and the corresponding eigenvalues as function of the relative uncertainty on b for two different values of the design eigenvalue λ_c (minus the tuning parameter λ) are indicated for the input-output linearizing controller.

Recall that with the polynomial method two equilibrium substrate concentrations are obtained. The relative error on the control objective is presented for both solutions. It is clear that the solution, resulting in a large error (right figure) is not feasible and not stable. Figures 7.3 and 7.4 show the relative error on the control objective (deviation of the equilibrium substrate concentration $C_{S,e}$ from the setpoint C_S^*) and the corresponding eigenvalues as function of the (relative) uncertainty on b for two different values of the design eigenvalue λ_c (minus the tuning parameter λ), when the input-state linearizing controller is used. Notice that here only one solution of the fifth order polynomial is retained. This is the only solution resulting in a feasible equilibrium point. From Figures 7.1 and 7.2 one can conclude that increasing the convergence rate of the input-output nonlinear linearizing controller results in a lower equilibrium error on the control objective when parametric uncertainty is involved. Analysis of the eigenvalues also indicates that a small increase in dynamical robustness is obtained when the convergence rate is increased. For the design eigenvalue $\lambda_c = 5$ the worst case eigenvalue of -0.78 is obtained when an underestimate of the parameter b of 50 percent is used while for the design eigenvalue $\lambda_c = 10$ this worst case eigenvalue becomes -0.95. Notice that for a zero error on the parameter b one of the eigenvalues equals the design eigenvalue.

Figure 7.3 and 7.4 indicates that decreasing the convergence rate of the controller based on input-state linearization results in a higher equilibrium error on the control objective and even to a loss of stability for certain errors

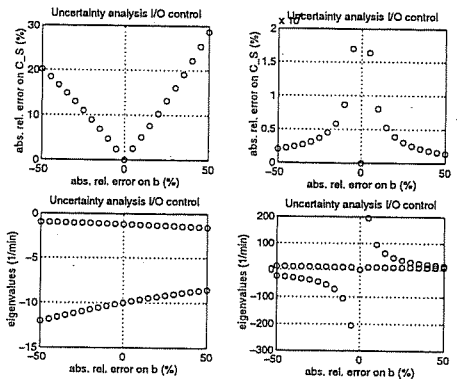


Figure 7.2: Robustness analysis of the input-output linearizing controller. Equilibruim and dynamical analysis. Design eigenvalue $\lambda_c = -10$.

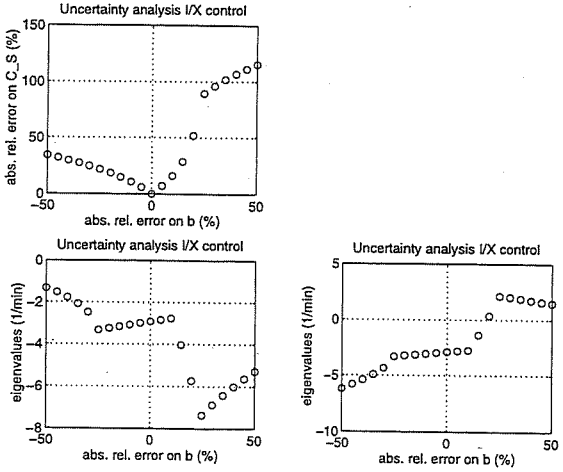


Figure 7.3: Robustness analysis of the input-state linearizing controller. Equilibruim and dynamical analysis. Design eigenvalue $\lambda_c = -5$.

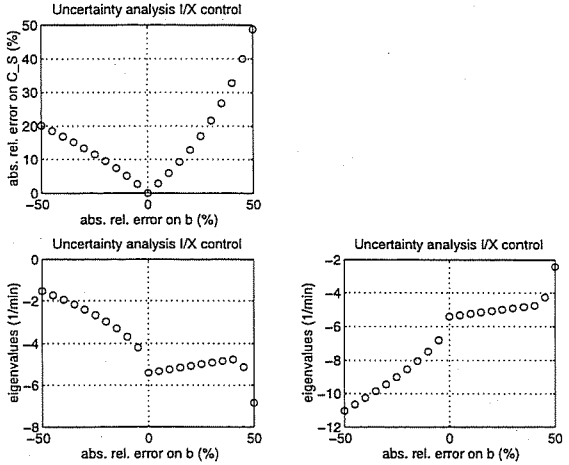


Figure 7.4: Robustness analysis of the input-state linearizing controller. Equilibruim and dynamical analysis. Design eigenvalue $\lambda_c = -10$.

on the parameter b. Notice that the eigenvalues are different from the design eigenvalues even when no parametric error is present. This is due to the fact that the design is performed in another coordinate system than the one considered here.

When the input-output linearizing controller and the controller based on input-state linearization are compared, one can conclude that parametric uncertainty on the parameter b results for the input-state linearizing controller in a higher equilibrium error on the control objective although the dynamical robustness of this controller is better.

When comparing the two control laws (7.2), (7.12) it can observed that (i) the part proportional with the tuning parameter λ is equal for both controllers, (ii) the controller based on input-state linearization contains a part of the controller based on input-output linearization, multiplied with a certain factor and (iii) the controller based on input-state linearization contains an extra part, not found in the controller based on input-output linearization. Note that the difference in dynamics will become more clear when small values of λ are used because for high values of λ the feedback action becomes dominant.

7.2.4 Conclusions

Two nonlinear controller design methodologies are illustrated on a prototype model for bioprocesses. The robustness against parametric uncertainty of the resulting controllers is analyzed. Both the error on the control objective and the stability of the equilibrium point are examined.

The obtained results are obviously depending on the structure of the prototype model and the model parameters. The main goal is however to introduce the tools for performing the robustness analysis, rather than stating general conclusions about the robustness of a certain design methodology.

The case study performed here shows that the obtained robustness is quite sufficient. From this observation one can conclude that, although exact linearization methods are often criticized in literature, their performance can be rather good. Careful analysis for the system under consideration must be performed before conclusions can be stated. Notice also that the robustness against parametric uncertainty can easily be improved by adding an extra integral action. More in general the controllers, resulting from these techniques, can serve as excellent starting point for other more robust techniques [Sepulchre *et al.* 1996].

The work presented here differs from the literature [Bastin and Dochain 1990], [Proll and Karim 1994], [Henson and Seborg 1992] in the sense that in most contributions the robustness analysis is performed with dynamical simulations, rather than explicit calculation of the resulting errors and stability. The results obtained by dynamical simulations are quite parameter dependent and do not provide much insight in the problem under consideration. When explicit relations are determined parameter independent conclusions can be drawn more easily.

Notice that here only robustness (against parametric uncertainty) is analyzed because this is the main criticism on the linearization methods. Naturally also other performance criteria must be examined in detail before a controller can be selected.

7.3 Combined observers-controllers

7.3.1 Problem statement

The application of modern model based control theory to biotechnological processes is hampered due to the fact that cheap, accurate on-line sensors for the biological states of the systems do not exist.

The measurement problem can however be relaxed by using *nonlinear observers* (Chapter 5). The estimated state can be used in the control algorithms if a *nonlinear separation principle* is satisfied. Although the estimated state of the system is used in the *nonlinear controller* instead of the real state, the combination of the observer-controller should be stable.

For a nonlinear observer, based on exact linearization up to an output injection and a controller, based on input-state linearization, it is shown that a local nonlinear separation principle is satisfied. This is first illustrated for the combination of the input-state linearizing controller and an observer, based on exact linearization up to an output injection, without derivatives of the input signal.

In Appendix C it is shown that this observer design technique is not suited for the biotechnological prototype model under consideration. Therefore the observer design is extended to observers which allow derivatives of the input signal. When combining this type of observers with a feedback controller certain existence problems can arise. For the biotechnological prototype under consideration it is shown that the local nonlinear separation principle still holds.

In [Krstic 1995] it is indicated that mainly two approaches to the combined estimator-controller problem can be distinguished. The first approach is based on *modularity*. The estimator and controller are designed independently and a *certainly equivalence property* is used for proving the stability of the combined estimator-controller. The second approach is to design both estimator and controller together for instance in a Lyapunov framework by using backstepping. The first approach has as advantages that it results in two less complex subproblems but the major drawback is that severe restrictions on the nonlinearities must be posed. The second approach is less restrictive but more complicated. It is clear that the approach used in this chapter is based on *modularity*. In [Hunt and Madanpal 1994] and [Teel and Praly 1995] *combined design* of nonlinear observers and controllers is considered.

In Section 7.3.2 and 7.3.3 the input-state feedback linearizing controller and the observer (without derivatives) based on exact linearization up to an output injection are shortly stated. In Section 7.3.4 the nonlinear separation principle is discussed in detail for the case with an observer without derivatives of the input. In Section 7.3.5 the observer design method which allows derivatives of the input signal is presented. In Section 7.3.6 the nonlinear separation principle is discussed for this type of observers and then illustrated for the biotechnological prototype model in Section 7.3.7. Notice that the design of the nonlinear observer based on exact linearization up to an output injection with derivatives of the input is considered here in a differential algebraic framework, while the same observer is discussed in the differential geometric framework in Appendix C. In Section 7.3.8 some conclusions are presented.

7.3.2 Nonlinear controller design

State feedback linearization is described in literature [Marino and Tomei 1995], [Isidori 1989]. By applying a state transformation $\mathbf{t}_1(\mathbf{x})$ and introducing a new control input v (7.17) a linear system (7.18) is obtained. $g_1(\mathbf{x})$

and $g_2(\mathbf{x})$ are nonlinear functions of the state $\mathbf{x}$.

The system matrix $\mathbf{A_C}$ is in controllability form (Appendix C) while $\mathbf{b}_n$ is a vector with all zero entries, except the last element which is one. Notice that the use of such a canonical form is not a limited description because any controllable linear system can be transformed to this form.

$$\mathbf{z} = \mathbf{t}_1(\mathbf{x}) \quad ; \quad v = g_1(\mathbf{x})u + g_2(\mathbf{x}) \tag{7.17}$$

$$\frac{d\mathbf{z}}{dt} = \mathbf{A_C} \cdot \mathbf{z} + \mathbf{b}_n \cdot v \tag{7.18}$$

An often used controller design technique for linear systems is the eigenvalue assignment method. The control input v is defined as the sum of a state feedback and a reference signal v_{ref}. By a proper choice of the feedback vector $\mathbf{p}$ the eigenvalues of the system can be altered.

$$\begin{aligned} \frac{d\mathbf{z}}{dt} &= (\mathbf{A_C} + \mathbf{b}_n\mathbf{p}^T) \cdot \mathbf{z} + \mathbf{b}_n \cdot v_{ref} \\ v &= \mathbf{p}^T \cdot \mathbf{z} + v_{ref} \end{aligned} \tag{7.19}$$

Due to the special structure of the dynamics of the error system an easy procedure for determining the tuning parameters (the elements of the vector $\mathbf{p}^T(p_1, \ldots, p_n)$) is possible. Suppose that the eigenvalues of the error system must be given by the characteristic equation (7.20), then the tuning parameters p_i are the coefficients of this polynomial.

$$\lambda^n - p_n\lambda^{n-1} - p_{n-1}\lambda^{n-2} - \ldots - p_1 = 0 \tag{7.20}$$

7.3.3 Nonlinear observer design I

The observer design problem can be considered to be the dual problem of controller design. Exact linearization up to an output injection as technique for observer design is introduced in literature [Keller 1987].

By using a state transformation $\mathbf{t}_2(\mathbf{x})$ (7.21) the nonlinear system is transformed into a system (7.22) consisting of a linear part and a nonlinear part $\gamma(y, u)$, which is only function of the measured output y and possibly the input u. Actually in the work of [Keller 1987], a larger class of transformations is used. This is further discussed in Section 7.3.5.

The system matrix $\mathbf{A_O}$ is in observability form (Appendix C) while the output of the system y and the state w_n are related by a nonlinear function. Notice that the use of this canonical form does not limit the generality of the approach, because every observable linear system can be transformed into this form.

$$\mathbf{w} = \mathbf{t}_2(\mathbf{x}) \quad ; \quad w_n = c(y) \tag{7.21}$$

$$\frac{d\mathbf{w}}{dt} = \mathbf{A_O} \cdot \mathbf{w} + \gamma(y, u) \tag{7.22}$$

An observer can then be constructed consisting of a copy of the system and a correction term, proportional with the error between the estimate $\widehat{w_n}$ and the measurement of the last state, which is a nonlinear function of the actual output of the system y. $\mathbf{k}$ is the gain vector. Note that the estimates of the states are denoted $\widehat{\mathbf{w}}$.

$$\frac{d\widehat{\mathbf{w}}}{dt} = \mathbf{A_O} \cdot \widehat{\mathbf{w}} + \gamma(y, u) + \mathbf{k} \cdot (c(y) - \widehat{w_n}) \tag{7.23}$$

The behavior of this observer can easily be understood when the dynamics of the error $\mathbf{e}_w = \mathbf{w} - \widehat{\mathbf{w}}$ between the actual state $\mathbf{w}$ and the estimates of the state $\widehat{\mathbf{w}}$ is studied. The error dynamics is described by a linear model. The eigenvalues can be assigned by a proper choice of the elements of the gain vector $\mathbf{k}^T(k_n, \ldots, k_1)$. Notice that $\mathbf{b}_n$ is a vector with zero entries, except for the last element equal to one.

$$\frac{d\mathbf{e}_w}{dt} = (\mathbf{A_O} - \mathbf{k}\mathbf{b}_n^T) \cdot \mathbf{e}_w \tag{7.24}$$

Due to the special structure of the dynamics of the error system an easy procedure for determining the tuning parameters k_i is possible. Suppose that the eigenvalues of the error system must be given by the characteristic equation (7.25), then the tuning parameters are the coefficients of this polynomial.

$$\lambda^n + k_n\lambda^{n-1} + k_{n-1}\lambda^{n-2} + \ldots + k_1 = 0 \tag{7.25}$$

7.3.4 Nonlinear separation principle I

When the feedback linearization method for controller design and the exact linearization up to an output injection for observer design, is applicable, the question arises whether the combination of both algorithms will still converge.

In the sequal the dynamics of the control and estimation error for a combined observer-controller are derived.

The combination of the system, controller and observer can be described in different coordinate systems. The **x**-coordinate system is the physical domain. The **z**-coordinate system is the canonical space, useful for controller design while the **w**-space is the canonical space, useful for observer design. These spaces are related through the transformations $\mathbf{t}_1$ and $\mathbf{t}_2$ introduced earlier. The following definitions are introduced. Notice that these definitions are given in the three different coordinate systems.

Designed states x,w,z. These are the states that would be obtained when the feedback linearizing controller is applied with full knowledge of the state.

Estimated states $\widehat{\mathbf{x}},\widehat{\mathbf{w}},\widehat{\mathbf{z}}$. These are the estimates of the states of the system obtained with the observer, based on exact linearization up to an output injection.

Obtained states $\widetilde{\mathbf{x}},\widetilde{\mathbf{w}},\widetilde{\mathbf{z}}$. These are the states obtained by applying the feedback linearizing controller in combination with the observer.

When the feedback linearizing controller is applied to the system (described in the z-coordinate system) in combination with the observer, the following behavior is obtained.

$$\begin{aligned} \frac{d\widetilde{\mathbf{z}}}{dt} &= \mathbf{A_C}\cdot\widetilde{\mathbf{z}} + \mathbf{b}_n\mathbf{p}^T\cdot\widehat{\mathbf{z}} + \mathbf{b}_n\cdot v_{ref} \\ v &= \mathbf{p}^T\cdot\widehat{\mathbf{z}} + v_{ref} \end{aligned} \tag{7.26}$$

For the error $\mathbf{e}_w = \widetilde{\mathbf{w}} - \widehat{\mathbf{w}}$ between the estimated state and the obtained state (both described in the w-coordinate system), the observer convergence property is still valid.

$$\frac{d\mathbf{e}_w}{dt} = (\mathbf{A_O} - \mathbf{k}\mathbf{b}_n^T)\cdot\mathbf{e}_w \tag{7.27}$$

Now it is shown that the error $\mathbf{e}_z = \widetilde{\mathbf{z}} - \mathbf{z}$ between the obtained state and the designed state is converging to zero, or after some transient the combination of the controller and the observer will still provide the desired, designed behavior of the system. Recall that $\mathbf{t}_1$ and $\mathbf{t}_2$ are the transformations from the x-domain to the z-domain (used in the controller design), w-domain (used in the observer design) respectively. A new transformation $\mathbf{t}$ from the w-domain to the z-domain can now be defined for the (designed, obtained and estimated) states.

$$\begin{aligned} \mathbf{z} &= \mathbf{t}_1(\mathbf{x}) = \mathbf{t}_1(\mathbf{t}_2^{-1}(\mathbf{w})) = \mathbf{t}(\mathbf{w}) \\ \widehat{\mathbf{z}} &= \mathbf{t}_1(\widehat{\mathbf{x}}) = \mathbf{t}_1(\mathbf{t}_2^{-1}(\widehat{\mathbf{w}})) = \mathbf{t}(\widehat{\mathbf{w}}) \\ \widetilde{\mathbf{z}} &= \mathbf{t}_1(\widetilde{\mathbf{x}}) = \mathbf{t}_1(\mathbf{t}_2^{-1}(\widetilde{\mathbf{w}})) = \mathbf{t}(\widetilde{\mathbf{w}}) \end{aligned} \tag{7.28}$$

The dynamics of the error $\mathbf{e}_z$ can be described by using the dynamics of the designed system (7.19) and the obtained system (7.26). Notice that the dynamics of the observer error are not altered by combining the observer and the controller. $\mathbf{e}_{cw} = \widetilde{\mathbf{w}} - \mathbf{w}$ is the control error, described in the w-coordinate system.

$$\begin{aligned} &\frac{d\mathbf{e}_z}{dt} = \mathbf{A_C}\cdot\mathbf{e}_z + \mathbf{b}_n\mathbf{p}^T\cdot(\widehat{\mathbf{z}}-\mathbf{z}) = \mathbf{A_C}\cdot\mathbf{e}_z + \mathbf{b}_n\mathbf{p}^T\cdot(\widehat{\mathbf{z}}+\mathbf{e}_z-\widetilde{\mathbf{z}}) \\ &= (\mathbf{A_C}+\mathbf{b}_n\mathbf{p}^T)\cdot\mathbf{e}_z + \mathbf{b}_n\mathbf{p}^T\cdot(\mathbf{t}(\widehat{\mathbf{w}}) - \mathbf{t}(\widehat{\mathbf{w}}+\mathbf{e}_w)) \\ &= (\mathbf{A_C}+\mathbf{b}_n\mathbf{p}^T)\cdot\mathbf{e}_z + \mathbf{b}_n\mathbf{p}^T\cdot(\mathbf{t}(\mathbf{w}+\mathbf{e}_{cw}-\mathbf{e}_w) - \mathbf{t}(\mathbf{w}+\mathbf{e}_{cw})) \\ &= (\mathbf{A_C}+\mathbf{b}_n\mathbf{p}^T)\cdot\mathbf{e}_z + \mathbf{b}_n\mathbf{p}^T\cdot(\mathbf{t}(\mathbf{w}+\mathbf{t}_{\mathbf{w}}^{-1}(\mathbf{e}_z)-\mathbf{e}_w) - \mathbf{t}(\mathbf{w}+\mathbf{t}_{\mathbf{w}}{}^{-1}(\mathbf{e}_z))) \\ &\frac{d\mathbf{e}_w}{dt} = (\mathbf{A_O}-\mathbf{k}\mathbf{b}_n^T)\cdot\mathbf{e}_w \end{aligned} \tag{7.29}$$

$$\mathbf{e}_z = \mathbf{t}_{\mathbf{w}}(\mathbf{e}_{cw}) = \mathbf{t}(\mathbf{w}+\mathbf{e}_{cw}) - \mathbf{t}(\mathbf{w}) \tag{7.30}$$

It can be concluded that the dynamics of the control and estimation error are given by the following equations.

$$\begin{aligned} \frac{d\mathbf{r}}{dt} &= \mathbf{A_r}\cdot\mathbf{r} + \delta(\mathbf{m}(t),\mathbf{r},\mathbf{s}) \\ \frac{d\mathbf{s}}{dt} &= \mathbf{A_S}\cdot\mathbf{s} \\ \delta(\mathbf{m}(t),\mathbf{r},0) &= 0 \end{aligned} \tag{7.31}$$

The vectors s, r represents the estimation and control error $\mathbf{e}_w$, $\mathbf{e}_z$ respectively. $\mathbf{m}(t)(=\mathbf{w}(t))$ represents the designed system dynamics. The matrices $\mathbf{A_r}$, $\mathbf{A_S}$ are stable matrices by design and represent the dynamics of the controller and observer respectively. The second equation is a stable linear equation. The estimation error s will converge to zero. The first equation can be considered as a linear equation plus a nonlinear time-varying disturbance δ, depending on an external signal $\mathbf{m}(t)$ (related to the designed system behavior and behaving properly), $\mathbf{r}(t)$ the control error and $\mathbf{s}(t)$ the estimation error. The disturbance $\delta(\mathbf{m}(t),\mathbf{r},\mathbf{s})$ is zero when the estimation error $\mathbf{s}(t)$ becomes zero.

$$\delta(\mathbf{m}(t),\mathbf{r},\mathbf{s}) = \mathbf{p}^T\cdot(\mathbf{t}(\mathbf{m}(t)+\mathbf{t}_{\mathbf{m}(t)}^{-1}(\mathbf{r})-\mathbf{s}) - \mathbf{t}(\mathbf{m}(t)+\mathbf{t}^{-1}(\mathbf{r}))) \tag{7.32}$$

The special structure of the error system can be exploited in the analysis of the local stability for instance with Lyapunov stability theory.

Consider the following Lyapunov function $v_L(\mathbf{r},\mathbf{s})$.

$$v_L(\mathbf{r},\mathbf{s}) = \mathbf{r}^T\mathbf{P_r}\mathbf{r} + \mathbf{s}^T\mathbf{P_S}\mathbf{s} \tag{7.33}$$

When the time derivative of the function v_L is calculated the following result is found with $\mathbf{Q_r}$ and $\mathbf{Q_S}$ two positive definite functions, solutions of the two Lyapunov equations (7.35), (7.36).

$$\frac{dv_L}{dt} = -\mathbf{r}^T\mathbf{Q_r}\mathbf{r} - \mathbf{s}^T\mathbf{Q_S}\mathbf{s} + \mathbf{r}^T(\mathbf{P_r}+\mathbf{P_r}^T)\delta(\mathbf{m}(t),\mathbf{r},\mathbf{s}) \tag{7.34}$$

$$\mathbf{P_r}\mathbf{A_r} + \mathbf{A_r}\mathbf{P_r} = -\mathbf{Q_r} \tag{7.35}$$

$$\mathbf{P_S}\mathbf{A_S} + \mathbf{A_S}\mathbf{P_S} = -\mathbf{Q_S} \tag{7.36}$$

It is found that the local approximation around the origin of the function $h(\mathbf{r},\mathbf{s})$ (7.37), has the structure (7.38).

$$h(\mathbf{r},\mathbf{s}) = \mathbf{r}^T(\mathbf{P_r}+\mathbf{P_r}^T)\delta(\mathbf{m}(t),\mathbf{r},\mathbf{s}) = \delta^T(\mathbf{m}(t),\mathbf{r},\mathbf{s})(\mathbf{P_r}+\mathbf{P_r}^T)\mathbf{r}^T \tag{7.37}$$

$$\begin{aligned} h(\mathbf{r},\mathbf{s}) &\approx \mathbf{r}^T\mathbf{V}(\mathbf{P_r},\delta)\mathbf{s} \\ \mathbf{V}(\mathbf{P_r},\delta) &= (\mathbf{P_r}+\mathbf{P_r}^T)\left(\frac{\partial\delta(\mathbf{m}(t),\mathbf{r},\mathbf{s})}{\partial\mathbf{s}}\right)_{(\mathbf{0},\mathbf{0})} \end{aligned} \tag{7.38}$$

The time derivative of the Lyapunov function v_L around the origin can then be approximated as follows.

$$\frac{dv_L}{dt} = \begin{pmatrix} \mathbf{r}^T \mathbf{s}^T \end{pmatrix} \cdot \mathbf{L} \cdot \begin{pmatrix} \mathbf{r} \\ \mathbf{s} \end{pmatrix} \tag{7.39}$$

$$\mathbf{L} = \begin{pmatrix} -\mathbf{Q_r} & (\mathbf{P_r} + \mathbf{P_r}^T)(\frac{\partial \delta(\mathbf{m}(t), \mathbf{r}, \mathbf{s})}{\partial \mathbf{s}})_{(0,0)} \\ 0 & -\mathbf{Q_s} \end{pmatrix} \tag{7.40}$$

From the derivation above one can conclude that local asymptotic stability of the combined observer-controller is obtained when the matrix $\mathbf{L}$ is negative definite. This condition can easily be evaluated.

7.3.5 Nonlinear observer design II

An extended observer design technique, compared to the method introduced in Section 7.3.3 [Isidori 1989, Marino and Tomei 1995], is presented by [Keller 1987]. This method is applicable to a larger class of systems.

The original system is now transformed to the observer canonical form (7.42) by a transformation (7.41). $u^{(i)}$ denotes the i^{th} order time derivative of u.

$$\mathbf{w} = \mathbf{t_2}(\mathbf{x}, u, \ldots, u^{(n-1)}) \tag{7.41}$$

$$\frac{d\mathbf{w}}{dt} = \mathbf{A_O} \cdot \mathbf{w} + \gamma(y, u, \ldots, u^{(n)}) \quad ; \quad w_n = c(y, u) \tag{7.42}$$

The observer design is unchanged. The main difference is the use of input dependent transformations, resulting in problems in combined observer-controller design.

Notice that differentiability of the input u is assumed. When a feedback control strategy is used, this assumption is fulfilled.

7.3.6 Nonlinear separation principle II

The combination of the controller, based on input-state linearization and the observer, based on exact linearization up to an output injection and using input dependent transformations, results in some specific problems, such that extra conditions must be imposed.

For a n-dimensional system it can be shown that the observer system can formally be written as follows.

$$\frac{d\widehat{\mathbf{x}}}{dt} = \mathbf{v}(\widehat{\mathbf{x}}, y, u, u^{(1)}, u^{(2)}, \ldots, u^{(n)}) \quad ; \quad y = h(\mathbf{x}) \tag{7.43}$$

Note that the observer system is function of the input u and its time derivatives up to order n. The input is given by the feedback controller and is

function of the estimate of the state, provided by the observer, which is dependent on the input and its derivatives. It is this dependency that causes an existence problem. Notice that the convergence property of the observer is independent of the inputs.

The existence problem is made clear as follows. Let γ_1 be the feedback controller. The following definitions are introduced.

$$\begin{aligned}
u^{(0)} &= \gamma_1(\widehat{\mathbf{x}}) \\
u^{(1)} &= \gamma_2(\widehat{\mathbf{x}}, y, u^{(0)}, u^{(1)}, u^{(2)}, \ldots, u^{(n)}) \\
u^{(2)} &= \gamma_3(\widehat{\mathbf{x}}, y, u^{(0)}, u^{(1)}, u^{(2)}, \ldots, u^{(n)}, u^{(n+1)}) \\
&\ldots \\
u^{(j-1)} &= \gamma_j(\widehat{\mathbf{x}}, y, u^{(0)}, u^{(1)}, u^{(2)}, u^{(3)}, \ldots, u^{(n)}, \ldots, u^{(n+j-2)}) \\
u^{(j)} &= \gamma_{j+1}(\widehat{\mathbf{x}}, y, u^{(0)}, u^{(1)}, u^{(2)}, u^{(3)}, \ldots, u^{(n)}, \ldots, u^{(n+j-1)})
\end{aligned} \tag{7.44}$$

Observe that the dependence of the m^{th}-order derivative of the input on the time derivative of the input up to order $(m+n-1)$ causes the problem. A condition, enabling the implementation of the combination of the extended observer and feedback controller, is that this chain must end for a finite m.

> The combination of the extended observer with a feedback controller is possible if and only if there exists a finite j such that γ_j is independent of $u^{(j)}, \ldots, u^{(n+j-2)}$.

Notice that (n-1) conditions must be fulfilled for an n-dimensional system, which causes severe restrictions on the practical applicability of the combined observer-controller.

7.3.7 Application

The combination of the extended observer design method and feedback controller design, based on input-state feedback linearization, is now illustrated for the biotechnological prototype system.

The control objective is to keep the substrate concentration at a setpoint C_S^*. Only on-line biomass measurements are available.

First the input-state linearizing controller design method is illustrated shortly. Second, the extended observer design method based on exact linearization up to an output injection is applied on the prototype model. Finally some comments on the combined observer-controller are given.

Input-state linearizing controller

The input-state linearizing controller, discussed in Section 7.2.2, is slightly modified such that the dynamics of the error system fits the formalism used in Section 7.3.2.

The following linear design procedure can now be used. Let E_1 and E_2 respectively be the error between the actual states Z_1, Z_2 and the designed

states $Z_1^\star$, $Z_2^\star$. The required states are on the manifold, defined by the control objective. The dynamics of the states $Z_1^\star$ and $Z_2^\star$ is given by the Brunovsky canonical form with as input V_{ref}. The (linear) dynamics of the error system is then given as follows:

$$\begin{array}{rcl} \frac{dE_1}{dt} & = & E_2 \\ \frac{dE_2}{dt} & = & V - V_{ref} \;=\; p_1E_1 + p_2E_2 \end{array} \tag{7.45}$$

With the following choice of $p_1 = -\lambda_c^2$ and $p_2 = 2\lambda_c$ an eigenvalue λ_c with a double multiplicity is obtained. The obtained control law V has then the following form:

$$V \;=\; p_1Z_1 + p_2Z_2 + V_{ref} - p_1Z_1^\star - p_2Z_2^\star \tag{7.46}$$

Notice that the only feasible equilibruim point for the designed states is $Z_1^\star = -A^{-1}\cdot B$ and $Z_2^\star = 0$. The stability of the dynamics of the designed states $Z_1^\star$, $Z_2^\star$ along the manifold is trivial from the dynamic equations.

Nonlinear observer design

In [Keller 1987] a nonlinear observer design technique using input derivatives and output transformations is presented. Recall that this observer design method and the related canonical forms are described in Chapter 5. In that chapter it is assumed that the input U is constant. The design consists of two steps. In the first step the system is transformed into the so-called generalized observability canonical form (GOBCF) system by the transformation (7.47). The state C_X is on-line measured and is considered as the output of the system Y.

$$Z_1 \;=\; C_X \quad ; \quad Z_2 \;=\; aC_XC_S - UC_X \tag{7.47}$$

With this state diffeomorphism the following nonlinear system is obtained.

$$\begin{array}{rcl} \frac{dZ_1}{dt} & = & Z_2 \\ \frac{dZ_2}{dt} & = & -(b_2Z_2^2 + b_1Z_2 + b_o) \\ b_2(Y) & = & -\frac{1}{Y} \\ b_1(Y,U) & = & -bY + U \\ b_o(Y,U,U^{(1)}) & = & -bY^2U + U^2Y - aUYC_{S,in} + YU^{(1)} \end{array} \tag{7.48}$$

Notice that in the canonical form the first order time derivative $U^{(1)}$ of the input U appears. The right-hand side of the dynamical equation of Z_2 is written as a polynomial in Z_2. The fact that this term can be written as a polynomial is a necessary and sufficient condition for the existence of a

transformation, which transforms the original system into the generalized observer canonical form (GOCF). This form is linear up to an output injection. The canonical form, described by the state $\mathbf{w}$, is obtained by solving partial differential equations. The first partial differential equation (7.49) determines the relation $c(y,u)$ (7.50) between the state W_2 and the output Y and possibly the input U. c_1 and c_2 are undetermined functions of the input U.

$$\frac{\partial^2 c(Y,U)}{\partial Y^2} \;=\; -\frac{1}{Y}\frac{\partial c(Y,U)}{\partial Y} \tag{7.49}$$

$$c(U,Y) \;=\; c_1(U)\ln(Y) + c_2(U) \tag{7.50}$$

The solution of the second partial differential equation (7.51) results in a nonlinear function of the output Y. The dynamics of W_2 is equal to W_1 minus this nonlinear function. c_3 is an undetermined function of the input U and its first derivative $U^{(1)}$.

$$\frac{\partial a_1(Y,U,U^{(1)})}{\partial Y} \;=\; (-bY + U)c_1(U)\frac{1}{Y} - 2\frac{\partial c_1(U)}{\partial U}\frac{1}{Y}U^{(1)} \tag{7.51}$$

$$a_1(Y,U,U^{(1)}) \;=\; c_1(U)(-bY + U\ln(Y)) - 2\frac{\partial c_1(U)}{\partial U}U^{(1)}\ln(Y) + c_3(U,U^{(1)}) \tag{7.52}$$

The last Equation (7.53) is a direct expression for the function a_o, which equals minus the right-hand side of the dynamic equation of W_1.

$$\begin{array}{rcl} a_o(Y,U,U^{(1)},U^{(2)}) & = & (-bY^2U + U^2Y - aUYC_{S,in} + YU^{(1)})\frac{1}{Y} + \\ & & (-\frac{\partial c_1(U)}{\partial U}\ln(Y) - \frac{\partial c_2(U)}{\partial U} + 2\frac{\partial c_1(U)}{\partial U}\ln(Y))\cdot U^{(2)} \\ & & -\frac{\partial c_3(U,U^{(1)})}{\partial U^{(1)}}U^{(2)} - \frac{\partial c_1(U)}{\partial U}(-bY + U\ln(Y))U^{(1)} - \\ & & c_1(U)\ln(Y)U^{(1)} + (2\frac{\partial^2 c_1(U)}{\partial U^2}\ln(Y) + \frac{\partial^2 c_2(U)}{\partial U^2})\cdot U^{(1)^2} \\ & & (-\frac{\partial^2 c_1(U)}{\partial U^2}\ln(Y)U^{(1)} - \frac{\partial c_3(U,U^{(1)})}{\partial U})\cdot U^{(1)} \end{array} \tag{7.53}$$

With the following choice of the functions $c_1(U) = 1$, $c_2(U) = 0$ and $c_3(U,U^{(1)}) = U$, the functions $c(Y,U)$, $a_o(Y,U,U^{(1)},U^{(2)})$ and $a_1(Y,U,U^{(1)})$ can be determined explicitly.

$$\begin{array}{rcl} c(U,Y) & = & \ln(Y) \\ a_1(Y,U,U^{(1)}) & = & -bY + U\ln(Y) + U \\ a_o(Y,U,U^{(1)},U^{(2)}) & = & -bYU + U^2 - aUC_{S,in} - \ln(Y)U^{(1)} \end{array} \tag{7.54}$$

The state diffeomorphism between the original coordinate system and the observer coordinates can now be calculated with the relations (7.55).

$$\begin{array}{rcccl} W_2 & = & c(Y,U) & = & \ln(C_X) \\ W_1 & = & \frac{\partial c(Y,U)}{\partial Y} + a_1(Y,U,U^{(1)}) & = & aC_S - bC_X + U\ln(C_X) \end{array} \tag{7.55}$$

The system in observer coordinates is given by a dynamical model, which is linear in the state W_1, W_2 and contains a nonlinear known function of the output Y. The observer consists of a copy of the system (written in observer coordinates) and a correction term, proportional with the error between the estimated state $\widehat{W_2}$ and the measured state W_2, which is a nonlinear function of the output Y. k_1 and k_2 are tuning parameters of the observer.

$$\begin{aligned} \frac{d\widehat{W_1}}{dt} &= bUY + aUC_{S,in} - U^2 + \ln(Y)U^{(1)} + k_1(W_2 - \widehat{W_2}) \\ \frac{d\widehat{W_2}}{dt} &= \widehat{W_1} + bY - U\ln(Y) - U + k_2(W_2 - \widehat{W_2}) \end{aligned} \tag{7.56}$$

The tuning of the observer results now in a linear problem. When the following tuning parameters are used $k_1 = \lambda_o^2$ and $k_2 = -2\lambda_o$ the eigendynamics of the error system is stable with a (negative) eigenvalue of double multiplicity λ_o. By using the inverse transformation from **w**-coordinates to **x**-coordinates the observer system can be described in the original coordinates as follows.

$$\begin{aligned} \frac{d\widehat{C_X}}{dt} &= a\widehat{C_X}\widehat{C_S} - \widehat{C_X}U + l_1(Y,\widehat{C_X}) \\ \frac{d\widehat{C_S}}{dt} &= b\widehat{C_X}\widehat{C_S} - \widehat{C_S}U + C_{S,in}U + l_2(Y,\widehat{C_X}) \end{aligned} \tag{7.57}$$

$$\begin{aligned} l_1(Y,\widehat{C_X}) &= m_1(\widehat{C_X})\cdot(\ln(\widehat{C_X}) - \ln(Y)) + m_2(\widehat{C_X})\cdot(\widehat{C_X} - Y) \\ l_2(Y,\widehat{C_X}) &= m_3(\widehat{C_X})\cdot(\ln(\widehat{C_X}) - \ln(Y)) + m_4(\widehat{C_X})\cdot(\widehat{C_X} - Y) \end{aligned} \tag{7.58}$$

$$\begin{aligned} m_1(\widehat{C_X}) &= (k_2 + U)\cdot\widehat{C_X} \\ m_2(\widehat{C_X}) &= -b\cdot\widehat{C_X} \\ m_3(\widehat{C_X}) &= \frac{1}{a}(k_1 - U^{(1)} + bU\widehat{C_X} + b\widehat{C_X}k_2 - Uk_2 - U^2) \\ m_4(\widehat{C_X}) &= -\frac{b^2}{a}\widehat{C_X} \end{aligned} \tag{7.59}$$

Recall that here the observer design method is presented in a differential algebraic framework while in Appendix C the same observer design method is reformulated in the differential geometric framework.

Combined observer-controller

Both the stability and occurence of existance problems are evaluated. The matrices $\mathbf{A_r}$ and $\mathbf{A_s}$ describe the controller and observer dynamics respectively. The tuning parameters λ_c and λ_o represent the convergence rate of

the controller and the observer.

$$\mathbf{A_r} = \begin{pmatrix} 0 & 1 \\ -\lambda_c^2 & 2\lambda_c \end{pmatrix} \; ; \; \mathbf{A_s} = \begin{pmatrix} 0 & -\lambda_o^2 \\ 1 & 2\lambda_o \end{pmatrix} \tag{7.60}$$

With the diagonal positive definite matrices $\mathbf{P_r}$ and $\mathbf{P_s}$ (7.61), the positive definite matrices $\mathbf{Q_r}$ and $\mathbf{Q_s}$ (7.62) are obtained with q_1 and q_2 positive parameters.

$$\mathbf{P_r} = \begin{pmatrix} q_1 & 0 \\ 0 & q_1 \end{pmatrix} \; ; \; \mathbf{P_s} = \begin{pmatrix} q_2 & 0 \\ 0 & q_2 \end{pmatrix} \tag{7.61}$$

$$\mathbf{Q_r} = -2q_1\mathbf{A_r} \; ; \; \mathbf{Q_s} = -2q_2\mathbf{A_s} \tag{7.62}$$

The stability of the combined observer-controller algorithm can be evaluated by analysis of the negative definiteness of the matrix (7.40). When the eigenvalues of the observer and controller are respectively -10 and -5 with double multiplicity and q_1, q_2 equal 5, the eigenvalues of the matrix (7.40) are -50 and -100 with double multiplicity.

For the prototype model no existence problems occur when the observer based on exact linearization up to an output injection is combined with a feedback controller because the observer equations are only depending on the first order time derivative of the input U. The conditions of Section 7.3.6 are thus satisfied for j equal two.

7.3.8 Conclusions

The main conclusion of Section 7.3 is that the error system, resulting from combining a nonlinear observer based on exact linearization up to an output injection and a feedback linearizing controller, has a special structure, which can be exploited for analysis, for instance the study of the trade-off between noise sensitivity and extension of the convergence area. As such an alternative for the high-gain observer approach often used in literature is found [Atassi and Khalil 1997].

When observers using derivatives of the input signal are used, some extra technical conditions must be fulfilled in order to avoid existence problems.

7.4 Optimal tuning of nonlinear controllers

7.4.1 Problem statement

After selection of an appropriate nonlinear controller design methodology, possibly after a performance analysis, the optimal tuning parameters of the controller must be determined.

Two approaches, that can be used in tuning of nonlinear controllers, are (i) *performance analysis* and (ii) *trade-off analysis* [Bastin and Dochain

1990]. Performance and trade-off analysis are illustrated for tuning of a nonlinear input-output linearizing controller. Recall that a more detailed discussion can be found in Chapter 6.

The optimal tuning of the controller is illustrated for setpoint control of the substrate concentration in a fed-batch fermentation process.

The influent flow rate F [L/h] keeping the substrate concentration constant can easily be found by setting the time derivative of the substrate concentration equal to zero. Application of the resulting control law results in a feedforward control strategy. When the substrate concentration deviates from the substrate concentration, then the control law will not compensate for this. This problem is circumvented by adding a feedback part to the control law. When the input-output controller design method of Section 7.2.2 is used, the following controller is obtained.

$$\frac{F}{V} = \frac{\sigma C_X}{C_{S,in} - C_S} - \lambda_c \frac{C_S - C_S^*}{C_{S,in} - C_S} \tag{7.63}$$

The selection of the tuning parameter λ_c is now discussed. Both performance analysis (Section 7.4.2) and trade-off analysis (Section 7.4.3) with the objective function are presented as tools for optimal tuning. In Section 7.4.4 the tuning problem is illustrated with simulations.

7.4.2 Performance analysis

Convergence. The convergence analysis is trivial. The tuning parameter λ_c is equal to the convergence speed by design.

Discretisation. Because the biomass and substrate concentration are not *on-line* available, the control law can only be updated at the time instants where new measurements become available. These measurements can be direct measurements or obtained via a state estimator. Discretization effects are difficult to analyze. Although the control law is updated at discrete time instances, it is still applied on a real continuous process, described with a continuous model. An exact analysis results in the study of mixed discrete-continuous systems. An approximate approach is to analyze the dynamics of the linear error model (7.1). When this model is discretized via a forward Euler approximation, it is found that the maximal allowable discretization time T_{max} is inversely proportional with the tuning parameter λ_c.

$$T_{max} \leq \frac{2}{\lambda_c} \tag{7.64}$$

Noise sensitivity. Due to noise on both the substrate and the biomass concentration (obtained via direct measurements or via a state observer), one must analyze how sensitive the control law is with respect to this noise. An indication of this sensitivity is given by evaluating the derivative of the control law with respect to the substrate and biomass concentration. These

derivatives can be used as instantaneous noise sensitivity functions. It is assumed that there is no noise on the volume measurement.

$$\begin{aligned} \mathcal{R}^I_{C_X} &= \frac{\partial F}{\partial C_X} = \frac{\sigma}{C_{S,in} - C_S} V \\ \mathcal{R}^I_{C_S} &= \frac{\partial F}{\partial C_S} = \frac{(C_{S,in} - C_S)\sigma^S C_X + \lambda_c (C_S^* - C_{S,in}) + \sigma C_X}{(C_{S,in} - C_S)^2} V \end{aligned} \tag{7.65}$$

From this analysis one can observe that the noise sensitivity is inversely proportional with the difference between the substrate concentration and the substrate concentration in the input stream. This suggests that working on a low substrate concentration level is beneficial when noise sensitivity is considered. The sensitivity function of the substrate concentration is a function linear in the tuning parameter λ_c. Due to the fact that here a mixed discrete-continuous system is under consideration, the discretization and noise sensitivity analysis is only indicative. More detailed analysis would lead to an increase in complexity. Nevertheless the performance analysis indicates how the maximal allowable discretization time is dependent on the tuning parameter and the influence of the process conditions on the noise sensitivity is revealed.

7.4.3 Trade-off analysis

In trade-off analysis the optimal value of the tuning parameter λ_c is obtained by optimization of an objective function, indicating the goal of the nonlinear linearizing controller. The objective is to keep the substrate concentration at a constant optimal setpoint. The objective function is the integral of the norm of the deviation of the substrate concentration from the setpoint. p is an extra degree of freedom for the process engineer. T_r is the reference time considered in the analysis.

$$\lambda_c^* = \arg\min_{\lambda_c} \left(\int_0^{T_r} \mid C_S(t) - C_S^* \mid^p dt \right) \tag{7.66}$$

In the objective function two contributions can be considered. The first contribution is due to the transient behavior of the closed loop system while the second contribution results from the noise on the measurements.

Transient behavior of the controlled system. It is clear from the design procedure of the nonlinear linearizing controller that the dynamics of the control error (substrate concentration minus substrate concentration setpoint) is given by a linear system. $C_S(0)$ is the initial substrate concentration. It is found that the contribution of the initial error is inversely proportional with the tuning parameter λ_c.

$$\int_0^\infty \mid C_S(t) - C_S^* \mid dt = \mid C_S(0) - C_S^* \mid \frac{1}{\lambda_c} \tag{7.67}$$

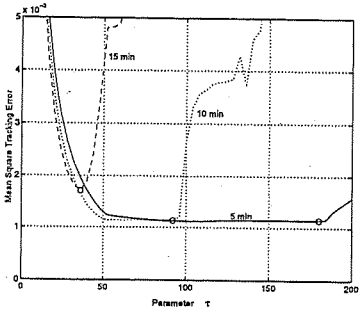


Figure 7.5: Optimal tuning of the substrate concentration setpoint controller with trade-off analysis. Transient behavior versus discretization errors. The mean square deviation of the substrate concentration from the setpoint as function of the tuning parameter λ_c for various values of the sampling time.

Noise sensitivity of the controller. Due to noise on both the substrate and biomass measurements a deviation from the control objective will appear. In the performance analysis the noise sensitivity of the control law itself is presented. The effects on the objective function are however difficult to determine.

Although it is difficult to indicate how the objective function is related to the tuning parameter λ_c, this is not a problem while using the trade-off analysis, because it does not rely on analytical expressions. When this method is used for determining the optimal tuning parameter a simulation is performed for various values of the tuning parameter. The tuning parameter, which optimizes the objective function, is selected.

7.4.4 Simulations

Simulations are made for a substrate concentration setpoint $C_{S,in} = 2$ [g/L]. In Figure 7.5 the integral of the squared error ($p = 2$) is shown as function of the tuning parameter λ_c for 3 different discretization times. It is assumed that the measurements of the biomass and substrate concentration are noise free. The figure indicates that an upperbound on the tuning parameter λ_c exist. Above this upperbound the error is increasing rapidly. The larger the discretization time, the lower the upperbound on λ_c is. This confirms qualitatively the result stated in the performance analysis. In Figure 7.6 the objective function is shown as function of the tuning parameter for two noise levels. A Gaussian noise is applied. The noise can here be quantified with its standard deviation. Recall that here both noise on the substrate

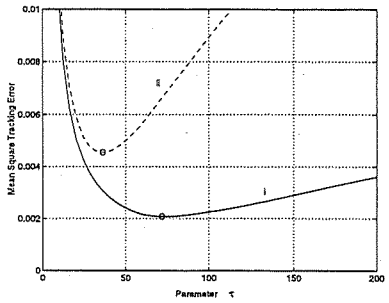


Figure 7.6: Optimal tuning of the substrate concentration setpoint controller with trade-off analysis. Transient behavior versus noise sensitivity. The mean square deviation of the substrate concentration from the setpoint as function of the tuning parameter λ_c for two noise levels and small sampling time.

measurements and the biomass measurements is assumed. For the noise on the biomass measurements the standard deviation is $0.05C_X$ for the first noise level. Notice that here the norm of the noise signal is function of the biomass concentration. For the second noise level is the standard deviation doubled. For the noise on the substrate concentration measurements the standard deviation is 0.1 for noise level one and doubled for the second noise level. To avoid discretization effects a discretization time of 0.5 minutes is used. In the figure it is clear that the noise contribution increases with larger values of λ_c. The optimal value of the tuning parameter λ_c depends on the noise level used during the simulation. Figure 7.7 shows the objective function for three different discretization times. Noise level one is used here. This figure shows the trade-off between the transient behavior and the noise sensitivity and includes discretization effects.

7.4.5 Conclusions

The tuning of an input-output linearizing controller is studied. Performance analysis reveals only a small set of relations between the process conditions, the tuning parameter and the performance measures. Nevertheless with these relations important insight in the tuning problem is gained. This insight can be used in the setup of the simulations, used in trade-off analysis. Trade-off analysis is found to be an easy applicable tool for tuning.

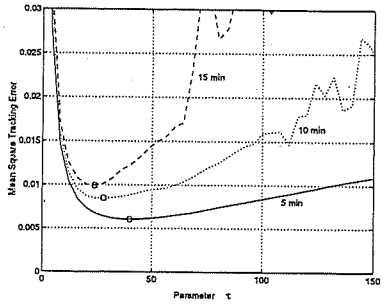


Figure 7.7: Optimal tuning of the substrate concentration setpoint controller with trade-off analysis. Transient behavior versus noise sensitivity and discretization effects. The mean square deviation of the substrate concentration from the setpoint as function of the tuning parameter λ_c for various values of the sampling time and noise level 1.

7.5 General conclusions

The robustness of an input-output and input-state linearizing controller is compared for a prototype model for bioprocesses. *Robustness analysis tools*, explicitly relating the uncertainty and the resulting performance, are introduced. Performance analysis serves as an alternative method for the dynamical simulations often presented in literature. Similar analysis tools are introduced in Chapter 5 for nonlinear observers.

Although the results of performance analysis are depending on the application under consideration, from the case study one can conclude that linearization techniques can have excellent robustness. These techniques should not be rejected a priori but evaluated for each case separately. The linearization methods can also be used as starting point for other more robust techniques [Sepulchre *et al.* 1996].

The combination of observers, based on exact linearization up to an output injection, and an input-state linearizing controller, is studied. It is shown that the error system of the combined observer-controller system has a special structure. Local asymptotic stability can be determined easily. When time derivatives of the input appear in the observer, existence problems can appear. The conditions, for which the combined observer-controller is feasible, are derived. This is illustrated for the biological prototype model.

The advantages and disadvantages of *performance* and *trade-off analysis*, introduced in Chapter 6, are compared for tuning of an input-output linearizing controller. It is found that the (limited) performance analysis reveals still important insight in the tuning problem. Trade-off analysis is

shown to be an easily applicable tool for tuning.

- *The global convergence property and acceptable robustness against model uncertainty of the exact linearization based controllers motivates their use for bioprocess control. The restricted applicability of this type of design methodology is a motivation for using low complexity models. The analysis of the combined observer-controller algorithm shows that separate design of the observer-controller is feasible (divide et impera strategy) although some technical conditions must be verified.*
  Although simple models are used, important insight in the tuning problem can be obtained.

Chapter 8

Conclusions

8.1 Overview of the contributions

In this thesis the applicability of *model based optimization and control techniques* to *bioprocesses* is analyzed. It is demonstrated that the decomposition of the model based approach in four subproblems (Modeling, Optimization, Monitoring and Control), reflected in the structure of the thesis, results in a feasible approach.

Modeling. Models are basic ingredients for (i) detailed analysis (e.g. dynamic and sensitivity analysis) of the bioprocess operation under consideration, (ii) (re-)design of the plant, (iii) improved process control and (iv) development of appropriate monitoring tools.

It must be emphasized that *models with low complexity* (process models) must and can be used because:

1. The mathematical (analytical) solvability of optimization, monitoring and controller design problems decreases rapidly as function of the model complexity.
2. Highly complex models (many states and parameters) intrinsically result in observability and identifiability problems due to the lack of on-line sensors, typically for bioprocesses.
3. Model inaccuracy does not pose a problem for the optimization, monitoring and controller design techniques. The optimal control strategy has model independent properties while the estimation and control algorithms are robust against approximations.

Optimization. Determination of the optimal control strategy must initially be decoupled from nonlinear controller design.

Straightforward application of optimal control theory (Minimum principle of Pontryagin) is not recommended due to the large model uncertainty, typically encountered when dealing with bioprocesses, and the intrinsic model sensitivity of the optimal control approach.

This model sensitivity problem can be circumvented by solving low complex optimization problems (requiring low complex models) analytically. From the analytical solution model independent properties of the optimal control strategy can be identified. Complex processes are delt with by considering a well motivated decomposition in easier subproblems.

Besides the actual determination of the optimal control strategy optimal control theory provides a framework for the treatment of the optimization of other degrees of freedom and reveals these parts of the model which are essential with respect to the optimization problem.

Monitoring. The monitoring problem consists of three subproblems.

Step 1. The identifiability and observability of the process model is analyzed for the measurement setup under consideration.

Step 2. An estimation algorithm is selected. This selection is based on a performance analysis of different estimation methods.

Step 3. The selected estimation algorithm is tuned.

Additional information can extracted from the *in bioprocess control* scarcely available *on-line measurements*. Estimation algorithms such as observers and observer based, incorporating the available process knowledge, can be used.

Due to the existence of different estimation algorithm design methodologies an *estimation algorithm selection* problem appears. Performance analysis tools evaluating performance measures such as convergence area, noise sensitivity, robustness against model uncertainty, ...guide the process engineer in the selection procedure.

It must be emphasized that the performance of the estimation algorithms is quite case sensitive. General rules for selection of an appropriate estimation algorithm do not exist.

Tuning of estimation algorithms is based on two complementary methods. *Performance analysis* provides insight into the tuning problem while with *trade-off analysis* the tuning parameters can be determined.

Although nonlinearities in the process model do require more advanced nonlinear estimator design techniques, local linearization should not be used a priori. The available process knowledge, incorporated in these nonlinearities, must be used in the estimator design as much as possible.

Control. Nonlinear controller design can be considered as the dual problem of monitoring. The existence of several nonlinear controller design techniques results in a similar selection problem, which can be approached by performance analysis.

Both performance analysis and trade-off analysis can be used for optimal tuning of the selected nonlinear controller.

Although nonlinear estimation and control design techniques are both quite complicated, the analysis of *combined estimators-controllers* remains feasible.

As a final conclusion it can be stated that *model based optimization and control of bioprocesses* is feasible when the specific nature of biotechnological processes (lack of on-line sensors and high model uncertainty) is taken into account in the different subproblems encountered.

8.2 Suggestions for further research

Chapter 1. Dynamic and sensitivity analysis is applied for model selection for a specific cyclically operated wastewater treatment systems for carbon removal. Application of these model selection tools to other wastewater treatment processes, e.g. nitrogen and phosphor removal, other configurations or even other biotechnological processes must be analyzed.

Fast and dedicated model construction is only feasible when advanced monitoring equipment is available. Recently developed sensors (NADH-sensor, settlometer, ...) must be evaluated in the context of process model design.

Chapters 2 and 3. It is shown that the Minimum Principle of Pontryagin can be applied for determining an optimal control strategy for complex systems such as fed-batch fermentation processes with multiple limiting substrates and cyclically operated wastewater treatment systems.

Because (i) the robustness of the resulting control strategy is based on extraction of model independent features and (ii) well motivated problem decomposition is found to be necessary, further mathematical analysis of these problems is necessary.

It must be evaluated whether new analytical developments in optimal control theory [Lamnabhi-Lagarrigue 1987] are useful for the processes under consideration.

Chapter 5, 6 and 7. The nonlinearities, found in the bioprocess models, should be incorporated in the observers and controllers. As such, advanced nonlinear design methodologies must be used.

Faster solving of the selection problem, resulting from the availability of numerous design methods, should be obtained by creating an environment, enabling fast performance analysis. Such an environment should also facilitate optimal tuning.

Instead of a posteriori evaluation of the observer and controller performance, constructive design methods should be considered.

It is shown in the thesis that the existing theoretical frameworks (optimal control, nonlinear estimation and control theory) are suitable for bioprocess optimization and control when the specific nature of these systems is taken into account. So further research should focus on evaluation and when necessary adaptation of existing techniques instead of developing new methods.

The 'divide et impera' strategy is shown to be feasible in practice. Nevertheless a firm theoretical basis for this decomposition must be developed by studying the interactions in detail between the subproblems (modeling, optimization, monitoring and control).

Transferability to the bioprocess industry can be enhanced by development of (i) concepts (performance measures, ...), which are inspired from process engineering point of view and (ii) tools (software environments), enabling fast design and analysis.

Part V

Appendices

Appendix A

Estimation theory

A.1 Introduction

The basic tools for performing the observability and identifiability analysis, presented in Chapter 4, are introduced. The methods are adopted from the work of Bastin and Dochain (1990).

The software sensors discussed here are based on the general dynamical model for biotechnological processes of Section A.2. *State observation*, *observer based parameter estimation* and *least squares estimation* are discussed in Section A.3, A.4 and A.5 respectively. *Linear transformations* and *reparameterizations* of the general dynamical model and the influence of these techniques on the state and parameter estimation problem are presented in Section A.6 and A.7.

Finally, some basic elements of adaptive state estimation are given in Section A.8.

A.2 General dynamical model for biotechnological processes

A general model for biotechnological systems is described by Bastin and Dochain (1990). ξ is the n-dimensional state of the process (described by the concentrations of each component in the liquid). $\mathbf{K}$ is the $n \times r$ yield matrix while $\varphi(\xi)$ is the r-dimensional vector of reaction rates. The transport terms are described by the $n \times n$ diagonal dilution matrix $\mathbf{D}$ and the n-dimensional input term $\mathbf{f}$.

$$\frac{d\xi}{dt} = \mathbf{K}\varphi(\xi) - \mathbf{D}\xi + \mathbf{f} \qquad \text{(A.1)}$$

A.3 State observers

The state of the process ξ can now be estimated from on-line measurements of a part of the state ξ_1 by the following algorithm.

$$\frac{d\hat{\xi}}{dt} = \mathbf{K}\varphi(\hat{\xi}) - \mathbf{D}\hat{\xi} + \mathbf{f} - \Omega(\hat{\xi})(\xi_1 - \hat{\xi}_1) \qquad \text{(A.2)}$$

$\hat{\xi}$ is the state estimate. Notice that this algorithm consists of a copy of the model plus a correction term, proportional with the difference between the measurements ξ_1 and the estimate of this part of the state $\hat{\xi}_1$. Ω is an $n \times p$-dimensional tuning function matrix if ξ_1 is a p-dimensional vector. In Chapter 5 a more general form for the correction term is presented.

The dynamics of the state estimator can be understood by examining the estimation error model. The estimation error $\mathbf{e}$ is defined as the difference between the actual state ξ of the process and the estimate of this state $\hat{\xi}$. The tuning matrix Ω must be constructed such that the error system is stable. Let $\hat{\xi}_1$ be written as $\mathbf{L}\hat{\xi}$ with $\mathbf{L}$ a $p \times n$ selection matrix then the error system can be written as follows.

$$\begin{aligned} \frac{d\mathbf{e}}{dt} &= \mathbf{K}\left[\varphi(\hat{\xi}+\mathbf{e}) - \varphi(\hat{\xi})\right] - \mathbf{D}\mathbf{e} - \Omega\mathbf{L}\mathbf{e} \\ &\approx \left[\mathbf{A}(\hat{\xi}) - \Omega\mathbf{L}\right]\mathbf{e} \qquad \text{(A.3)} \\ \mathbf{A}(\hat{\xi}) &\triangleq \mathbf{K}\left[\left.\frac{\partial\varphi(\xi)}{\partial\xi}\right|_{\xi=\hat{\xi}}\right] - \mathbf{D}\mathbf{I}_\mathbf{n} \end{aligned}$$

From the linearized tangent approximation of the error system around the estimated state $\hat{\xi}$ one can conclude that the stability of the system can be achieved by realizing strictly negative eigenvalues by a proper selection of the tuning functions $\Omega(\hat{\xi})$. Because the system is time-varying an extra condition stating that the time derivative of the matrix $A(\hat{\xi})$ is bounded must be fulfilled. This is generally fulfilled when the tuning functions are bounded in the region of interest. This can easily be proven by applying the global bounded input bounded state property of the general dynamical model [Bastin and Dochain 1990]. Two cases can be distinguished.

Exponential observers. When the eigenvalues of the matrix $\mathbf{A}(\hat{\xi})$ can be chosen arbitrary, the system is called exponentially observable and the observer is an *exponential observer*. A necessary condition for the process to be exponentially observable is that the following matrix is full rank.

$$\begin{bmatrix} \mathbf{L} \\ \mathbf{L}\mathbf{A}(\hat{\xi}) \\ \vdots \\ \mathbf{L}\mathbf{A}^{n-1}(\hat{\xi}) \end{bmatrix} \qquad \text{(A.4)}$$

Asymptotic observers. When the eigenvalues of the matrix $\mathbf{A}(\hat{\xi})$ can not be chosen arbitrary but the equilibrium point $\mathbf{e} = \mathbf{0}$ is still an asymptotically stable equilibrium point, the observer is called *asymptotic*. The convergence rate of the observer is determined by the dynamics of the system.

A.4 Observer based parameter estimators

Suppose that the reaction rate vector $\varphi(\xi)$ can be modeled as the product of a known $r \times q$ matrix $\mathbf{H}(\xi)$ and an unknown q-dimensional parameter vector ρ. The unknown parameters ρ can then be estimated by the following algorithm.

$$\begin{aligned} \frac{d\hat{\xi}}{dt} &= \mathbf{K}\mathbf{H}(\xi)\hat{\rho} - \mathbf{D}\xi + \mathbf{f} \\ &- \Omega(\hat{\xi})(\xi - \hat{\xi}) \\ \frac{d\hat{\rho}}{dt} &= (\mathbf{K}\mathbf{H}(\xi))^{\mathbf{T}}\Gamma(\hat{\xi})(\xi - \hat{\xi}) \end{aligned} \tag{A.5}$$

$\hat{\rho}$ is the estimate of the parameter vector. $\hat{\xi}$ is the estimate of the state while ξ is the on-line state measurement. Ω and Γ are again tuning function matrices. Notice that full state measurements are assumed.

The dynamics of the parameter estimator can be understood by examining the estimation error model. Two errors can now be defined. The state estimation error $\mathbf{e}_1$ is defined as the difference between the measurements ξ and the estimate of this state $\hat{\xi}$ while the parameter estimation error $\mathbf{e}_2$ is defined as the difference between the real process parameter ρ and the estimate of this parameter $\hat{\rho}$. The tuning matrices Ω and Γ must be constructed such that the error system (A.6) is stable.

The dynamics of the observer-based estimators are here shortly described. A detailed description can be found in [Bastin and Dochain 1990].

$$\begin{pmatrix} \frac{d\mathbf{e}_1}{dt} \\ \frac{d\mathbf{e}_2}{dt} \end{pmatrix} = \mathbf{A}(\xi) \cdot \begin{pmatrix} \mathbf{e}_1 \\ \mathbf{e}_2 \end{pmatrix} + \mathbf{v} \tag{A.6}$$

$$\mathbf{A}(\xi) = \begin{pmatrix} \Omega & \mathbf{K}\mathbf{H}(\xi) \\ -\mathbf{H}^T(\xi)\mathbf{K}^T\Gamma & \mathbf{0} \end{pmatrix} \tag{A.7}$$

$$\mathbf{v} = \begin{pmatrix} \mathbf{0} \\ \frac{d\rho}{dt} \end{pmatrix} \tag{A.8}$$

Exponential convergence of this observer based estimator is guaranteed if (i) the matrix Ω is stable, (ii) the matrix Γ is a symmetric positive definite

matrix such that the matrix Λ (A.9) is negative definite and (iii) the matrix $\Phi \triangleq \mathbf{K}\mathbf{H}(\xi)$ is persistently exciting.

$$\Lambda = \frac{d\Gamma}{dt} + \Gamma\Omega + \Omega^T\Gamma \tag{A.9}$$

A matrix Φ is called persistently exciting if there exist positive constants α and β such that the following inequality is satisfied for all time instances t. $\mathbf{I_n}$ is the $n \times n$-dimensional identity matrix.

$$\alpha\mathbf{I_n} \leq \int_t^{t+\beta} \Phi(\tau)\Phi^T(\tau)d\tau \tag{A.10}$$

Roughly spoken, this inequality means that Φ is not zero over a too long finite time interval. Notice that when Φ is zero, the dynamical equations of the errors $\mathbf{e}_1$ and $\mathbf{e}_2$ are decoupled.

A.5 Least squares estimation

The estimation of the yield coefficients (elements of the matrix $\mathbf{K}$) from full state measurements ξ when the reaction rates φ are unknown is considered here. When the matrix $\mathbf{K}$ has rank q the state ξ can be partitioned in a q-dimensional state ξ_a and an $(n\text{-}q)$-dimensional state ξ_b. This results in the following process model with $\mathbf{K_a}$,$\mathbf{K_b}$,$\mathbf{D_a}$, $\mathbf{D_b}$, $\mathbf{f}_b$ and $\mathbf{f}_a$ matrices and vectors induced by the partition and of appropriate dimensions.

$$\begin{aligned} \frac{d\xi_a}{dt} &= \mathbf{K_a}\varphi(\xi_a, \xi_b) - \mathbf{D_a}\xi_a + \mathbf{f}_a \\ \frac{d\xi_b}{dt} &= \mathbf{K_b}\varphi(\xi_a, \xi_b) - \mathbf{D_b}\xi_b + \mathbf{f}_b \end{aligned} \tag{A.11}$$

The new states η_a and η_b are introduced. These quantities represent the net change of the states ξ_a and ξ_b due to biotransformation only.

$$\begin{aligned} \eta_a &= \xi_a(t) - \xi_a(0) + \int_0^t (\mathbf{D_a}\xi_a - \mathbf{f}_a)d\tau \\ \eta_b &= \xi_b(t) - \xi_b(0) + \int_0^t (\mathbf{D_b}\xi_b - \mathbf{f}_b)d\tau \end{aligned} \tag{A.12}$$

The following linear relation between the state variables η_a and η_b can then be established with the matrix $\mathbf{A_o}$ the solution of a matrix equation. Notice that the elements of the matrix $\mathbf{A_o}$ are function of the yield coefficients.

$$\begin{aligned} \eta_b &= -\mathbf{A_o}\eta_a \\ \mathbf{A_o}\mathbf{K_a} + \mathbf{K_b} &= \mathbf{0} \end{aligned} \tag{A.13}$$

When the l-dimensional vector of elements of the matrix $\mathbf{A_o}$ is denoted θ Equation (A.14), linear in the parameter vector θ, is obtained. The $(n\text{-}q) \times l$ matrix $\mathbf{R}$ is function of the state η_a. The linear relation forms the basis for different least squares estimation schemes for determining the parameter vector θ and thus the yield coefficients independent of the reaction rates.

$$\eta_b = \mathbf{R}(\eta_a) \cdot \theta \tag{A.14}$$

A.6 Transformations

The potential of the above described methods can be enlarged when linear state transformations of the process model are allowed.

Recall that the aim of the observability and identifiability analysis is to determine which states and which parameters can be estimated with state observers, observer based parameter estimators and least squares estimation techniques when a certain state or combination of states are measured on-line and additional parameters are given. With these transformations observability and identifiability properties of the original model can be detected which are not obvious from the original model description.

The importance of linear state transformations is now illustrated. A two step procedure is introduced. In a first step an $(n\text{-}q)$-dimensional state vector $\mathbf{z}$ is introduced by the following state transformation.

$$\mathbf{z} = \mathbf{C_a} \cdot \xi_a + \mathbf{C_b} \cdot \xi_b \tag{A.15}$$

ξ_a is a q-dimensional vector of states ξ with q the rank of the matrix $\mathbf{K}$ and ξ_b is the $(n\text{-}q)$-dimensional vector containing the remainder of the states ξ. $\mathbf{C_a}$ and $\mathbf{C_b}$ are respectively $(n\text{-}q) \times q$ and $(n\text{-}q) \times (n\text{-}q)$ matrices. $\mathbf{C_b}$ is assumed to be invertible. The process model can now be reformulated.

$$\begin{aligned} \frac{d\mathbf{z}}{dt} &= (\mathbf{C_a} \cdot \mathbf{K_a} + \mathbf{C_b} \cdot \mathbf{K_b}) \cdot \varphi - \mathbf{C_b} \cdot \mathbf{D_b} \cdot \mathbf{C_b}^{-1} \cdot \mathbf{z} \\ &+ (\mathbf{C_a} \cdot \mathbf{f}_a + \mathbf{C_b} \cdot \mathbf{f}_b) + (\mathbf{C_b} \cdot \mathbf{D_b} \cdot \mathbf{C_b^{-1}} \cdot \mathbf{C_a} - \mathbf{C_a} \cdot \mathbf{D_a}) \cdot \xi_a \end{aligned} \tag{A.16}$$

$\mathbf{K_a}$, $\mathbf{K_b}$, $\mathbf{D_a}$, $\mathbf{D_b}$ are the corresponding submatrices of the yield matrix $\mathbf{K}$ and the dilution matrix $\mathbf{D}$ respectively induced by the state partitioning. By selecting $\mathbf{C_a}$ and $\mathbf{C_b}$ such that $\mathbf{C_a} \cdot \mathbf{K_a} + \mathbf{C_b} \cdot \mathbf{K_b} = 0$ the dynamics of $\mathbf{z}$ is given by differential equations which are *independent* of the reaction rates. The dynamical system given by (A.16) and the differential equations for ξ_a (expressed in terms of the states $\mathbf{z}$ and ξ_a only) are equivalent to the original process model.

The concept of transforming the system such that a dynamic system which is independent of the reaction rates originates from the work of Bastin and Dochain (1990), in which a diagonal dilution matrix $\mathbf{D}$, with the dilution rate D as diagonal element, is considered. In this appendix still a diagonal dilution matrix is used but the diagonal elements can differ from each other. This extension results in a more complicated dynamic equation for the state $\mathbf{z}$. For instance, the term containing ξ_a disappears when a diagonal matrix with the same element on the diagonal is used. These extensions are also discussed by Chen (1992) and Dochain and Perrier (1994).

In a second step the model is rewritten in terms of the state $\mathbf{z}$ and the measured state. Suppose that the definition of $\mathbf{C_a}$ and $\mathbf{C_b}$ results in a dynamical model which is independent from φ. Let ξ_{nm} and ξ_m be

the non-measured and measured states respectively and assume that the dimension of ξ_m is equal to the rank of the matrix $\mathbf{K}$. The $(n\text{-}q) \times (n\text{-}q)$ matrix $\mathbf{C_{nm}}$ and $(n\text{-}q) \times q$ matrix $\mathbf{C_m}$ define the relation of these states with $\mathbf{z}$. If the matrix $\mathbf{C_{nm}}$ is invertible and the state ξ_{nm} can be rewritten as a function of the measured state ξ_m and $\mathbf{z}$, then the dynamic model can be rewritten with $\mathbf{K_m}$, $\mathbf{f}_m$ and $\mathbf{D_m}$ the partition of the matrices induced by the partition of the state in ξ_m and ξ_{nm}. Assume that the state ξ_a can be rewritten as a combination of the state $\mathbf{z}$ and the measured state ξ_m, involving the $q \times (n\text{-}q)$ matrix $\mathbf{C_z}$ and the $q \times q$ matrix $\mathbf{C_{am}}$. Recall that ξ_a and $\mathbf{z}$ are the states involved in the dynamical model obtained after the first step of the two step model transformation procedure.

$$\mathbf{z} = \mathbf{C_a} \cdot \xi_a + \mathbf{C_b} \cdot \xi_b = \mathbf{C_m} \cdot \xi_m + \mathbf{C_{nm}} \cdot \xi_{nm} \tag{A.17}$$

$$\xi_a = \mathbf{C_z} \cdot \mathbf{z} + \mathbf{C_{am}} \cdot \xi_m \tag{A.18}$$

The general dynamical model can be rewritten as follows.

$$\begin{aligned} \frac{d\xi_m}{dt} &= \mathbf{K_m}\varphi(\xi_m, \mathbf{C_{nm}^{-1}} \cdot (\mathbf{z} - \mathbf{C_m}\xi_m)) + \mathbf{f}_m - \mathbf{D_m} \cdot \xi_m \\ \frac{d\mathbf{z}}{dt} &= -\mathbf{C_b} \cdot \mathbf{D_b} \cdot \mathbf{C_b}^{-1} \cdot \mathbf{z} + (\mathbf{C_a} \cdot \mathbf{f}_a + \mathbf{C_b} \cdot \mathbf{f}_b) \\ &+ (\mathbf{C_b} \cdot \mathbf{D_b} \cdot \mathbf{C_b^{-1}} \cdot \mathbf{C_a} - \mathbf{C_a} \cdot \mathbf{D_a}) \cdot (\mathbf{C_z} \cdot \mathbf{z} + \mathbf{C_{am}} \cdot \xi_m) \end{aligned} \tag{A.19}$$

Notice that the dynamics of $\mathbf{z}$ is now depending on the measured state. The following asymptotic observer is found by using the dynamic equation of $\mathbf{z}$. The nonmeasured state ξ_{nm} can then be retrieved via relation (A.21) by combining the estimate of $\mathbf{z}$ denoted $\widehat{\mathbf{z}}$ and the measured state ξ_m.

$$\begin{aligned} \frac{d\widehat{\mathbf{z}}}{dt} &= -\mathbf{C_b} \cdot \mathbf{D_b} \cdot \mathbf{C_b}^{-1} \cdot \widehat{\mathbf{z}} + (\mathbf{C_a} \cdot \mathbf{f}_a + \mathbf{C_b} \cdot \mathbf{f}_b) \\ &+ (\mathbf{C_b} \cdot \mathbf{D_b} \cdot \mathbf{C_b^{-1}} \cdot \mathbf{C_a} - \mathbf{C_a} \cdot \mathbf{D_a}) \cdot (\mathbf{C_z} \cdot \widehat{\mathbf{z}} + \mathbf{C_{am}} \cdot \xi_m) \end{aligned} \tag{A.20}$$

$$\xi_{nm} = \mathbf{C_{nm}}^{-1} \cdot (\mathbf{z} - \mathbf{C_m} \cdot \xi_m) \tag{A.21}$$

A.7 Reparametrizations

The potential of the state observers and observer based parameter estimators can be enlarged by considering reparametrizations of the models, possibly in combination with a transformation.

By considering reparametrization of the general dynamical model the joint estimation of yield coefficients and (specific) reaction rates from full state and/or partial state measurements and the estimation of (specific) reaction rates independently of the yield coefficients can be studied.

- Joint estimation of yield coefficients and (specific) reaction rates

Full state measurements.

Suppose that the full state ξ is measured and that the unknown reaction rate vector $\varphi(\xi)$ has been modeled as the product of a known $r \times q$ matrix $\mathbf{H}(\xi)$ and an unknown q-dimensional parameter vector ρ. The elements of the vector ρ can be considered as specific reaction rates. The joint estimation of the yield coefficients (elements of the matrix $\mathbf{K}$) and the parameter vector ρ can be performed with an observer based parameter estimator when the reparametrization (A.22) is used.

$$\mathbf{K} \cdot \mathbf{H}(\xi) \cdot \rho \;=\; \Phi(\xi) \cdot \theta \tag{A.22}$$

θ is the l-dimensional vector of unknown variables. The elements of θ are bilinear combinations of unknown yield coefficients and specific reaction rates. Φ is a known $n \times l$ matrix of functions of the state variables ξ. With $\mathbf{k}$ and ρ the vector of unknown yield coefficients and specific reaction rates respectively, the reparametrization can be written formally as follows.

$$\theta \;=\; \mathbf{r}(\rho, \mathbf{k}) \tag{A.23}$$

The estimation of the parameter θ can be performed with the observer based parameter estimator discussed in Section A.4.

$$\begin{aligned} \frac{d\hat{\xi}}{dt} &= \Phi(\xi)\hat{\theta} - \mathbf{D}\xi + \mathbf{f} + \Omega(\xi - \hat{\xi}) \\ \frac{d\hat{\theta}}{dt} &= \Phi^T(\xi)\Gamma(\xi - \hat{\xi}) \end{aligned} \tag{A.24}$$

From the estimate of the parameter $\hat{\theta}$ the yield coefficients and the specific rates are obtained due to the invertibility of the reparametrization.

$$\left(\hat{\rho}, \hat{\mathbf{k}} \right) \;=\; \mathbf{r}^{-1}(\hat{\theta}) \tag{A.25}$$

Partial state measurements.

By using the transformations discussed before and the separation of the reaction rate in a known and unknown part, the general dynamical model (A.19) can be used with φ written as follows.

$$\varphi \;=\; \mathbf{H}(\xi_m, \mathbf{C_{nm}^{-1}}(\mathbf{z} - \mathbf{C_m}\xi_m))\rho \tag{A.26}$$

The dynamics of the measured state ξ_m can now be rewritten with θ the unknown parameters (polynomial expressions of both yield coefficients and reaction rates) and Φ a matrix of polynomial expressions of $\mathbf{z}$ and ξ_m.

$$\begin{aligned} \frac{d\xi_m}{dt} &= \Phi(\mathbf{z}, \xi_m) \cdot \theta + \mathbf{f_m} - \mathbf{D_m} \cdot \xi_m \\ \frac{d\mathbf{z}}{dt} &= -\mathbf{C_b} \cdot \mathbf{D_b} \cdot \mathbf{C_b}^{-1} \cdot \mathbf{z} + (\mathbf{C_a} \cdot \mathbf{f}_a + \mathbf{C_b} \cdot \mathbf{f}_b) \\ &+ (\mathbf{C_b} \cdot \mathbf{D_b} \cdot \mathbf{C_b^{-1}} \cdot \mathbf{C_a} - \mathbf{C_a} \cdot \mathbf{D_a}) \cdot (\mathbf{C_z} \cdot \mathbf{z} + \mathbf{C_{am}} \cdot \xi_m) \end{aligned} \tag{A.27}$$

It is clear that an asymptotic observer based estimator for the reaction rates ρ and the yield vector $\mathbf{k}$ (containing the yield coefficients that must be estimated) can be written for the system described by (A.27) if the dynamics of the state $\mathbf{z}$ is independent from the yield vector $\mathbf{k}$ and the reparametrization (A.23) is invertible. Invertibility is not guaranteed in this case.

- Estimation of the reaction rates independent of the yield coefficients

The above mentioned approach can of course also be used for estimation of specific reaction rates, independently of some yield coefficients, from partial state measurements.

An observer based estimator for θ, independent of the some yield coefficient, can be built if the dynamics of $\mathbf{z}$ and the function Φ are independent of these yield coefficients.

A.8 Adaptive state estimation

The basic idea of adaptive state estimation is now introduced for a general state space model. Through combination of *on-line* measurements and model knowledge a process state, which is not measured, can be reconstructed with a state estimator when certain *observability conditions* are fulfilled. The state estimation algorithm is based on a relation between the *on-line* measurement and the state of the process under consideration. Changes in the parameters of this relation (and even of the model) is taken into account by adaptation.

- Non-adaptive state estimator

Consider the nonlinear model (A.28) with $\mathbf{x}$ the $n \times 1$ state vector and $\mathbf{u}$ the $m \times 1$ input vector. $\mathbf{f}$ is an n-dimensional vector field.

$$\frac{d\mathbf{x}}{dt} \;=\; \mathbf{f}(\mathbf{x}, \mathbf{u}) \qquad y \;=\; h(\mathbf{x}, \mathbf{p}) \tag{A.28}$$

The available *on-line* measurement y and the state of the process $\mathbf{x}$ are related by the following equation with $\mathbf{p}$ the known constant $r \times 1$ parameter vector. $h(\mathbf{x}, \mathbf{p})$ is a scalar output function.

The state estimator consist of two parts. The first part is a copy of the process model (A.28) while the second part is a correction term. The correction term is modeled as a product of tuning matrix $\mathbf{\Phi}$ and the error on the estimate of the output. The error is equal to the difference between the *on-line* measurement y and the estimate for this *on-line* measurement $h(\widehat{\mathbf{x}})$ estimated through the output relation with $\widehat{\mathbf{x}}$ the estimated process state of the system.

$$\frac{d\widehat{\mathbf{x}}}{dt} = \mathbf{f}(\widehat{\mathbf{x}}, \mathbf{u}) + \mathbf{\Phi}(\widehat{\mathbf{x}}, \mathbf{u}) \cdot (y - h(\widehat{\mathbf{x}}, \mathbf{p})) \tag{A.29}$$

- Adaptive state estimator

  Suppose that the $r \times 1$ parameter vector $\mathbf{p}(t)$ in the output relation is time-varying. The dynamics of this parameter vector is assumed to be slower that the main dynamics of the process state $\mathbf{x}$. When measurements of the state $\mathbf{x}(t_k)$ are available at some discrete time points t_k, then the parameter vector $\mathbf{p}(t)$ can be modified by using this extra information when some *identifiability conditions* are fulfilled. These conditions guarantee that the parameter vector $\mathbf{p}(t)$ can be determined from the available measurement set $\mathbf{x}(t_k)$.

  Notice that through the *on-line* measurements of y estimates of the state $\mathbf{x}$ are available continuously while with the few direct measurements of the state $\mathbf{x}$ itself the parameter vector $\mathbf{p}(t)$ can be determined. The state measurements $\mathbf{x}$ can also be used for state estimator reinitialization.

  The complete adaptive state estimator is then written by the following set of differential and difference equations.

$$\begin{aligned} \frac{d\widehat{\mathbf{x}}}{dt} &= \mathbf{f}(\widehat{\mathbf{x}}, \mathbf{u}) + \mathbf{\Phi}(\widehat{\mathbf{x}}, \mathbf{u}) \cdot (y - h(\widehat{\mathbf{x}}, \widehat{\mathbf{p}}(t_k))) \\ \widehat{\mathbf{p}}(t_{k+1}) &= \widehat{\mathbf{p}}(t_k) + \mathbf{\Psi}(\mathbf{x}_k, \widehat{\mathbf{p}}(t_k)) \cdot (y - h(\mathbf{x}_k, \widehat{\mathbf{p}}(t_k)) \end{aligned} \tag{A.30}$$

  Notice that the parameter adaptation is also driven by the error between the *on-line* measurement y and the value estimated on basis of the measured state $\mathbf{x}(t_k)$ and the estimated value of the parameter $\widehat{\mathbf{p}}(t_k)$ multiplied with a tuning matrix $\mathbf{\Psi}$.

Notice that the basic idea of adaptive state estimation is to use available measurements with different discretisation times in an optimal way. The on-line measurements y (small discretisation step) are used to obtain on-line estimates of the state $\mathbf{x}$ while the measurements of the state $\mathbf{x}(k)$ (large discretisation step) are used to update the relation between the measurement y and the state $\mathbf{x}(t_k)$. It is clear that the performance of this adaptive state estimation scheme will depend on the time variability of the relation y-$\mathbf{x}$ versus the discretisation step of the state measurements.

Appendix B

Technical lemmas

B.1 Introduction

Some Technical Lemmas, frequently used in Chapter 6, are given and proven. Lemmas (B.2) and (B.3) are relating the upper bound on the state of a linear system with an upper bound on the input of that system. Because Lemma (B.2) is a special case of Lemma (B.3), only the proof of the second Lemma is presented. Recall that the use of these Lemmas is only valid for linear time invariant system. These Lemmas can applied to linear time-varying systems and nonlinear systems by using a local linear approximation of the system. The obtained results are then only locally valid. In Lemma (B.4) both the design of tuning function of a nonlinear observer with a particuler design method and the implications of time discretization are analyzed.

B.2 Technical Lemma 1

For the linear system (B.1), with a eigenvalue λ, with multiplicity two, the upper bound (B.2) on the 2-dimensional state $\mathbf{x}(t_\infty)$ is found with B_1 and B_2 upper bounds on the input signals $b_1(t)$ and $b_2(t)$ respectively.

$$\begin{pmatrix} \frac{dx_1}{dt} \\ \frac{dx_2}{dt} \end{pmatrix} = \begin{pmatrix} 2\lambda & -1 \\ \lambda^2 & 0 \end{pmatrix} \cdot \begin{pmatrix} x_1 \\ x_2 \end{pmatrix} + \begin{pmatrix} b_1(t) \\ b_2(t) \end{pmatrix} \tag{B.1}$$

$$\begin{aligned} |\, x_1(t) \,| &\leq \frac{2}{|\,\lambda\,|\,e} B_1 + \frac{1}{\lambda^2} B_2 \\ |\, x_2(t) \,| &\leq B_1 + \frac{2}{|\,\lambda\,|} B_2 \end{aligned} \tag{B.2}$$

B.3 Technical Lemma 2

For the linear system (B.3), with eigenvalue λ, with multiplicity two, the upper bound (B.4) on the 2-dimensional state $\mathbf{x}(t_\infty)$ is found with B_1 and B_2 upper bounds on the input signals $b_1(t)$ and $b_2(t)$ respectively.

$$\begin{pmatrix} \frac{dx_1}{dt} \\ \frac{dx_2}{dt} \end{pmatrix} = \begin{pmatrix} a & b \\ c & d \end{pmatrix} \cdot \begin{pmatrix} x_1 \\ x_2 \end{pmatrix} + \begin{pmatrix} b_1(t) \\ b_2(t) \end{pmatrix} \tag{B.3}$$

$$\begin{aligned} |\, x_1(t) \,| \leq\ & |\, -\frac{1}{\lambda} + \frac{1}{\lambda^2}(a-\lambda) \,|\, B_1 && if \lambda \leq a \\ or\ & |\, -\frac{1}{\lambda} - \frac{(a-\lambda)}{\lambda^2}(2e^{\frac{\lambda}{\lambda-a}} - 1) \,|\, B_1 && if a \leq \lambda \\ +\ & |\, b \,|\, \frac{1}{\lambda^2} B_2 \\ |\, x_2(t) \,| \leq\ & |\, c \,|\, \frac{1}{\lambda^2} B_1 \\ +\ & |\, -\frac{1}{\lambda} + \frac{1}{\lambda^2}(d-\lambda) \,|\, B_2 && if \lambda \leq d \\ or\ & |\, -\frac{1}{\lambda} - \frac{(d-\lambda)}{\lambda^2}(2e^{\frac{\lambda}{\lambda-d}} - 1) \,|\, B_2 && if d \leq \lambda \end{aligned} \tag{B.4}$$

Proof

- An eigenvalue λ with double multiplicity is obtained if $a + d = 2\lambda$ en $ad - bc = \lambda^2$.
- The matrix exponential (B.5) is determined. $\mathbf{A}$ denotes the system matrix.

$$e^{\mathbf{A}t} = \begin{pmatrix} e^{\lambda t} + (a-\lambda)te^{\lambda t} & bte^{\lambda t} \\ cte^{\lambda t} & e^{\lambda t} + (d-\lambda)te^{\lambda t} \end{pmatrix} \tag{B.5}$$

- An upper bound on the absolute value of the state $\mathbf{x}$ is now calculated with $\mathbf{B}$ a bound on the input vector $\mathbf{b}$.

$$\begin{aligned} \mathbf{x(t)} &= e^{\mathbf{A}t} \cdot \mathbf{x(o)} + \int_0^t e^{\mathbf{A}\tau} \cdot \mathbf{b}(t-\tau) d\tau \\ |\, \mathbf{x(t)} \,| &\leq |\, e^{\mathbf{A}t} \,| \cdot |\, \mathbf{x(o)} \,| + \int_0^t |\, e^{\mathbf{A}\tau} \cdot \mathbf{B} \,|\, d\tau \end{aligned} \tag{B.6}$$

When the transient behavior is negligible (for t sufficiently large and a stable matrix $\mathbf{A}$) the following relations are obtained.

$$\begin{aligned} |\, x_1(t) \,| &\leq B_1 \int_0^t |\, e^{\lambda\tau} + (a-\lambda)\tau e^{\lambda\tau} \,|\, d\tau \\ &+ B_2 \int_0^t |\, b\tau e^{\lambda\tau} \,|\, d\tau \\ |\, x_2(t) \,| &= B_1 \int_0^t |\, c\tau e^{\lambda\tau} \,|\, d\tau \\ &+ B_2 \int_0^t |\, e^{\lambda\tau} + (d-\lambda)\tau e^{\lambda\tau} \,|\, d\tau \end{aligned} \tag{B.7}$$

- The integrals in the previous relations are now calculated. Because the integral of the absolute value of a function must be determined, the integral must be split up into different parts when the function changes sign. Whether this is necessary depends on the parameters of the system.

  - When $a \geq \lambda$ then the integral stated below can easily be solved.

$$\begin{aligned} &\int_0^t \mid e^{\lambda\tau} + (a-\lambda)\tau e^{\lambda\tau} \mid d\tau \quad = \\ &(a-\lambda)\cdot(\frac{te^{\lambda t}}{\lambda} - \frac{1}{\lambda^2}(e^{\lambda t}-1)) \quad + \quad (\frac{e^{\lambda t}}{\lambda} - \frac{1}{\lambda}) \end{aligned} \tag{B.8}$$

  - The integral below is determined in two parts because the integrand changes sign at the time instance t_* when $a \leq \lambda$.

$$t_* \quad = \quad \frac{1}{\lambda - a} \tag{B.9}$$

$$\begin{aligned} &\int_0^t \mid e^{\lambda\tau} + (a-\lambda)\tau e^{\lambda\tau} \mid d\tau = \\ &\int_0^{t_*} e^{\lambda\tau} + (a-\lambda)\tau e^{\lambda\tau} d\tau - \int_{t_*}^t e^{\lambda\tau} + (a-\lambda)\tau e^{\lambda\tau} d\tau \\ &= \\ &(a-\lambda)\cdot(\frac{t_* e^{\lambda t_*}}{\lambda} - \frac{1}{\lambda^2}(e^{\lambda t_*}-1)) + (\frac{e^{\lambda t_*}}{\lambda} - \frac{1}{\lambda}) \\ &-(a-\lambda)\cdot((\frac{te^{\lambda t}}{\lambda} - \frac{t_* e^{\lambda t_*}}{\lambda}) - \frac{1}{\lambda^2}(e^{\lambda t} - e^{\lambda t_*})) - (\frac{e^{\lambda t}}{\lambda} - \frac{e^{\lambda t_*}}{\lambda}) \\ &= \\ &\frac{1}{\lambda}(2e^{\lambda t_*} - e^{\lambda t} - 1) + \frac{(a-\lambda)}{\lambda}(2t^* e^{\lambda t_*} - te^{\lambda t}) \\ &-\frac{(a-\lambda)}{\lambda^2}(2e^{\lambda t_*} - e^{\lambda t} - 1) \\ &= \\ &\frac{1}{\lambda}(2e^{\frac{\lambda}{\lambda-a}} - e^{\lambda t} - 1) + \frac{(a-\lambda)}{\lambda}(2\frac{1}{\lambda-a}e^{\frac{\lambda}{\lambda-a}} - te^{\lambda t}) \\ &-\frac{(a-\lambda)}{\lambda^2}(2e^{\frac{\lambda}{\lambda-a}} - e^{\lambda t} - 1) \end{aligned} \tag{B.10}$$

  -

$$\int_0^t \mid \tau b e^{\lambda\tau} \mid d\tau \quad = \quad \frac{bte^{\lambda t}}{\lambda} - \frac{b}{\lambda^2}(e^{\lambda t} - 1) \tag{B.11}$$

The integrals involved in determining the bound on x_2 are the same as the ones determined. The parameters a and b must be replaced with d and c respectively. For t infinitely large the asymptotic bound (B.3) on the state $\mathbf{x}(t)$ is found.

B.4 Technical Lemma 3

Consider the 2-dimensional nonlinear system (B.12) and a nonlinear observer (B.13) for this system, using on-line measurements of the second state x_2. The tuning functions $\mathbf{k}(\mathbf{x})$ are determined via local linearization of the error system around the actual state estimate $\widehat{\mathbf{x}}$ such that the matrix of the error system has a eigenvalue λ with double multiplicity. The error $\mathbf{e}$ is equal to the state $\mathbf{x}$ minus the estimate of the state $\widehat{\mathbf{x}}$. The tuning functions are then determined by the equations (B.14). f_i^j are the partial derivatives of the function f_i with respect to the variable x_j.

$$\frac{d\mathbf{x}}{dt} \quad = \quad \mathbf{f}(\mathbf{x}) \tag{B.12}$$

$$\frac{d\widehat{\mathbf{x}}}{dt} \quad = \quad \mathbf{f}(\widehat{\mathbf{x}}) \quad + \quad \mathbf{k}(\widehat{\mathbf{x}})\cdot(x_2 - \widehat{x_2}) \tag{B.13}$$

$$\mathbf{k_1}(\widehat{\mathbf{x}}) \quad = \quad \frac{(\lambda - f_1^1)^2}{f_2^1} + f_1^2 \quad , \quad \mathbf{k_2}(\widehat{\mathbf{x}}) \quad = \quad -2\lambda + f_2^2 + f_1^1 \tag{B.14}$$

The matrix of the error system is presented below.

$$\begin{pmatrix} f_1^1 & -\frac{(\lambda - f_1^1)^2}{f_2^1} \\ f_2^1 & 2\lambda - f_1^1 \end{pmatrix} \tag{B.15}$$

When the nonlinear observer is implemented in discrete way with a forward Euler approximation of the derivatives, the matrix (B.16) of the linear approximation of the nonlinear state estimator can be determined. The eigenvalues of the discrete system (B.17) are then found.

$$\begin{pmatrix} 1 + T(f_1^1 - k_1^1 x_2) & T(f_1^2 - k_1 - k_1^2 x_2) \\ T(f_1^1 - k_2^1 x_2) & 1 + T(f_2^2 - k_2 - k_2^2 x_2) \end{pmatrix} \tag{B.16}$$

$$\lambda_T \quad = \quad 1 + \lambda T + T x_2 \Phi(\lambda, f_1, f_2) + \sqrt{\Psi(\lambda, T, x_2, f_1, f_2)} \tag{B.17}$$

The first two terms of equation (B.17) equals the relation between the eigenvalues of the discrete system and the continuous system as found for linear systems. The second part of equation contains the functions Φ and Ψ which are nonlinear functions of the derivatives of f_1 and f_2. It can be shown that these functions are zero when the second order derivatives of f_1 and f_2 are zero. The proof of this Lemma is not presented as it consists of straightforward tedious calculations.

Appendix C

Differential geometry in nonlinear controller and observer design

C.1 Introduction

In this appendix concepts used in *nonlinear observer design* and *nonlinear controller design* are shortly reviewed.

Basic definitions and theorems are presented in Sections C.2 and C.3 respectively. Two nonlinear controller design methods (*input-output linearization* and *input-state linearization*) are discussed in Section C.4. Nonlinear observer design based on *exact linearization up to an output injection* is treated in Section C.5. As an introduction some canonical forms are shortly reviewed. In the observer design method basically two cases can be distinguished:

Case 1. The state transformation, used in the design of the nonlinear observer, is *independent* from the input signal (Section C.5.2).

Case 2. The state transformation, used in the design of the nonlinear observer, is *depending* on the input and its time derivatives and a nonlinear transformation of the output is allowed (Section C.5.3).

The latter observer design method originates from *differential algebraic methods* while the other controller and observer design methods are based on *differential geometric approaches*. In Section C.5.3 the latter design method is reformulated in the differential geometric framework. The differences between the observer design methods are illustrated for a prototype model for biotechnological processes.

The nonlinear controller design methods and the observer design method without input derivatives, are found in [Marino and Tomei 1995] and [Isidori 1989]. The observer design method with input derivatives and output transformation originates from [Keller 1987].

The observer design method with output transformation is used in Chapter 5, with the assumption that the input is constant. Robustness of the input-output and input-state linearizing controller is analyzed in Chapter 7. The combination of nonlinear observers (both methods) with input-state linearizing controllers is also discussed in Chapter 7. The constant input assumption is violated here. Notice that by reformulation of the second observer design method in the differential geometric framework the combined observer-controller problem can be discussed in one framework.

C.2 Basic definitions

In this appendix the single input single output system (C.1) is considered. $\mathbf{x}$ is the n-dimensional state, u the input and y the output. It is assumed that $\mathbf{f}(\mathbf{x})$, $\mathbf{g}(\mathbf{x})$ are smooth vector fields in $\mathcal{R}^n$ and $h(\mathbf{x})$ is a smooth function from $\mathcal{R}^n$ to $\mathcal{R}$.

$$\frac{d\mathbf{x}}{dt} = \mathbf{f}(\mathbf{x}) + \mathbf{g}(\mathbf{x})u \qquad y = h(\mathbf{x}) \tag{C.1}$$

Some definitions and concepts are now introduced.

- The Jacobian of a vector field $\mathbf{f}$ is a map from $\mathcal{R}^n$ to $\mathcal{R}^{n\times n}$ defined by:

$$\frac{\partial \mathbf{f}}{\partial \mathbf{x}} = \begin{pmatrix} \frac{\partial f_1}{\partial x_1} & \frac{\partial f_1}{\partial x_2} & \cdots & \frac{\partial f_1}{\partial x_n} \\ \frac{\partial f_2}{\partial x_1} & \cdots & \cdots & \frac{\partial f_2}{\partial x_n} \\ \vdots & \vdots & \vdots & \vdots \\ \frac{\partial f_n}{\partial x_1} & \frac{\partial f_n}{\partial x_2} & \cdots & \frac{\partial f_n}{\partial x_n} \end{pmatrix} \tag{C.2}$$

- If $\mathbf{w}$ and $\mathbf{v}$ are respectively n-dimensional row and column vectors, then $< \mathbf{w}, \mathbf{v} >$ denotes the inner product of these two vectors.

- The Lie bracket $[\mathbf{f}, \mathbf{g}]$ of two vector fields $\mathbf{f}$ and $\mathbf{g}$ is a vector field defined by (C.3). The Lie bracket $[\mathbf{f}, \mathbf{g}]$ is also denoted as $ad_{\mathbf{f}}\mathbf{g}$. Repeated Lie brackets can then be defined by (C.4).

$$[\mathbf{f}, \mathbf{g}] = \frac{\partial \mathbf{g}}{\partial \mathbf{x}}\mathbf{f} - \frac{\partial \mathbf{f}}{\partial \mathbf{x}}\mathbf{g} \tag{C.3}$$

$$ad^n_{\mathbf{f}}\mathbf{g} = ad_{\mathbf{f}}(ad^{(n-1)}_{\mathbf{f}}\mathbf{g}) \tag{C.4}$$

- The Lie derivative $L_{\mathbf{f}}h$ of a function $h(\mathbf{x})$ along the vector field $\mathbf{f}(\mathbf{x})$ is a function defined as the inner product of $\mathbf{dh}$, the differential of the function $h(\mathbf{x})$, which is a row vector with the partial derivatives of the function $h(\mathbf{x})$ with respect to the state, with the vector field $\mathbf{f}$. Notice that the Lie derivative represent the time derivative of the function $h(\mathbf{x})$. Repeated Lie derivatives can be defined by (C.6).

$$L_{\mathbf{f}}h = < \mathbf{dh}, \mathbf{f} > \tag{C.5}$$

$$L^0_{\mathbf{f}}h = h \qquad L^1_{\mathbf{f}}h = \mathbf{dh} \cdot \mathbf{f} \qquad L^n_{\mathbf{f}}h = \mathbf{d}(L^{(n-1)}_{\mathbf{f}}h) \cdot \mathbf{f} \tag{C.6}$$

- The relative degree of system (C.1) is defined as the integer ρ such that in a neighborhood $\mathcal{U}_o$ of the origin the following conditions hold true:

$$\begin{aligned} L_{\mathbf{g}}L^i_{\mathbf{f}}h(\mathbf{x}) &= 0 \qquad 0 \leq i \leq \rho - 2 \\ L_{\mathbf{g}}L^{(\rho-1)}_{\mathbf{f}}h(\mathbf{x}) &\neq 0 \end{aligned} \tag{C.7}$$

- A homeomorphism (bijection) ϕ from $\mathcal{U}$ to $\mathcal{V}$, two neighborhoods in $\mathcal{R}^n$ of the origin, is a diffeomorphism if both ϕ and its inverse are continuous.

- A r-dimensional distribution $\mathbf{D}$ on $\mathcal{D}$, a subset of $\mathcal{R}^n$, is a map which assigns to each point of $\mathcal{D}$, a r-dimensional subspace of $\mathcal{R}^n$. A distribution $\mathbf{D}$ is called *involutive* if for any two vector field $\mathbf{f}$ and $\mathbf{g}$, belonging to the distribution, the Lie bracket $[\mathbf{f}, \mathbf{g}]$ belongs to the distribution.

- The notation (C.8) for the vector field $\mathbf{f}$ denotes that in $\mathbf{x}$-coordinates only the i-component is different from zero.

$$\mathbf{f} = \frac{\partial}{\partial x_i} \tag{C.8}$$

C.3 Basic theorems

C.3.1 Leibniz formula

Given two smooth vector fields $\mathbf{f}$, $\mathbf{g}$ and a smooth function $h(\mathbf{x})$, the following formula can be written:

$$L_{\mathbf{f}} < \mathbf{dh}, \mathbf{g} > = < \mathbf{dh}, ad_{\mathbf{f}}\mathbf{g} > + < \mathbf{d}(L_{\mathbf{f}}h), \mathbf{g} > \tag{C.9}$$

C.3.2 Lemma

If for two smooth vector fields $\mathbf{f}$, $\mathbf{g}$ and a smooth function $h(\mathbf{x})$ in $\mathcal{U}$, a subset of $\mathcal{R}^n$, for some integer $\rho, 1 < \rho < n$, the condition (C.10) is fulfilled for all $\mathbf{x}$ in $\mathcal{U}$ with $\gamma(\mathbf{x})$ a function, then the property (C.11) holds true.

$$\begin{aligned} < \mathbf{d}(L^i_{\mathbf{f}}h), \mathbf{g} > &= 0 \qquad 0 \leq i \leq \rho - 2 \\ < \mathbf{d}(L^{\rho-1}_{\mathbf{f}}h), \mathbf{g} > &= \gamma \neq 0 \end{aligned} \tag{C.10}$$

$$\begin{aligned} < \mathbf{d}(L^i_{\mathbf{f}}h), ad^j_{\mathbf{f}}\mathbf{g} > &= 0 \qquad 0 \leq i+j \leq \rho - 2 \\ < \mathbf{d}(L^i_{\mathbf{f}}h), ad^j_{\mathbf{f}}\mathbf{g} > &= \gamma \neq 0 \qquad i+j = \rho - 1 \end{aligned} \tag{C.11}$$

C.3.3 Inverse Function Theorem

Let $\mathcal{D}$ be an open subset of $\mathcal{R}^n$ and let ϕ be a smooth map from $\mathcal{D}$ to $\mathcal{R}^n$. If the Jacobian of ϕ is nonsingular at some point p of $\mathcal{D}$ then there exists a neighborhood $\mathcal{V}$, subset of $\mathcal{D}$, such that ϕ is a diffeomorphism from $\mathcal{V}$ to $\phi(\mathcal{V})$, subset of $\mathcal{R}^n$.

C.3.4 Frobenius Theorem

Let $\mathbf{D}$ be an r-dimensional distribution on $\mathcal{D}$, a subset of $\mathcal{R}^n$. For every point p of $\mathcal{D}$, there exist a mapping ϕ $(\phi_1, \ldots, \phi_n)$ such that for every vector field $\mathbf{f}$ in $\mathbf{D}$ the conditions (C.12) hold true if and only if $\mathbf{D}$ is an involutive distribution.

$$< \mathbf{d}\phi_i, \mathbf{f} > = 0 \quad r+1 \leq i \leq n \tag{C.12}$$

C.3.5 Simultaneous Rectification Theorem

Let $\mathbf{f}_1, \mathbf{f}_2, \ldots, \mathbf{f}_r$, $r \leq n$, be smooth vector fields on $\mathcal{R}^n$ and p a point of $\mathcal{R}^n$ such that these vector fields $\mathbf{f}_1(p), \mathbf{f}_2(p), \ldots, \mathbf{f}_r(p)$ are linearly independent then there exists a coordinate system around $\mathcal{U}$, a neighborhood of p, such that property (C.13) is fulfilled, if and only if conditions (C.14) hold true for these vector fields.

$$\mathbf{f}_i = \frac{\partial}{\partial x_i} \tag{C.13}$$

$$[\mathbf{f}_i, \mathbf{f}_j] = 0 \quad 1 \leq i, j \leq r \tag{C.14}$$

C.3.6 Remarks

In the theorems discussed further several transformations are introduced. The fact that these transformations are diffeomorphisms is based on the *Inverse Function Theorem* by showing that their Jacobian matrix is nonsingular. This is proven by using some of the assumptions of the theorem in combination with *Leibniz formula* and Lemma C.3.2. The existence of a set

of linearly independent vector fields, which form the basis for an involutive distribution, enables the use of the *Frobenius Theorem* (generating functions with differentials orthogonal with respect to these vector fields) or the *Simultaneous Rectification Theorem* (generating a coordinate transformation, such that these vector fields are orthogonal in this coordinate space).

C.4 Nonlinear controller design

C.4.1 Input-output linearizing controller

The single input system (C.1) is *locally state feedback input-output linearizable* in a neighborhood of the origin $\mathcal{U}_o$ if there exists a state feedback $u(\mathbf{x}) = k(\mathbf{x}) + \beta(\mathbf{x})v$ with $k(\mathbf{x})$, $\beta(\mathbf{x})$ smooth functions and $\beta \neq 0$ in $\mathcal{U}_o$ such that the input-output dynamics are given by the linear differential equation (C.15) with y the output, r a positive constant and v the new input of the system.

$$\frac{d^r y}{dt^r} = v \tag{C.15}$$

Theorem. The single input system (C.1) is *locally state feedback input-output linearizable* if the relative degree $\rho \leq n$.

Proof. 1. It is clear that equation (C.15) is fulfilled when the system (C.1) can be transformed into the canonical form (C.16) (tracking form). $\mathbf{w}$ is an $(n\text{-}r)$-dimensional state vector. The output y equals the state z_1.

$$\begin{aligned} \frac{d\mathbf{w}}{dt} &= \phi(\mathbf{w}, \mathbf{z}) \\ \frac{dz_i}{dt} &= z_{i+1} \qquad 1 \leq i \leq r-1 \\ \frac{dz_r}{dt} &= v \end{aligned} \tag{C.16}$$

2. It can be shown that the condition $\rho \leq n$ implies that the system (C.1) can be transformed into the canonical form (C.16) with $r = \rho$. This is first proven for $\rho = n$ and secondly for $\rho < n$.

$\boxed{\rho = n}$

(a) It can be shown that the matrix $\mathbf{M}_{n-1}(\mathbf{x})$ (C.17) is full rank. This is proven by showing that the rank of the $n \times n$ matrix $\mathbf{N}(\mathbf{x})$ has rank n. The definition of relative degree and Lemma C.3.2 is used.

$$\mathbf{M}_{n-1}(\mathbf{x}) = \left(\mathbf{dh}, \ldots, \mathbf{d}(L_{\mathbf{f}}^{(n-1)}\mathbf{h})\right)^T \tag{C.17}$$

$$\mathbf{G}_{n-1}(\mathbf{x}) = \left(\mathbf{g}, \ldots, ad_{\mathbf{f}}^{n-1}\mathbf{g}\right) \tag{C.18}$$

$$\mathbf{N}(\mathbf{x}) = \mathbf{M}_{n-1}(\mathbf{x}) \cdot \mathbf{G}_{n-1}(\mathbf{x}) \tag{C.19}$$

(b) From the Inverse Function Theorem it follows that (C.20) is a coordinate transformation. It is clear that this local diffeomorphism transforms the system (C.1) into the canonical form (C.16) with $r = \rho$.

$$\mathbf{z} = \mathbf{t}(\mathbf{x}) = (h(\mathbf{x}), L_{\mathbf{f}}h(\mathbf{x}), \ldots, L_{\mathbf{f}}^{(n-1)}h(\mathbf{x}))^T \tag{C.20}$$

$\boxed{\rho < n}$

(a) The existence of $n - \rho$ functions $w_i(\mathbf{x}), 1 \leq i \leq n - \rho$, satisfying conditions (C.21) is proven by applying the Frobenius Theorem for the distribution $\mathbf{D} = span(\mathbf{g})$. Combined with the definition of the relative degree condition (C.22) is established.

$$< \mathbf{dw}_i, \mathbf{g} > = 0 \quad 1 \leq i \leq n - \rho \tag{C.21}$$

$$rank\left(\mathbf{dh}, \ldots, \mathbf{d}(L_{\mathbf{f}}^{\rho-2}h), \mathbf{dw_1}, \ldots, \mathbf{dw}_{n-\rho}\right) = n - 1 \tag{C.22}$$

(b) The nonsingularity of the matrix (C.23) $\mathbf{M}_{\rho-1}(\mathbf{x})$ is trivial from the definition of the relative degree and (C.22). With the Inverse Function Theorem it follows that (C.24) is a coordinate transformation. It is clear that this local diffeomorphism transforms the system (C.1) into the canonical form (C.16). $\mathbf{w}$ and $\mathbf{z}$ are respectively n-ρ-dimensional and ρ-dimensional vectors.

$$\mathbf{M}_{\rho-1}(\mathbf{x}) = \left(\mathbf{dh}, \ldots, \mathbf{d}(L_{\mathbf{f}}^{\rho-1}\mathbf{h}), \mathbf{dw_1}, \ldots, \mathbf{dw}_{n-\rho}\right)^T \tag{C.23}$$

$$\begin{aligned} \mathbf{w} &= \mathbf{w}(\mathbf{x}) \\ \mathbf{z} &= \mathbf{t}(\mathbf{x}) = (h(\mathbf{x}), L_{\mathbf{f}}h(\mathbf{x}), \ldots, L_{\mathbf{f}}^{\rho-1}h(\mathbf{x}))^T \end{aligned} \tag{C.24}$$

C.4.2 Input-state linearizing controller

The single input system (C.1) is said to be *locally feedback linearizable* in a neighborhood $\mathcal{U}_o$ of the origin if there exist a local diffeomorphism $\mathbf{z} = \mathbf{t}(\mathbf{x})$ and a state feedback $u(\mathbf{x}) = k(\mathbf{x}) + \beta(\mathbf{x})v$, with $k(\mathbf{x})$, $\beta(\mathbf{x})$ smooth and $\beta(\mathbf{x}) \neq 0$ in $\mathcal{U}_o$ transforming the system in the canonical form (C.25) (Brunovsky controller form). v is considered as new input.

$$\frac{d\mathbf{z}}{dt} = \mathbf{A_c} \cdot \mathbf{z} + \mathbf{b_c} \cdot v \tag{C.25}$$

$$\mathbf{A_c} = \begin{pmatrix} 0 & 1 & 0 & \dots & 0 \\ 0 & 0 & 1 & \dots & 0 \\ \vdots & \vdots & \vdots & \vdots & \vdots \\ 0 & 0 & 0 & \dots & 0 \end{pmatrix} \quad \mathbf{b_c} = \begin{pmatrix} 0 \\ 0 \\ 0 \\ \vdots \\ 1 \end{pmatrix} \tag{C.26}$$

Theorem. The single input system (C.1) is *locally state feedback linearizable* if, and only if, in $\mathcal{U}_o$, a neighborhood of the origin:

1. $$span\left(\mathrm{g}, \dots, ad_{\mathbf{f}}^{(n-1)}\mathrm{g}\right) = \mathcal{R}^n \tag{C.27}$$

2. the distribution $\mathbf{G}_{n-2}$ is involutive and of constant rank $n-1$.

$$\mathbf{G}_{n-2}(\mathbf{x}) = span\left(\mathrm{g}, \dots, ad_{\mathbf{f}}^{(n-2)}\mathrm{g}\right) \tag{C.28}$$

Proof. 1. From the assumptions and the Frobenius theorem the existence of a smooth function h from $\mathcal{R}^n$ to $\mathcal{R}$, which satisfies the conditions (C.29), is guaranteed.

$$(< \mathbf{dh}, \mathrm{g} >, < \mathbf{dh}, ad_{(-\mathbf{f})}\mathrm{g} >, \dots, < ad_{(-\mathbf{f})}^{(n-1)}\mathrm{g} >) = (0, \dots, \gamma) \tag{C.29}$$

2. The transformation $\mathbf{z} = \mathbf{t}(\mathbf{x})$, defined by (C.30), is shown to be a local diffeomorphism by proving that its Jacobian $\dfrac{\partial \mathbf{t}}{\partial \mathbf{x}}$ is nonsingular (Inverse Function Theorem).

$$\mathbf{z} = \mathbf{t}(\mathbf{x}) = (h(\mathbf{x}), L_{\mathbf{f}}h(\mathbf{x}), \dots, L_{\mathbf{f}}^{(n-1)}h(\mathbf{x}))^T \tag{C.30}$$

3. The nonsingularity of the Jacobian of $\mathbf{t}(\mathbf{x})$ is proven by showing the nonsingularity of the matrix $\mathbf{N}(\mathbf{x})$ (C.32) (by using Leibniz formula and the conditions (C.29)) and the first condition of the theorem (nonsingularity of the matrix $\mathbf{G}_{n-1}(\mathbf{x})$).

$$\mathbf{G}_{n-1}(\mathbf{x}) = \left(\mathrm{g}, \dots, ad_{\mathbf{f}}^{(n-2)}\mathrm{g}\right) \tag{C.31}$$

$$\mathbf{N}(\mathbf{x}) = \frac{\partial \mathbf{t}(\mathbf{x})}{\partial \mathbf{x}} \cdot \mathbf{G}_{n-1}(\mathbf{x}) \tag{C.32}$$

4. The fact that the dynamics of the system in the z-space is in Brunovsky controller form follows from the definition (C.30) and from using Leibniz formula in combination with the conditions (C.29).

C.5 Nonlinear observer design

C.5.1 Canonical forms

Three canonical forms, often used in observer design, are shortly reviewed. Canonical forms are used because observer design for systems in canonical form is easier than for the original system. Without loss of generality single input (U)/single output (Y) nonlinear (time invariant) systems with 2 state variables (X_1, X_2) are considered in order to simplify the notations. The model system considered is of the general form (C.33). where g_1, g_2 and h are nonlinear functions.

$$\begin{aligned} \frac{dX_1}{dt} &= g_1(X_1, X_2, U) \\ \frac{dX_2}{dt} &= g_2(X_1, X_2, U) \\ Y &= h(X_1, X_2, U) \end{aligned} \tag{C.33}$$

1. Generalized observer canonical form (GOCF) [Keller 1987].
For the above 2 dimensional system (C.33) the GOCF reads as follows.

$$\begin{aligned} \frac{dZ_1}{dt} &= -\ a_0(Y, U, U^{(1)}, U^{(2)}) \\ \frac{dZ_2}{dt} &= Z_1 - a_1(Y, U, U^{(1)}) \end{aligned} \tag{C.34}$$

The state Z_2 is a nonlinear function $c(Y, U)$ of the output Y and the input U. $U^{(n)}$ denotes the n-th derivative of U with respect to time. This canonical form is used by Keller for time invariant nonlinear systems (C.33). The input is considered explicitly in a general way. Two variants can be mentioned. Isidori uses this form for *autonomous* systems. Bestle and Zeitz consider *time varying* systems without considering an input explicitly. In that case the functions a_0 and a_1 are time varying.
2. Generalized observability canonical form (GOBCF) [Keller 1987].
In this canonical form, which is used as an intermediate form in the method of Keller, the output Y equals the state Z_1.

$$\begin{aligned} \frac{dZ_1}{dt} &= Z_2 \\ \frac{dZ_2}{dt} &= -a_{nl}(Z_1, Z_2, U, U^{(1)}, U^{(2)}) \end{aligned} \tag{C.35}$$

3. Observer canonical form [Gauthier *et al.* 1992].
This canonical form, which is used in the design of high gain observers, is only defined for models *affine* in the input U. The output Y again equals the state Z_1.

$$\begin{aligned} \frac{dZ_1}{dt} &= Z_2 + a_1(Z_1) \cdot U \\ \frac{dZ_2}{dt} &= -a(Z_1, Z_2) + a_2(Z_1, Z_2) \cdot U \end{aligned} \tag{C.36}$$

C.5.2 Observers without input derivatives

Exact linearization up to an output injection

The single input system (C.1) is said to be *locally exact linearizable up to an output injection* if there exist a diffeomorphism $\mathbf{z} = \mathbf{t}(\mathbf{x})$ in a neighborhood $\mathcal{U}_o$ of the origin transforming the system into the canonical form (C.37) with z_n equal to the output y.

$$\frac{d\mathbf{z}}{dt} = \mathbf{A_O} \cdot \mathbf{z} + \gamma(y,u) \tag{C.37}$$

$$\mathbf{A_O} = \begin{pmatrix} 0 & 0 & 0 & \dots & 0 & 0 \\ 1 & 0 & 0 & \dots & 0 & 0 \\ \vdots & \vdots & \vdots & \vdots & \vdots & \\ 0 & 0 & 0 & \dots & 1 & 0 \end{pmatrix} \tag{C.38}$$

Theorem. The single input system (C.1) is *locally exact linearizable up to an output injection* if, and only if, in $\mathcal{U}_o$, a neighborhood of the origin and for the vector field $\mathbf{r}(\mathbf{x})$, defined by the equations (C.39), the conditions (C.40, C.41, C.42) hold true.

$$\begin{pmatrix} < \mathbf{dh}, \mathbf{r} > \\ \vdots \\ < \mathbf{d}(L_\mathbf{f}^{(n-1)}\mathbf{h}), \mathbf{r} > \end{pmatrix} = \begin{pmatrix} 0 \\ \vdots \\ 1 \end{pmatrix} \tag{C.39}$$

1.

$$rank(\mathbf{H}_{n-1}(\mathbf{x})) = rank\left(\mathbf{dh}, \mathbf{d}(L_\mathbf{f}\mathbf{h}), .., \mathbf{d}(L_\mathbf{f}^{(n-1)}\mathbf{h})\right) = n \tag{C.40}$$

2.

$$\left[ad_\mathbf{f}^i\mathbf{r}, ad_\mathbf{f}^j\mathbf{r}\right] = 0 \quad 0 \le i,j \le n-1 \tag{C.41}$$

3.

$$\left[\mathbf{g}, ad_\mathbf{f}^j\mathbf{r}\right] = 0 \quad 0 \le j \le n-2 \tag{C.42}$$

Proof. 1. It is shown from the definition of the vector field $\mathbf{r}(\mathbf{x})$ and the first condition of the theorem that the vector fields (C.43) are linearly independent by applying Lemma C.3.2. This is proven by showing the nonsingularity of the matrix $\mathbf{N}(\mathbf{x})$.

$$\mathbf{R}_{n-1}(\mathbf{x}) = \left(\mathbf{r}, ad_{(-\mathbf{f})}\mathbf{r}, \dots, ad_{(-\mathbf{f})}^{(n-1)}\mathbf{r}\right) \tag{C.43}$$

$$\mathbf{N}(\mathbf{x}) = \mathbf{H}_{n-1}(\mathbf{x}) \cdot \mathbf{R}_{n-1}(\mathbf{x}) \tag{C.44}$$

2. From the linearly independence of the vector fields (C.43) and the second condition of the theorem one can observe that the Simultaneous Rectification Theorem holds true. This implies the existence of a local diffeomorphism, which simultaneously rectifies the vector fields (C.43). This results in the property (C.45).

$$ad_{(-\mathbf{f})}^i\mathbf{r} = \frac{\partial}{\partial z_{j+1}} \quad 0 \le j \le n-1 \tag{C.45}$$

3. From the property (C.45) the structure of $\mathbf{f}$ described in the $\mathbf{z}$-coordinates can be derived. From the property (C.45) and the third condition of the theorem the structure of $\mathbf{g}$ described in the $\mathbf{z}$-coordinates can be derived. From the structure of $\mathbf{f}$ and $\mathbf{g}$ one can show that the dynamics of the system in the $\mathbf{z}$-coordinates is in the required canonical form.

C.5.3 Observers with input derivatives

The nonlinear observer design method based on exact linearization up to an output injection, allowing input derivatives and an additional transformation of the output, is discussed. First the design method is shortly presented. Then this design methodology is compared with the method presented in Section C.5.2 and reformulated in the differential geometric framework. Finally the conditions appearing in the observer design methods are illustrated for a prototype model for biotechnological systems.

Exact linearisation up to an output injection

The single input system (C.1) is said to be *locally exact linearizable up to an output injection* if there exist a diffeomorphism $\mathbf{z} = \mathbf{t}(\mathbf{x}, u, u^{(1)}, \dots, u^{(n-1)})$ in a neighborhood $\mathcal{U}_o$ of the origin transforming the system into the canonical form (C.46) with $z_n = c(y,u)$ a nonlinear function of input u and output y.

$$\frac{d\mathbf{z}}{dt} = \mathbf{A_O} \cdot \mathbf{z} + \gamma(y, u, u^{(1)}, \dots, u^{(n)}) \tag{C.46}$$

The determination of the functions $\gamma_i, 1 \le i \le n$ and $c(y,u)$ is based on a two-step transformation. These functions are found by solving sets of partial differential equations. Conditions for a priori checking of the solvability of these sets of partial differential equations exist. The design method originates from differential algebraic techniques. *This design procedure is discussed in detail in Chapter 5 and 7.*

Reformulation in the differential geometric framework

In this section it is described how the nonlinear observer design method discussed here is related to the one treated in Section C.5.2. As such the

method, which originates from differential algebraic techniques, is reformulated in the differential geometric framework.

Step 1. Nonlinear transform of the output.

It is clear that the design method discussed here introduces *an extra degree of freedom* by allowing a nonlinear transformation of the output. Suppose that the state diffeomorphism is independent from the input and its derivatives. The observer design method can then be reformulated in the differential geometry framework as follows.

The single input system (C.1) is said to be *locally exact linearizable up to an output injection* if there exist a diffeomorphism $\mathbf{z} = \mathbf{t}(\mathbf{x})$ in a neighborhood $\mathcal{U}_o$ of the origin transforming the system into the canonical form (C.47) with $z_n = c(y)$ a nonlinear function of y.

$$\frac{dz}{dt} = \mathbf{A_O} \cdot \mathbf{z} + \gamma(y, u) \tag{C.47}$$

Theorem. The single input system (C.1) is *locally exact linearizable up to an output injection* if, and only if, in $\mathcal{U}_o$, a neighborhood of the origin, there exists a nonlinear function $c(y)$ of the output, such that for $h^\star(\mathbf{x}) = c(h(\mathbf{x}))$ and for the vector field $\mathbf{r}(\mathbf{x})$, defined by the partial differential equation (C.39), using $h^\star$ instead of h, the conditions (C.40), (C.41), (C.42) also expressed in $h^\star$ hold true.

It is easy to see that by considering $y^\star = c(y) = c(h(\mathbf{x})) = h^\star(\mathbf{x})$ as the new output of the system the method of Section C.5.2 can be applied. z_n will then equal the new output $y^\star$. The main difference is that now a transformation of the output has been performed.

Step 2. State diffeomorphism, dependent on the input signal.

Suppose that now a state diffeomorphism is allowed which is dependent on the input signal u but that the time-derivatives of the input signal are zero or u is constant. In fact the system can then be written in the form (C.48).

$$\frac{dx}{dt} = \mathbf{f}(\mathbf{x}) + \mathbf{g}(\mathbf{x})u = \mathbf{f}^\star(\mathbf{x}, u) \qquad y = h(\mathbf{x}) \tag{C.48}$$

The single input system (C.48) is said to be *locally exact linearizable up to an output injection* if there exist a diffeomorphism $\mathbf{z} = \mathbf{t}(\mathbf{x}, u)$ in a neighborhood $\mathcal{U}_o$ of the origin, which can be explicitly dependent on the input u, transforming the system into the canonical form (C.49) with $z_n = c(y, u)$ a nonlinear function of y and u.

$$\frac{dz}{dt} = \mathbf{A_O} \cdot \mathbf{z} + \gamma(y, u) \tag{C.49}$$

Theorem. The single input system (C.48) is *locally exact linearizable up to an output injection* if, and only if, in $\mathcal{U}_o$, a neighborhood of the origin, there exists a nonlinear function $c(y, u)$ of the output, such that for

$h^\star(\mathbf{x}) = c(h(\mathbf{x}), u)$ and for the vector field $\mathbf{r}(\mathbf{x})$, defined by the partial differential equation (C.39), expressed in $h^\star$ and $f^\star$, the conditions (C.40), (C.41) also expressed in $h^\star$ and $\mathbf{f}^\star$ hold true.

It is trivial that in this case again an *extra degree of freedom* is introduced by allowing the state diffeomorphism to be dependent on the input u. Notice that the input u can just be considered as a parameter because u is assumed to be constant. Observe that the conditions on g are removed. This model part is however included in $\mathbf{f}^\star$ by definition.

Step 3. State diffeomorphism, dependent on the input signal and its derivatives.

Suppose that now the assumption that the input u is constant, is removed and that a state diffeomorphism is allowed depending on the input signal u and its time-derivatives $u^{(1)}, \ldots, u^{(n-1)}$.

The single input system (C.48) is *locally exact linearizable up to an output injection* if there exist a diffeomorphism $\mathbf{z} = \mathbf{t}(\mathbf{x}, u, u^{(1)}, \ldots, u^{(n-1)})$ in a neighborhood $\mathcal{U}_o$ of the origin, which can be explicitly dependent on the input u and its time-derivatives up to order $(n\text{-}1)$, transforming the system into the canonical form (C.50) with $z_n = c(y, u)$ a nonlinear function of y and u.

$$\frac{dz}{dt} = \mathbf{A_O} \cdot \mathbf{z} + \gamma(y, u, u^{(1)}, \ldots, u^{(n-1)}) \tag{C.50}$$

The dynamics of $\mathbf{z}$ are found by applying the chain rule for differentiation on the state transformation and results in equation (C.51).

$$\frac{dz}{dt} = \frac{\partial \mathbf{t}(\mathbf{x}, u, u^{(1)}, .., u^{(n-1)})}{\partial \mathbf{x}} \mathbf{f}^\star(\mathbf{x}, u) + \sum_{i=0}^{n-1} \frac{\partial \mathbf{t}(\mathbf{x}, u, u^{(1)}, .., u^{(n-1)})}{\partial u^{(i)}} \frac{du^i}{dt} \tag{C.51}$$

Theorem. The single input system (C.48) is *locally exact linearizable up to an output injection* if, and only if, in U_o, a neighborhood of the origin, there exists a nonlinear function $c(y, u)$ of the output, such that for $h^\star(\mathbf{x}) = c(h(\mathbf{x}), u)$ and for the vector field $\mathbf{r}$, defined by the partial differential equations (C.39), expressed in $h^\star$ and $\mathbf{f}^\star$, the conditions (C.40), (C.41), also expressed in $h^\star$ and $\mathbf{f}^\star$, and condition (C.52) hold true.

$$\left[\frac{\partial \mathbf{t}(\mathbf{x}, u, u^{(1)}, \ldots, u^{(n-1)})}{\partial u^{(i)}}, ad^j_{\mathbf{f}} \mathbf{r} \right] = 0 \quad 0 \leq j \leq n-2 \quad 0 \leq i \leq n-1 \tag{C.52}$$

The condition (C.41) guarantees that the part of the equation (C.51) due to the partial derivative of the state transformation with respect to the state $\mathbf{x}$ is in the suitable form. The extra condition (C.52) ensures that the part of the equation (C.51) related to the partial derivative of the state transformation with respect to the input signal and its derivatives is only function of the state z_n. Notice that this condition is similar to the condition, required for g, in the method presented in Section C.5.2.

Example The system under consideration (C.53) is a prototype model for biotechnological processes. C_X and C_S are the biomass and substrate concentration in a reactor. On-line biomass measurements are assumed to be available ($Y = C_X$). The goal is to design a nonlinear observer for estimation of the substrate concentration.

$$\begin{array}{rcl} \frac{dC_X}{dt} &=& aC_XC_S - C_XU \\ \frac{dC_S}{dt} &=& bC_XC_S - C_SU + C_{S,in}U \end{array} \qquad \text{(C.53)}$$

Step 1. Observer design without output transformation and state diffeomorphism independent from the input.
It can easily be verified that the conditions of the theorem of Section C.5.2 are not fulfilled. In a first step the observability vector field $\mathbf{r}$ is determined from the set of partial differential equations (C.54).

$$\begin{pmatrix} < \mathbf{dh}, \mathbf{r} > \\ < \mathbf{d}(L_\mathbf{f}\mathbf{h}), \mathbf{r} > \end{pmatrix} = \begin{pmatrix} 0 \\ 1 \end{pmatrix} \quad \mathbf{r} = \begin{pmatrix} 0 \\ \frac{1}{aC_X} \end{pmatrix} \qquad \text{(C.54)}$$

The Lie-brackets $ad^0_\mathbf{f}\mathbf{r}$ and $ad^1_\mathbf{f}\mathbf{r}$ are first determined.

$$ad^0_\mathbf{f}\mathbf{r} = \mathbf{r} \quad ad_\mathbf{f}\mathbf{r} = \begin{pmatrix} -1 \\ -\frac{C_S}{C_X} - \frac{b}{a} \end{pmatrix} \qquad \text{(C.55)}$$

$$[ad^0_\mathbf{f}\mathbf{r}, ad^1_\mathbf{f}\mathbf{r}] = \begin{pmatrix} 0 \\ -\frac{2}{aC_X^2} \end{pmatrix} \quad [\mathbf{g}, \mathbf{r}] = \begin{pmatrix} 0 \\ \frac{2}{aC_X} \end{pmatrix} \qquad \text{(C.56)}$$

From equation (C.56) it is clear that the conditions of the theorem of Section C.5.2 are not fulfilled.
Step 2. Observer design based on nonlinear transformation of the output and a state diffeomorphism, dependent on the constant input signal.
Suppose that not the output Y is used in the observer but a new input $Y^\star = \ln(Y)$ or $h^\star = \ln(C_X)$. Further it is assumed that the input U is constant. The vector field $\mathbf{f}^\star$ is given below.

$$\mathbf{f}^\star = \begin{pmatrix} \mathbf{f}_1^\star \\ \mathbf{f}_2^\star \end{pmatrix} = \begin{pmatrix} aC_XC_S - UC_X \\ bC_XC_S - UC_S + UC_{S,in} \end{pmatrix} \qquad \text{(C.57)}$$

Again the observability vector field $\mathbf{r}$ is determined from the set of partial differential equations (C.58).

$$\begin{pmatrix} < \mathbf{dh}^\star, \mathbf{r} > \\ < \mathbf{d}(L_{\mathbf{f}^\star}\mathbf{h}^\star), \mathbf{r} > \end{pmatrix} = \begin{pmatrix} 0 \\ 1 \end{pmatrix} \quad \mathbf{r} = \begin{pmatrix} 0 \\ \frac{1}{a} \end{pmatrix} \qquad \text{(C.58)}$$

$$ad_{\mathbf{f}^\star}\mathbf{r} = -\begin{pmatrix} C_X \\ \frac{bC_X}{a} - \frac{U}{a} \end{pmatrix} \quad [ad^0_{\mathbf{f}^\star}\mathbf{r}, ad^1_{\mathbf{f}^\star}\mathbf{r}] = \begin{pmatrix} 0 \\ 0 \end{pmatrix} \qquad \text{(C.59)}$$

It can easily be verified that the observability condition (C.40) is fulfilled. From (C.59) it follows that the conditions of the theorem, discussed in Section C.5.3, step 2 are fulfilled. The state transformation (C.60) results in the canonical form (C.61), enabling a linear design up to an output injection.

$$W_1 = aC_S - bC_X + U\ln(C_X) \quad W_2 = \ln(C_X) \qquad \text{(C.60)}$$

$$\begin{array}{rcl} \frac{dW_1}{dt} &=& aUC_{S,in} + bUe^{Y^\star} - U^2 \\ \frac{dW_2}{dt} &=& W_1 + be^{Y^\star} - UY^\star - U \end{array} \qquad \text{(C.61)}$$

Step 3. Observer design based on nonlinear transformation of the output and a state diffeomorphism, dependent on the input signal and its time derivatives.
When the input U is not constant and the state diffeomorphism (C.60) is used, the canonical form (C.62) is obtained. Condition (C.52) guarantees that the vector field, related to the input derivatives, is only function of $y^\star = \ln(C_X)$. Equation (C.63) shows that the condition (C.52) is fulfilled.

$$\begin{array}{rcl} \frac{dW_1}{dt} &=& aUC_{S,in} + bUe^{Y^\star} - U^2 + \ln(C_X)\frac{dU}{dt} \\ \frac{dW_2}{dt} &=& W_1 + be^{Y^\star} - UY^\star - U + 0\frac{dU}{dt} \end{array} \qquad \text{(C.62)}$$

$$[\begin{pmatrix} \ln(C_X) \\ 0 \end{pmatrix}, \mathbf{r}] = -\begin{pmatrix} -\frac{1}{C_X} & 0 \\ 0 & 0 \end{pmatrix}\begin{pmatrix} 0 \\ \frac{1}{a} \end{pmatrix} = \begin{pmatrix} 0 \\ 0 \end{pmatrix} \qquad \text{(C.63)}$$

C.6 Conclusions

In this appendix *observer* and *controller* design methods, used in Chapters 5 and 7, are presented.

It is illustrated that the observer design method, using a state transformation which is function of the input and a nonlinear transformation of the output, is suited for the prototype model for bioprocesses.

This method, which originates from *differential algebraic* techniques, is reformulated in the *differential geometric* framework. This reformulation enables the study of the combined observer-controller problem in the same framework (Chapter 7).

Appendix D

Notations, units and parameter values

In this appendix some information on the hard- and software used is provided. Also the notation and units of the variables and the parameter values, used throughout the different chapters, are given.

Hard- and software

The simulations are performed under the operating system DOS-WINDOWS in a PC-environment. The programming language FORTRAN in combination with the NAG-library (Numerical Algorithm Group) and MATLAB for WINDOWS are used. Some calculations are done in MATHEMATICA. The text processing is performed in EMTEX.

The data-acquisition software WISCON and the RODTOX-sensor (KELMA B.V.B.A.) is used on the wastewater treatment plants of SEGHERSengineeringWater NV.

Data-acquisition for the fermentation processes is realized with a combination of AFS (New Brunswick Scientific Inc.) and LABVIEW (National Instruments Co.). A Bioflo III fermentor (New Brunswick Scientific Inc.) is used.

Parameter	Dimension
Substrate concentration C_S	kgBOD/m^3
Biomass concentration C_X	kgBOD/m^3
Inert biomass concentration C_{X_d}	kgBOD/m^3
Substrate concentration in the influent $C_{S,in}$	kgBOD/m^3
Specific biomass growth rate μ_{max}	1/h
Monod constant K_S	kgBOD/m^3
Yield biomass on substrate $Y_{X/S}$	-
Specific biomass decay rate K_d	1/h
Sludge thickening coefficient β	-
Sludge waste fraction w	-
Influent flow rate F	m^3/h
Volume of a single tank V	m^3
Duration of the main phase T_{main}	h
Duration of the intermediate phase T_{inter}	h

Table D.1: Notations used in Chapter 1 for the single stage system

Parameter	Dimension	Value
μ_{max}	1/h	0.16
K_S	kgBOD/m^3	0.016
K_d	1/h	0.0075
$Y_{X/S}$	-	0.73
$C_{S,in}$	kgBOD/m^3	0.8
V	m^3	290
β	-	3
w	-	0.033
F	m^3/h	75
T_{main}	h	3
T_{inter}	h	1

Table D.2: Parameter values used in Chapter 1 for the single stage system

Parameter	Dimension
Rapidly degradable substrate concentration $C_{S,r}$	kgBOD/m^3
Slowly degradable substrate concentration $C_{S,s}$	kgBOD/m^3
Biomass concentration C_X	kgBOD/m^3
Inert biomass concentration C_{X_d}	kgBOD/m^3
Substrate concentration in the influent $C_{S,in}$	kgBOD/m^3
Specific biomass growth rate $\mu_{max,r}$	1/h
Specific biomass growth rate $\mu_{max,s}$	1/h
Monod constant K_{S_r}	kgBOD/m^3
Monod constant K_{S_s}	kgBOD/m^3
Yield biomass on rapidly degradable substrate $Y_{X/S,r}$	-
Yield biomass on slowly degradable substrate $Y_{X/S,s}$	-
Specific biomass decay rate $K_{d,r}$	1/h
Specific biomass decay rate $K_{d,s}$	1/h
Sludge thickening coefficient β	-
Sludge waste fraction w	-
Influent flow rate F	m^3/h
Volume of a single tank V	m^3
Duration of the main phase T_{main}	h
Duration of the intermediate phase T_{inter}	h

Table D.3: Notations used in Chapter 1 for the two stage system

Parameter	Dimension	Value
$\mu_{max,r}$	1/h	0.05
$\mu_{max,s}$	1/h	0.05
$K_{S,r}$	kgBOD/m^3	0.016
$K_{S,s}$	kgBOD/m^3	0.016
$K_{d,r}$	1/h	0
$K_{d,s}$	1/h	0
$Y_{X/S,r}$	-	0.5
$Y_{X/S,s}$	-	0.5
$C_{S,in}$	kgBOD/m^3	0.8
V	m^3	875
β	-	1
w	-	0.1
F	m^3/h	50
T_{main}	h	3
T_{inter}	h	1

Table D.4: Parameter values used in Chapter 1 for the two stage system

Parameter	Dimension	Value
μ'_m	1/h	2.1
K_{S_1}	g/L	10
K_{I_1}	g/L	0.1
K_{S_2}	g/L	40
K_{I_2}	g/L	0.1
Y_1	gDW/g	0.4
Y_2	gDW/g	0.6
m_1	g/h	0.2
m_2	g/h	0.4
K_{M_1}	g/L	10
K_{M_2}	g/L	40
$C^\star_{S_1}$	g/L	1
$C^\star_{S_2}$	g/L	2
V_{Max}	L	10
$V_\star$	L	7
u_1^{max}	L/h	0.8
u_2^{max}	L/h	1.2
$C_{S_1,in}$	g/L	400
$C_{S_2,in}$	g/L	600
α_1	g	800
α_2	g	400

Table D.5: Parameter values and constraints used in Chapter 2

Parameter	Dimension
Biomass amount in the reactor X	gMLSS
Biomass concentration C_X	gMLSS/L
Substrate amount in the reactor S	COD
Substrate concentration C_S	mgCOD/L
Oxygen amount in the reactor O	mgO_2
Oxygen concentration C_O	mgO_2/L
Volume of the reactor V	L
The specific biomass growth rate μ	1/h
The specific substrate consumption rate σ	mgCOD/gMLSS h
The maximal specific biomass growth rate μ_{max}	1/h
The Monod constant K_S	mgCOD/L
Yield biomass on substrate $Y_{X/S}$	gMLSS/mgCOD
Yield biomass on oxygen $Y_{X/O}$	mgO_2/gMLSS
Endogenous respiration coefficient m	mgO_2/gMLSS h
Dilution rate D	1/h
Flow rate F	L/h
Dose of wastewater to be treated ξ	L
Dose of wastewater added κ	L
Substrate concentration in the influent $C_{S,in}$	mgCOD/L
Unit cost due to effluent disposal α	\$ L/mgCOD
Unit cost due to aeration β	\$ L/mg O_2
Duration of the treatment process T	h
Oxygen uptake rate OUR	mgO_2/L h
Endogenous respiration OUR_{end}	mgO_2/L h
Exogenous respiration OUR_{ex}	mgO_2/L h

Table D.6: Notations used in Chapter 3

Parameter	Dimension	Value
μ_{max}	1/min	0.01
K_S	kgCOD/m^3	0.9
$Y_{X/S}$	kgMLSS/kgCOD	0.5
$Y_{X/O}$	kgMLSS/kgO_2	2
m	kgO_2/gMLSS min	0.0001
$C_{S,in}$	kgCOD/m^3	4
V	m^3	1000
β	\$ L/mgCOD	1
α	\$ L/mgO_2	1

Table D.7: Parameters values used in Chapter 3

Parameter	Dimension
Substrate concentration C_S	mgCOD/L
Biomass concentration C_X	gMLSS/L
Oxygen concentration C_O	mgO_2/L
Substrate concentration in the influent $C_{S,in}$	mgCOD/L
Biomass concentration in the influenht $C_{X,in}$	gMLSS/L
Inverse of the yield biomass on substrate k_1	mgCOD/gMLSS
Inverse of the yield biomass on oxygen k_3	mgO_2/gMLSS
Specific biomass growth rate μ	1/h
Dilution rate D	1/h
Oxygen transfer coefficient k_La	1/h
Oxygen saturation concentration C_{SAT}	mgO_2/L

Table D.8: Notations used in Chapter 4, Section 4.2

Parameter	Dimension	Value
$C_{X_A}(0)$	gMLSS/L	0.4
$C_{X_H}(0)$	gMLSS/L	4
$C_{NH_4}(0)$	kg/m^3	0.05
$C_{NO_X}(0)$	kg/m^3	0.04
$C_C(0)$	kg/m^3	0.1
$C_O(0)$	kg/m^3	0
V	m^3	0.4
$C_{NH_4,in}$	kg/m^3	0.1
F	m^3/min	1
p_1	mV	-100
p_2	mV	300
p_3	mV	-100
p_4	mV	200

Table D.9: Parameter values used in Chapter 4, Section 4.3

Parameter	Dimension	Value
$C_{S,in}$	g/L	6
a	L/gh	1
b	L/gh	-2
μ_{max}	1/h	0.20
K_S	g/L	0.40
K_I	g/L	40
$Y_{X/S}$	-	0.5
m	1/h	0.05

Table D.10: Parameter values used in Chapter 7

Appendix E

Bibliography

1. J.P. Axelsson 1989. Modelling and control of fermentation processes. *PhD thesis*, Lund Institute of Technology (Sweden)

2. A.N. Atassi and H.K. Khalil 1997. A nonlinear separation principle for the stabilization of a class of nonlinear systems. *Proceedings of the 1997 European Control Conference*, Brussels (Belgium), 2 WE-A-A 1-6

3. S.P. Banks 1981. A note on non-linear observers. *Int. J. Control*, 34 (1), 185-190

4. G. Bastin and D. Dochain 1990. *On-line estimation and adaptive control of bioreactors.* Elsevier Science Publishing Co., Amsterdam (The Netherlands)

5. M.B. Beck 1986. Identification, estimation and control of biological wastewater treatment processes. *IEE Proceedings*, 133 (5), 254-264

6. D. Bestle and M. Zeitz 1983. Canonical form observer design for non-linear time variable systems. *Int. J. Control*, 38 (2), 419-431

7. M. Bieswal 1995. *Modelisation mathematique de stations d'epuration d'eau par boues activees selon le systeme UNITANK®* . Mémoire, Faculté des Sciences Agronomiques, Universite Catholique De Louvain

8. A.E. Bryson and Y.C. Ho 1975. *Applied optimal control.* Hemisphere, Washington (USA)

9. J.B. Busby and J.F. Andrews 1975. Dynamical modeling and control strategies for the activated sludge process. *Journal WPCF*, 47 (5), 1055-1080

10. L. Cazzador 1987. On the optimal control of fed-batch reactors with substrate-inhibited kinetics. *Biotechnology and Bioengineering*, 31, 670-674

11. C. Cenens, V. Ryckaert and J. Van Impe 1997. On the interaction between biodegradation and sedimentation in activated sludge wastewater treatment systems. *Mededelingen Fac. Landbouww. Univ. Gent*, 62 (4b), 1633-1640

12. L. Chen 1992. Modelling, identifiability and control of complex biotechnological processes. *PhD thesis*, Université Catholique de Louvain (Belgium)

13. J.E. Claes, V.G. Ryckaert, J.F. Van Impe, R. Gerards and L. Vriens 1996a. Mathematical modeling and identification of UNITANK® wastewater treatment systems. *European Water Pollution Control*, 6 (6), 34-44

14. J.E. Claes, V.G. Ryckaert and J.F. Van Impe 1996b. Modelling and identification of the specific growth rate and the oxygen uptake rate on a full scale wastewater treatment system. P. Borne, R. Soenen, Y. Sallez and S. El Khattabi (Eds.), *Computational Engineering in Systems Applications 1996, Volume 1: Modelling, Analysis and Simulation*, GERF EC Lille - Cité Scientifique, Villeneuve d'Ascq, 142-147

15. J.E. Claes, V.G. Ryckaert, R. Gerards, L. Vriens and J.F. Van Impe 1997. Modeling, monitoring and control of cyclically operated biological wastewater treatment plants. *Proceedings of the 1997 European Control Conference*, Brussels (Belgium), 4 TH-A H1 1-6

16. C. de Prada, R. Moreno, M. Poch and J. Robuste 1991. Recursive estimation of OUR in activated sludge processes. *Proceeding of the 1991 European Control Conference*, Grenoble (France), 2, 1648-1653

17. I. Derese and E.J. Noldus 1980. Nonlinear control of bilinear systems. *IEE Proc.*, 127 (4), 169-175

18. D. Dochain and M. Perrier 1994. Recent approaches to the dynamical modelling, analysis, monitoring and control design for nonlinear bioprocesses. *Trends in Chem. Engineering*, 2, 215-251

19. D. Dochain and M. Perrier 1995. Adaptive linearizing control of the activated sludge process. *Pulp and Paper Canada*, 96 (12), 421-425

20. H.E. Emara-Shabaik and C.T. Leondes 1981. Non-linear filtering-the link between Kalman and extended Kalman filters. *Int. J. Control*, 34 (6), 1207-1214

21. J.P. Gauthier, H. Hammouri and S. Othman 1992. A simple observer for nonlinear systems, applications to bioreactors. *IEEE Transactions on Automatic Control*, 37 (6), 875-880

22. S. Ghekiere, L. Vriens, P. Delaplace, A. Van Haute and H. Verachtert 1990. The application of enhanced biological nitrogen and phosphorus removal on UNITANK® systems: optimisation, simulation and modelling of the process configurations. *Proc. Int. Conf. Environmental planning and management*, Roorkee (India), 472-479

23. G.J. Haarsma and K. Keesman 1995. Robust model predictive dissolved oxygen control. *Mededelingen Fac. Landbouww. Univ. Gent*, 60 (4b), 2415-2425

24. H. Hammouri and J.P. Gauthier 1992. Global time varying linearisation up to output injection. *SIAM J. Control and Optimization*, 30 (6), 1295-1310

25. H. Hammouri and J.P. Gauthier 1988. Bilinearisation up to output injection. *Systems and Control Letters*, 11, 139-149

26. H. Hammouri and M. Kinnaert 1994. A new procedure for time varying linearisation up to output injection. *Technical Report*, Faculté des Sciences Appliquées, Service d'Automatique, Université Libre de Bruxelles (Belgium)

27. A. Héduit and D.R. Thévenot 1989. Relation between redoxpotential and oxygen levels in activated sludge reactors. *Water Science and Technology*, 21, 946-956

28. A. Héduit and D.R. Thévenot 1992. Elements in the interpretation of platinium electrode potentials in biological treatment. *Water Science and Technology*, 26, 1335-1344

29. M.A. Henson and D.E. Seborg 1992. Nonlinear control strategies for continuous fermentors. *Chem. Eng. Sci.*, 47, 821-835

30. M. Henze, W. Gujer, T. Mino, T. Matsuo, M.C. Wentzel and G.v.R. Marais G.v.R. 1995. *Activated Sludge Model No. 2.* Scientific and Technical Report No. 3, International Association on Water Quality, London (UK)

31. C. Herremans, V. Ryckaert and J. Van Impe 1997. Calculation of carbon addition during biological nitrogen removal by using optimal control theory. *Mededelingen Fac. Landbouww. Univ. Gent*, 62 (4b), 1691-1694

32. A. Holmberg 1982. Modelling of the activated sludge process for microprocessor-based state estimation and control. *Water Research*, 16, 1233-1246

33. A. Holmberg 1982. On the practical identifiability of microbial growth models. Incorporating Michaelis-Menten type nonlinearities. *Mathematical Biosciences*, 62, 23-43

34. L.R. Hunt and S. Verma Madanpal 1994. Observers for nonlinear systems in steady state. *IEEE Transactions on Automatic Control*, 39 (10), 2113-2117

35. S. Isaacs 1996. Short horizon control strategies for an alternating activated sludge process. *Proceedings of the IAWQ Water Quality Conference*, Singapore, June

36. A. Isidori 1989. *Nonlinear control systems.* Springer-Verlag, Berlin (Germany)

37. T. Kailath 1980. *Linear systems.* Prentice Hall, Englewood Cliffs (New Jersey)

38. H. Khalil 1992. *Nonlinear systems.* Macmillan Publishing Company, New York

39. H. Keller 1987. Nonlinear observer design by transformation into generalized observer canonical form. *Int. J. Control*, 46 (6), 1915-1930

40. M. Keulers 1993. Identification and control of a fed-batch process - application to culture of *Saccharomyces cerevisiae*. *PhD thesis*, Technische Universiteit Eindhoven (The Netherlands)

41. D.E. Kirk 1970. *Optimal control theory: an introduction.* Prentice Hall, Englewood Cliffs (New Jersey)

42. FA. Koch and W.K. Oldham 1985. Oxidation-reduction potential: a tool for monitoring control and optimization of biological nutrient removal systems. *Water Science and Technology*, 17, 259-281

43. A.J. Krener and W. Respondek 1985. Nonlinear observers with linearizable error dynamics. *SIAM J. Control and Optimization*, 23 (2), 197-216

44. M. Krstic, I. Kanellakopoulos and P. Kokotovic 1995. *Nonlinear and adaptive control design.* John Wiley & Sons, New York (USA)

45. F. Lamnabhi-Lagarrigue 1987. Singular optimal control problems - on the order of a singular arc. *Systems and Control Letters*, 9, 173-182

46. A. Levin 1992. Neural network in dynamical systems. *PhD thesis*, Yale University (USA)

47. H.C. Lim, Y.J. Tayeb, J.M. Modak and P. Bonte 1986. Computation algorithms for optimal feed rate for a class of fed-batch fermentation: numerical results for prenicillin and cell mass production. *Biotechnology and Bioengineering*, 28, 1408-1420

48. R. Marino and P. Tomei 1995. *Nonlinear control design - geometric, adaptive and robust*, Prentice Hall, London (UK)

49. S. Marsili-Libelli 1989. Modelling, identification and control of the activated sludge process. *Advances in Biochemical Engineering/Biotechnology*, 38, 89-148

50. S. Marsili-Libelli 1992. Deterministic and fuzzy control of the sedimentation process. *Mededelingen Fac. Landbouww. Univ. Gent*, 61 (4a), 2229-2239 [*Proceedings of the 1992 Forum for Applied Biotechnology*, Brugge (Belgium)]

51. P.E. Moraal and J.W. Grizzle 1995. Observer design for nonlinear systems with discrete time measurements. *IEEE Transactions on Automatic Control*, 40 (3), 395-404

52. J.M. Modak, H.C. Lim and Y.J. Tayeb 1986. General characteristics of optimal feed rate profiles for various fed-batch fermentation processes. *Biotechnology and Bioengineering*, 28, 1396-1407

53. J.M. Modak and H.C. Lim 1987. Feedback optimization of fed-batch fermentations. *Biotechnology and Bioengineering*, 30, 528-540

54. J.M. Modak and H.C. Lim 1989. Simple nonsingular control approach to fed-batch fermentation optimization. *Biotechnology and Bioengineering*, 33, 11-15

55. J. Moubaraki, G. Bastin and J. Levine 1993. Nonlinear control of biotechnological processes with growth-production decoupling. *Mathematical biosciences*, 116, 21-44.

56. T. Proll and N.M. Karim 1994. Nonlinear control of a bioreactor model using exact and input/output linearization. *Int. J. Control*, 60 (4), 499-519

57. S.J. Parulekar and H.C. Lim 1985. Modeling, optimization and control of semi-batch bioreactors. *Advances in Biochemical Engineering*, 32, 207-258

58. S.J. Parulekar 1992. Analytical optimization of some single-cycle and repeated fed-batch fermentations. *Chemical Engineering Science*, 47, 4077-4077

59. L.S. Pontryagin, V.G. Boltyanskii, R.V. Gamkrelidze and E.F. Mishchenko 1962. *The mathematical theory of optimal processes.* Wiley Interscience, New York (USA)

60. V.G. Ryckaert, J.F. Van Impe, J. Curinckx and K. Van Gool 1994. State space analysis of periodic biological wastewater treatment plants. *Mededelingen Fac. Landbouww. Univ. Gent*, 59 (4a), 2047-2055

61. V.G. Ryckaert, J.E. Claes, C.H. Herremans, J.F. Van Impe, R. Gerards and L. Vriens 1995. Observer based estimation of oxygen uptake rates in cyclically operated wastewater treatment plants. *Mededelingen Fac. Landbouww. Univ. Gent*, 60 (4b), 2377-2384

62. V.G. Ryckaert, J.F. Van Impe, M. Feyaerts and L. Vriens 1996a Modelgebaseerde interpretatie van oxydo-reductie metingen. In: K. Gernaey (Editor), *Milieutechnologie in beweging*, ISBN 90 76019 02 9 - Technologisch Instituut VZW, Antwerpen (Belgie)

63. V.G. Ryckaert, J.E. Claes and J.F. Van Impe 1996b. Intelligent temperature control of an oven cavity for optimal microbiological safety and food quality. *Second European Symposium on Sous Vide*, 78-99, Acco, Leuven (Belgium)

64. V.G. Ryckaert and J.F. Van Impe 1996c. Design methodologies for nonlinear observers - application to biological models. P. Borne, R. Soenen, Y. Sallez and S. El Khattabi (Eds.), *Computational Engineering in Systems Applications 1996, Volume 1: Modelling, Analysis and Simulation*, GERF EC Lille - Cité Scientifique, Villeneuve d'Ascq, 1052-1057

65. V.G. Ryckaert, J.E. Claes, J.F. Van Impe, R. Gerards and L. Vriens 1996d. Optimal design and control of UNITANK® wastewater treatment systems. *Mededelingen Fac. Landbouww. Univ. Gent*, 61 (4a), 1799-1802

66. V.G. Ryckaert, C.H. Herremans, J.E. Claes, J.F. Van Impe, R. Gerards and L. Vriens 1997a. Modelling and dynamical analysis of UNITANK® wastewater treatment systems. *Mathematical Modelling of Systems*, 3(2), 159-180

67. V.G. Ryckaert and J.F. Van Impe 1997b. State and parameter estimation of bioprocess models - a case study. L.T. Grujić, P. Borne, A. El Moudni and M. Ferney (Eds.), *Control of Industrial Systems*, 3, 576-581, published for IFAC by Ecole Nationale d'Ingénieurs de Belfort

68. V.G. Ryckaert and J.F. Van Impe 1997c. Robustness analysis of nonlinear observers. *Proceedings of the 1997 European Control Conference*, Brussels (Belgium), 1 TU-E F5 1-6

69. V.G. Ryckaert, T. Boelen, R. Sepulchre and J.F. Van Impe 1997d. Constructive nonlinear observer design. *Book of abstracts BeNeLux meeting on Systems and Control 1998*

70. V.G. Ryckaert, M. Feyaerts, L. Vriens, H. Verachtert and J.F. Van Impe 1998a. Redox based control in a UNITANK® nitrogen removal system. *Accepted for publication in European Water Management*

71. V.G. Ryckaert and J.F. Van Impe 1998b. Optimal tuning of software sensors for bioprocess control. *Proceedings of the ACoFoP, Automatic Control of Food and Biological Processes Conference*, Göteborg (Zweden)

72. V.G. Ryckaert, T. Boelen and J.F. Van Impe 1998c. Robustness of nonlinear observers. *Proceedings of NOLCOS98, IFAC Nonlinear Control Systems Design Symposium*, Enschede (The Netherlands)

73. V.G. Ryckaert and J.F. Van Impe 1998d. Optimal design and control of cyclically operated biological wastewater treatment plants. *Proceedings of CAB7, IFAC Conference on Computer Applications in Biotechnology*, Osaka (Japan)

74. V.G. Ryckaert and J.F. Van Impe 1998e. Optimal control of complex fed-batch bioprocesses. Part 1: generic properties, Part 2: case study. *Submitted to Control Engineering Practice*, [Technical Report BioTeC 97-03, Laboratory for Industrial Microbiology and Biochemistry, Katholieke Universiteit Leuven (Belgium)]

75. V.G. Ryckaert, T. Boelen, E. Jacobs and Jan F. Van Impe 1998f. Nonlinear observers for bioprocess monitoring. *Submitted to Mathematical Biosciences* [Technical Report BioTeC 98-04, Laboratory for Industrial Microbiology and Biochemistry, Katholieke Universiteit Leuven (Belgium)]

76. V.G. Ryckaert and J.F. Van Impe 1998g. Combined nonlinear observer-controllers Application to a prototype bioprocess model. *Submitted to IEEE Conference on Control Applications - Control Applications in Biological and Medical Systems*, Trieste (Italy) [Technical Report BioTeC 98-03, Laboratory for Industrial Microbiology and Biochemistry, Katholieke Universiteit Leuven (Belgium)]

77. V.G. Ryckaert, J.E. Claes and J.F. Van Impe 1998h. Model-based temperature control in ovens. *Submitted to Journal of Food Engineering*

78. R. Sepulchre, M. Jankovic and P. Kokotovic 1996. *Constructive nonlinear control.* Springer-Verlag, London (UK)

79. A. Teel and L. Praly 1995. Tools for semiglobal stabilization by partial state and output feedback. *SIAM J. Control and Optimization*, 33, 1443-1488

80. L. Van Campenhout and D. Iserentant 1996. The respiratory activity of barley and its natural microflora during germination in the malting process. Mededelingen Fac. Landbouww. Univ. Gent, 61 (4a), 1657-1660

81. K. Vandenbroeck 1996. *Identificatie van modelparameters voor een actief slib waterzuiveringsinstallatie volgens het UNITANK® principe.* Eindwerk, Departement Levensmiddelen- en Microbiële Technologie, Faculteit Landbouwkundige en Toegepaste Biologische Wetenschappen, Katholieke Universiteit Leuven

82. A.J. Van der schaft 1985. On nonlinear observers. *IEEE Transactions on Automatic Control*, AC-30 (12), 1254-1256

83. J.F. Van Impe, J. Vandewalle, P. Vanrolleghem and W. Verstraete 1992a. New trends in model-based monitoring and control of the activated sludge wastewater treatment process. *Journal A, Special Issue on Environmental Control*, 33 (3), 19-29

84. J.F. Van Impe, B. Nicola, T. Martens, J. De Baerdemaker and J. Vandewalle 1992b. Dynamic mathematical model to predict microbial growth and inactivation during food processing. *Applied and Environmental Microbiology*, 58 (9), 2901-2909

85. J.F. Van Impe 1993a. *Modeling and optimal adaptive control of biotechnological processes.* Birkhäuser, Boston (USA). Also available as: *PhD thesis*, Katholieke Universiteit Leuven (Belgium)

86. J.F. Van Impe and G. Bastin 1993b. Optimal adaptive control of fed-batch fermentation processes with multiple substrates. *Proceedings of the 2nd* IEEE *Conference on Control Applications , Vancouver, British Columbia (Canada), September 13-16, 1993*, 469-474, IEEE Catalog Number: 93CH3243-3

87. J.F. Van Impe and G. Bastin 1995a. Optimal adaptive control of fed-batch fermentation processes. *Control Eng. Practice*, 3(7), 939-954

88. J.F. Van Impe 1995b. Advanced monitoring and control of biotechnological processes - application to wastewater treatment processes. *Technical Report LIMB 1996-05*, Laboratory for Industrial Microbiology and Biochemistry, Katholieke Universiteit Leuven, 84 p. *Scientific Prize Barco N.V. 1995 of the Belgian National Fund for Scientific Research*

89. P. Vanrolleghem 1994. On-line modelling of activated sludge processes: development of an adaptive sensor. *PhD thesis*, Rijksuniversiteit Gent (Belgium)

90. M. Vidyasagar 1993. *Nonlinear systems analysis.* Prentice-Hall, London

91. D. Williamson 1977. Observation of bilinear systems with application to biological control. *Automatica*, 13, 243-254

92. Xiao-Hua Xia and Wei-Bin Gao 1989. Nonlinear observer design by observer error linearisation. *SIAM J. Control and Optimization*, 27, 199-216

93. C.B. Youssef, G. Roux and B. Dahhou 1995. Multivariable adaptive predictive control of nonlinear systems: application to a multistage wastewater treatment process. *Proceedings of the 1995 European Control Conference*, Rome (Italy), 3585-3590

Appendix F

Nederlandse samenvatting

F.1 Motivatie

Modelgebaseerde optimalisering en regeling van bioprocessen

Van theorie naar praktijk

Modelgebaseerde optimalisering en regeling is een algemeen geaccepteerde methodologie in toepassingsdomeinen zoals elektronica, thermodynamica en hydraulica. Het gebruik van een modelgebaseerde aanpak voor biologische processen, waarvan de hoofddynamica bepaald wordt door *levende* materie zoals bijvoorbeeld micro-organismen, wordt vaak bekritiseerd. Naast technische redenen, zoals de intrinsieke complexe, tijdsvariërende en niet-lineaire dynamica van biotechnologische processen, wordt feitelijk het mathematisch modelleren van dergelijke systemen in vraag gesteld. Twee belangrijke redenen voor het verwerpen van de modelleerbaarheid van bioprocessen kunnen worden aangeduid. Ten eerste is er het psychologisch feit dat mensen moeilijk accepteren dat systemen waarbij levende materie (in de limiet ook mensen) mathematisch beschrijfbaar zijn. Ten tweede is er vaak een verkeerd begrip van wat een model feitelijk is. Als de vergelijking met andere toepassingsdomeinen zoals elektronica en mechanica wordt gemaakt, wordt vaak gesteld dat voor de klasse van systemen in die disciplines basiswetten bekend zijn terwijl dit voor de biotechnologische processen slechts zelden het geval is. Men realiseert zich op dat moment onvoldoende dat deze fameuze fysische wetten slechts, zij het dan behoorlijk accuraat, modellen zijn van de realiteit.

Een eerste thema van dit doctoraatswerk is het beschrijven van de rol van het gebruikte procesmodel bij het modelgebaseerd optimaliseren en regelen van biotechnologische processen. Er wordt aangetoond dat excellente performantie met modelgebaseerde technieken kan worden bekomen zelfs al is het model slechts een ruwe benadering van de realiteit. Het is de robuustheidseigenschap van deze methodologieën dat de toepassing op bioprocessen mogelijk maakt.

Dit eerste thema wordt in de verschillende hoofdstukken als volgt uitgewerkt.

Hoofdstuk 1. Het modelleren van een biologisch afvalwaterzuiveringssysteem wordt bestudeerd. Er wordt aangetoond dat een eenvoudig procesmodel volstaat voor een diepgaande analyse van de hoofddynamica van een dergelijk proces. Daarenboven zijn de parameters van het bekomen model te bepalen in de praktijk.

Hoofdstuk 2 en 3. Optimale regelstrategieën voor bioprocessen worden afgeleid. De belangrijkste eigenschappen van de bekomen regelstrate-

gieën worden voornamelijk bepaald door *kwalitatieve* kennis van proceskinetiek.

Hoofdstuk 4. Observeerbaarheid van de toestanden en identifieerbaarheid van de modelparameters zijn bestudeerd. Het model fungeert hier als kader voor data interpretatie. Het concept van *minimale modellering* duidt hier aan dat een complete specificatie van het model absoluut onnodig is.

Hoofdstuk 5 en 7. De robuustheid van niet-lineaire toestandschatters en regelaars tegen zowel parametrische als structurele onzekerheid van het ontwerpmodel is gekarakteristeerd. De performantie van de diverse algoritmes blijft acceptabel voor behoorlijk realistische ordes van onzekerheid.

Hoofdstuk 6 en 7. Modelgebaseerde afstelling van niet-lineaire schatters en regelaars is bestudeerd. Er is aangetoond dat zelfs met modellen met een lage complexiteit belangrijke inzichten in het optimaal afstelprobleem worden bekomen.

Modelgebaseerde technieken in de elektronica en de mechanica zijn vaak ontwikkeld in het kader van lineaire tijdsinvariante systemen. Deze lineaire technieken zijn algemeen verspreid en erkend. Eventuele veranderingen in tijd en niet-lineair gedrag kan worden opgevangen door adaptieve methodes, gebaseerd op de beschikbaarheid van snelle en accurate *on-line* sensoren.

Door het intrinsieke niet-lineaire tijdsvariërende gedrag van bioprocessen en het gebrek aan goedkope, betrouwbare en accurate *on-line* sensoren dient men modelgebaseerde technieken voor biotechnologische processen in de eerste plaats binnen het kader van de niet-lineaire systeem en regeltechniek te ontwikkelen. Dit onderzoeksdomein is echter in volle ontwikkeling. Dit resulteert in een grote verscheidenheid aan concepten en notaties, die meestal vanuit puur mathematisch oogpunt worden ingevoerd. De in de literatuur beschreven methodes zijn op het eerste zicht trouwens niet altijd direct toepasbaar.

Het tweede thema van dit doctoraatsonderzoek omvat, in plaats van het ontwikkelen van nieuwe niet-lineaire technieken, het illustreren van het potentieel van de bestaande technieken, via diverse voorbeelden, en het introduceren van algemene concepten ter evaluatie van deze methodes vanuit het standpunt van de procesingenieur.

Dit thema is als volgt uitgewerkt in de verschillende hoofdstukken.

Hoofdstuk 1. Dynamische simulatie, toestandsruimte analyse en gevoeligheidsanalyse worden geïntroduceerd als technieken waarmee de hoofddynamica van het proces kan worden geanalyseerd.

Hoofdstuk 2 en 3. Er wordt aangetoond dat *optimal control* theorie (het minimum principe van Pontryagin) een krachtige wiskundige techniek is waarmee optimale regelingangen kunnen worden bepaald en dit ondanks de intrinsieke sensitiviteit van deze techniek voor modelonnauwkeurigheden. De resulterende optimale regelstrategieën fungeren als basis voor het ontwerp van praktisch implementeerbare regelaars.

Hoofdstuk 4. Analyse van de observeerbaarheid en identifieerbaarheid van de toestanden en parameters van het model is meer dan het evalueren van een aantal wiskundige eigenschappen van een model. Met dergelijke analyses kan een direct verband tussen het ontwerp van de installatie en de meetbaarheid ervan worden vastgesteld. Deze analyse kan eveneens worden gebruikt als een techniek voor het bepalen van een optimale investeringspolitiek met betrekking tot sensoren.

Hoofdstuk 5 en 7. Diverse ontwerpmethodologieën voor niet-lineaire toestandschatters en regelaars worden vergeleken en toegepast op een prototype model voor biotechnologische processen. Performantie-analyse wordt geïntroduceerd en blijkt een uitstekende techniek voor selectie van de geschikte toestandschatter en regelaar. De selectie-criteria zijn geïnspireerd vanuit het standpunt van de procesingenieur.

Hoofdstuk 6 en 7. De juiste afstelling van de diverse algoritmes (schatters en regelaars) is uitermate belangrijk. Optimale afstelling door middel van gecombineerde performantie en *trade-off* analyse is bestudeerd.

Een derde thema van dit doctoraatsonderzoek is het demonstreren van het potentieel van modelgebaseerd optimaliseren en regelen voor bioprocessen via het toepassen van deze technieken voor verschillende systemen.

De volgende voorbeelden worden bestudeerd.

Actief slib afvalwaterzuiveringssystemen. Het modelleren van koolstofverwijderingssystemen wordt bestudeerd in **Hoofdstuk 1**. Ook nitraat verwijderingssystemen worden kort beschreven in dit hoofdstuk. Een optimale regelstrategie voor het koolstofverwijderingssysteem wordt afgeleid in **Hoofdstuk 3**. De resultaten van de observeerbaarheids- en identifieerbaarheidsanalyse voor het prototype model worden geïnterpreteerd in het kader van koolstofverwijderingssystemen in **Hoofdstuk 4**. In hetzelfde hoofdstuk wordt het potentieel van de redoxpotentiaal als extra *on-line* meting in nitraatverwijderingssystemen aangegeven. Het optimaal afstellen van parameterschatters, toepasbaar bij koolstofverwijdering, wordt geïllustreerd in

Hoofdstuk 6. De resultaten, bekomen via deze schatters, worden gebruikt in **Hoofstuk 1** over modelleren.

Fermentatieprocessen. In **Hoofdstuk 2** worden optimale regelstrategieën afgeleid voor een fermentatieproces met 1 biomassa en meerdere limiterende substraten door middel van het minimum principe van Pontryagin. De optimale afstelling van parameter en toestandschatters voor een fermentatieproces wordt geanalyseerd in **Hoofdstuk 6**. De performantie van parameterschatters wordt geïllustreerd met echte data. Het afstelling van een niet-lineaire regelaar wordt eveneens besproken voor fermentatieprocessen in **Hoofdstuk 7**.

Het moet worden benadrukt dat het prototype model, gebruikt voor identifieerbaarheids- en observeerbaarheidsanalyse (**Hoofdstuk 4**), performantie analyse van niet-lineaire toestandschatters (**Hoofdstuk 5**) en regelaars (**Hoofdstuk 7**), zowel voor afvalwaterzuiveringssystemen als voor fermentatieprocessen kan worden gebruikt.

Conceptueel gezien zijn modelleren, optimaliseren, meten en regelen van (bio-)processen sterk gerelateerde problemen. De resulterende optimale regelstrategie hangt af van het model terwijl de implementeerbaarheid van de bekomen strategie afhangt van eigenschappen zoals meetbaarheid en stuurbaarheid van het model. Vanuit deze observatie zou men kunnen besluiten dat het modelleren, optimaliseren en het ontwerp van schatters en regelaars simultaan moet gebeuren. Dit is praktisch niet haalbaar.

Een vierde en laatste thema van dit doctoraatswerk is het illustreren dat modelgebaseerde optimalisering en regeling grofweg in vier subproblemen kan worden verdeeld: (i) modelleren, (ii) afleiden van een optimale regelstrategie, (iii) ontwerp van schatters en (iv) ontwerp van regelaars. Problemen ten gevolge van interacties tussen de verschillende subproblemen kunnen worden vermeden mits in acht nemen van een aantal vuistregels. De opdeling in vier subproblemen wordt ook weerspiegeld in de structuur van het doctoraat.

Modellering. In **Hoofdstuk 1** wordt het modelleren van een cyclisch opererend actief slib afvalwaterzuiveringssysteem voor koolstofverwijdering bestudeerd.

Het ontwerp van modellen met een lage complexiteit voorkomt problemen bij de optimalisering van het proces en ontwerp van schatters en regelaars.

Optimalisering. In **Hoofdstuk 2 en 3** worden de optimalisering van respectievelijk fermentatieprocessen en afvalwaterzuiveringssystemen bestudeerd.

Via inzicht in het optimaliseringsvraagstuk worden de delen van het model belangrijk voor het optimaliseringsprobleem bepaald.

Meten. Een eerste stap in het oplossen van het meetprobleem is het uitvoeren van een observeerbaarheids- en identifieerbaarheidsanalyse (**Hoofdstuk 4**).

In **Hoofdstuk 5** wordt het ontwerp van schatters en de performantieanalyse bestudeerd. Met een dergelijke analyse kan een geschikte schatter worden geselecteerd. Deze selectie is de tweede stap in het oplossen van het meetprobleem.

Een derde en laatste stap is het optimaal afstellen van schatters. In **Hoofdstuk 6** worden performantie- en *trade-off* analyse voorgesteld als complementaire technieken voor optimale afstelling.

Observeerbaarheids- en identifieerbaarheidsanalyse tonen aan welke delen van het model belangrijk zijn voor het oplossen van het meetprobleem.

Regeling. In **Hoofdstuk 7** wordt performantie-analyse en optimale afstelling van niet-lineaire regelaars bestudeerd, alsook de combinatie van schatters en regelaars.

Hoofdstukken 2, 5, 7 zijn theoretisch van aard terwijl **Hoofdstukken 1, 3, 4, 6** meer practisch georiënteerd zijn omdat een specifiek systeem wordt bestudeerd en/of echte data worden gebruikt.

Het proefschrift toont aan dat het modelleren van bioprocessen **geen** *basisprobleem is dat het toepassen van modelgebaseerde technieken voor optimalisering en regeling van biotechnologische systemen onmogelijk maakt. De typische karakteristieken van bioprocessen (complex, tijdsvariërend niet- lineaire dynamica met grote onzekerheid) vergen alleen een specifieke aanpak bij het gebruik van modelgebaseerde technieken. De presentatie van diverse technieken en methodes voor evaluatie van deze technieken vanuit het standpunt van de procesingenieur zou de toepassing van deze technieken in de industrie moeten vergemakkelijken. Het potentieel van de gebruikte methodes is geïllustreerd met diverse toepassingen. De verdeel en heers strategie, weerspiegeld in de structuur van de tekst, toont aan dat modelgebaseerde optimalisering en regeling van bioprocessen in een aantal relatief eenvoudig oplosbare subproblemen kan worden opgesplitst.*

F.2 Eigen bijdragen

F.2.1 Hoofdstuk 1. Modellering van cyclisch opererende actief slib afvalwaterzuiveringsinstallaties

Verschillende wiskundige modellen voor beschrijving van klassieke afvalwaterzuiveringssystemen zijn reeds bekend in de literatuur. De complexiteit van deze modellen hangt sterk af van de modelleringsdoelstelling. Modellen voor simulatie van afvalwaterzuiveringssystemen hebben veel toestanden en parameters en zijn gebaseerd op biologische kennis. Modellen, bruikbaar voor *on-line* procesregeling, hebben bij voorkeur een minimum aantal procesvariabelen (minimaal modelleringsconcept), omdat voor bioprocesregeling slechts een beperkte set *on-line* sensoren ter beschikking zijn.

De hoofddoelstelling van dit hoofdstuk is het modelleren van cyclisch opererende actief slib afvalwaterzuiveringssystemen. Eenvoudige modellen, die experimenteel kunnen worden gevalideerd en bruikbaar zijn voor het optimaliseren, schatten van procesvariabelen en regelen, worden gebruikt. Dergelijke modellen volstaan voor het beschrijven van de hoofddynamica van het bioproces. Een aantal modelselectietechnieken worden eveneens geïntroduceerd.

Er wordt aangetoond dat *dynamische analyse* en *sensitiviteitsanalyse* bruikbare technieken zijn om een geschikte modelstructuur te bepalen voor de beschrijving van een koolstofverwijderingssysteem.

Twee types van cyclisch opererende systemen (1-trap en 2-trap systemen) worden bestudeerd. Een ongestructureerd model voor het beschrijven van een 1-trap systeem wordt voorgesteld. Het gedrag van het systeem wordt in detail geanalyseerd in de toestandsruimte door middel van evenwichtslijnen. Voor het 2-trap systeem worden een ongestructureerd en gestructureerd model vergeleken door middel van dynamische- en sensitiviteitsanalyse. Het blijkt dat voor een 2-trap systeem een gestructureerd model, dat de ontwerpfilosofie van een dergelijk systeem bevat, noodzakelijk is voor een goede beschrijving.

Ook modelvalidatie door middel van laboratoriumproeven (o.a. respirometrie, ...) en proeven op een industriële installatie wordt voorgesteld.

De ontwikkelde modellen zijn bruikbaar voor het optimaliseren van dergelijke systemen (Hoofdstuk 3). Respirometrie is het basisconcept, gebruikt in het ontwerp van een geavanceerd meetsysteem, bruikbaar voor de implementatie van een optimale regelstrategie. Metingen, verwerkt met de algoritmes van Hoofdstuk 6, worden gebruikt tijdens het modelleren.

F.2.2 Hoofdstuk 2. Optimale regeling van fed-batch fermentatieprocessen met meerdere limiterende substraten

Optimalisering van bioprocessen door middel van *optimale controle* theorie lijkt in eerste opzicht niet aangewezen. Het is bekend dat de resultaten, bekomen met deze aanpak, modelsensitief zijn terwijl grote modelonzekerheid typisch is voor bioprocessen.

Een interessante aanpak bestaat uit een tweestaps procedure. In een eerste fase wordt het *optimale controle* probleem opgelost. De bekomen optimale regelstrategie wordt dan geherformuleerd als een niet-lineair regelprobleem. Deze tweestaps procedure combineert de voordelen van *optimale controle* theorie en niet-lineaire regeling. Het toepassen van *optimale controle* theorie resulteert in een optimale regelstrategie terwijl het inpassen van deze strategie in een geavanceerde niet-lineaire regelaar een robuuste performantie garandeert.

De hoofddoelstelling van dit hoofdstuk is het illustreren van de toepasbaarheid van de tweestapsprocedure voor optimalisering van fed-batch fermentatieprocessen met meerdere limiterende substraten.

Eerst wordt het *optimale controle* probleem bestudeerd voor een algemeen model voor biotechnologische processen. De cotoestandvergelijkingen en condities voor het voorkomen van singuliere regeling worden afgeleid. De bekomen formules worden dan verfijnd voor een model met één biomassa en meerdere limiterende substraten. De optimale regelstrategie wordt afgeleid. Een stopcriterium en een algemene uitdrukking voor de singuliere regelwetten worden gespecifeerd zonder *a priori* relaties tussen de specifieke reactiesnelheden aan te nemen. De resultaten worden uitvoerig geïllustreerd voor een systeem met één biomassa en twee substraten. Het blijkt dat enkel kwalitatieve kennis van de reactiesnelheden volstaat voor het volledig karakterisen van de optimale regelstrategie. Optimalisering van de overblijvende vrijheidsgraden (initiële condities, instelpunten, hoeveelheid toegevoegd substraat) wordt eveneens bestudeerd.

F.2.3 Hoofdstuk 3. Optimale regeling van cyclisch opererende actief slib afvalwaterzuiveringsinstallaties

De strengere milieunormen vereisen een meer adequate procesregeling van de bestaande afvalwaterzuiveringsinstallaties. Het combineren van geavanceerde procesregeling en moderne ontwerpprocedures resulteert in kleinere performante systemen en verhoogt de capaciteit van bestaande installaties.

Het toepassen van modelgebaseerde regeltechniek (adaptieve, neurale, fuzzy en predictieve regeling) voor koolstof- en nitraatverwijderingssyste-

men is reeds uitvoerig besproken in de literatuur. Deze technieken vereisen echter vaak een referentietraject, dat meestal niet gekend is.

In dit hoofdstuk wordt geïllustreerd dat met *optimale controle* theorie het referentietraject kan worden bepaald. Optimalisering van multi-tank cyclisch opererende koolstofverwijderingssystemen wordt bestudeerd. De volgende oplossingsstrategie wordt gebruikt.

Stap 1. Het optimaliseringsprobleem van een hypothetisch 1-tank systeem wordt bestudeerd. Een kostcriterium dat zowel beluchtingskosten als milieu-aspecten in rekening brengt wordt geoptimaliseerd. De bekomen optimale regelstrategie wordt geïllustreerd met simulaties.

Stap 2. Er wordt nagegaan wat de implicaties zijn voor de optimale regelstrategie als een cyclische bedrijfsvoering vereist is.

Stap 3. De invloed van de uitbreiding van het 1-tank systeem naar een niet cyclisch opererend multitank systeem op de optimale strategie wordt bestudeerd.

Stap 4. Met de inzichten verworven in de stappen 1 tot 3 wordt een heuristische bijna-optimale regelstrategie voor een 2-tank cyclisch opererend systeem geconstrueerd.

Stap 5. De bekomen strategie wordt uitgebreid voor 3-tank systemen zoals het UNITANK® systeem. Een aantal implementatie-aspecten worden bestudeerd.

Naast de resultaten bekomen voor de koolstofverwijderingsinstallatie, wordt in dit hoofdstuk geïllustreerd hoe *optimale control* theorie belangrijke eigenschappen van de optimale regelstrategie onthult zonder het numerisch oplossen van het *optimale control* probleem. Ook een methode voor het oplossen van *optimal control* vraagstukken voor complexe geïnterconnecteerde systemen wordt gepresenteerd. Het basisidee van deze methode bestaat erin de oplossingen van vereenvoudigde *optimale controle* problemen op een gemotiveerde manier te combineren.

F.2.4 Hoofdstuk 4. Toestand- en parameterschatters voor bioprocesmodellen

De toepassing van moderne modelgebaseerde regeling voor bioprocessen zoals afvalwaterzuivering en fermentatieprocessen wordt bemoeilijkt door het gebrek aan goedkope betrouwbare accurate *on-line* sensoren. Dit probleem kan gedeeltelijk worden verholpen door middel van zogenaamde *software sensoren*.

Een *software sensor* is een (parameter of toestand) schattingsalgoritme, gebaseerd op het procesmodel en beschikbare *on-line* metingen. De volgende vraag kan worden gesteld.

Gegeven een meetset (gegenereerd met een hardware sensor) en kennis over het systeem (modelstructuur en een aantal modelparameters), welke ongemeten toestanden en parameters kunnen uit die meetset worden geëxtraheerd?

Analyse van de observeerbaarheid van ongemeten toestanden en identifieerbaarheid van onbekende modelparameters is de eerste stap in het ontwerp van *software sensoren*.

In dit hoofdstuk wordt een observeerbaarheids- en identifieerbaarheidsanalyse van een prototype model voor bioprocessen uitgevoerd. De resultaten worden geïnterpreteerd in de context van koolstofverwijderingssystemen.

Ook de observeerbaarheid van de toestanden in een model voor nitraatverwijderingssystemen bekomen wanneer men de oxydoreductiepotentiaal gebruikt als *on-line* meting wordt bepaald.

De belangrijkste doelstelling van het hoofdstuk is aantonen dat observeerbaarheids- en identifieerbaarheidsanalyse niet enkel het evalueren van een aantal wiskundige condities is, maar een kader voor datainterpretatie.

F.2.5 Hoofdstuk 5. Performantie van niet-lineaire toestandschatters

Toestandschatters zijn algoritmes die uitgaande van een procesmodel en beschikbare *on-line* metingen niet gemeten toestandsvariabelen schatten. Voor bioprocesregeling, waar gebrek aan *on-line* sensoren typisch is, zijn toestandschatters een mogelijk alternatief.

Een overzicht van 4 niet-lineaire toestandschatterontwerpmethodologieën wordt gegeven en geïllustreerd voor een prototype model voor bioprocessen. De resultaten van een exhaustieve performantieanalyse (convergentiegebied, convergentiesnelheid, ruisgevoeligheid, robuustheid, ...) van de verschillende schatters worden gepresenteerd.

De hoofddoelstelling van het hoofdstuk is, naast het evalueren van de toepasbaarheid van de schatters voor het prototype model, het introduceren van concepten voor performantieanalyse.

Een eerste klasse van schatters is gebaseerd op een coördinatentranformatie, die het systeem transformeert naar een lineair systeem plus een niet-lineair gedeelte dat enkel afhankelijk is van de beschikbare meting. Het ontwerp van de schatters is dan gebaseerd op een lineaire techniek.

Een andere klasse van schatters is gebaseerd op een lokale linearisatie rond de geschatte toestand. Dit kan zowel gebeuren in het oorspronkelijke coördinatensysteem als in een getransformeerde ruimte.

Een derde klasse van schatters is gebaseerd op *high-gain* technieken. De niet-lineariteiten worden gecompenseerd door dominantie.

De performantieanalyseconcepten, geïntroduceerd in dit hoofdstuk, zijn geïnspireerd vanuit het standpunt van de procesingenieur.

F.2.6 Hoofdstuk 6. Optimale afstelling van toestand- en parameterschatters

In dit hoofdstuk wordt het optimaal afstellen van toestand- en parameterschatters besproken. Twee methodes worden toegelicht.

Performantieanalyse De invloed van de afstelparameters op performantiecriteria zoals ruisgevoeligheid, convergentiegebied en de maximaal toelaatbare discretisatie tijd wordt geanalyseerd. Hoewel deze aanpak resulteert voor zowel lineaire als niet-lineaire schatters in analytische uitdrukkingen voor de performantiecriteria in functie van de afstelparameters, blijft de actuele selectie van deze parameters moeilijk omdat geen globaal beeld van de performantie wordt bekomen. Ook mogelijke interacties worden verwaarloosd. Het belangrijkste voordeel van de performantieanalyse is dat een aantal structurele relaties tussen de performantie en de procescondities aan het licht komen.

Trade-off analyse De invloed van de afstelparameters op een kostfunctie, die de doelstelling van het algoritme (schatting van een variabele) beschrijft, wordt geanalyseerd door middel van simulaties. In feite is deze kostfunctie een impliciete functie van de eerder beschreven performantiecriteria. De afstelparameters, waarvoor deze functie optimaal wordt, worden geselecteerd. Het voordeel van deze methode is dat de *trade-off* tussen deze verschillende performantiecriteria nu duidelijk is met inbegrip van mogelijke interacties. Het belangrijkste nadeel is dat deze methode slechts goed functioneert in de praktijk wanneer realistische simulaties worden uitgevoerd. De analyse toont hoe de performantie is maar geeft niet aan hoe deze eventueel kan worden verbeterd.

Door middel van een aantal gevalstudies wordt aangetoond dat *performantie-* en *trade-off* analyse complementaire methodes zijn. Door middel van performantieanalyse kunnen realistische simulaties worden geconstrueerd terwijl *trade-off* analyse tot de uiteindelijke selectie van afstelwaarden leidt.

F.2.7 Hoofdstuk 7. Niet-lineaire regeling van bioprocessen

Het bestaan van diverse ontwerptechnieken voor niet-lineaire regelaars introduceert een selectieprobleem voor de procesingenieur. Een eerste bijdrage van het hoofdstuk omvat het analyseren van de robuustheid van twee ontwerpmethodes (*input-output linearisatie* en *input-state linearisatie*). Deze methodes zijn toegepast voor het prototype model voor bioprocessen.

Implementatie van de niet-lineaire regelaars is slechts mogelijk indien de regelaar wordt gekoppeld aan een toestandschatter. De convergentie-eigenschappen van een schatter, gebaseerd op exacte linearisatie en een

regelaar, gebaseerd op *input-state* linearisatie, zijn bestudeerd. Er is aangetoond dat combinatie van deze algoritmes leidt tot een bepaalde structuur in de dynamica van de regel- en schattingsfout. Omdat de toestandschatter gebruik maakt van afgeleiden van het ingangssignaal bepaald door de regelaar moet aan een aantal extra technische condities voldaan zijn.

Ook de optimale afstelling van regelaars door middel van *performantie-* en *trade-off* analyse wordt geïllustreerd.

F.2.8 Appendix C. Differential geometry in niet-lineaire regelaar en toestandschatterontwerp

Concepten gebruikt in niet-lineaire toestandschatter en regelaarontwerp worden kort geïntroduceerd. Een aantal basisdefinities en theoremas worden aangebracht. Twee niet-linear regelaarontwerpmethodes (*input-output linearisatie* en *input-state linearisatie*) worden beschreven. Niet-lineair toestandschatterontwerp gebaseerd op *exacte linearisatie modulo een output injectie* wordt bestudeerd. In de bovenstaande toestandschatterontwerpmethodes kunnen twee gevallen worden onderscheiden. In het eerste geval is de gebruikte coördinaattransformatie onafhankelijk van de ingang van het systeem. In het tweede geval is deze transformatie afhankelijk van de ingang van het systeem en zijn tijdsafgeleiden. Ook een extra niet-lineaire transformatie van de meting is toegestaan. Deze laatste toestandschatter ontwerpmethode is gebaseerd op *differential algebra* technieken terwijl de andere schatter- en regelaar ontwerptechnieken gebaseerd zijn op *differential geometry*.

In de appendix wordt de tweede toestandschatterontwerpmethode geherformuleerd in het kader van *differential geometry*. De verschillen tussen de schatterontwerptechnieken worden in detail geïllustreerd voor een prototype model voor bioprocessen.

F.3 Conclusies

In het proefschrift wordt de toepasbaarheid van modelgebaseerde optimalisering en regeling van bioprocessen geanalyseerd. Er wordt aangetoond dat de opdeling in vier subproblemen (modelleren, optimaliseren, meten en regelen) resulteert in een bruikbare aanpak.

Modellering. Modellen zijn basisingrediënten voor (i) een gedetailleerde analyse (b.v. dynamische en sensitiviteitsanalyse) van de dynamica van het te bestuderen bioproces, (ii) het (her-)ontwerp van de installatie, (iii) een verbeterde procesregeling en (iv) het ontwerp van geavanceerde meetapparatuur.

Het moet worden benadrukt dat modellen met een lage complexiteit moeten en mogen worden gebruikt voor de volgende redenen:

- De wiskundige (analytische) oplosbaarheid van optimalisering, schatter- en regelaarontwerp neemt snel af met de modelcomplexiteit.
- Complexe modellen (met veel toestanden en parameters) resulteren onvermijdelijk in observeerbaarheids- en identifieerbaarheidsproblemen door het gebrek aan sensoren.
- De modelgebaseerde technieken zijn robuust tegen modelfouten. De optimale regelstrategieën vertonen model onafhankelijke karakteristieken terwijl de schattings- en regelalgoritmes robuust zijn voor zowel parametrische als structurele onzekerheid.

Optimalisering. Het bepalen van een optimale regelstrategie moet initieel worden ontkoppeld van het niet-lineaire regelaarontwerp.

Optimal control theorie (minimum principe van Pontryagin) kan niet zomaar worden toegepast voor bioproces optimalisering ten gevolge van de voor bioprocessen typische modelfouten en de grote modelsensitiviteit van de *optimal control* aanpak.

De modelsensitiviteit kan worden omzeild door analytische oplossingen te bepalen voor problemen met een lage complexiteit. Uitgaande van deze analytische resultaten kunnen dan een aantal model onafhankelijke eigenschappen van de optimale regelstrategie worden afgeleid. Het oplossen van complexe regelproblemen is mogelijk via een goed gemotiveerde probleemdecompositie.

Naast het bepalen van de optimale regelstrategie blijkt *optimal control* theorie ook een geschikt kader voor het optimaliseren van de andere vrijheidsgraden van het systeem.

Meten. Het meetprobleem bestaat uit drie deelproblemen.

Stap 1. De identifieerbaarheid en observeerbaarheid van de parameters en toestanden van het procesmodel wordt onderzocht.

Stap 2. Een schattingsalgoritme wordt geselecteerd op basis van een performantie-analyse van een klasse van algoritmes.

Stap 3. Het geselecteerde algoritme wordt optimaal afgesteld op basis van een gecombineerde *performantie-* en *trade-off* analyse.

Door middel van schattingsalgoritmes zoals toestand- en parameterschatters wordt extra informatie uit de in bioprocesregeling schaarse *on-line* metingen gehaald.

Door het bestaan van diverse schattingsalgoritmes ontstaat er een selectieprobleem. Analyse van performantie-criteria zoals het convergentiedomein, ruisgevoeligheid, robuustheid tegen modelfouten, ... helpt de procesingenieur om een optimale selectie te maken.

Optimale afstelling van het schattingsalgoritme is gebaseerd op twee complementaire methodes. Met performantie-analyse wordt inzicht in het afstelprobleem bekomen terwijl met *trade-off* analyse de optimale parameterset wordt bepaald.

Het expliciet insluiten van niet-lineariteiten in de algoritmes impliceert het gebruik van meer geavanceerde ontwerptechnieken. Deze technieken integreren de beschikbare proceskennis echter op een optimale manier, wat resulteert in een verhoogde performantie.

Regeling. Niet-lineair regelaarontwerp kan worden beschouwd als duaal aan het ontwerp van schatters. Het bestaan van diverse ontwerpmethodologieën resulteert in een analoog selectieprobleem. Performantie analyse kan hier opnieuw worden gebruikt.

Ondanks de complexiteit van zowel schatter- en regelaarontwerp blijft de analyse van gecombineerde schatters en regelaars mogelijk.

Als uiteindelijke conclusie kan worden gesteld dat modelgebaseerde optimalisering en regeling van bioprocessen mogelijk is als de typische kenmerken van biotechnologische systemen in rekening worden gebracht bij de toepassing van de diverse methodes.

CURRICULUM VITAE

Personalia

Naam Vincent Gerard Paul Ryckaert

Thuisadres IJzerenmolenstraat 143 bus 7 3001 Heverlee (Tel. 016/201105)

Geboorteplaats Kortrijk

Geboortedatum 20 juli 1970

Nationaliteit Belg

Burgerlijke stand Gehuwd met Ingrid Reynaert op 20 april 1996

Opleiding

Middelbaar onderwijs 1982-1988, Wetenschappelijke A, *St-Jozefscollege*, Izegem

Universitair onderwijs 1988-1993, Burgerlijk Elektrotechnisch-Werktuigkundig ingenieur, Specialisatie: Automatisatie, Katholieke Universiteit Leuven

Eindwerk Study of the sensitivity problem of modelparameters for submicron circuit simulation, *Interuniversitair Microelectronica Centrum IMEC*, Heverlee (Leuven), Promotor: Prof. Dr. Ir. K. Demeyer

Doctoraat Model based optimization and control of bioprocesses - from theory to practice, *Faculteit Toegepaste Wetenschappen - Departement Elektrotechniek*, Promotoren: Prof. Dr. Ir. J. Van Impe en Prof. Dr. Ir. B. De Moor

Doctoraatsopleiding

1. *Optimal Linear Quadratic and Predictive Control*, Prof. M. Gevers
2. *Adaptive Control*, Prof. B. Wittenmark
3. *Nonlinear Control*, Dr. R. Sepulchre
4. *Neural Networks - Applications in Systems and Control*, Prof. J. Vandewalle
5. *Control System Analysis & Design via Convex Optimization*, Prof. El. Ghaoui
6. *Stochastic Systems, Estimation and Filtering*, Prof. R. Boel
7. *Numerical Linear Algebra: Signals, Systems & Control*, Prof. P. Vandooren
8. *Advanced Linear Systems Theory for Robust control*, Prof. B. De Moor
9. *Robust Control Design*, Prof. A. Tits
10. *Fundamental Limitations in Filtering & Control*, Dr. M. Seron & J. Braslavsky
11. *Environmental Bioprocesses*, ETH Zurich
12. *Workshop on Nonlinear Systems and Control*, IHP Paris
13. *Bioreactors and Bioapplications*, COMETT course, Lissabon
14. *Advanced Instrumentation, Data Interpretation, and Control of Biotechnological Processes*, COMETT course, Gent
15. *Integrated Wastewater Management*, COST-682, Budapest
16. *Nutriëntverwijdering over de grens - laatste ontwikkelingen*, Antwerpen
17. *Optimalisering van biotechnologische processen - een modelgebaseerde benadering*, Wommelgem

Onderzoeksprojecten

Augustus 1991 Zomerstage aan het Interuniversitair Microelektronica Centrum IMEC, *Evaluatie van de circuitsimulatie-omgeving CADENCE.*

15 september 1993 - 15 januari 1994, 1995 Contractonderzoek in samenwerking met ALMA Sous-Vide Competence Center en Zanussi Italië, *Development of a temperature measurement system for an industrial oven* and *Intelligent temperature control of an oven cavity for optimal microbiological safety and food quality.*

15 januari 1994 - 28 februari 1994 Wetenschappelijk medewerker aan de K.U.Leuven - Faculteit Toegepaste Wetenschappen - ESAT/SISTA

1 maart 1994 - 31 december 1994 Contractonderzoek in samenwerking met Aqualeuven/Seghersengineering en I.W.T./VL.I.M. [Vlaams Instituut voor bevordering van Wetenschappelijk-Technologisch onderzoek in industrie - VLaams Impulsprogramma Milieu], *Modelgebaseerde Optimale Adaptieve Controle van een UNITANK® Systeem gesteund op Microbiologische Kennis.*

1 januari 1995 - 31 december 1998 I.W.T.-bursaal [Vlaams Instituut voor bevordering van Wetenschappelijk-Technologisch onderzoek in industrie], *Optimale adaptieve controle van complexe biotechnologische processen - Toepassing op afvalwaterzuiveringssystemen.*

Publicaties

1. V.G. Ryckaert, J.F. Van Impe, J. Curinckx and K. Van Gool 1994. State space analysis of periodic biological wastewater treatment plants. In: *Mededelingen Fac. Landbouww. Univ. Gent*, 59 (4a): 2047-2055
2. V.G. Ryckaert, J.F. Van Impe and J.E. Claes 1995. State and parameter estimation of bioprocess models - a case study. *BeNeLux meeting*, Houthalen, 1p.
3. V.G. Ryckaert, J.E. Claes, C.H. Herremans, J.F. Van Impe, R. Gerards and L. Vriens 1995. Observer based estimation of oxygen uptake rates in cyclically operated waste water treatment plants. In: *Mededelingen Fac. Landbouww. Univ. Gent*, 60 (4b): 2377–2384
4. V.G. Ryckaert, J.E. Claes and J.F. Van Impe 1996. Intelligent temperature control of an oven cavity for optimal microbiological safety and food quality. In: *Second European Symposium on Sous Vide*, 78-99, Acco, Leuven
5. V.G. Ryckaert and J.F. Van Impe 1996. Design methodologies for nonlinear observers - application to biological models. In: P. Borne, R. Soenen, Y. Sallez and S. El Khattabi (Eds.), *Computational Engineering in Systems Applications 1996, Volume 1: Modelling, Analysis and Simulation*, GERF EC Lille - Cité Scientifique, Villeneuve d'Ascq, 1052-1057
6. V.G. Ryckaert, J.E. Claes, J.F. Van Impe, R. Gerards and L. Vriens 1996. Optimal design and control of UNITANK® wastewater treatment systems. In: *Mededelingen Fac. Landbouww. Univ. Gent*, 61 (4a): 1799-1802
7. V.G. Ryckaert, J.F. Van Impe, M. Feyaerts and L. Vriens 1996. Modelgebaseerde interpretatie van oxydo-reductie metingen. In: K. Gernaey (Editor), *Milieutechnologie in beweging*, ISBN 90 76019 02 9 - Technologisch Instituut VZW, Antwerpen

8. V.G. Ryckaert, J.E. Claes and J.F. Van Impe 1996. Optimal design and control of UNITANK® wastewater treatment systems. *BeNeLux meeting*, Mierlo (The Nederlands), 1p.
9. V.G. Ryckaert, C.H. Herremans, J.E. Claes, J.F. Van Impe, R. Gerards and L. Vriens 1997. Modelling and dynamical analysis of UNITANK® wastewater treatment systems. *Mathematical Modelling of Systems*, 3, (2), 159-180
10. V.G. Ryckaert and J.F. Van Impe 1997. State and parameter estimation of bioprocess models - a case study. In: L.T. Grujić, P. Borne, A. El Moudni and M. Ferney (Eds.), *Control of Industrial Systems*, 3, 576-581, published for IFAC by Ecole Nationale d'Ingénieurs de Belfort, Belfort, 6p.
11. V.G. Ryckaert, E. Jacobs and J.F. Van Impe 1997. Robustness of nonlinear observers - application to biological models. In: *Proceedings of the 1997 European Control Conference*, 1, TU-E F5 1-6, 6 p.
12. V.G. Ryckaert and J.F. Van Impe 1997. Combined nonlinear observers and nonlinear controllers. *BeNeLux meeting* , Houffalize, 1p.
13. V.G. Ryckaert, M. Feyaerts, L. Vriens, H. Verachtert and J.F. Van Impe 1998. Redox based control in a UNITANK® nitrogen removal system. *Accepted for publication in European Water Management*
14. V.G. Ryckaert and J.F. Van Impe 1998. Optimal tuning of software sensors for bioprocess control. *Proceedings of the ACoFoP, Automatic Control of Food and Biological Processes Conference*, Göteborg (Zweden)
15. V.G. Ryckaert, T. Boelen and J.F. Van Impe 1998. Robustness of nonlinear observers. *Proceedings of NOLCOS98, IFAC Nonlinear Control Systems Design Symposium*, Enschede (The Netherlands)
16. V.G. Ryckaert and J.F. Van Impe 1998. Optimal design & control of cyclically operated biological wastewater treatment plants. *Proceedings of CAB7, IFAC Conference on Computer Applications in Biotechnology*, Osaka (Japan)
17. V.G. Ryckaert, T. Boelen, R. Sepulchre and J.F. Van Impe 1998. Constructive nonlinear observer design. *BeNeLux meeting*, Mierlo (The Netherlands), 1p.
18. J.E. Claes, V.G. Ryckaert, J.F. Van Impe, R. Gerards and L. Vriens 1996. Mathematical modeling and identification of UNITANK® wastewater treatment systems. *European Water Pollution Control*, 6(6), 34-44
19. C.H. Herremans, V.G. Ryckaert, J.F. Van Impe en H. Verachtert 1996. Dynamisch Gedrag van Actief Slib Waterzuiveringsinstallaties volgens het UNITANK® systeem: Systeemtheoretische Analyse. *WATER*, 91, 289-293

Review activiteiten voor

1. *IFAC SYmposium on System IDentification* 1994, Copenhagen (Danmark)
2. *8th European Signal Processing Conference EUSIPCO-96* 1996, Trieste (Italy)
3. *European Control Conference ECC* 1997, Brussels (Belgium)
4. *The Journal of the Franklin Institute*, 1997
5. *IEEE Transactions on Automatic Control*, 1998